Efficient carbon utilization to dimethyl ether by steam adsorption enhancement

Jasper van Kampen

Efficient carbon utilization to dimethyl ether by steam adsorption enhancement

EINDHOVEN UNIVERSITY OF TECHNOLOGY

TNO

The research presented in this thesis has been carried out at the research group Sustainable Technologies for Industrial Processes (STIP) from the Netherlands Organisation for applied scientific research (TNO) and at the research group Chemical Process Intensification (SPI) within the department of Chemical Engineering and Chemistry at the Eindhoven University of Technology (TU/e). The research was supported by the European Union's Horizon research and innovation programme under grant agreement no. 727600, the FLEDGED project.

FSC
www.fsc.org
MIX
Paper from responsible sources

A catalogue record is available from the Eindhoven University of Technology Library
ISBN 978-90-386-5269-6

Cover design Jasper van Kampen
Printed by Gildeprint - The Netherlands

Efficient carbon utilization to dimethyl ether by steam adsorption enhancement

PROEFSCHRIFT

ter verkrijging van de graad van doctor aan de Technische Universiteit Eindhoven, op gezag van de rector magnificus prof.dr.ir. F.P.T. Baaijens, voor een commissie aangewezen door het College voor Promoties, in het openbaar te verdedigen op vrijdag 4 juni 2021 om 16:00 uur

door

Jasper van Kampen

geboren te Sint-Oedenrode

Dit proefschrift is goedgekeurd door de promotoren en de samenstelling van de promotiecommissie is als volgt:

voorzitter:	prof.dr. F. Gallucci
1e promotor:	prof.dr.ir. M. van Sint Annaland
copromotor:	dr.ir. J. Boon (TNO)
leden:	dr. L.M.P. Madeira (Universidade do Porto)
	prof.dr.ir. W. de Jong (TUD)
	prof.dr.ir. J. van der Schaaf
	prof.dr.ir. D.W.F. Brilman (UT)
	dr. M.C. Romano (Politecnico di Milano)

Het onderzoek of ontwerp dat in dit proefschrift wordt beschreven is uitgevoerd in overeenstemming met de TU/e Gedragscode Wetenschapsbeoefening.

μάλα γὰρ φιλοσόφου τοῦτο τὸ πάθος, τὸ θαυμάζειν:
οὐ γὰρ ἄλλη ἀρχὴ φιλοσοφίας ἢ αὕτη
Σωκράτης

Wonder is the beginning of wisdom

Socrates (Plato, *Theaetetus*)

Efficient carbon utilization to dimethyl ether by steam adsorption enhancement

Dimethyl ether (DME), due to its chemical and physical properties as well as its combustion characteristics, is one of the most promising alternative fuel solutions among the various ultra-clean, renewable, and low-carbon fuels under consideration worldwide. DME is also one of the valuable products considered for chemical recycling by carbon dioxide conversion, direct (carbon capture and utilization) as well as indirect conversion via biomass-based syngas. Conventionally, DME is produced from synthesis gas with methanol as an intermediate chemical. The incomplete methanol and DME yields require extensive separation sections and recycles. In recent years a lot of attention has been going to the direct production of DME in a single-step process. The single-step direct DME synthesis also proceeds via intermediate methanol, yet offers a reduction in process steps and increased overall conversion to DME. Although the direct DME synthesis process outperforms the indirect process in terms of efficiency, separation and recycling remain a requirement. In the direct DME synthesis, the oxygen surplus of the feed ends up in CO_2, resulting in equal molar amounts of DME and CO_2 produced. Since the reaction is equilibrium limited, the downstream separation section produces recycle streams of synthesis gas ($CO+H_2$), CO_2, and methanol. Synthesis gas and methanol can be recycled back to the DME synthesis reactor, while the CO_2 is at best recycled in synthesis gas generation via dry or tri-reforming. However, starting from a renewable, CO_2-rich feedstock and/or captured CO_2 to produce DME, this is not an option. In fact, one of the major challenges in power-to-liquid (PtL) processes is the direct utilization of CO_2, making most approaches for renewable fuel production unattractive. For CO_2 utilization, the production and efficient handling of steam remains a major bottleneck. Separation enhancement is a proven process intensification, providing a strategy to overcome conversion problems in equilibrium-limited reactions. According to Le Chatelier's principle, the removal of one of the products will shift the equilibrium-limited conversion to the products' side. In particular, sorption enhanced DME synthesis (SEDMES) is a novel process route for the production of DME. It is based on the in situ removal of water by a solid adsorbent, typically a LTA zeolite. The in situ removal of H_2O assures that the oxygen surplus of the feed no longer ends up as CO_2, as is the case for direct DME synthesis. As a result, CO_2 can be used directly as feed, rather than being the main by-product of DME synthesis.

SEDMES is a cyclic process, that comprises high pressure adsorption and low pressure regeneration, possibly at elevated temperatures. A dynamic SEDMES reactor model is developed, allowing the study of the full cyclic process of adsorption and inherent

regeneration. The SEDMES process is a promising process intensification, already achieving over 80% single-pass CO_2 conversion and more than 70% single-pass DME (carbon) yield for a non-optimized three-reactor column system. A key parameter for optimizing the SEDMES process further is the working adsorption capacity of the system. The regeneration, inherent to a reactive adsorption process, has a large influence on the adsorption capacity of the system. A combination of temperature and pressure swing regeneration results in the best system performance regarding the DME yield and CO_2 conversion. However, first indication is given that both TSA and PSA alone could be an option in the SEDMES process development. Especially, PSA is generally preferred for its facilitated design and possibly improved productivity. Finally, under the TPSA conditions, cooled reactor operation of the reactive adsorption step is required to achieve high performance of the system. SEDMES temperature control in a multi-tubular fixed bed reactor, however, is shown not to be a critical issue.

Modelling studies on sorption enhanced reactions strongly rely on the understanding of the interaction of steam and the adsorbent under relevant conditions. One of the most promising high-temperature steam adsorbents, molecular sieve zeolite 3A, is studied under relevant conditions for the sorption enhanced conversion of CO_2 by a combined experimental and modelling approach. Quantitative data for water adsorption at elevated temperature (200-350 °C) and partial pressure (0.05-4.5 bar) allows development of a suitable adsorption isotherm under these conditions. Besides the adsorption capacity, the kinetics of adsorption are essential the for modelling and evaluation of applications of the adsorbent in sorption enhanced reaction processes. Therefore, a kinetic description of water adsorption is developed by means of a mass transfer rate model, which is sufficiently accurate for all reactor and process modelling purposes.

The direct synthesis of DME, with or without sorption enhancement, entails the use of two different catalytic phases, one for the synthesis of methanol from syngas and one for the subsequent dehydration to DME. Copper-Zinc Oxide-Alumina (CZA) materials are the benchmark catalysts for the synthesis of methanol from syngas, whereas acidic solids such as γ-Al_2O_3 are the most active catalysts for the methanol dehydration to DME. An experimental proof-of-concept for sorption enhanced DME synthesis, with commercial and novel catalyst materials, is shown. To extend the knowledge on catalyst inhibition and deactivation by steam, an investigation of the boehmite to γ-Al_2O_3 phase transition is presented in the temperature and partial pressure ranges of 250-400 °C and pressures up to 15 bar respectively. Reaction kinetics for the commercial dehydration catalyst, as well as the methanol synthesis catalyst, have been determined. The activation energies determined for both the methanol synthesis and methanol dehydration kinetics are lower than the values originally reported, attributed to the higher activity of present-day catalysts.

The study of the adsorbent material, the investigation of the catalysts, and the combination of all materials involved in SEDMES result in a validated dynamic reactor model, allowing adequate upscaling of the SEDMES technology and predictions of large scale DME synthesis.

Confirming model indications, a validated pressure swing regeneration cycle for sorption enhanced DME synthesis is demonstrated on a bench-scale reactor. SEDMES is again demonstrated to be a highly flexible process for converting CO_2-rich (bio-based) syngas and CO_2 directly to DME with a high single-pass conversion. Here, 80% single-pass carbon selectivity to DME is demonstrated with pressure swing regeneration, which already allows for a factor four increase in productivity with further optimization still possible. SEDMES technology is developed even further by experimental validation on a multi-column test-rig under industrially relevant conditions. In this setup the continuous production of DME by sorption enhancement is demonstrated for the first time in open literature. The essential pressure swing regeneration, key to an economic attractive process, is confirmed as the mode of regeneration. The developed SEDMES reactor model describes both the transient nature of the process during the cyclic-steady-state, as well as the approach to the cyclic steady-state. Additionally, the dynamic operation is studied in more detail, including lower temperatures than previously reported for SEDMES. Elaboration on SEDMES cycle design is presented to give direction for further process systems engineering, techno-economic analysis and life cycle analysis. A three column cycle design has shown good cyclic performance. When pressure equalization is disregarded to minimize the number of columns, and therefore reduce the capital cost, the blowdown recycle becomes important. Also, from a techno-economic perspective, a small recycle of non-condensables (CO and H_2) after a simple flash separation would be of interest to achieve high productivity at high, but not maximum, carbon selectivity. This example illustrates the importance of combining the SEDMES cycle design, the overall process systems engineering and techno-economic evaluation. Combined these aspects can be used to optimize SEDMES further for the desired use case and address the economic and carbon mitigating benefits of SEDMES over conventional DME synthesis technology. In contrast to conventional DME synthesis, SEDMES allows more efficient carbon and renewable hydrogen utilization to DME.

In conclusion, sorption enhanced DME synthesis has matured from a technology concept to a technology validated in a relevant environment. Crucial to the understanding of steam separation enhanced processes, SEDMES has been investigated by a combined experimental and modelling approach. With the technology validated and the modelling framework available, techno-economic and life cycle analyses have to be performed to investigate the economic and carbon mitigating benefits of the high efficiency carbon and hydrogen utilization by the SEDMES technology.

Contents

List of Figures

List of Tables

Chapter 1. Introduction

Abstract

This chapter introduces the research questions addressed in this thesis and discusses the motivation for the development of a novel process for the production of dimethyl ether.
Dimethyl ether is one of the most promising alternative fuel solutions. It is also one of the valuable products considered for chemical recycling by carbon dioxide conversion. However for efficient carbon dioxide utilization, the production and efficient handling of steam is a major bottleneck. In this chapter the novel sorption enhanced dimethyl ether synthesis (SEDMES) process is introduced, which uses a solid adsorbent for the in situ removal of water. The in situ removal of water assures that the oxygen surplus of the feed does not end up in carbon dioxide, as is the case for conventional synthesis. As a result, carbon dioxide can be used directly as feed, rather than being the main by-product of dimethyl ether synthesis. The chapter concludes with an overview of the thesis in which various aspects of the novel SEDMES process are investigated.

Efficient carbon utilization to dimethyl ether by steam adsorption enhancement

Dimethyl ether (DME) is the simplest ether compound, represented by the chemical formula CH_3OCH_3. DME is gaseous at ambient conditions, which is easy to liquefy and transport. It is safely stored and handled and does not form explosive peroxides in contrast to several other ethers. Its chemical and physical properties as well as its combustion characteristics make that DME can be used as fuel in domestic applications replacing LPG, both in compression ignition engines (100% DME) and spark ignition engines (30% DME/70% LPG), and in power generation. Consequently, DME is one of the most promising alternative fuel solutions among the various ultra clean, renewable, and low-carbon fuels under consideration worldwide [1-3]. DME is also one of the valuable products considered for chemical recycling by carbon dioxide conversion [4], direct (CCU) as well as indirect conversion via biomass-based syngas. Conventionally, DME is produced from synthesis gas with methanol as an intermediate chemical. The following equilibrium reactions are involved:

Methanol synthesis	$CO_2+3H_2 \rightleftharpoons CH_3OH+H_2O$	ΔH^0 = -49 kJ/mol	(1)
	$CO+2H_2 \rightleftharpoons CH_3OH$	ΔH^0 = -90 kJ/mol	(2)
Water-gas shift	$CO+H_2O \rightleftharpoons H_2+CO_2$	ΔH^0 = -41 kJ/mol	(3)
Methanol dehydration	$2CH_3OH \rightleftharpoons CH_3OCH_3+H_2O$	ΔH^0 = -24 kJ/mol	(4)

Indirect DME production (Figure 1-1a) comprises the production of intermediate methanol (1,2), and subsequent methanol dehydration (4). The incomplete methanol and DME yields require extensive separation sections and recycles. In recent years a lot of attention is going to the direct production of DME in a single-step process (Figure 1-1b), including a major contribution for the development of hybrid catalysts [5-18]. The single-step direct DME synthesis proceeds via intermediate methanol as well, yet offers a reduction in process steps and increased overall conversion to DME [17, 19-21]. Although the direct DME synthesis process outperforms the indirect process in terms of efficiency, separation and recycling remain a requirement. In the direct DME synthesis, the O-surplus of the feed ends up in CO_2, resulting in equal molar amounts of DME and CO_2 produced. Since the reaction is equilibrium limited, the downstream separation section produces recycle streams of synthesis gas ($CO+H_2$), CO_2, and methanol. Synthesis gas and methanol can be recycled back to the DME synthesis reactor, while the CO_2 is at best recycled in synthesis gas generation via dry or tri-reforming [15, 22-28]. However, starting from a renewable, CO_2-rich feedstock and/or captured CO_2 to produce DME, this is not an option. In fact, one of the major challenges in power-to-liquid (PtL) processes is the direct utilization of CO_2 [29], making

most approaches for renewable fuel production unattractive [30]. For CO_2 utilization, the production and efficient handling of steam remains a major bottleneck [4, 31, 32].

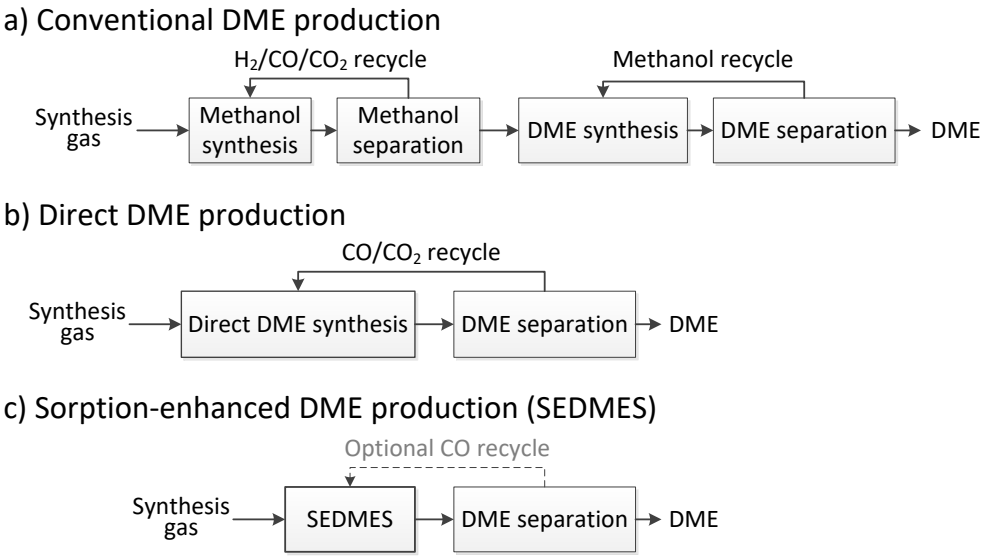

FIGURE 1-1: SCHEMATIC OVERVIEW OF DME PRODUCTION ROUTES.

Separation enhancement is a proven strategy to overcome conversion problems in equilibrium-limited reactions. According to Le Chatelier's principle, the removal of one of the products shifts the equilibrium-limited conversion to the products' side, which is utilized mainly for various CO_2 separation and utilization processes [22, 33, 34]. In particular, sorption enhanced DME synthesis (SEDMES, Figure 1-1c) is a novel process route for the production of DME [35-37]. It is based on the in situ removal of water by a solid adsorbent, typically a LTA zeolite [22, 38]. The in situ removal of H_2O assures that the oxygen surplus of the feed no longer ends up as CO_2, as is the case for direct DME synthesis. As a result, CO_2 can be used directly as feed, rather than being the main by-product of DME synthesis. In this thesis the technical potential of sorption enhanced DME synthesis is investigated by modelling and experimental studies. Figure 1-2 shows an illustration of the SEDMES reactor concept, indicating the materials involved and their functionalities in the process, which are investigated in the chapters throughout this thesis.

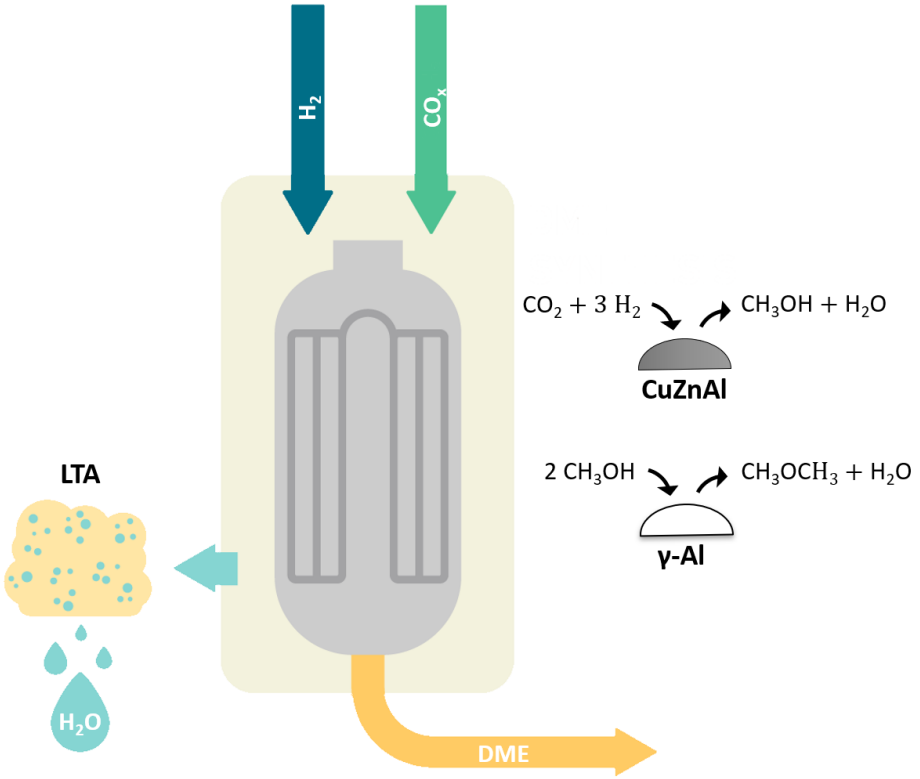

FIGURE 1-2: SCHEMATIC REPRESENTATION OF THE SEDMES REACTOR CONCEPT.

Dehydration reactions are common in the chemical industry, and similarly the utilization of carbon dioxide often starts with its chemical reduction with hydrogen and the formation of steam. In fact, the effective handling of steam is one of the biggest bottlenecks for CO_2 utilization in industry [4, 31]. In **Chapter 2** the advantages of process intensification through steam separation enhanced reactions are discussed and a critical review of adsorption and membrane technologies is given.

In **Chapter 3** the development of a dynamic SEDMES reactor model is described. The chapter introduces an elaborate model description, followed by a first comparison of the model with experimental results. SEDMES is studied as a full cyclic process of adsorption and inherent regeneration, and its performance is extensively analyzed. Finally, an initial comparison of SEDMES and direct DME synthesis is made.

Modelling studies on sorption enhanced reactions strongly rely on the accuracy of the description of the interaction of steam and the adsorbent under relevant conditions. **Chapter 4** studies one of the most promising high-temperature steam adsorbents, molecular sieve zeolite 3A, under relevant conditions for the sorption enhanced conversion of CO_2 by a combined experimental and modelling approach. Quantitative data for water adsorption at elevated temperature (200-350 °C) and partial pressure (0.05-4.5 bar) allows evaluation of a suitable adsorption isotherm under these conditions. Besides the adsorption capacity, the kinetics of adsorption are essential the for modelling and evaluation of applications of the adsorbent in sorption enhanced reaction processes. Therefore, a kinetic description of water adsorption is developed by means of a mass transfer rate model.

The direct synthesis of DME, with or without sorption enhancement, entails the use of two different catalytic phases, one for the synthesis of methanol from syngas and one for the subsequent dehydration to DME. Copper-Zinc Oxide-Alumina (CZA) materials are the benchmark catalysts for the synthesis of methanol from syngas [39-41], whereas acidic solids such as γ-Al_2O_3 [40, 42], zeolites [43, 44], acidic oxides [45] or heteropoly acids [46-49] are the most active catalysts for methanol dehydration. **Chapter 5** presents a proof-of-concept for the sorption enhanced DME synthesis with commercial and novel catalyst materials.
To extend the knowledge on catalyst inhibition and deactivation by steam, an investigation of the boehmite to γ-Al_2O_3 phase transition is presented in the temperature and partial pressure ranges of 250-400 °C and pressures up to 15 bar respectively. Finally, in this chapter the reaction kinetics for the commercial materials (CZA and γ-Al_2O_3), selected for SEDMES scale-up, are determined for model validation purposes.

In **Chapter 6** the results of an experimental investigation into the bench-scale sorption enhanced production of DME are described and discussed. The investigation of the materials involved in SEDMES, separately under relevant conditions and combined for sorption enhanced DME production, have resulted in a validated model. Sorption enhanced DME synthesis technology is validated with the best (commercially available) materials, and model development and validation under relevant conditions is performed. Special attention is paid to the mode of regeneration, as the key to an economically attractive process.

SEDMES is developed further in **Chapter 7**. The results of an experimental investigation into the multi-column, continuous sorption enhanced production of DME are discussed. The SEDMES reactor model is used for data interpretation. The confirmation of pressure swing regeneration during the continuous production of DME is amongst the points of attention. Additionally, the dynamic operation is studied in more detail, including the possibility to

operate at lower temperatures than previously reported for SEDMES. An elaboration on the SEDMES cycle design is presented to give direction for further process flow sheeting, techno-economic analysis and life cycle analysis of SEDMES.

Finally, the research in this thesis on the efficient carbon utilization to dimethyl ether by steam adsorption enhancement is summarized. A short outlook is given, discussing possible SEDMES applications and the way forward in SEDMES technology development.

Bibliography

[1] T.A. Semelsberger, R.L. Borup, H.L. Greene, Dimethyl ether (DME) as an alternative fuel, Journal of Power Sources 156 (2006) 497-511.
[2] C. Arcoumanis, C. Bae, R. Crookes, E. Kinoshita, The potential of di-methyl ether (DME) as an alternative fuel for compression-ignition engines: A review, Fuel 87 (2008) 1014-1030.
[3] G.A. Olah, A. Goeppert, G.K.S. Prakash, Chemical Recycling of Carbon Dioxide to Methanol and Dimethyl Ether, J. Org. Chem. 74 (2009) 487–498.
[4] G. Centi, S. Perathoner, Opportunities and prospects in the chemical recycling of carbon dioxide to fuels, Catalysis Today 148 (2009) 191-205.
[5] G. Bonura, M. Cordaro, C. Cannilla, A. Mezzapica, L. Spadaro, F. Arena, F. Frusteri, Catalytic behaviour of a bifunctional system for the one step synthesis of DME by CO_2 hydrogenation, Catalysis Today 228 (2014) 51-57.
[6] M. Cai, A. Palčić, V. Subramanian, S. Moldovan, O. Ersen, V. Valtchev, V.V. Ordomsky, A.Y. Khodakov, Direct dimethyl ether synthesis from syngas on copper-zeolite hybrid catalysts with a wide range of zeolite particle sizes, Journal of Catalysis 338 (2016) 227-238.
[7] E. Catizzone, A. Aloise, M. Migliori, G. Giordano, Dimethyl ether synthesis via methanol dehydration: Effect of zeolite structure, Applied Catalysis A: General 502 (2015) 215-220.
[8] W.H. Chen, C.L. Hsu, X.D. Wang, Thermodynamic approach and comparison of two-step and single step DME (dimethyl ether) syntheses with carbon dioxide utilization, Energy 109 (2016) 326-340.
[9] F. Dadgar, R. Myrstad, P. Pfeifer, A. Holmen, H.J. Venvik, Catalyst Deactivation During One-Step Dimethyl Ether Synthesis from Synthesis Gas, Catalysis Letters 147 (2017) 865-879.
[10] M.D. Falco, M. Capocelli, A. Basile, Selective membrane application for the industrial one-step DME production process fed by CO_2 rich streams: Modeling and simulation, International Journal of Hydrogen Energy (2017) 6771-6786.
[11] F. Frusteri, M. Migliori, C. Cannilla, L. Frusteri, E. Catizzone, A. Aloise, G. Giordano, G. Bonura, Direct CO_2-to-DME hydrogenation reaction: New evidences of a superior behaviour of FER-based hybrid systems to obtain high DME yield, Journal of CO_2 Utilization 18 (2017) 353-361.

[12] A. García-Trenco, A. Martínez, The influence of zeolite surface-aluminum species on the deactivation of CuZnAl/zeolite hybrid catalysts for the direct DME synthesis, Catalysis Today 227 (2014) 144-153.
[13] I.A. Kurzina, S.I. Reshetnikov, N.I. Karakchieva, L.N. Kurina, Direct synthesis of dimethyl ether from synthesis gas: Experimental study and mathematical modeling, Chemical Engineering Journal 329 (2017) 135-141.
[14] Y. Li, T. Wang, X. Yin, C. Wu, L. Ma, H. Li, X. Zhang, Y. Lv, Pilot-scale tests of direct dimethyl ether synthesis from biomass-derived syngas, Asia-Pacific Power and Energy Engineering Conference (APPEEC), Wuhan, 2009.
[15] S.-H. Lee, W. Cho, T. Song, Y.-J. Ra, Scale up study of DME direct synthesis technology, Proceedings of World gas conference, 2009.
[16] S.P. Naik, T. Ryu, V. Bui, J.D. Miller, N.B. Drinnan, W. Zmierczak, Synthesis of DME from CO_2/H_2 gas mixture, Chemical Engineering Journal 167 (2011) 362-368.
[17] K.L. Ng, D. Chadwick, B.A. Toseland, Kinetics and modelling of dimethyl ether synthesis from synthesis gas, Chemical Engineering Science 54 (1999) 3587-3592.
[18] V.M. Lebarbier, R.A. Dagle, L. Kovarik, J.A. Lizarazo-Adarme, D.L. King, D.R. Palo, Synthesis of methanol and dimethyl ether from syngas over Pd/ZnO/Al2O3 catalysts, Catalysis Science & Technology 2 (2012) 2116–2127.
[19] U. Mondal, G.D. Yadav, Perspective of dimethyl ether as fuel: Part I. Catalysis, Journal of CO2 Utilization 32 (2019) 299-320.
[20] F. Dadgar, R. Myrstad, P. Pfeifer, A. Holmen, H.J. Venvik, Direct dimethyl ether synthesis from synthesis gas: The influence of methanol dehydration on methanol synthesis reaction, Catalysis Today 270 (2016) 76-84.
[21] D. Liuzzi, C. Peinado, M.A. Peña, J. van Kampen, J. Boon, S. Rojas, Increasing dimethyl ether production from biomass-derived syngas via sorption enhanced dimethyl ether synthesis, Sustainable Energy & Fuels 4 (2020) 5674-5681.
[22] J. van Kampen, J. Boon, F. van Berkel, J. Vente, M. van Sint Annaland, Steam separation enhanced reactions: Review and outlook, Chemical Engineering Journal 374 (2019) 1286–1303.
[23] T.B.H. Nguyen, E. Zondervan, Methanol production from captured CO2 using hydrogenation and reforming technologies: environmental and economic evaluation, Journal of CO2 Utilization 34 (2019) 1-11.
[24] A. Rafiee, K. Rajab Khalilpour, D. Milani, M. Panahi, Trends in CO2 conversion and utilization: A review from process systems perspective, Journal of Environmental Chemical Engineering 6 (2018) 5771-5794.
[25] M.T. Luu, D. Milani, M. Wake, A. Abbas, Analysis of di-methyl ether production routes : Process performance evaluations at various syngas compositions, Chemical Engineering Science 149 (2016) 143-155.

[26] S.-H. Lee, W. Cho, W.-S. Ju, B.-H. Cho, Y.-C. Lee, Y.-S. Baek, Tri-reforming of CH4 using CO2 for production of synthesis gas to dimethyl ether, Catalysis Today 87 (2003) 133-137.
[27] W. Cho, T. Song, A. Mitsos, J.T. McKinnon, G.H. Ko, J.E. Tolsma, D. Denholm, T. Park, Optimal design and operation of a natural gas tri-reforming reactor for DME synthesis, Catalysis Today 139 (2009) 261-267.
[28] I.H. Kim, S. Kim, W. Cho, E.S. Yoon, Simulation of commercial dimethyl ether production plant, in: S. Pierucci, G.B. Ferraris (Eds.) 20th European Symposium on Computer Aided Process Engineering – ESCAPE20, 2010, pp. 799-804.
[29] V. Dieterich, A. Buttler, A. Hanel, H. Spliethoff, S. Fendt, Power-to-liquid via synthesis of methanol, DME or Fischer–Tropsch-fuels: a review, Energy & Environmental Science 13 (2020) 3207-3252.
[30] R.J. Detz, J.N.H. Reek, B.C.C. van der Zwaan, The future of solar fuels: when could they become competitive?, Energy & Environmental Science 11 (2018) 1653-1669.
[31] Accelerating Breakthrough Innovation in Carbon Capture, Utilization, and Storage, Report of the Mission Innovation Carbon Capture, Utilization, and Storage Expert's Workshop, 2017.
[32] A. Katelhon, R. Meys, S. Deutz, S. Suh, A. Bardow, Climate change mitigation potential of carbon capture and utilization in the chemical industry, Proc Natl Acad Sci U S A 116 (2019) 11187-11194.
[33] A.E. Rodrigues, L.M. Madeira, Y.-J. Wu, R. Faria, Sorption Enhanced Reaction Processes, World Scientific, 2017.
[34] J.C. Abanades, J. Boon, P. Cobden, K. Coenen, D.S.M. Constantino, R.P.V. Faria, J.R. Fernández, F. Gallucci, M.C. Iliuta, A.E. Rodrigues, E. van Dijk, M. van Sint Annaland, Sorption Enhancement of Chemical Processes, 1 ed., Academic Press, 2017.
[35] J. Boon, F. van Berkel, H. van Dijk, J. Vente, Separation enhanced dimethyl ether synthesis, 5th TMFB International Conference, Aachen, 2017.
[36] I. Iliuta, M.C. Iliuta, F. Larachi, Sorption-enhanced dimethyl ether synthesis — Multiscale reactor modeling, Chemical Engineering Science 66 (2011) 2241-2251.
[37] J. van Kampen, J. Boon, F. van Berkel, H. van Dijk, J. Vente, M. van Sint Annaland, Regeneration conditions as the key to sorption enhanced dimethyl ether synthesis, 25th International Symposium on Chemical Reaction Engineering, Florence, 2018.
[38] J. van Kampen, J. Boon, J. Vente, M. van Sint Annaland, Sorption enhanced dimethyl ether synthesis for high efficiency carbon conversion: Modelling and cycle design, Journal of CO_2 Utilization 37 (2020) 295-308.
[39] R. Khoshbin, M. Haghighi, Direct conversion of syngas to dimethyl ether as a green fuel over ultrasound-assisted synthesized CuO–ZnO–Al2O3/HZSM-5 nanocatalyst: effect of active phase ratio on physicochemical and catalytic properties at different process conditions, Catal. Sci. Technol. 4 (2014) 1779-1792.

[40] R. Peláez, P. Marín, S. Ordóñez, Direct synthesis of dimethyl ether from syngas over mechanical mixtures of CuO/ZnO/Al2O3 and γ-Al2O3: Process optimization and kinetic modelling, Fuel Processing Technology 168 (2017) 40-49.
[41] C. Baltes, S. Vukojevic, F. Schuth, Correlations between synthesis, precursor, and catalyst structure and activity of a large set of CuO/ZnO/Al2O3 catalysts for methanol synthesis, Journal of Catalysis 258 (2008) 334-344.
[42] F. Song, Y. Tan, H. Xie, Q. Zhang, Y. Han, Direct synthesis of dimethyl ether from biomass-derived syngas over Cu–ZnO–Al2O3–ZrO2(x)/γ-Al2O3 bifunctional catalysts: Effect of Zr-loading, Fuel Processing Technology 126 (2014) 88-94.
[43] D. Mao, X. Guo, Dimethyl Ether Synthesis from Syngas over the Admixed Cu/ZnO/Al2O3Catalyst and Alkaline Earth Oxide-Modified HZSM-5 Zeolite, Energy Technology 2 (2014) 882-888.
[44] X.-J. Tang, J.-H. Fei, Z.-Y. Hou, X.-M. Zheng, H. Lou, Characterization of Cu−Mn/Zeolite-Y Catalyst for One-Step Synthesis of Dimethyl Ether from CO−H2, Energy & Fuels 22 (2008) 2877–2884.
[45] R. Ladera, E. Finocchio, S. Rojas, J.L.G. Fierro, M. Ojeda, Supported niobium catalysts for methanol dehydration to dimethyl ether: FTIR studies of acid properties, Catalysis Today 192 (2012) 136-143.
[46] R.M. Ladera, J.L.G. Fierro, M. Ojeda, S. Rojas, TiO2-supported heteropoly acids for low-temperature synthesis of dimethyl ether from methanol, Journal of Catalysis 312 (2014) 195-203.
[47] R.M. Ladera, M. Ojeda, J.L.G. Fierro, S. Rojas, TiO2-supported heteropoly acid catalysts for dehydration of methanol to dimethyl ether: relevance of dispersion and support interaction, Catalysis Science & Technology 5 (2015) 484-491.
[48] A. Kornas, M. Śliwa, M. Ruggiero-Mikołajczyk, K. Samson, J. Podobiński, R. Karcz, D. Duraczyńska, D. Rutkowska-Zbik, R. Grabowski, Direct hydrogenation of CO2 to dimethyl ether (DME) over hybrid catalysts containing CuO/ZrO2 as a metallic function and heteropolyacids as an acidic function, Reaction Kinetics, Mechanisms and Catalysis 130 (2020) 179-194.
[49] C. Peinado, D. Liuzzi, R.M. Ladera-Gallardo, M. Retuerto, M. Ojeda, M.A. Pena, S. Rojas, Effects of support and reaction pressure for the synthesis of dimethyl ether over heteropolyacid catalysts, Sci Rep 10 (2020) 8551.

Chapter 2. Steam separation enhanced reactions

Abstract

This chapter contains a review of the advances, and an assessment of the potential and the challenges, in the field of steam separation enhanced technologies. Enhancement by steam separation is a promising process intensification for many types of reactions in which water is formed as a byproduct. For this, two main technologies are reactive vapor permeation (membrane technology) and reactive adsorption. Both can achieve significant conversion enhancement of equilibrium limited reactions by in situ removal of the by-product steam, while additionally it may help protecting catalysts from steam-induced deactivation.

In general, reactive permeation or reactive adsorption would be preferable for distinctly different process conditions and requirements. However, although some advantages of reactive steam separation are readily apparent from a theoretical, thermodynamic point of view, the developments in several research lines make clear that the feasibility of in situ steam removal should be addressed case specifically and not only from a theoretical point of view. This includes the hydrothermal stability of the membranes and their permselectivity for reactive steam permeation, whereas high-temperature working capacities and heat management are crucial aspects for reactive steam adsorption. Together, these developments can accelerate further discovery, innovation and the rollout of steam separation enhanced reaction processes for CO_2 utilization.

This chapter is based on published work:
J. van Kampen et al., Steam separation enhanced reactions: Review and outlook, Chemical Engineering Journal 374 (2019) 1286–1303.

2.1. Introduction

Dehydration reactions are common in chemical industry, and similarly the utilization of carbon dioxide often starts with its chemical reduction with hydrogen and the formation of steam. In fact, the effective handling of steam is one of the biggest bottlenecks for CO_2 utilization in industry [1, 2]. Whereas H_2O is the main byproduct of many equilibrium limited reactions, such as the reverse water-gas shift reaction and dimethyl ether synthesis, its in situ removal will result in significant conversion enhancements and thus process intensification. This is based on Le Chatelier's principle, according to which the reactant conversion to products in an equilibrium limited reaction is increased by selectively removing reaction products. In chemical process intensification this concept is used in reactive separations, where reaction and separation take place in a single process step [3]. Another benefit of in situ steam removal involves the mitigation of catalyst deactivation. Thermally induced deactivation (such as sintering or phase transformation at high temperatures) is generally accelerated by H_2O [4]. For reactions in which H_2O is a main byproduct, such as Fischer-Tropsch synthesis, catalyst deactivation by the formed H_2O could be detrimental. On the catalyst level, tuning of catalyst support, promoters and crystallite size has been applied to the increase H_2O resistance and extend catalyst lifetime. Additionally, on a reactor and process level, in situ removal of steam would benefit catalyst stability, enhancing catalyst lifetime and process efficiency in these cases as well. While the advantages of process intensification through steam separation enhanced reactions has become apparent from several experimental and theoretical studies, a critical review is lacking.

Several possibilities exist to enhance process efficiency by steam separation. Staged ex situ separation, using for example interstage cooling and condensation, could be applied when the conversion per reactor stage is reasonably high. Otherwise, the required large number of sequential reaction and separation steps to achieve low steam levels makes this a less efficient approach [5, 6], or entails the use of a large recycle stream. In situ steam separation by means of a reactive separation method is often required to achieve efficient process intensification.

Although reactive distillation (RD) is one of the best-known examples of integrated reaction and separation and therefore a widespread implemented method [7, 8], its use is limited to systems with a product in the liquid phase. For gas phase systems, membrane (reactive vapor permeation) and (reactive) adsorption technologies are the most important separation methods that could be implemented.

Also membrane technology has been extensively studied and has found various commercial applications, for example in hydrogen separation and filtration applications. Many different types of membranes exist, which are applicable to gas and/or liquid processes. Key factors for application of membrane separation processes or membrane reactors, irrespective of

the specific process or reactor, are permeability, selectivity or separation factor and material stability [9]. Over the past decades dehydration of organic streams using membranes gained attention with the first steam selective membranes being reported [10]. This development has made membranes available for in situ H_2O removal during steam producing reactions, i.e. reactive vapor permeation.

Adsorption technology is widely used in pressure swing adsorption (PSA) applications, where high purity requirements have to be reached. While the concept of reactive adsorption has long been known [11], the use of an adsorbent and catalyst mixture in a reactor and its periodic operation have been studied in the open literature since the 1980s [12-15]. The most common application of this concept is the conversion enhancement in a reversible reaction to overcome equilibrium limitations. However, selectivity control could also be obtained by the selective removal of a byproduct. The use of a solid adsorbent requires periodic regeneration to regain the adsorptive capacity of the system. Several reactor and regeneration concepts exist for various adsorption technologies. Typically, a fixed-bed reactor configuration is combined with regeneration cycles. The method of regeneration can be divided into pressure swing, temperature swing, concentration swing, reactive regeneration, displacement regeneration or a combination of these operations [16-18]. In fact, in adsorptive reactors the regeneration process is often the rate determining step and the regeneration determines the cycle times and the required equipment, and therefore the efficiency and feasibility of the process. However, the regeneration procedure is determined by the requirements and the possibilities of the reactive separation system. Carvill et al. (1996) were the first to experimentally investigate the reactive adsorption of steam in the reverse water-gas shift reaction [19]. They showed the potential of reactive adsorption for the in situ removal of steam during a chemical reaction.

Thus, over the past decades the relevance of reactive separation has been established, as many authors have investigated the possibility of reactive steam separation for their studied processes by theoretical and experimental means. At this point in time, lessons can be drawn about the strategies for developing steam separation enhanced reactions, combining insights from experimental and modelling work in the literature. As the interest in the development of steam separation enhanced reactions is strongly increasing with the development of CO_2 utilization processes, these lessons may serve as a guidance for future developments in this field.

In this chapter the possibilities of in situ steam separation from dehydration reactions are reviewed. The advances in reactive steam separation by membrane and adsorption technologies are highlighted and the potential of both reactive separation methods is discussed, based on process requirements. Whereas the processes relevant in this field are operated at higher temperatures, a general temperature window starting from 200 °C up to maximally 400 °C is considered. Finally, critical aspects for future development and optimization of reactive steam separation technologies are identified.

2.2. Reactive separation of steam

2.2.1. General considerations

The conversion of equilibrium limited dehydration reactions can be enhanced due to an equilibrium displacement by selectively separating steam, resulting in lower remaining steam partial pressures. This is illustrated in Figure 2-1, where on the left the thermodynamic carbon distribution for direct dimethyl ether (DME) synthesis is depicted and on the right the experimentally obtained results for sorption enhanced DME synthesis are shown [20]. Not only does the DME yield increase from a conventionally limited 9% for CO_2 feed, or 55% for CO feed, to more than 80%, also the CO_2 content in the product is decreased to less than 1%. This results in an increased single-pass conversion, less demand on downstream separation units, and smaller recycle streams for all CO_2 to CO syngas ratios and especially for CO_2 feed.

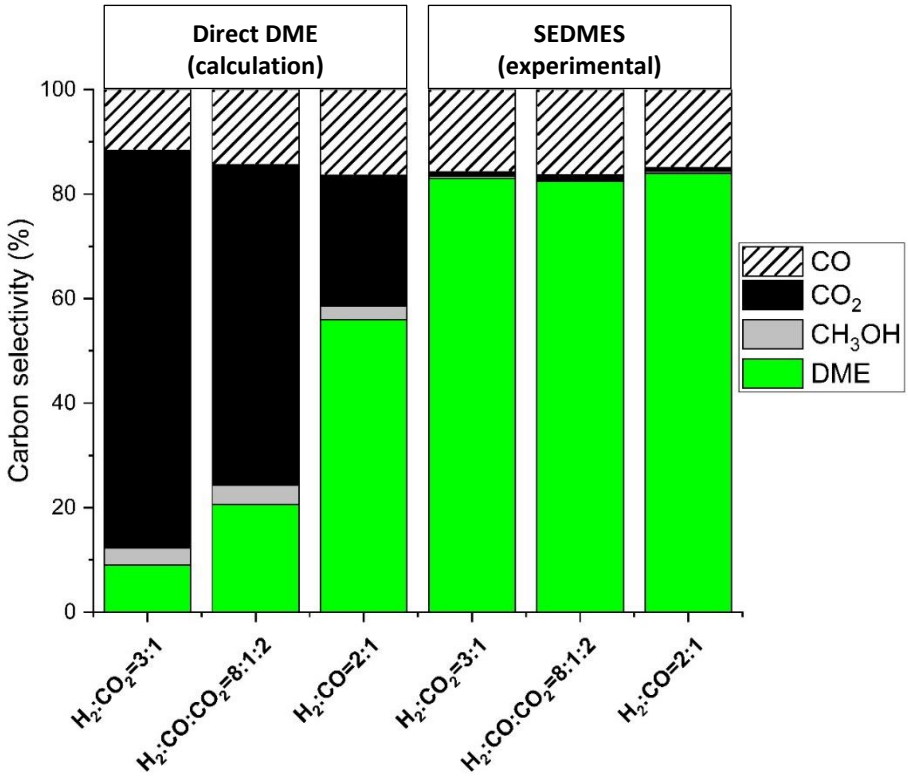

FIGURE 2-1: THERMODYNAMIC (MAXIMALLY POSSIBLE) CARBON DISTRIBUTION (LEFT) VERSUS EXPERIMENTALLY OBTAINED RESULTS FOR SORPTION ENHANCED DME SYNTHESIS (RIGHT). CONDITIONS: STOICHIOMETRIC H_2 TO CO_x FEED, CO_x FEED IS CO_2, CO_2:CO 2:1 AND CO, INCLUDING 30% INERT, 275 °C AND 40 BAR [20].

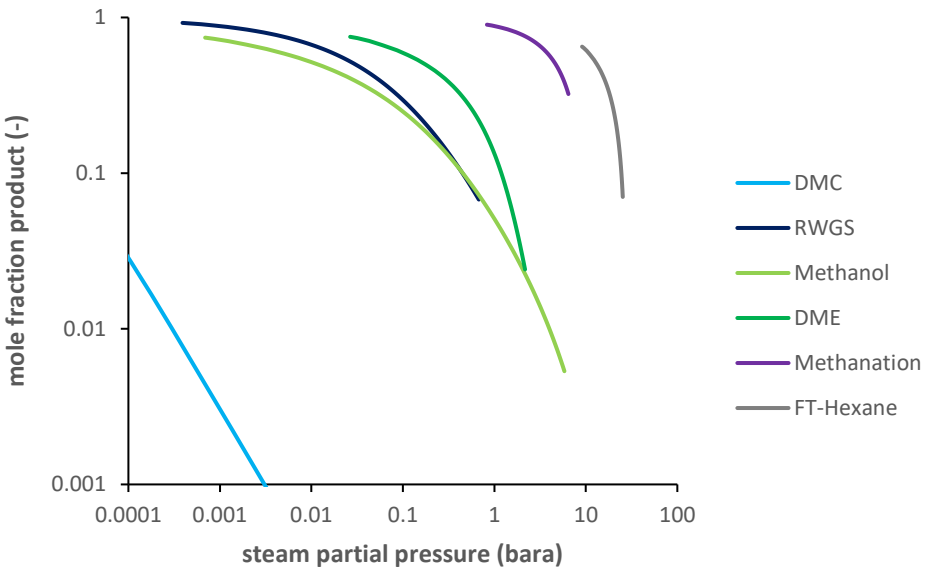

FIGURE 2-2: MOLAR FRACTION OF PRODUCT, CO FOR RWGS, CH_3OH FOR METHANOL SYNTHESIS, DME FOR DIRECT DME SYNTHESIS, CH_4 FOR METHANATION, HEXANE FOR FISCHER-TROPSCH AND DMC FOR DIRECT DMC SYNTHESIS, AS A FUNCTION OF THE REMAINING STEAM PARTIAL PRESSURE BASED ON MINIMIZATION OF THE GIBBS FREE ENERGY OF REACTION. CONDITIONS: STOICHIOMETRIC H_2, CO_2 FEED FOR ALL REACTIONS; RWGS 300 °C, 10 BAR; METHANOL 250 °C, 30 BAR; DME 275 °C, 30 BAR; METHANATION 300 °C, 10 BAR; FT 250 °C, 30 BAR; DMC 200 °C, 30 BAR.

In Figure 2-2 the yield as a function of the remaining steam partial pressure is shown for some important reactions studied in literature, clearly indicating the possible increase in equilibrium conversion at lower steam partial pressures for the different reactions. On the one hand, very low steam partial pressures are required to gain a high CO yield in the reverse-WGS, or even extremely low partial pressures for the direct synthesis of dimethyl carbonate (DMC). On the other hand, for the Fischer-Tropsch synthesis of hexane a steam partial pressure of 10 bar would already result in significant conversion enhancement. Besides conversion enhancement due to equilibrium displacement, the decrease in the steam partial pressure by in situ separation can also affect the reaction kinetics, reaction selectivity, catalyst deactivation and thus catalyst lifetime. All these positive and/or negative effects are different for each case and must be addressed case specific. For example, in the case of methanation, the primary advantage of employing sorption enhancement is not to increase the (already high) conversion, but to enhance product purity by converting remaining hydrogen [21] or carbon dioxide [22]. Other opportunities are operation at milder reaction conditions to achieve the same conversion and yield as conventional processes, such as in [19].

The sections below discuss adsorptive and membrane-based processes, respectively, for steam separation enhanced reaction processes. It is followed by a third section discussing their relative merits.

2.2.2. Reactive steam adsorption

Steam adsorption enhanced reverse water-gas shift experiments in a bench scale reactor by Carvill et al. were the first to be reported in the open literature [19]. Since then, in situ steam adsorption has been studied for various reactions, including the reverse water-gas shift, the Claus process, the Sabatier process, dimethyl ether (DME) synthesis and dimethyl carbonate (DMC) synthesis. A shortlist of steam adsorption studies is presented in Table 2-1.

TABLE 2-1: SHORTLIST OVERVIEW OF EXPERIMENTAL WORK ON REACTIVE STEAM ADSORPTION.

Reaction	Sorbent	Regeneration	Reference
r-WGS	13X	Pressure swing	Carvill et al. [19]
r-WGS	4A	-	Haije et al. [23]
r-WGS	13X, 4A, SOD	-	Ghodhbene et al. [24]
Claus	3A	Purge & Temperature swing	Agar [25]
Claus	3A	Purge & Temperature swing	Elsner et al. [26, 27]
DME	$MgSO_4$	-	Kim et al. [28]
DME	3A	Pressure swing	Ressler et al. [29]
DME	LTA	Temperature & Pressure swing	Boon et al. [5]
DME	LTA	Temperature & Pressure swing	van Kampen et al. [20, 30]
Methanation	4A	Purge & Temperature swing	Walspurger et al. [21]
Methanation	3A, 5A	-	Borgschulte et al. [22, 31]
Methanation	5A, 13X	Purge	Delmelle et al. [32, 33]
DMC	3A	-	Choi et al. [34]
Glycerol carbonate	13X	-	George et al. [35]

Only few authors have conducted studies that combine theory and experiments in a fundamental way, which is crucial for a proper understanding of this type of process as argued below.

Essential for an adsorptive reactor is the capacity of the adsorbent and its affinity for separation of the desired component. However, the capacity of the adsorbent is finite, which makes periodic regeneration inherent to any adsorption process. The periodic regeneration restores the adsorptive capacity and therefore gives an extra degree of freedom to the process, making the method of regeneration another essential aspect for reactive steam adsorption. In this respect, a distinction has to be made between the total capacity and the working capacity of an adsorbent material. The working capacity of the material is its apparent capacity over many consecutive cycles of adsorption and regeneration, whereas the total capacity is a material characteristic given by its isotherm. A large amount of adsorbent material is necessary when its working capacity is low (while a large amount of steam has to be separated). Evidently, a large amount of adsorbent would make the implementation of an adsorptive reactor less feasible. Another factor of interest is the selectivity for the adsorption of steam relative to other components, which determines the loss of reactants and/or products. Non-selective adsorption results in an impure desorption gas stream, which can or has to be separated for economic or environmental reasons. Additional separation units and possible recycle streams make the process more complex, more costly and less viable. Besides separation affinity and capacity, the kinetics of separation could also play an important role. Ideally, the rate of steam adsorption matches the rate of steam production. The latter, however, is influenced by the adsorption of steam due the changed kinetics of the desired reaction and/or undesired side-reactions. Moreover, mass transfer limitations between catalytically active sites and adsorption sites could affect the outcome of a reactive adsorption process. In addition to mass transfer, heat transfer is often an important aspect in chemical reactors. Especially for highly exothermic or highly endothermic reactions heat transfer limitations could be problematic and heat management is essential. In addition to the heat of reaction(s), the heat of adsorption has to be managed as well for reactive adsorption processes. This makes the heat management possibly more complex. Consequently, the complexity of operating reactive adsorption processes has led to the proposal of very different contactor types for its implementation. Among others, these contactor types include a moving bed adsorptive reactor, a packed bed adsorptive reactor and a fluidized bed adsorptive reactor. The choice of contactor type influences all other aspects, from heat and mass transfer characteristics to possible regeneration modes. Therefore, one contactor type could be preferred over another depending on specific issues. For instance, a fluidized bed reactor could be beneficial in case of heat transfer limitations. However, a contactor type could also increase the complexity of the process, for example in the case of a moving bed reactor. These aspects of reactive adsorption processes are discussed in more detail below.

Selectivity

For in situ steam removal by solid adsorbents, zeolite type materials are often preferred, as can also be deduced from Table 2-1. These structured materials have well-defined pore sizes and geometries. Because of their characteristics, zeolite materials can have a high affinity and selectivity for the desired adsorbate. Zeolite types 3A and 4A are especially suitable for the removal of steam (~0.2-0.3 nm kinetic diameter [36, 37]) due to their micropores with a diameter of around 0.3-0.4 nm [16], preventing the adsorption of other, larger components that are present during reaction. Conversely, Carvill et al. (1996) used zeolite NaX as water-selective adsorbent at moderately high temperatures for the reverse water-gas shift reaction [19]. Although zeolite NaX typically has a larger pore opening of 0.8 nm, possible co-adsorption of other components is not observed nor discussed. Similarly, zeolite 13X (NaX) is used as solid adsorbent for steam in the formation of larger, cyclic carbonates (e.g. ethylene carbonate, propylene carbonate and glycerol carbonate). Also in this study, enhanced product yields with almost 100% selectivity were obtained [35].

Although co-adsorption is not always observed nor discussed, competitive adsorption of steam and CO_2 is well-known for various materials [36, 38]. In line with this, Walspurger et al. (2014) show competitive adsorption of CO_2 on zeolite 4A adsorbent. Although the adsorption capacity of CO_2 itself seems very low, the capacity for steam adsorption decreases significantly in the presence of CO_2 [21]. Recently, Delmelle et al. (2018) gave evidence of a decrease in water diffusion kinetics during adsorbent regeneration due to pore blocking by reaction intermediates and products [32]. Moreover, Vaporciyan and Kadlec (1987,1989) even use the slightly larger pore zeolite 5A for the separation of CO_2 [14, 15]. For zeolites 5A and 4A, authors also showed co-adsorption of other components, such as carbon monoxide, methanol and DME [36, 39, 40]. For zeolite type 3A adsorbent, co-adsorption is less well-known. Its smaller pore size (0.3 nm) physically restricts slightly larger molecules to adsorb, which is why zeolite type 3A is used for drying both polar gases and reactive gases [37]. However, other authors have shown that the presence of methanol influences steam adsorption, even for zeolite type 3A [41], and that DMC can also adsorb on 3A, although at high pressures (20 MPa) [42].

Capacity

Physical adsorption is an exothermic process, which makes that the capacity of all adsorbents decreases with an increase in temperature. A physical sorbent is typically characterized by a low adsorption heat, a low activation energy, high adsorption/desorption rates and excellent reversibility [43]. Contrastingly, chemisorption is characterized by the reaction between adsorbate and surface-active sites of the adsorbent. Therefore, chemisorption features high adsorption heat and activation energy compared to physisorption. Typical chemical adsorbents are base-metal oxides. Although steam will

adsorb chemically on base metal oxides, at high temperatures and pressures carbonates will likely be formed in the presence of CO_2 [44, 45]. Hydrotalcites, a class of double hydroxides with the general formula $Mg_{(1-x)}Al_x(OH)_2(CO_3)(x/2)\cdot nH_2O$, are typically used for CO_2 adsorption. However, they show a capacity for steam adsorption as well [38, 46]. With respect to the sorption capacity, it is important to focus on materials which retain sufficient capacity at elevated temperatures. The steam adsorption capacity of the hydrotalcites, as well as for the base metal oxides, is however limited [46, 47].

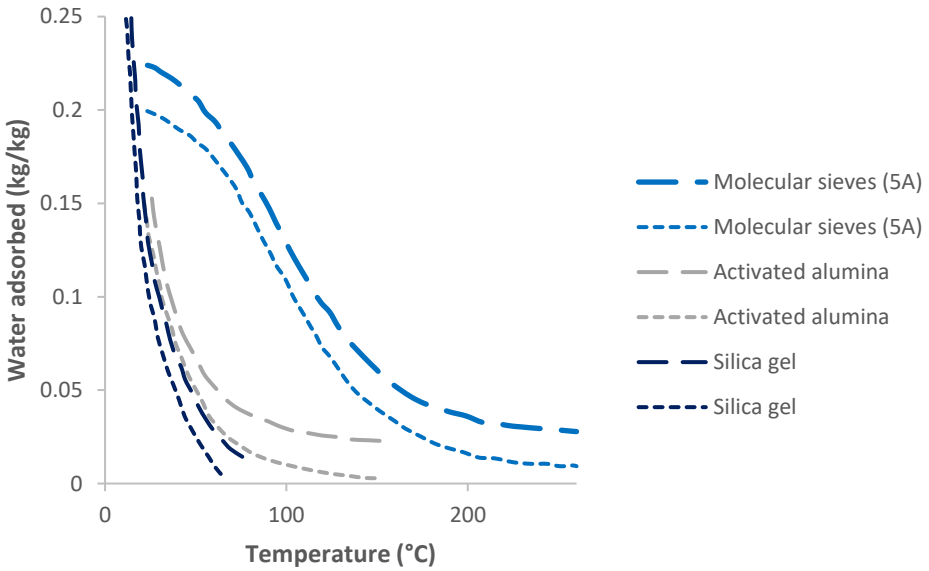

FIGURE 2-3: WATER ADSORPTION CAPACITY VERSUS TEMPERATURE IN EQUILIBRIUM WITH 13.33 MBAR WATER VAPOR PARTIAL PRESSURE FOR MOLECULAR SIEVES (ZEOLITE 5A), SILICA GEL, AND ACTIVATED ALUMINA (STRIPED LINES). DOTTED LINES SHOW THE EFFECT OF THE 2WT% OF RESIDUAL WATER AT THE START OF THE ADSORPTION (ADAPTED FROM [48]).

In Figure 2-3 (adapted from [48]) the water adsorption capacity of three physical adsorbents is plotted against temperature. Zeolites are well-known molecular sieves, and are used at relatively low to moderate temperatures. Possible steam separation enhanced reactions on the other hand are typically operated at higher temperatures (200-400 °C), which requires sufficient adsorption capacity at these temperatures. Although zeolite molecular sieves have an adsorption capacity for water at slightly elevated temperatures (Figure 2-3), little information about the adsorption of steam on zeolite materials under higher temperatures is known in the open literature. Elsner et al. (2002) encountered this issue and experimentally determined a Freundlich isotherm for a zeolite type 3A under sorption enhanced Claus conditions [27]. Other authors, focusing on modeling a sorption enhanced reaction process, use a variety of adsorption isotherm descriptions besides Freundlich models, such as Unilan and Langmuir models, derived from material studies [49-51]. Gabrus

et al. (2015) experimentally studied the water adsorption isotherm for zeolite types 3A and 4A, and Mette et al. (2014) similarly performed a study on binderless zeolite type 13X up to 250 °C [52, 53]. However, it was reported that the latter material has reduced hydrothermal stability at temperatures above 200 °C. Although the Langmuir-Freundlich and the dual-site Langmuir-Langmuir models proposed by Gabrus et al. (2015) are fitted for temperatures up to 250 °C, these, and other descriptions have been determined under different conditions than those of the studied sorption enhanced reactions, which means that the models have to be extrapolated to unverified conditions. In contrast, the more experimental studies regarding sorption enhanced reactions do not explicitly consider isotherm models for the used adsorbent material. The focus in these contributions is merely on the enhancement effect of the adsorbent on the reaction, not on a description of the intrinsic adsorption behavior of the material [19, 22, 28, 29, 34].

Regeneration

Besides the adsorption capacity at high temperature, the adsorbent material should also have good adsorption kinetics under the sorption enhanced reaction conditions [24]. Preferably the rates of adsorption and production of steam match. However, especially the desorption kinetics of the adsorbent material are of interest. The desorption is often the time-limiting step in a sorption enhanced reaction process, determining the length of the regeneration. The most common regeneration procedures are pressure swing, temperature swing or a combination of both operations, possibly with the use of a purge gas. In theoretical evaluations often pressure swing regeneration is considered [25, 49, 50], because its fast response and therefore short regeneration time is preferred over the slower temperature swing. However, in practical applications of zeolite molecular sieves, the drying beds at moderate temperatures are often regenerated by increasing the temperature [36, 37]. For the use of a purge gas, a suitable stream must be available in the process and its partial back mixing must not cause complications.

In the study by Carvill et al. (1996) on sorption enhanced reverse water-gas shift, pressure swing regeneration was shown to be suitable for periodic regeneration of the zeolite NaX adsorbent [19]. Using product to repressurize the reactor they could achieve a high purity product, whereas reactant repressurization led to sorption enhanced conversions without high purity product. The product CO concentrations were initially low due to the displacement of the pressurization gas from the reactor and only reached a maximum of 80% before reaction equilibrium values were obtained. Although the benefits of sorption enhancement have been demonstrated experimentally for the reverse WGS reaction, further optimization of the adsorption and regeneration process is required to roll out the sorption enhanced reverse water-gas shift process and achieve high conversion of CO_2 to CO combined with high purity. To optimize the sorption enhanced reverse WGS in a solar fuel process Haije et al. (2011) suggest using the heat released from Fischer-Tropsch

synthesis, downstream of the rWGS unit, to regenerate the adsorbent by temperature swing regeneration [23].

In the sorption enhanced methanation process temperature swing regeneration with the use of a purge gas has been applied in cyclic experiments, as reported by Walspurger et al. [21]. The regeneration temperature, ranging from 350 to 450 °C, had no significant effect on the working capacity of the used zeolite material, which could be due to either the extensive regeneration time or the excess of purge gas used. Delmelle et al. (2016) observed a significant improvement in regeneration for a hybrid Ni/13X adsorbent using air rather than hydrogen as purge gas in their sorption enhanced methanation process [33]. The purge gas did not affect the regeneration of hybrid Ni/5A, suggesting that the larger pores of 13X allow for faster transport and better regeneration. Whereas the methanation experiments have been performed at atmospheric pressure, the choice of regeneration method and appropriate conditions, however, is critical for the feasibility of the reactor concept. Design and optimization of the regeneration step will be key in optimizing the energy requirement and the associated operational costs.

In successive studies on the Claus process, the regeneration was analyzed in more detail [26, 27]. Based on the thermal inertia of the fixed bed, the study concludes that regeneration by temperature swing is not feasible. This makes pressure swing regeneration the most viable option. Abufares et al. (2007) evaluate an optimization model for vacuum swing regeneration for the same Claus process [54]. They show that a high-performance adsorptive reaction process is possible by means of optimized vacuum swing regeneration. In addition to previous studies, van Kampen et al. (2017) also explicitly looked into the effect of the regeneration conditions on the sorption enhanced DME process [20, 30]. They have shown that the used zeolite adsorbents can be readily regenerated by pressure swing regeneration. Increasing the temperature during regeneration (temperature swing) improves the extent of regeneration even further by increasing the working capacity of the adsorbent.

Catalyst activity, reaction kinetics, and mass transfer

Studies have clearly indicated that the adsorbent regeneration not only influences the adsorptive capacity of the system, but that periodic exposure to regeneration conditions may also affect the catalyst performance. In a study of the regeneration conditions in sorption enhanced DME synthesis, van Kampen et al. [20] have shown that periodic exposure to temperature swing conditions of 400 °C not only improves the performance of the adsorbent, which can be judged from the extended period before breakthrough, but also improves the activity of the $Cu/ZnO/Al_2O_3$ catalyst, which can be judged from the equilibrium conversion after breakthrough and stabilization (see Figure 2-4 and Figure 2-5).

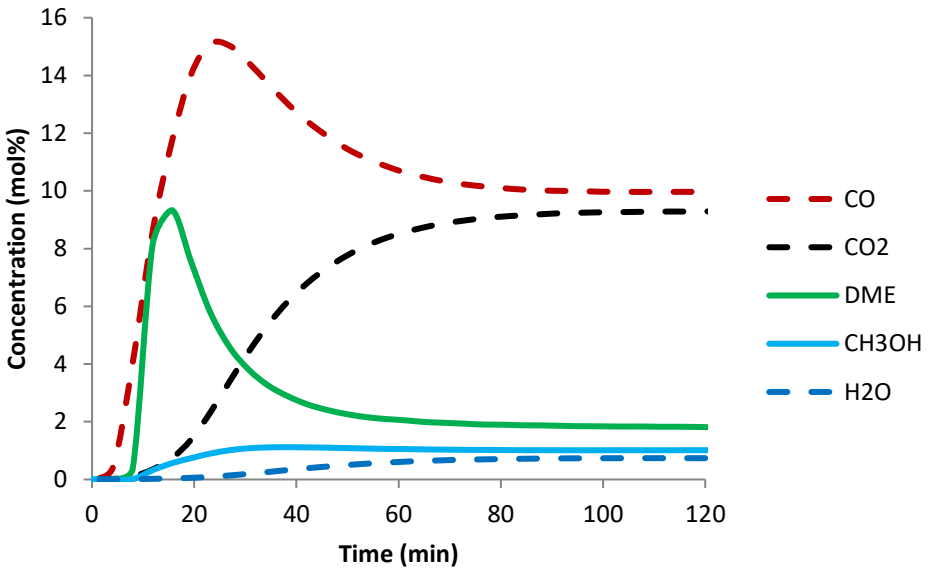

FIGURE 2-4: TYPICAL BREAKTHROUGH PROFILE FOR CZA CATALYST + LTA ADSORBENT SYSTEM. CONDITIONS: STOICHIOMETRIC H_2, CO, CO_2 FEED FOR ALL REACTIONS; CO_2:CO = 1:2; 275 °C, 25 BAR(A); 300 °C REGENERATION [20].

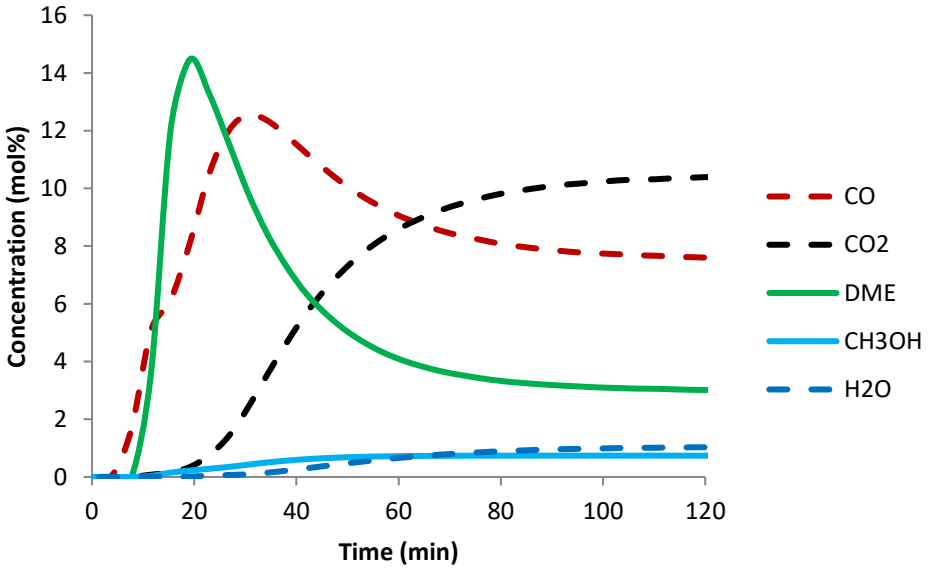

FIGURE 2-5: TYPICAL BREAKTHROUGH PROFILE FOR CZA CATALYST + LTA ADSORBENT SYSTEM. CONDITIONS: STOICHIOMETRIC H_2, CO, CO_2 FEED FOR ALL REACTIONS; CO_2:CO = 1:2; 275 °C, 25 BAR(A); 400 °C REGENERATION [20].

Regarding the effect on catalyst activity and reaction kinetics, Reßler et al. (2005), employing adsorbent zeolite 3A in sorption enhanced DME formation, posit that the removal of steam has a conflicting role. Methanol and DME producing reactions are enhanced, but the opposite holds for the water-gas shift reaction [29]. It is widely known that a low content of CO_2 enhances the reaction kinetics for methanol synthesis over CZA catalysts, although CO_2 limits the reaction equilibrium [55]. Whereas the extent of regeneration in sorption enhanced DME synthesis influences the amount of CO_2 present, it also directly influences the reaction kinetics. This gives the regeneration of this reactive adsorption system extra importance, although it is an important parameter in adsorptive reactors in general.

Although sorption enhanced methanation is shown by Walspurger et al. (2014) for a physical mixture of a methanation catalyst and a zeolite adsorbent [21], there are indications that a hybrid catalyst adsorbent particle could perform better than a physical mixture [22, 31]. It is clear that the effective transport of species between, and therefore the proximity of catalytically active sites and adsorbent sites can have an important role in sorption enhanced processes. In addition, this also suggests that the major mass transport resistance comprises the transport from the catalyst, via the bulk phase, to the sorbent. The relatively low space velocities for many adsorption processes increases the likelihood of mass transfer limitations. However, recent developments in rapid PSA cycling seem promising for improving these aspects.

As mentioned previously, by modification of the reaction conditions the conversion of the desired reaction can be enhanced, but undesired parallel or consecutive reactions may be enhanced as well. In the Claus process this aspect of reactive adsorption appears. To a small extent, the formation of undesirable carbonyl sulfide (COS) was observed. In the conventional Claus process COS is hydrolyzed by the steam present in the reactor. Whereas steam is selectively removed in the adsorptive reactor concept, this hydrolyzation is suppressed as well and even more COS could be formed compared to the conventional process [27]. This example of COS formation clearly illustrates the possible enhancement of undesired side-reactions due to inherent concentration or temperature profiles in reactive adsorption processes.

Heat management

Heat management is very important for chemical reactions, especially in the case of high exothermicity or endothermicity, and thus also for reactive adsorption processes. The adsorption of steam is an exothermic process, which is therefore favored at low temperatures (and high pressures). The adsorbent material requires a high affinity for steam to obtain sufficient working capacity and subsequent sorption enhancement at higher reaction temperatures (between 200 and 400 °C). This was shown for the zeolite type adsorbents used by various authors (see Table 2-1).

For exothermic reactions, such as the methanation reaction, the Claus reaction and (direct) DME synthesis, the adiabatic temperature rise could be very high (up to 500 °C for methanation). Besides the influence this already would have on the conventional reactions, these temperature profiles affect the adsorption capacity of steam, the kinetics and the concentration profiles in adsorptive reactions. For this reason, Walspurger et al. (2014) considered an adsorptive reactor as a third reactor in a (conventional) series of three adiabatic reactors, in which the main part of the reaction heat is mitigated to the first and second reactor. In this way they motivate the use of an adiabatic reactor instead of a more complex and costly isothermal reactor [21]. Elsner et al. (2003), on the other hand, claim that the thermal inertia of the fixed bed adsorptive reactor avoids interference of the reaction heat with the adsorption process [27], which would make adiabatic operation feasible. In addition, for a fixed bed reactor in chemical looping combustion it is shown that as long as the velocity of the reaction front is larger than that of the heat front, the maximum temperature increase is only affected by the gas and solid properties [56, 57]. Also other authors assessed the possibilities of adiabatic and non-adiabatic reactor operation. Sorption enhanced reverse WGS couples the endothermic rWGS reaction with the exothermic steam adsorption, possibly minimizing external heat input required for rWGS [58]. In a fixed bed reactor Parra et al. (2017) show that in the optimal configuration the temperature is close to the set maximum temperature of 260 °C. Although a higher temperature limits the adsorption capacity, the reaction kinetics are faster. For the adiabatic case this optimization towards the highest allowable temperature means that the feed temperature has to be low to not exceed 260 °C inside the reactor. In the non-adiabatic case, a profile of the wall temperature allows for the highest productivity. Near the reactor inlet a lower wall temperature results in more adsorption due to the higher allowable heat of adsorption. Throughout the reactor the rates of reaction and adsorption converge, allowing operation at higher (wall) temperatures [58]. This shows the advantage of non-adiabatic operation, the temperature can be tuned to favor the dominant phenomenon, reaction or adsorption. Contrastingly, for adiabatic operation the temperature is determined by (the exo- or endothermicity of) the dominant phenomenon, which is also shown for sorption enhanced reverse WGS in a moving bed reactor [59].

Contactor type and reactor configuration

In the literature focusing on reactive steam adsorption, a packed bed adsorptive reactor is the most commonly selected reactor configuration [19-21, 27]. This reactor configuration is relatively easy to implement compared to a less mature technology, such as a fluidized bed adsorptive reactor. By optimizing the reactor operation, the ideal performance of a moving bed reactor can be achieved. Parra et al. (2017,2018) showed that a moving bed adsorptive reactor could be more beneficial than a packed bed adsorptive reactor for the reverse WGS reaction with an order of magnitude difference in space time yield [58, 59]. Similarly, Santos

et al. (2015) proved the potential of a moving bed chromatograph reactor for the separation of water and DMC, in its direct synthesis [60]. Although other contactor types are less apparent in research on reactive steam adsorption, they could be beneficial for specific steam sorption enhanced reaction processes. In the previous sections the importance of mass transfer and heat management is discussed. If transfer limitations are a serious issue for a process, fluidized bed technology would be a good candidate for its great mass and heat transfer properties. For these reasons Bayat et al. have suggested several configurations for sorption enhanced methanol synthesis and sorption enhanced Fischer-Tropsch synthesis [51, 61], including a dual (moving) bed reactor and a fluidized bed reactor, thermally coupled to a fixed bed reactor.

2.2.3. Reactive steam permeation (membrane steam separation)

The second reactive steam separation method is reactive steam permeation or reactive membrane separation. Few studies have been published on steam separation enhanced reactions, including DME and DMC synthesis [62-72], however the Fischer-Tropsch (FT) reaction has received the most attention [73-78]. A shortlist is given in Table 2-2.

TABLE 2-2: SHORTLIST OVERVIEW OF EXPERIMENTAL & MODELLING LITERATURE ON REACTIVE STEAM PERMEATION (AND PERVAPORATION). MEMBRANE REACTORS (MR), PACKED BED MEMBRANE REACTORS (PBMR), CATALYTIC MEMBRANE REACTORS (CMR) AND SIMULATED MOVING BED MEMBRANE REACTORS (PERMSMBR) ARE LISTED.

Reaction	Membrane material	Process	Reference
FT	Zeolite: MOR, ZSM-5	MR: gas phase & slurry	Espinoza et al. [73, 74]
FT	Ceramic (TEOS coated)	PBMR	Rohde et al. [75]
FT	Zeolite: H-SOD	MR	Rohde et al. [77]
FT	Ceramic supported polymer (CSP)	PBMR	Rohde et al. [76]
DME	Silica	PBMR	Lee et al. [79]
DME	NaA	MR & PBMR	Fedosov et al. [80]
DME	Zeolite model	PBMR model	Iliuta et al. [62]
DME	Microporous zeolite: ZSM5/MFI	PBMR model	De Falco et al. [64]
DME	Zeolite model: ZSM5, MOR or SIL	PBMR model	Diban et al. [63, 69]
MeOH	Zeolite	PBMR & PBMR model	Gallucci et al. [81, 82]

Steam selective/ MeOH synthesis	Mordenite	MR (permeation)	Sawamura et al. [83]
MeOH	Nafion	PBMR & PBMR model	Struis et al. [84]
Steam selective/ MeOH synthesis	Zeolite: A	MR	Gorbe et al. [85]
MeOH	Inorganic: carbon & zeolite	-	Gallucci [10]
Flue gas dehydration	SPEEK	MR	Sijbesma et al. [86]
DMC	SPEEK	MR & CMR model	Mengers et al. [66]
DMC	SPEEK model & SPEEK chitosan model (up to 200C)	(C)MR model	Kuenen et al. [67, 68]
DMC	Composite membrane (PERVAP 1255)	MR assisted RD: MeOH permeation	Holtbruegge et al. [87, 88]
Water selective membranes	Zeolite: 4A	MR	Zhu et al. [39]
Water selective membranes	Zeolite: H-SOD	MR (pervaporation)	Khajavi et al. [89]
Water selective membranes	Zeolite: H-SOD	MR (permeation)	Lafleur et al. [90]
Steam selective membranes (MeOH, DME, DMC)	Zeolite: SOD	MR (permeation)	Wang et al. [91, 92]
Acetals	Silica	PermSMBR	Pereira et al. [93]
Acetals	Silica	PermSMBR	Silva et al. [94]

Espinoza et al. (1999,2000) were the first to show that zeolite type membranes can selectively separate steam under FT-reaction conditions [73, 74]. However, especially the selectivity tends to decrease at increasing temperatures. This brings us to the requirements for reactive steam separation by membranes. Similar to the capacity for reactive adsorption, the steam flux through the membrane (given by the membrane permeance) has to be sufficient. Whereas the rate of steam separation has to match the rate of steam production, the membrane permeance directly determines the required membrane area. The membrane area, however, is limited, depending on the membrane reactor configuration, and therefore defines the feasibility of the concept. As already mentioned in

the example by Espinoza et al., another aspect determining the viability of the reactive steam permeation concept, is the permselectivity of the membrane. A low separation selectivity could result in a reduced separation enhancement and loss of reactants and/or product, which means that an extra, costly recovery is necessary for economic, legislative or environmental reasons. A third principal requirement for reactive steam permeation is the hydrothermal stability of the membrane. Many membranes typically operate at low to moderate temperatures [95]. In contrast, operation at high temperatures and high pressures is necessary for reactive steam permeation. Aside from these aspects, kinetic effects and mass and heat transfer limitations could be of importance. As already mentioned, the rate of steam separation should match the rate of steam production. However, the production rate could be influenced by the separation of steam due altered kinetics of the desired reaction and/or undesired side-reactions (with beneficial or adverse effects on the product selectivity). Furthermore, mass and heat transfer limitations in the membrane reactor, and especially between catalytically active sites and the membrane, could largely affect the reactive steam permeation process. Finally, also for reactive steam separation by membranes several contactor types are possible for implementation. The fixed bed membrane reactor, catalytic membrane reactor and fluidized bed membrane reactor are examples of the many possible types available. These contactor types have different characteristics and therefore influence all other aspects. For example, in case of mass transfer limitations due to the (non-)proximity of catalytically active material and the membrane a catalytic membrane would help overcoming this issue by bringing the functionalities closer together. A fluidized bed membrane reactor could also become an option in the case of (severe) mass or heat transfer limitations due to its good mass and heat characteristics.

Flux and permeance

Many authors who have theoretically evaluated membrane steam separation enhanced reactions have relied on permeance and permselectivity data taken from literature that has been obtained during membrane characterization studies [62, 64, 67]. Rohde et al. (2008) already have presented an overview of the state-of-the-art membranes for in situ H_2O removal, dividing them in three different types: zeolite membranes, amorphous membranes and polymer membranes [77]. Their work is used as a basis and extended to a summary on H_2O permeances at higher temperatures (200-400 °C) (Figure 2-6).

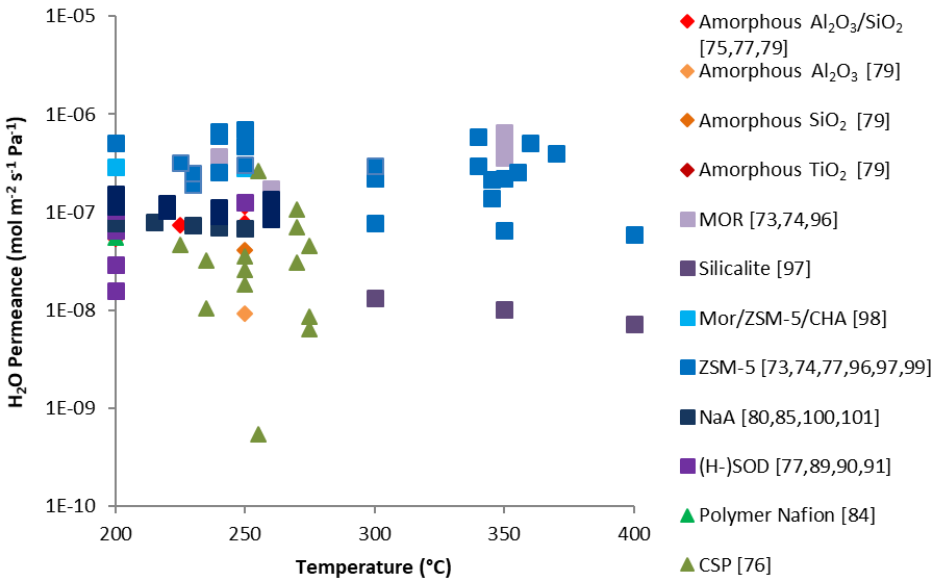

FIGURE 2-6: H_2O PERMEANCES FOR ZEOLITE, AMORPHOUS AND POLYMER MEMBRANES BETWEEN 200 AND 400 °C [73-77, 79, 80, 84, 85, 89-91, 96-101].

As already mentioned, many membranes were applied at low to moderate temperatures. For example, Holtbruegge et al. (2014) gave a maximum temperature of 90 °C related to the polymer layers in PERVAP 1255 [88]. Due to these temperatures various membranes depicted in Figure 2-6 have only been tested up to 200 °C, and only few membranes have been tested above 300 °C.

Although pervaporation, in which the liquid feed/retentate changes phase to the vapor permeate, is outside the scope of this article due to its temperature window (generally well below 200 °C), some membranes, that are in principle also suitable for reactive steam permeation, have only been tested for pervaporation applications. Rohde et al. (2008) and Khajavi et al. (2009) tested their hydroxy sodalite (H-SOD) membrane for steam pervaporation [77, 89]. Although the membrane performed well for pervaporation and should be suitable for vapor permeation, the processes are different and their applicability in steam separation is not guaranteed. Both systems have different modes of operation. Where in vapor permeation the steam pressure difference determines the driving force, in pervaporation the liquid feed/retentate changes phase to the vapor permeate driven by a concentration gradient. Wang et al. (2014) and Lafleur et al. (2017), however, developed (hydroxy) sodalite membranes suitable for steam permeation, indeed showing good permeances [90, 91].

From Figure 2-6 it can be seen that zeolite membranes, specifically ZSM-5 and mordenite type membranes, outperform the amorphous and polymer membranes in steam

permeance at higher temperatures. In general, these zeolite membranes have a permeance between $1 \cdot 10^{-7}$ and $1 \cdot 10^{-6}$ mol Pa^{-1} m^{-2} s^{-1}. Except from Wang et al. (2012), who tested self-made membranes even up to 550 °C [97], no clear trend in steam permeance is observed for the mentioned zeolite membranes within this temperature range, which is promising for the thermal stability of these membranes. Although duration experiments are required for actual membrane stability measurements.

Permselectivity

Considering the permselectivities of the different membrane types, in general the selectivities of H_2O towards H_2 and of H_2O towards alcohols, such as methanol are considered critical [62, 63, 95]. The permselectivity of H_2O towards H_2 for various types of membranes at elevated temperatures is shown in Figure 2-7. Increasing the temperature results in a decreased permselectivity for all types of membranes. As discussed in the previous section on reactive steam adsorption, zeolite materials are well-structured with specific pore diameters. Both steam and hydrogen are small enough to enter these pores. However, the loading of steam on zeolite membranes is prone to block the permeation of hydrogen [39, 83, 85, 97]. With increasing temperature both the steam loading and the permselectivity decrease. Polymer membranes tend to have a decrease in vapor permeance and an increase in gas permeance with increasing temperatures, resulting in a drop in the H_2O/H_2 permselectivity [86]. For amorphous membranes the decrease in H_2O/H_2 permselectivity is explained by an increase in the H_2 permeance due to degradation of the membrane at higher temperatures [77]. Again, the zeolite membranes seem to outperform the other membranes with permselectivities over 10, and even up to 1000, for the temperature range 200-300 °C. For example the permselectivities for the polymer membranes are in the range between 1 and 10. Although some higher values have been obtained for ECN's ceramic supported polymer tested by Rohde et al. [76, 77]. For even higher temperatures (> 300 °C) only data for zeolite membranes are available. And at these temperatures the permselectivity of the zeolite membranes drops to values ranging from 1 till 10, as explained above.

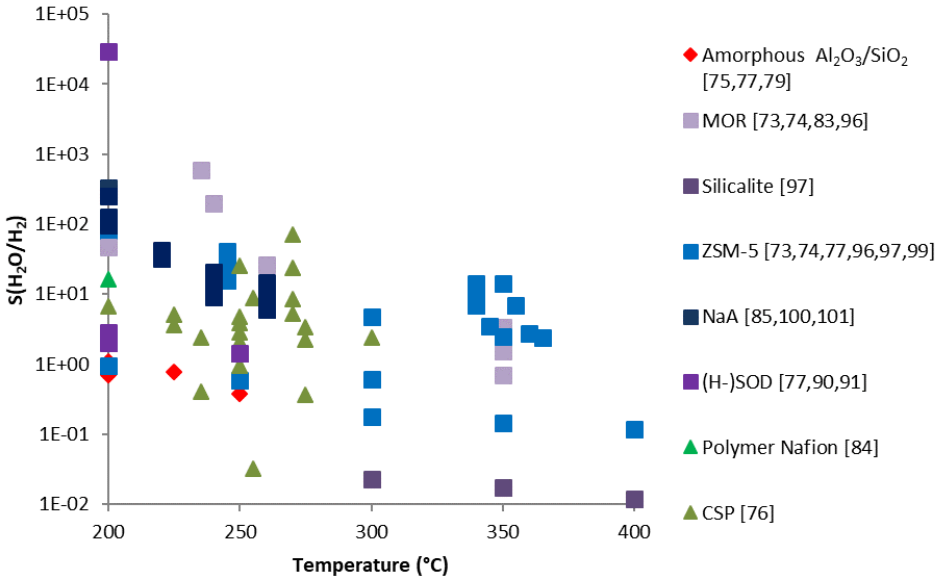

FIGURE 2-7: PERMSELECTIVITY OF H_2O TOWARDS H_2 FOR ZEOLITE, AMORPHOUS AND POLYMER MEMBRANES BETWEEN 200 AND 400 °C [73-77, 79, 83-85, 90, 91, 96, 97, 99-101].

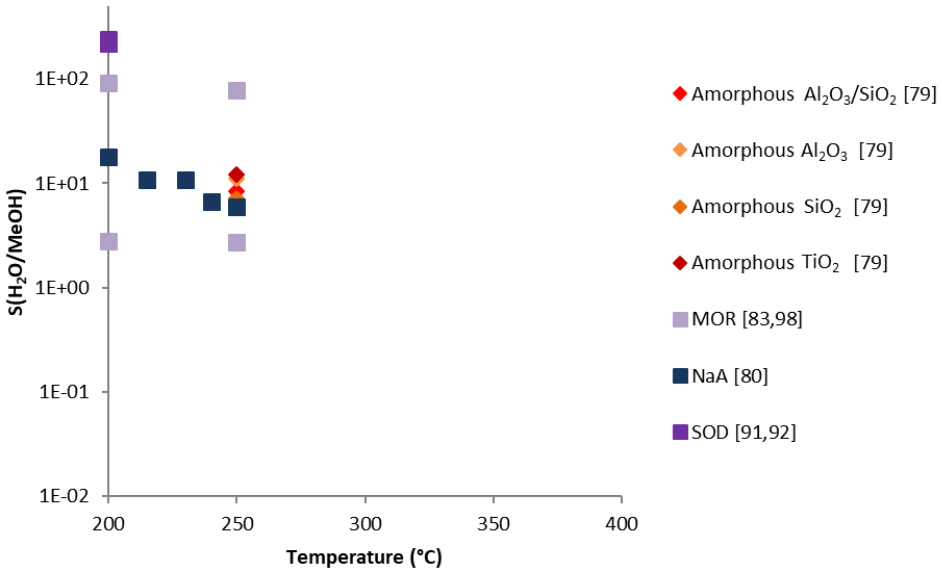

FIGURE 2-8: PERMSELECTIVITY OF H_2O TOWARDS METHANOL FOR ZEOLITE AND AMORPHOUS MEMBRANES BETWEEN 200 AND 400 °C [79, 80, 83, 91, 92, 98].

Another important aspect is the permselectitivity of H_2O towards condensable (vapor) components in a reaction mixture. The separation enhanced yield for a PBMR can be even lower than the yield of a PBR due high losses over the membrane, as shown for methanol permselectivity in DME synthesis [63, 69]. In Figure 2-8 the permselectivity of H_2O towards methanol (as the hardest to separate alcohol) is presented for various types of membranes at elevated temperatures.

The first thing to notice from Figure 2-8 is that the available data is limited and the temperature range only goes up to 250 °C. Secondly, relatively low permselectivities are achieved for the separation of steam and methanol. However, more recent work on zeolite membranes shows more promising permselectivities of steam towards methanol [83, 91, 92]. The difficult separation, due to the preferential permeation of polar molecules, can be explained by a preferential adsorption mechanism rather than a size exclusion mechanism [95]. This supports the previous statement that the presence of steam limits the permeation of hydrogen in zeolite membranes, which is observed by several authors. Although not only the presence of steam limits hydrogen permeation, also the presence of methanol does.

Due to this difficult separation often the separation of condensables (vapor), such as steam and methanol, from non-condensable gases is considered [67, 68, 81, 82]. Some authors even use these hydrophilic membranes to separate methanol in a process where they exclude the presence of steam, in particular for polymer membranes [87, 88].

Stability

Also the hydrothermal stability of the considered membranes is of great importance. Zeolite type membranes are tested at higher temperatures (200-400 °C), as could be seen in Figure 2-6 and Figure 2-7. In contrast, polymer membranes are generally operated at lower temperatures and tend to break down at higher temperatures [88]. This is also the reason that there is little experimental data available for polymer membranes at elevated temperatures. The ceramic supported polymer membrane is a notable exception to this, this membrane was tested up to 300 °C and was reported to be stable under hydrothermal conditions, which would make it suitable for practical applications of in situ steam removal. Amorphous membranes have not been tested over 250 °C. They are reported to degrade at higher temperatures and are therefore considered not suitable for operation at elevated temperatures [77]. Although zeolite type membranes are used at higher temperatures, also their stability is not always optimal. Thermal expansion, adsorbate-induced structural changes and the effect of the framework cations influence the membrane stability [102]. In line with these observations, LTA membranes have been stated to be unstable towards hydrolysis [103]. Therefore ZSM-5 membranes are dominant in the window between 300 and 400 °C. These membranes, however, often show less permeance due to reduced hydrophilicity [103, 104]. Either increasing the hydrophilicity or increasing the stability by Si enrichment are promising developments in further improving zeolite type membranes.

Mass transfer and kinetics

Besides permeance, permselectivity and stability, also kinetic effects and mass transfer limitations could be of importance. Some authors express the kinetic compatibility as the product of the modified Péclet number (Pe) and the Damköhler number (Da), and give a range between 0.1 and 10 for this expression [77, 105]. The modified Péclet number relates the rate of transport by convection (and therefore the residence time) to rate of transport through the membrane, whereas the Damköhler number relates the rate of reaction to the rate of transport by convection. As the rate of reaction and the rate of separation have to be balanced, the product of Pe and Da should be balanced as well. Although this approach could work for many cases, the rate of reaction is evaluated with kinetics that do not account for separation enhancement conditions. Therefore, it neglects the possible influence of reactive separation on the kinetics of the system. Not only the kinetics, but also mass transfer limitations could affect the reactive steam permeation. In most cases the transport from the catalyst to the membrane via the bulk phase is rate determining. On the one hand, the relatively low space velocities for many separation enhanced processes adds to the probability of mass transfer limitations. On the other hand, radial convection can significantly contribute to the transport to/from the membrane [106, 107]. Whereas transfer limitations between the different functional areas could influence the kinetics of reaction and separation, and the overall reactive separation performance, it is important to assess the limitations of the steam separation enhanced system, kinetics and/or mass transfer, so that the best configuration and reactor tuning can be applied.

Heat management

In addition, heat transfer limitations could have a large effect on the performance of reactive steam permeation. Heat management is important for chemical reactions in general, especially in the case of high exothermicity or endothermicity. Temperature profiles in reactive separation, however, does not only influence the local reaction rate, but also the separation, thereby changing the overall behavior of the reactive permeation process. Gorbe et al. (2018) even suggest the application of a temperature gradient over their zeolite membrane to improve its performance [85]. In general, the behavior of a reactive permeation process can be controlled relatively easy by heat management due to the steady-state characteristics of a membrane reactor.

Contactor types and reactor configuration

The most common implementation of reactive steam permeation is as packed bed membrane reactor (PBMR), in which a membrane reactor is filled with catalyst material [66, 70, 71, 73-76, 78, 80, 108]. Although this is a relatively easy way to implement membrane separation, other contactor types could be beneficial for different reactions and operating

conditions. For example, in case of mass transfer limitations due to the (non-)proximity of catalytic active material and the membrane a catalytic membrane could help overcoming this issue by bringing the functionalities closer together. A fluidized bed membrane reactor could also become an option in the case of (severe) heat transfer limitations due to its good heat transfer characteristics.

Besides the characteristics of the various membrane reactor types, also the choice of using a sweep determines the behavior of the reactive steam permeation system. Basically, the system is regenerated using a pressure swing, whereas the partial pressure difference over the membrane is the driving force for steam separation. Nevertheless, a degree of freedom remains in the choice for a vacuum or sweep gas at the permeate side. Sweeping the permeate side of the membrane with a low pressure, inert gas can increase the driving force over the membrane. On the other hand, diffusional resistances due to penetration of sweep gas into the membrane support can increase as well [107]. However, the increase in the driving force will be more dominant than the increase in mass transfer resistances and therefore the use of sweep gas can enhance steam separation. Another example is the recirculation of the sweep gas stream. In the case of a PBMR for DME synthesis, the recirculation of the sweep gas stream reduces the driving force for methanol over the membrane. The minimized loss of methanol across the membrane results in increased DME yields at high recirculation factors [69].

For the (reactive) separation of steam, although permeation was not used in all cases, many reactor configurations are reported. Hydrophilic membranes were tested in slurry, fixed-bed and fluidized-bed reactors [62, 77]. Dual membrane reactors have been suggested, utilizing both a steam selective membrane and a hydrogen selective membrane [70, 71]. A simulated moving bed membrane reactor was developed for acetal synthesis [93, 94] and steam permeation was combined with reactive distillation [87, 88]. All these configurations could result in potential benefits regarding the specific reactions and process conditions. Therefore, the optimal contactor type is case specific.

2.3. Selection of separation method

To benefit from the full potential of process intensification (PI), many ongoing research activities focus on new methodologies, frameworks and toolboxes for this level of process synthesis [3, 109-112]. Although design methods for reaction-separation processes have been reviewed and revised [109, 110], in practice a superstructure method is not applied in the design of completely new processes due to its high complexity [113, 114]. Instead, process engineering decisions are often based on expert knowledge. Commonly this knowledge is formulated in so-called heuristic rules or rules-of-thumb [18, 113]. The potential of in situ steam removal as PI is discussed with regard to selection criteria and process requirements.

2.3.1. Potential of in situ steam removal

Process selection criteria

In process selection, commonly a cost optimization is performed in which the overall economy of the process is guiding the selection of the best option or configuration. This includes the material and energy efficiency, as well as the required separation technologies and recycles. In situ steam removal could result in a more complex reactor design by means of the implementation of membrane area or adsorbent in the reactor. However, the reduction of the downstream separation and recycle section, as well as possible operation at milder reaction conditions, could lower the capital expenditure significantly. The higher energy efficiency of an in situ steam removal process compared to the conventional process reduces the energy costs and therefore operational expenditure. The operational expenditure could be lowered as well by means of improved resource efficiency for in situ separation. Often such an energy (or resource) efficient process also results in reduction of the capital expenditure cost (satisfying the classic optimization equation), based on a reduction in the number of steps [112, 114]. Moreover, not only costs can be a criterion for process selection, also its environmental impact can be a selection criterion. For such a 'license to operate' the energy efficiency and global warming potential of the process have to be assessed. The climate change mitigation potential of a process could be assessed by quantifying the CO_2 emissions avoided through a life cycle analysis [115]. This quantification could be a good method to evaluate different technologies and select an optimum process, especially for carbon capture and utilization technologies.

Criteria for in situ steam removal

For the feasibility of reactive steam separation, various aspects have to be evaluated. The first aspect to be addressed is the advantage of in situ steam separation in terms of reaction equilibrium and/or kinetics. Secondly, the steam concentration, which has to be reached, has to be evaluated and therefore the amount of steam that has to be separated. Thirdly, the technical aspect of the required in situ separation has to be attended. Finally, the process selection criteria such as the process economics and the reduction of the overall global warming potential can be addressed. The last aspects can only be fully considered if the first aspects have been evaluated and answered sufficiently.

Although the advantages of the first aspects for reactive steam separation may be apparent from a theoretical point of view, the developments in several research lines have demonstrated that the actual performance of the reactive steam adsorption system is often determined by the chemistry of the system and therefore impossible to be determined on a general level [20, 30]. This makes clear that the feasibility of in situ steam removal should be addressed for each specific case and not only from a theoretical point of view. Nonetheless, some general aspects can be outlined.

General considerations: Impact of steam removal

To discuss general aspects for steam separation enhanced reactions a simple equilibrium reaction 1 is assumed:

$$aA + bB \leftrightarrow cP + dH_2O \quad (1)$$

In this reaction, reactants A and B form the desired product P and by-product H_2O, such as the reverse water-gas shift, etherification or esterification reactions. The impact of steam removal on this reaction can be assessed by the amount of steam present in equilibrium:

$$P_{H2O} = \sqrt[d]{K_{eq} \frac{{P_A}^a {P_B}^b}{{P_P}^c}} \quad (2)$$

Secondly, reaction kinetics can be influenced by steam due to inhibition or even deactivation. This is generalized in equation 3 using a stoichiometry of one. The equation includes catalyst inhibition by H_2O as a surface coverage effect with an inhibition factor *f*.

$$r = k \frac{P_A P_B - P_P P_{H2O}/K_{eq}}{(1 + f P_{H2O})^2} \quad (3)$$

To evaluate the potential advantage of in situ steam removal equations (1), (2) and (3) are used in a simple plug flow reactor model [116]. Steam is removed instantaneously from the reaction mixture and the possible influence on the residence time is neglected for simplification. The parameters and conditions can be found in Table 2-3. The potential advantage of in situ steam removal is illustrated in Figure 2-9, where the reactant conversion to product is shown as a function of the equilibrium constant which represents different type of reactions.

TABLE 2-3: PARAMETERS AND CONDITIONS FOR PFR MODEL.

Operating conditions	Data	Operating conditions	Data
Reactor length	6 m	Superficial gas velocity	0.15 m·s^{-1}
Reactor temperature	250 °C	Kinetic rate constant	10^{-3} s^{-1}
Reactor pressure	50 bar(a)		

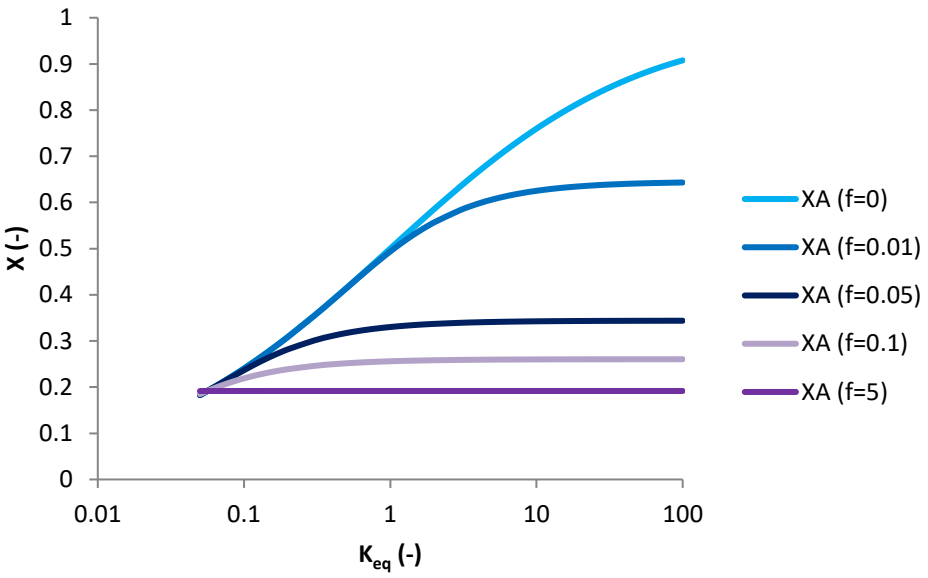

FIGURE 2-9: CONVERSION X IN A PFR REACTOR AS A FUNCTION OF THE EQUILIBRIUM CONSTANT K_{EQ} FOR DIFFERENT STEAM INHIBITION FACTORS *F* (CONDITIONS LISTED IN TABLE 2-3).

As can be expected, for reactions with large values for the equilibrium constant the conversion to product is significantly larger due to the equilibrium position. The effect of steam inhibition on the reaction rate, and therefore on the conversion is especially significant for a reaction with larger values for their equilibrium constant. The larger K_{eq}, the more favored is the formation of product and of steam. However, the formed steam inhibits the reaction and therefore suppresses the product yield. The Fischer-Tropsch synthesis is a typical example of this situation. In Figure 2-10 the impact of in situ steam removal (*R*) on reactions with and without steam inhibition is shown. Clearly in situ H_2O removal is an interesting option for a large range of conditions and therefore reactions. The conversion of reactions with a small equilibrium constant, such as the reverse-WGS (K_{eq}(300 °C) ≈ $2 \cdot 10^{-2}$), can be significantly enhanced by in situ separation, although low steam levels have to be achieved. At the other end of the range, for reactions with a large equilibrium constant, such as Fischer-Tropsch (K_{eq}(250 °C, H_2-CO to C_6H_{14}) ≈ $1 \cdot 10^{20}$), the effect of steam removal is less pronounced, unless steam inhibition (Equation 3) plays a role, as is the case for Fischer-Tropsch. Whereas inhibition by steam has a large effect on the conversion for reactions with a large K_{eq} (Figure 2-9), the impact of in situ steam removal increases if steam inhibition is more pronounced (Figure 2-10).

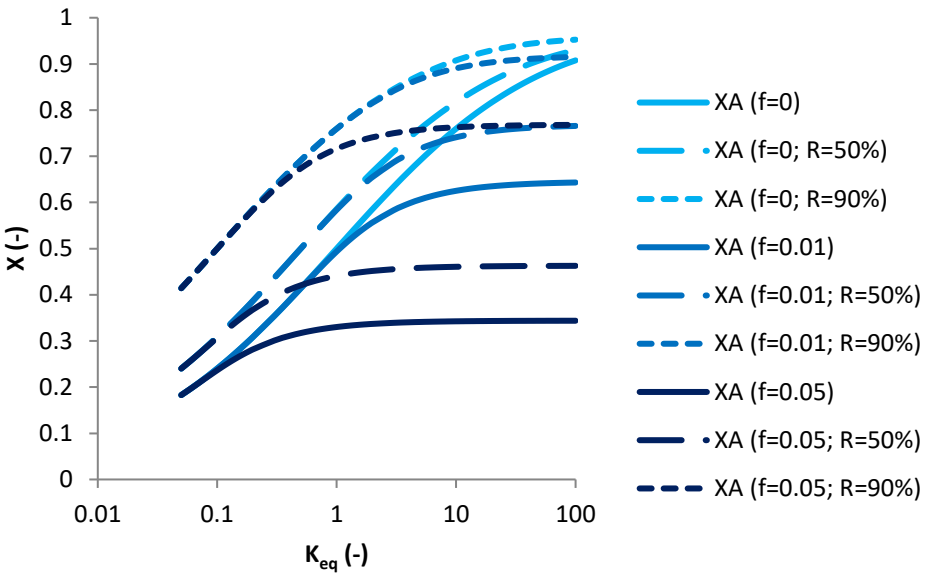

FIGURE 2-10: IMPACT OF 50 AND 90% STEAM REMOVAL *R* (INSTANTANEOUS) ON PFR CONVERSION AS A FUNCTION OF THE EQUILIBRIUM CONSTANT K_{EQ} (CONDITIONS LISTED IN TABLE 2-3).

Selectivity and permselectivity

Another aspect of the feasibility of reactive steam separation is the selectivity. Reactive steam permeation (membrane separation) requires high permselectivities and reactive steam adsorption requires high selectivity of the adsorbent material. As depicted in Figure 2-11, the (perm)selectivity for steam separation (compared to reactant A) has only a limited influence on the conversion towards the product. For the case of a reaction with a K_{eq} of 10 and 90% steam removal, a selectivity above 30 hardly further improves the conversion and the largest improvement is already made towards a selectivity of 10. For the other cases shown in this figure, this threshold is even lower. This is different concerning the selectivity for steam separation compared to the product P: if product P is unselectively separated as well, this could improve conversion enhancement. However, not only the effect of the (perm)selectivity on the conversion is important. The impact on the process complexity and (economic) viability determines the requirements for the (perm)selectivity. The necessity of extra separation and purification due to economic (recovery of costly reactant/product), environmental and/or legislative (pollution) reasons, would make the process even more complex than reactive separation already can be and could reduce the (economic) viability of the reactive separation process. If for one, or more, of these reasons the reactant loss has to be limited to 5%, a (perm)selectivity higher than 15 is already sufficient for the

depicted conditions, as shown in Figure 2-12. However, if the loss has to be below 1%, (perm)selectivities of 100 or larger are required.

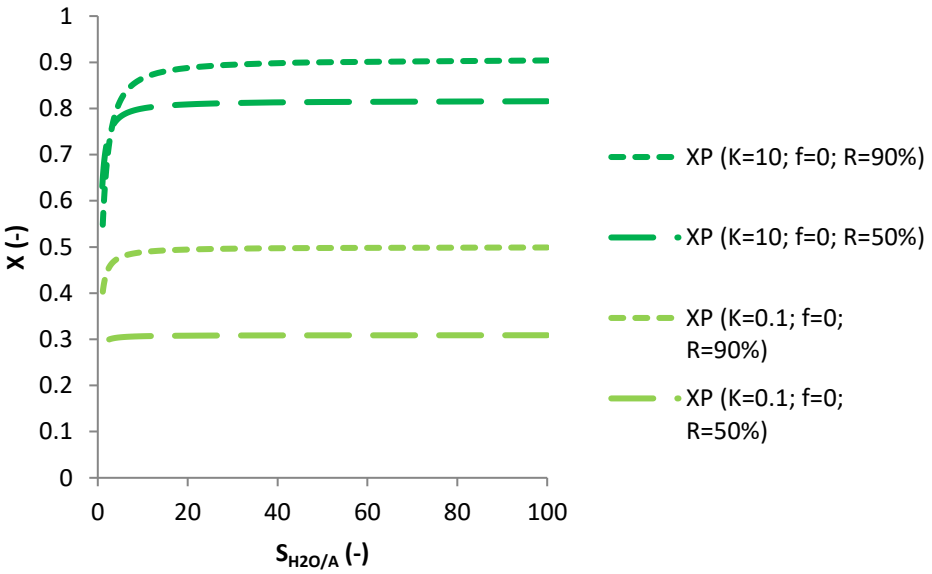

FIGURE 2-11: PFR CONVERSION AS A FUNCTION OF (PERM)SELECTIVITY OF STEAM TOWARDS REACTANT A (CONDITIONS LISTED IN TABLE 2-3).

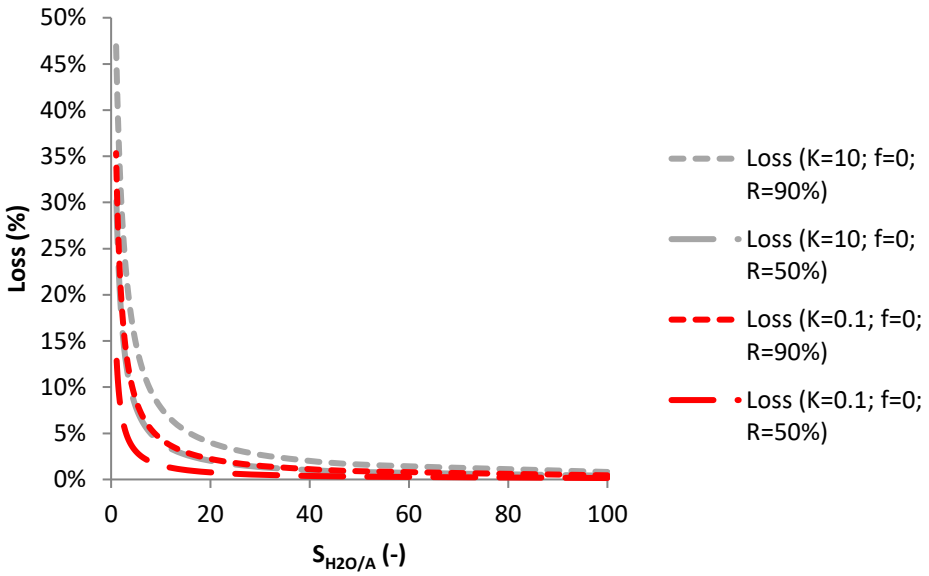

FIGURE 2-12: LOSS OF REACTANT A AS A FUNCTION OF (PERM)SELECTIVITY OF STEAM TOWARDS REACTANT A (CONDITIONS LISTED IN TABLE 2-3).

Kinetics and mass transfer limitations

Besides displacement of the reaction equilibrium, the removal of steam may also change the reaction kinetics. When the reaction is faster than the rate of separation, the separation enhanced process is limited by the separation and the enhancement could become minimal. Vice versa, with faster separation than reaction, not only the desired reaction could become separation enhanced. Even a conventionally insignificant side reaction could become the dominant reaction, as is the case for the formation of COS in the Claus process [27].

In addition to matching reaction and separation rates, also the proximity of reaction and separation plays an important role. It was observed that the performance of the reactive steam adsorption system is determined by the chemistry of local conditions in the system [22, 30]. This close proximity reduces possible mass transfer limitations between reaction and separation which is the case for both adsorption and vapor permeation, and therefore improves the performance of the reactive separation process. The choice of contactor type/reactor configuration could help in this regard. An adsorption reactor, as well as a catalytic membrane reactor could provide a closer proximity of reaction and separation compared to a packed bed membrane reactor.

Capacity and permeance

The fourth aspect of the criteria for in situ steam removal to be considered is the capacity of separation. In the case of reactive adsorption this is the adsorption capacity of the adsorbent material, in the case of reactive membrane separation the membrane permeance determines the capacity of separation. As plotted in section 2.2.3, membrane steam permeances range from 10^{-8} to 10^{-6} mol m^{-2} s^{-1} Pa^{-1}, and adsorbent steam capacities can range from 2 to 20 wt.% [16, 37]. The resulting capacity of separation should match the amount of steam produced, as was also shown by varying the sorbent volume capacity in a thermodynamic analysis of sorption enhanced methanol synthesis [117]. In order to match the steam production, the separation capacity determines the membrane area or adsorbent weight required. In its turn the required membrane area or adsorbent weight results in the size of the reactive separation system and therefore determines a large part of the capital costs.

2.3.2. System sizing: membrane area and sorbent weight

The rate of separation and the rate of formation have to be compatible to implement reactive separation. The necessary membrane area can be computed from the production rate, the membrane permeance and the steam pressure difference over the membrane:

$$a_m = \frac{A_m}{V_R} = \frac{R_{H2O}}{Q_{H2O}\,\Delta P_{H2O}} \tag{4}$$

A maximum of 250 m^2 membrane area/ m^3 reactor volume can be incorporated in a standard shell-tube reactor configuration [118]. Furthermore, zeolite-type membranes achieve permeance values of $1{\cdot}10^{-7}$ mol/(s m^2 Pa). For a case of Fischer-Tropsch synthesis with in situ steam removal a production rate of 193 kg H_2O/(hr m^3 reactor volume) is assumed. For this rate together with 2.5 bar steam pressure difference over the membrane, almost 50% of the reactor volume would be occupied for in situ steam separation [77].

The current state-of-the-art membranes as discussed in section 2.2.3, with a tenfold increased permeance, will drastically decrease the occupied reactor volume. Besides a good indication of the minimum permeance required for application of membranes for in situ steam separation, $1{\cdot}10^{-7}$ mol/(s m^2 Pa), this example also gives a good indication of a minimum steam pressure difference required over the length of the membrane. Rohde et al. [77] state that pressure differences less than 2.5 bar steam are technically not feasible. Depending on the specific conditions, it can be argued that a steam partial pressure of 1 bar is the minimum to be considered for membrane separation utilizing the maximum 250 m^2 membrane area/m^3 reactor in equation (4).

Similar to the membrane area, the amount of adsorbent material required can be estimated. For this, one needs to know the production rate, the adsorption capacity and the adsorption (cycle) time.

$$\frac{w_{ads}}{V_R} = \frac{R_{H2O}t}{q_{H2O}} \quad (5)$$

Where for reactive vapor permeation (not for reactive pervaporation) the pressure difference over the membrane is an extra parameter influencing the system sizing and design, for reactive adsorption this is the adsorption (cycle) time. The cycle time gives an extra degree of freedom to reactive adsorption systems.

As an example, the same case of Fischer-Tropsch synthesis with in situ steam removal is considered, again assuming a 193 kg H_2O/(hr m^3 reactor volume) production rate. A typical working capacity for zeolite type adsorbents for gas drying is stated to readily be 10 wt.% and a bulk density of 720 kg/m^3 is given [37]. Using short cycle times of 15 minutes already two-thirds of the reactor volume would be filled by adsorbent, leaving the remaining space available for catalyst material. To design a system with longer cycle times, more adsorbent material and/or higher working capacities are required.

2.3.3. System: contactor type and regeneration

Regeneration

Another important degree of freedom for reactive steam adsorption is the method of sorbent regeneration, which can be divided into pressure swing, temperature swing, concentration swing, reactive regeneration, displacement regeneration or combinations of these operations [16-18]. Inherently, regeneration is slow compared to adsorption because of the shape of the isotherm [17]. Therefore, the regeneration determines the cycle times, the extent of equipment required, and therefore the efficiency and feasibility of the process. Pressure swing regeneration, possibly vacuum or in combination with a purge gas, is the most commonly used regeneration mode for reactive adsorption [19, 20, 26, 27, 29]. This operation is relatively easily implemented and fast in operation, making short cycle times and efficient use of adsorbent feasible [16]. Temperature swing on the other hand, commonly used for molecular sieves, is generally a slower method of regeneration and therefore results in less freedom for the selection of cycle times.

In contrast to reactive steam adsorption, reactive steam permeation has no extra degree of freedom in the choice of regeneration. Basically, membrane technology involves pressure swing regeneration by means of a partial pressure difference across the membrane. Restricting the operational choice to vacuum or sweep gas operation, where the use of a sweep gas can increase the driving force and therefore the separation, although diffusion resistances could arise (as discussed in Section 2.2.3).

Contactor type and reactor configuration

The contactor type is another variable in the design of a reactive separation process. Although different technologies have been developed for (reactive) separation by membranes and adsorption, analogies can be drawn. Implementation of membrane separation can be done in various contactor types, each with their own pros and cons. Among others, membrane contactors are a packed bed membrane reactor (PBMR), a catalytic membrane reactor (CMR) and a fluidized bed membrane reactor (FBMR).

The PBMR generally consists of a membrane reactor, standard shell-tube configuration, filled with a catalyst bed. This is the easiest configuration to design and operate, therefore it is the most commonly used configuration in reactive steam permeation literature [66, 73-76, 78, 80, 108]. However, possible downsides include mass and heat transfer limitations. A CMR reduces mass transfer limitations between reaction and separation by integrating the catalytic functionality on the membrane. The performance of a catalytic membrane reactor is determined by the catalytic layer thickness, of which the optimum is a function of the reaction kinetics and the membrane permeability [119]. Where on the one hand the close integration could be beneficial, on the other hand membrane fabrication becomes more complex and the system loses degrees of freedom compared to a PBMR. In addition to PBMR, the FBMR integrates membranes in a fluidized bed reactor, which is especially suitable for situations in which mass and/or heat transfer limitations are important. This technology is still in early stages of development and main challenges include particle attrition and membrane deterioration due to the particle fluidization. Applications of FBMR technology for reactive steam separation are lacking in the open literature.

Similar to membrane separation, integration of adsorption is possible with various contactor types. Some possibilities include a packed bed reactor, a (simulated) moving bed reactor and a fluidized bed reactor. The most commonly used configuration for (reactive) adsorption is a packed bed reactor. Inherent to the use of a solid adsorbent, periodic regeneration is required to regain the adsorptive capacity of the system. Typically, multiple fixed-bed reactor configurations are combined in a process cycle, switching between adsorption and regeneration steps, resembling a temperature or pressure swing adsorption system [16]. Examples of packed bed reactors in reactive steam adsorption show process considerations regarding regeneration, including heat management [21, 27], separation enhanced kinetics [20] and repressurization [19]. Although the multiple reactor concept works well, the performance of a fixed-bed reactor could be improved by using a moving bed reactor as contactor type. In this reactor configuration the solids are circulated between adsorption and regeneration reactors, thus reducing the total solids inventory. The reactors can be operated continuously in the same mode of operation, removing the transient behavior which is typical for a fixed-bed configuration. Advantageous is also the decoupling of adsorption and regeneration, which therefore could be separately optimized. Parra et al. (2018) discussed the advantages of a moving bed reactor over a fixed-bed reactor for steam

separation enhanced reverse-WGS [59]. Santos et al. (2015) have demonstrated true moving bed reactor (TMBR) technology for the direct synthesis of DMC [60]. However, they also indicate a major drawback of the technology. Disadvantageous is the moving of solids, which would result in a more complex system with accompanying issues such as particle attrition and mechanical failure (solid transport). For these reasons the moving bed reactor can be simulated by means of a simulated moving bed reactor (SMBR), which retains the advantages of a TMBR without introducing the problems associated with the actual movement of solids [120]. In a conventional SMBR the solids are fixed in a packed bed and instead the feed is switched periodically to a different reactor to simulate the behavior of a moving bed reactor. This is most commonly done in a configuration of multiple packed bed reactors [93, 94]. Finally, a fluidized bed reactor (FBR) can be considered as a type of moving bed reactor. The solids are generally well mixed due to fluidization, and by interconnection of two fluidized bed reactors adsorption and regeneration can be done in different reactors. This would assure continuous operation of a reactor and decoupling of adsorption and regeneration. The biggest advantage of fluidized bed reactors are the good specifications with regard to heat transfer, due to the well mixed particles. Whereas the gas phase is generally in plug flow, also good mass transfer is achievable. However, back-mixing of particles could be an issue. Applications of FBR for reactive steam adsorption have not appeared in the open literature, although these systems are studied for CO_2 adsorption [121].

2.3.4. Adsorption and membrane technology

Following the criteria for in situ steam removal, the first aspect to be discussed is the steam partial pressure difference: what amount of steam has to be removed and what remaining steam level is acceptable? For example, Rohde et al. [77] stated that at least a partial pressure difference of 2.5 bar steam is necessary for membrane technology to be feasible in Fischer-Tropsch synthesis. In addition, even with vacuum on the permeate side, a minimum achievable steam partial pressure in the reactor product arguably seems to be 1 bar. In situ steam removal by adsorption on the other hand does not have this minimum steam partial pressure difference and could be used to remove trace amounts of steam, provided sufficient regeneration is possible. This regeneration, however, results in the driving force for adsorption. Where the driving force for permeation is determined by the partial pressure difference, the driving force for adsorption is determined by the difference between the actual adsorbent loading and the equilibrium loading, defined by an isotherm [16, 17]. Therefore the, often nonlinear, shape of the isotherm results in a different behavior compared to membrane separation.

Regarding selectivity, this has only a limited influence on the conversion towards the product. As discussed, the influence on the loss of reactant is probably more significant.

For both technologies, materials (adsorbents and membranes) are available which can achieve reasonable selectivity towards steam removal, although methanol selectivity is a well-known bottleneck. Unselective separation of the product together with steam could benefit conversion enhancement, for example in methanol synthesis [81, 82]. Additional separation of product and steam would determine the viability in this case. Unselective separation of reactant could result in significant losses and/or costly recovery, definitively in the case of reactive steam permeation. For reactive steam adsorption, co-adsorption of reactant could possibly be handled by holding the reactant in the system, keeping it available for reaction. The required selectivity depends however on the specific case. Furthermore, the selectivity could be a trade-off with separation capacity, permeance and kinetics of the system. Examples are the use of large pore zeolites in adsorption [16, 37] or reducing membrane thickness to reduce diffusion resistances [95, 107], although losing some selectivity.

Some examples [27, 30] show that the kinetics of in situ steam removal could also play an important role. In the case of mass transfer limitations between catalytic reaction and steam separation a catalytic membrane reactor could be beneficial compared to a packed bed membrane reactor. Reactive adsorption would be beneficial as well, whereas the catalytic and separation functionalities are closer together (depending on mixing scales).

The separation capacity, or permeance in the case of membrane technology, mainly determines the system sizing (as discussed in section 2.3.2.). Large amounts of steam produced help the separation via membranes due to a larger pressure difference over the membrane. For steam adsorption the capacity is limited, so the larger the amount of steam to be separated, the more adsorbent material is required. Although some extra degree of freedom is present in the form of cycle times, the required membrane area tends to be advantageous compared to the necessary adsorbent material for large amounts of steam to be separated. For this reason a large part of the literature on reactive steam permeation is dedicated to Fischer-Tropsch synthesis, where large amounts of steam have to be separated [73-78]. Whereas reactive steam adsorption literature mainly focuses on reactions where the remaining steam content is crucial, such as the reverse-WGS and DME synthesis [5, 19, 20, 24, 28-30, 58, 59]. All of these reactions have great opportunities in the direct or indirect conversion of CO_2 towards fuels and chemicals in order to reduce CO_2 emissions and to create value [2].

In summary, as graphically presented in Figure 2-13, membrane technology would be preferable for larger steam pressures (>1 bar), where the remaining steam content is less restricted. Reactive adsorption would be preferable for lower steam pressure processes (<1 bar) and particularly for steam level reduction as low as trace amounts. Finally, all aspects have to be evaluated case specific and supported by experimental corroboration.

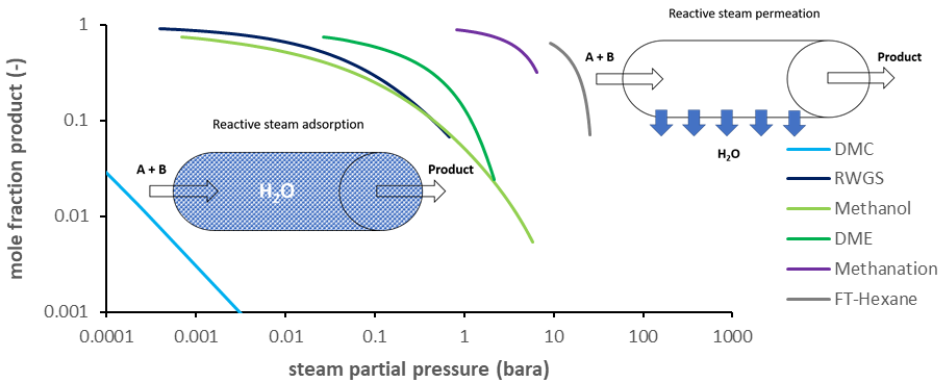

FIGURE 2-13: GRAPHICAL PRESENTATION OF THE STEAM SEPARATION ENHANCED REACTIONS AND THE SUITABLE STEAM SEPARATION ENHANCED TECHNOLOGIES.

2.3.5. Future developments in steam separation enhancement

Although reactive steam separation shows great potential for process intensification, and therefore energy efficiency and reduced environmental impact, currently limited industrial applications exist. In this section the main obstacles, bottlenecks and the directions for future developments in steam separation enhancement are elucidated.

Sorbents

Reactive steam adsorption requires a high working capacity of the adsorbent material at elevated temperatures. However, many adsorbents are used at relatively low to moderate temperatures. Although some materials, such as zeolite molecular sieves, still have a working capacity at slightly elevated temperatures (Figure 2-3), in general little information about the adsorption of steam under high temperatures is known in the open literature. This makes the working capacity one of the main obstacles to overcome prior to industrial practice. Another bottleneck comprises heat management. The adsorption of steam is an exothermic process, which is therefore favored at low temperatures. Hence, the requirement of sufficient working capacities at higher temperatures. In addition, many dehydration reactions, such as the methanation reaction, the Claus reaction and (direct) DME synthesis, are exothermic as well. The resulting temperature profiles could affect the adsorption capacity, the kinetics and the concentration profiles in adsorptive reactions. Again, case specific reaction, reactor and process conditions determine the importance of heat management and the best way to overcome possible obstacles. The combination of theory and experiments in a fundamental way is crucial for a proper understanding of steam adsorption enhanced processes and to overcome its bottlenecks. Although theoretical frameworks and model predictions give an overview of the potential of in situ steam

adsorption (especially for the reverse-WGS, DME synthesis and methanation reactions), often isotherm models are used that have not been validated under the actual reaction conditions and only provide indicative results. Therefore, closer investigation of steam adsorption at elevated reaction temperatures has to be performed. Secondly, although co-adsorption of various reactants may be suspected for regularly used adsorbents, it is rarely studied. Thus, improved understanding of selectivity and co-adsorption at reaction conditions are a second aspect that need to be addressed for the future development of reactive steam adsorption. Thirdly, kinetic and mass transfer behavior is different for sorption enhanced reactions compared to conventional reaction systems. Nevertheless, conventional descriptions are often used for reactive steam separation. Although it could possibly describe the system well, the difference between sorption enhanced and conventional kinetics need to be further investigated. Besides mass transfer, also heat transfer, and heat management in general, is a fourth aspect presently receiving little attention in studies on reactive steam adsorption. Whereas many steam sorption enhanced reactions, as well as steam adsorption itself, are exothermic, proper heat management will be of large significance in the further development of these processes. Furthermore, the regeneration of the reactive steam adsorption system will have a large impact on the overall process and its feasibility. On the one hand, the overall process design would benefit from a quick and energy efficient regeneration procedure, while on the other hand the reaction system could require a slow and energy intensive regeneration procedure. Interfering with all other aspects, regeneration is a fifth and important aspect for the future development of reactive steam adsorption processes. Finally, after all these aspects have been evaluated and answered sufficiently, criteria such as the process economics and the reduction of the overall global warming potential can be addressed.

Membranes

For reactive steam permeation hydrothermal stability is a major bottleneck for industrial application. Typically, amorphous membranes are reported to degrade at higher temperatures (over 250 °C) and are therefore considered unsuitable at these temperatures [77]. Polymer membranes tend to break down at higher temperatures as well [88], to which the ceramic supported polymer membrane is a notable exception with reported hydrothermal stability up to 300 °C. Although zeolite type membranes are tested at higher temperatures, thermal expansion, adsorbate-induced structural changes and the effect of the framework cations influence membrane stability [102]. Enhancing the flux by increasing hydrophilicity of stable membranes or increasing stability by Si enrichment of less stable membranes are promising developments in further improving zeolite type membranes. In addition to the stability, the seal and the loading of membranes at high temperatures and pressures are an essential aspect for industrial application. However, detailed discussion on this aspect is often missing in the open literature [122]. In general, high pressures are less

of an issue at low temperatures and vice versa. The combination of high pressure and high temperature becomes increasingly challenging for more severe conditions and therefore could become a bottleneck. Another obstacle to overcome for reactive steam permeation is the permselectivity. In general, the permselectivities of H_2O towards H_2 and of H_2O towards alcohols, such as methanol are considered most important [62, 63, 95]. For all types of membranes higher temperatures result in a decreased permselectivity. In addition to this, due to the difficult separation of steam and methanol, often the separation of condensables (vapor) from non-condensable gases is considered and even exploited [67, 68, 81, 82].

Similar to reactive steam adsorption, several authors developing theoretical frameworks for reactive steam permeation rely on experimentally obtained membrane permeance and selectivity, that were not validated at reaction conditions. Other authors have focused on experimental work, specifically looking at membrane performance (permeance/flux) and less on the overall reactive separation system. Firstly, whereas experimental data at higher temperatures is limited, steam permeation at elevated reaction temperatures has to be investigated more closely. Permselectivity data is often limited to hydrogen and steam, up to moderate temperatures. Therefore, membrane selectivity for relevant reaction components (under reaction conditions) is a second aspect for the future development of reactive steam permeation. A third aspect is membrane stability. The hydrothermal stability, as well as the chemical stability, of the membranes is often unknown or considered critical, making both duration tests under relevant conditions and the development of new stable membranes the third important aspect for future development. Kinetic and mass transfer limitations also play an important role in steam permeation enhanced reactions and therefore they are a fourth aspect requiring closer investigation. Similar to mass transfer, this also holds for heat transfer. Whereas the reactor configuration directly influences mass and heat transfer behavior, the benefits of (novel) reactor configurations, other than packed bed membrane reactors, for reactive steam permeation is a fifth important aspect in the development of these novel processes. Lastly, although the regeneration mode is fixed being a pressure swing over the membrane, the importance of the sweep gas or the choice for a vacuum affects the reactive steam permeation. Again, criteria such as the process economics and the reduction of the overall global warming potential can only be addressed after all other aspects have been evaluated and answered sufficiently.

2.4. Conclusions

In this chapter, reactive separation of steam has been discussed. Reducing the steam partial pressure by in situ separation results in conversion enhancement due to equilibrium displacement. However, it could affect reaction kinetics, reaction selectivity, catalyst

deactivation and therefore catalyst lifetime. All these opportunities (positive and negative) are case specific and have to be addressed as such. Nonetheless, some general aspects have been outlined in this review.

Membrane technology requires larger steam partial pressure differences (>1 bar) and may be preferred when the remaining steam content is less restricted, when there are no kinetic and mass transfer limitations, and when the (perm)selectivity is high, at least of steam compared to the reactants. Reactive adsorption would be preferable to consider for achieving lower steam partial pressures (<1 bar), for steam level reductions as low as trace amounts and if transfer limitations between catalytic activity and separation are important. With respect to DME synthesis, both membrane and adsorption technology are of interest for in situ steam separation. However, sorption enhanced DME synthesis appears to be the most promising from a carbon efficiency point of view due to its high single-pass conversion of CO_2 to DME.

Before process design and selection criteria, such as the process economics, energy efficiency, and environmental impact, can be regarded, various aspects of the reactive steam separation process need to be addressed. Essential aspects for reactive steam adsorption include high temperature working capacities and heat management. Crucial to further our understanding of steam separation enhanced processes are studies that combine theory and experiments in a fundamental way. Not only material performance under relevant conditions has to be investigated, but also different reactor and process configurations. The next chapters will elaborate on these aspects for sorption enhanced DME synthesis.

Nomenclature

A_m	Membrane area (m^2)
a_m	Membrane area per reactor volume (m^2 m^{-3})
Da	Damköhler number (-)
f	Inhibition factor (-)
k	Reaction rate constant (s^{-1})
K_{eq}	Equilibrium constant (-)
P_i	Partial pressure of component i (bar)
Pe	Péclet number (-)
Q_i	Permeance of component i (mol s^{-1} m^{-2} Pa^{-1})
q_i	Adsorbent loading (kg kg^{-1})
r	Reaction rate (mol m^{-3} s^{-1})
R_i	Production rate of component i (kg hr^{-1} m^{-3})
R	Steam removal (%)
S	Selectivity (-)

t	Time (s)
V_R	Reactor volume (m^3)
w_{ads}	Weight of adsorbent (kg)
X	Conversion (-)

Abbreviations

CMR	Catalytic membrane reactor
COS	Carbonyl Sulphide
CSP	Ceramic supported polymer
CZA	Copper/Zinc Oxide/Alumina
DMC	Dimethyl carbonate
DME	Dimethyl ether
FBMR	Fluidized bed membrane reactor
FBR	Fluidized bed reactor
FT	Fischer-Tropsch
LTA	Linde Type A
MOR	Mordenite
MR	Membrane reactor
PBMR	Packed bed membrane reactor
PBR	Packed bed reactor
PI	Process Intensification
PSA	Pressure swing adsorption
RD	Reactive distillation
rWGS	Reverse water-gas shift
SMBR	Simulated moving bed reactor
SOD	Sodalite
TMBR	True moving bed reactor
TSA	Temperature swing adsorption
WGS	Water-gas shift
ZSM-5	Zeolite Socony Mobil-5

Bibliography

[1] Accelerating Breakthrough Innovation in Carbon Capture, Utilization, and Storage, Report of the Mission Innovation Carbon Capture, Utilization, and Storage Expert's Workshop, 2017.

[2] G. Centi, S. Perathoner, Opportunities and prospects in the chemical recycling of carbon dioxide to fuels, Catalysis Today 148 (2009) 191-205.

[3] A. Stankiewicz, J.A. Moulijn, Process Intensification: transforming chemical engineering, Chemical Engineering Progress (2000) 22-34.
[4] C. Bartholomew, R. Farrauto, Fundamentals of industrial catalytic processes, second ed., Wiley2006.
[5] J. Boon, F. van Berkel, H. van Dijk, J. Vente, Separation enhanced dimethyl ether synthesis, 5th TMFB International Conference, Aachen, 2017.
[6] S. Guffanti, C. Visconti, G. Groppi, Sorption enhanced dimethyl ether synthesis: process analysis and reactor modelling, 25th International Symposium on Chemical Reaction Engineering, Florence, 2018.
[7] V. Agreda, L. Partin, W. Heise, High-purity methyl acetate via reactive distillation, Chemical Engineering Progress 86 (1990).
[8] V. Agreda, L. Partin, Reactive distillation process for the production of methyl acetate, U.S., 1984.
[9] H. Strathmann, Membranes and Membrane Separation Processes, Ullmann's Encyclopedia of Industrial Chemistry, Wiley-VHC Verlag, 2005.
[10] F. Gallucci, Inorganic Membrane Reactors for Methanol Synthesis, Methanol Science and Engineering, Elsevier, 2018.
[11] W. Gluud, K. Keller, R. Schonfelder, W. Klempt, Production of Hydrogen, 1931.
[12] M. Kuczynski, M. Oyevaar, R. Pieters, K. Westerterp, Methanol synthesis in a counter-current gas–solid–solid trickle flow reactor, Chemical Engineering Science 42 (1987) 1887-1898.
[13] D. Agar, W. Ruppel, Extended reactor concept for dynamic DeNox design, Chemical Engineering Science 43 (1988) 2079-2085.
[14] G.G. Vaporciyan, R.H. Kadlec, Equilibrium-Limited Periodic Separating Reactors, AIChE Journal 33 (1987) 1334-1343.
[15] G.G. Vaporciyan, R.H. Kadlec, Periodic Separating Reactors : Experiments and Theory, AIChE Journal 35 (1989) 831-844.
[16] D.M. Ruthven, Principles of Adsorption and Adsorption Processes, Wiley, 1984.
[17] R.T. Yang, Gas Separation by Adsorption Processes, Imperial College Press, 1997.
[18] H. Schmidt-Traub, A. Gorak, Integrated Reaction and Separation Operations, Springer, 2006.
[19] B.T. Carvill, J.R. Hufton, M. Anand, S. Sircar, Sorption-enhanced reaction process, AIChE Journal 42 (1996) 2765-2772.
[20] J. van Kampen, J. Boon, F. van Berkel, H. van Dijk, J. Vente, M. van Sint Annaland, Regeneration conditions as the key to sorption enhanced dimethyl ether synthesis, 25th International Symposium on Chemical Reaction Engineering, Florence, 2018.
[21] S. Walspurger, G.D. Elzinga, J.W. Dijkstra, M. Saric, W.G. Haije, Sorption enhanced methanation for substitute natural gas production: Experimental results and thermodynamic considerations, Chemical Engineering Journal 242 (2014) 379-386.

[22] A. Borgschulte, N. Gallandat, B. Probst, R. Suter, E. Callini, D. Ferri, Y. Arroyo, R. Erni, H. Geerlings, A. Züttel, Sorption enhanced CO_2 methanation, Physical Chemistry Chemical Physics 15 (2013) 9620-9620.
[23] W. Haije, H. Geerlings, Efficient Production of Solar Fuel Using Existing Large Scale Production Technologies, Environmental Science & Technology 45 (2011) 8609–8610.
[24] M. Ghodhbene, F. Bougie, P. Fongarland, M.C. Iliuta, Hydrophilic zeolite sorbents for in-situ water removal in high temperature processes, The Canadian Journal of Chemical Engineering 95 (2017) 1842-1849.
[25] D.W. Agar, Multifunctional reactors : Old preconceptions and new dimensions, Chemical Engineering Science 54 (1999) 1299-1305.
[26] M.P. Elsner, C. Dittrich, D.W. Agar, Adsorptive reactors for enhancing equilibrium gas-phase reactions — two case studies, Chemical Engineering Science 57 (2002) 1607-1619.
[27] M.P. Elsner, M. Menge, C. Müller, D.W. Agar, The Claus process : teaching an old dog new tricks, Catalysis Today 79-80 (2003) 487-494.
[28] H.-J. Kim, H. Jung, K.-Y. Lee, Effect of Water on Liquid Phase DME Synthesis from Syngas over Hybrid Catalysts Composed of Cu/ZnO/Al_2O_3 and γ-Al_2O_3, Korean Journal of Chemical Engineering 18 (2001) 838-841.
[29] S. Ressler, M. Elsner, C. Dittrich, D. Agar, S. Geisler, O. Hinrichsen, Reactive gas adsorption, Integrated Reaction and Separation Operations, Springer, 2006.
[30] J. van Kampen, S. Booneveld, J. Boon, M. van Sint Annaland, Catalytic aspects of sorption enhanced dimethyl ether synthesis, CHAINS 2017, Veldhoven, 2017.
[31] A. Borgschulte, E. Callini, N. Stadie, Y. Arroyo, M.D. Rossell, R. Erni, H. Geerlings, A. Züttel, D. Ferri, Manipulating the reaction path of the CO_2 hydrogenation reaction in molecular sieves, Catalysis Science & Technology 5 (2015) 4613-4621.
[32] R. Delmelle, J. Terreni, A. Remhof, A. Heel, J. Proost, A. Borgschulte, Evolution of Water Diffusion in a Sorption-Enhanced Methanation Catalyst, Catalysts 8 (2018) 341-355.
[33] R. Delmelle, R.B. Duarte, T. Franken, D. Burnat, L. Holzer, A. Borgschulte, A. Heel, Development of improved nickel catalysts for sorption enhanced CO_2 methanation, International Journal of Hydrogen Energy 41 (2016) 20185-20191.
[34] J.-C. Choi, L.-N. He, H. Yasuda, T. Sakakura, Selective and high yield synthesis of dimethyl carbonate directly from carbon dioxide and methanol, Green Chemistry 4 (2002) 230-234.
[35] J. George, Y. Patel, S.M. Pillai, P. Munshi, Methanol assisted selective formation of 1,2-glycerol carbonate from glycerol and carbon dioxide using $^nBu_2SnO$ as a catalyst, Journal of Molecular Catalysis A: Chemical 304 (2009) 1-7.
[36] H. Secker, V. Zafirakis, Choosing 3A or 4A Molecular Sieve for Natural Gas Dehydration, Gas Processors Association - Europe (2016) 1-15.
[37] S. Sircar, A. Myers, Gas Separation by Zeolites, Handbook of Zeolite Science and Technology, CRC, 2003.

[38] K. Coenen, F. Gallucci, G. Pio, P. Cobden, E.V. Dijk, E. Hensen, M.V. Sint, On the influence of steam on the CO 2 chemisorption capacity of a hydrotalcite-based adsorbent for SEWGS applications, Chemical Engineering Journal 314 (2017) 554-569.
[39] W. Zhu, L. Gora, A.W.C. van den Berg, F. Kapteijn, J.C. Jansen, J.A. Moulijn, Water vapour separation from permanent gases by a zeolite-4A membrane, Journal of Membrane Science 253 (2005) 57-66.
[40] J.B. Lad, Y.T. Makkawi, Adsorption of dimethyl ether (DME) on zeolite molecular sieves, Chemical Engineering Journal 256 (2014) 335-346.
[41] B. Peng, H. Dou, H. Shi, E.E. Ember, J.A. Lercher, Overcoming Thermodynamic Limitations in Dimethyl Carbonate Synthesis from Methanol and CO_2, Catalysis Letters 148 (2018) 1914-1919.
[42] B.A.V. Santos, V.M.T.M. Silva, J.M. Loureiro, E. Rodrigues, Adsorption of H_2O and Dimethyl Carbonate at High Pressure over Zeolite 3A in Fixed Bed Column, Industrial & Engineering Chemistry Research 53 (2014) 2473−2483.
[43] Y. Yuan, H. Zhang, F. Yang, N. Zhang, X. Cao, Inorganic composite sorbents for water vapor sorption: A research progress, Renewable and Sustainable Energy Reviews 54 (2016) 761-776.
[44] Z. Pan, C.Y. Zhao, Dehydration/hydration of MgO/H_2O chemical thermal storage system, Energy 82 (2015) 611-618.
[45] B. Dou, C. Wang, Y. Song, H. Chen, B. Jiang, M. Yang, Y. Xu, Solid sorbents for in-situ CO_2 removal during sorption-enhanced steam reforming process: A review, Renewable and Sustainable Energy Reviews 53 (2016) 536-546.
[46] J. Boon, P.D. Cobden, H.A.J. van Dijk, C. Hoogland, E.R. van Selow, M. van Sint Annaland, Isotherm model for high-temperature, high-pressure adsorption of and on K-promoted hydrotalcite, Chemical Engineering Journal 248 (2014) 406-414.
[47] C. Unluer, A. Al-Tabbaa, Characterization of Light and Heavy Hydrated Magnesium Carbonates Using Thermal Analysis, Journal of Thermal Analysis and Calorimetry 115 (2014) 595-607.
[48] A. Kohl, R. Nielsen, Gas Dehydration and Purification by Adsorption, Gas Purification, Gulf Publishing Company, 1997.
[49] P.S. Lawrence, M. Gru, W. Dietrich, D.W. Agar, Optimal Distribution of Catalyst and Adsorbent in an Adsorptive Reactor at the Reactor Level, Industrial & Engineering Chemistry Research 45 (2006) 4911-4917.
[50] I. Iliuta, M.C. Iliuta, F. Larachi, Sorption-enhanced dimethyl ether synthesis — Multiscale reactor modeling, Chemical Engineering Science 66 (2011) 2241-2251.
[51] M. Bayat, M. Heravi, M.R. Rahimpour, Sorption enhanced process by integrated heat-exchanger reactor assisted by fluidization concept for methanol synthesis, Chemical Engineering and Processing: Process Intensification 110 (2016) 30-43.

[52] E. Gabruś, J. Nastaj, P. Tabero, T. Aleksandrzak, Experimental studies on 3A and 4A zeolite molecular sieves regeneration in TSA process: Aliphatic alcohols dewatering-water desorption, Chemical Engineering Journal 259 (2015) 232-242.
[53] B. Mette, H. Kerskes, H. Drück, H. Müller-Steinhagen, Experimental and numerical investigations on the water vapor adsorption isotherms and kinetics of binderless zeolite 13X, International Journal of Heat and Mass Transfer 71 (2014) 555-561.
[54] A. Abufares, S. Engell, Optimal Operation of the Cyclic Claus Process, in: V. Plesu, P.S. Agachi (Eds.) 17th European Symposium on Computer Aided Process Engineering – ESCAPE17, 2007.
[55] K. Klier, V. Chatikavanij, R.G. Herman, G.W. Simmons, Catalytic synthesis of methanol from CO/H_2, Journal of Catalysis 74 (1982) 343-360.
[56] S. Noorman, Packed bed reactor technology for chemical-looping combustion, University of Twente, Enschede, 2009.
[57] S. Noorman, M.v.S. Annaland, H. Kuipers, Packed Bed Reactor Technology for Chemical-Looping Combustion, Indutrial & Engineering Chemistry Research 46 (2007) 4212-4220.
[58] A.A.M. Parra, C. Asmanoglo, D.W. Agar, Cyclic Steady-State Behavior of a Fixed-Bed Adsorptive Reactor for Reverse Water-Gas Shift Reaction, Chemical & Engineering Technology 40 (2017) 915-926.
[59] A.A.M. Parra, C. Asmanoglo, D.W. Agar, Modelling and optimization of a moving-bed adsorptive reactor for the reverse water-gas shift reaction, Computers and Chemical Engineering 109 (2018) 203-215.
[60] B.A.V. Santos, C.S.M. Pereira, V.M.T.M. Silva, J.M. Loureiro, A.E. Rodrigues, Design of a true moving bed reactor for the direct synthesis of dimethyl carbonate, Chemical Engineering Science 123 (2015) 406-419.
[61] M. Bayat, Conversion of syngas to liquid hydrocarbons via a sorption-enhanced dual bed reactor, Petroleum Science and Technology 35 (2017) 1839-1845.
[62] I. Iliuta, F. Larachi, P. Fongarland, Dimethyl Ether Synthesis with in situ H_2O Removal in Fixed-Bed Membrane Reactor: Model and Simulations, Industrial & Engineering Chemistry Research 49 (2010) 6870-6877.
[63] N. Diban, A.M. Urtiaga, I. Ortiz, J. Ereña, J. Bilbao, A.T. Aguayo, Influence of the membrane properties on the catalytic production of dimethyl ether with in situ water removal for the successful capture of CO_2, Chemical Engineering Journal 234 (2013) 140-148.
[64] M.D. Falco, M. Capocelli, A. Basile, Selective membrane application for the industrial one-step DME production process fed by CO_2 rich streams: Modeling and simulation, International Journal of Hydrogen Energy (2017) 6771-6786.
[65] M.D. Falco, M. Capocelli, G. Centi, Dimethyl ether production from CO_2 rich feedstocks in a one-step process: thermodynamic evaluation and reactor simulation, Chemical Engineering Journal (2016) 400-409.

[66] H. Mengers, Membrane reactors for the direct conversion of CO_2 to dimethyl carbonate, University of Twente, Enschede, 2015.
[67] H.J. Kuenen, H.J. Mengers, A.G.J.V.D. Ham, A. Kiss, Novel Process for Conversion of CO_2 to Dimethyl Carbonate using Catalytic Membrane Reactors, in: Z. Kravanja, M. Bogataj (Eds.) 26th European Symposium on Computer Aided Process Engineering – ESCAPE 26, Elsevier, Portorož, 2016.
[68] H.J. Kuenen, H.J. Mengers, D.C. Nijmeijer, A.G.J.V.D. Ham, A.A. Kiss, Techno-economic evaluation of the direct conversion of CO_2 to dimethyl carbonate using catalytic membrane reactors, Computers and Chemical Engineering 86 (2016) 136-147.
[69] N. Diban, A.M. Urtiaga, I. Ortiz, J. Ereña, J. Bilbao, A.T. Aguayo, Improved Performance of a PBM Reactor for Simultaneous CO_2 Capture and DME Synthesis, Industrial & Engineering Chemistry Research 53 (2014) 19479-19487.
[70] M. Farniaei, M. Abbasi, A. Rasoolzadeh, M.R. Rahimpour, Performance enhancement of thermally coupling of methanol synthesis, DME synthesis and cyclohexane dehydrogenation processes: Employment of water and hydrogen perm-selective membranes via different recycle streams, Chemical Engineering and Processing: Process Intensification 85 (2014) 24-37.
[71] M. Farsi, A. Hallaji Sani, P. Riasatian, Modeling and operability of DME production from syngas in a dual membrane reactor, Chemical Engineering Research and Design 112 (2016) 190-198.
[72] B. Santos, V. Silva, J. Loureiro, A. Rodrigues, Review for the Direct Synthesis of Dimethyl Carbonate, ChemBioEng Reviews 1 (2014) 214-229.
[73] R.L. Espinoza, E. Toit, J. Santamaria, M. Menendez, J. Coronas, S. Irusta, Use of membranes in Fischer-Tropsch reactors, Studies in Surface Science and Catalysis 130 (2000) 389-394.
[74] R. Espinoza, E.d. Toit, J. Santamaria, M. Menendez, J. Coronas, S. Irusta, Production of Hydrocarbons, 1999.
[75] M. Rohde, D. Unruh, G. Schaub, Membrane application in Fischer-Tropsch synthesis to enhance CO_2 hydrogenation, Industrial & Engineering Chemistry Research (2005) 9653-9658.
[76] M. Rohde, G. Schaub, J. Vente, H.v. Veen, Fischer-Tropsch synthesis with in-situ H2O removal by a new hydrophilic membrane - An experimental and modelling study, DGMK Tagungsbericht (2006) 215-222.
[77] M.P. Rohde, G. Schaub, S. Khajavi, J.C. Jansen, F. Kapteijn, Fischer – Tropsch synthesis with in situ H_2O removal – Directions of membrane development, Microporous and Mesoporous Materials 115 (2008) 123-136.
[78] M. Rohde, In situ H_2O removal via hydrophilic membranes during Fischer-Tropsch and other fuel-related synthesis reactions, Karlsruhe Institut für Technologie, Karlsruhe, 2010.

[79] K.-H. Lee, M.-Y. Youn, B. Sea, Preparation of hydrophilic ceramic membranes for a dehydration membrane reactor, Desalination 191 (2006) 296-302.
[80] D.A. Fedosov, A.V. Smirnov, V.V. Shkirskiy, T. Voskoboynikov, I.I. Ivanova, Methanol dehydration in NaA zeolite membrane reactor, Journal of Membrane Science 486 (2015) 189-194.
[81] F. Gallucci, L. Paturzo, A. Basile, An experimental study of CO_2 hydrogenation into methanol involving a zeolite membrane reactor, Chemical Engineering and Processing 43 (2004) 1029-1036.
[82] F. Gallucci, A. Basile, A theoretical analysis of methanol synthesis from CO_2 and H_2 in a ceramic membrane reactor, International Journal of Hydrogen Energy 32 (2007) 5050-5058.
[83] K.-I. Sawamura, T. Shirai, M. Takada, Selective permeation and separation of steam from water–methanol–hydrogen gas mixtures through mordenite membrane, Catalysis Today 132 (2008) 182-187.
[84] R.P.W.J. Struis, S. Stucki, Verification of the membrane reactor concept for the methanol synthesis, Applied Catalysis A: General 216 (2001) 117-129.
[85] J. Gorbe, J. Lasobras, E. Francés, J. Herguido, M. Menéndez, I. Kumakiri, H. Kita, Preliminary study on the feasibility of using a zeolite A membrane in a membrane reactor for methanol production, Separation and Purification Technology 200 (2018) 164-168.
[86] H. Sijbesma, K. Nymeijer, R.V. Marwijk, R. Heijboer, J. Potreck, M. Wessling, Flue gas dehydration using polymer membranes, Journal of Membrane Science 313 (2008) 263-276.
[87] J. Holtbruegge, M. Wierschem, S. Steinruecken, D. Voss, L. Parhomenko, P. Lutze, Experimental investigation, modeling and scale-up of hydrophilic vapor permeation membranes: Separation of azeotropic dimethyl carbonate/methanol mixtures, Separation and Purification Technology 118 (2013) 862-878.
[88] J. Holtbruegge, M. Wierschem, P. Lutze, Chemical Engineering and Processing : Process Intensification Synthesis of dimethyl carbonate and propylene glycol in a membrane-assisted reactive distillation process : Pilot-scale experiments , modeling and process analysis, Chemical Engineering & Processing: Process Intensification 84 (2014) 54-70.
[89] S. Khajavi, J.C. Jansen, F. Kapteijn, Application of hydroxy sodalite films as novel water selective membranes, Journal of Membrane Science 326 (2009) 153-160.
[90] M. Lafleur, F. Bougie, N. Guilhaume, F. Larachi, P. Fongarland, M.C. Iliuta, Development of a water-selective zeolite composite membrane by a new pore-plugging technique, Microporous and Mesoporous Materials 237 (2017) 49-59.
[91] N. Wang, Y. Liu, A. Huang, J. Caro, Supported SOD membrane with steam selectivity by a two-step repeated hydrothermal synthesis, Microporous and Mesoporous Materials 192 (2014) 8-13.
[92] N. Wang, Y. Liu, A. Huang, J. Caro, Hydrophilic SOD and LTA membranes for membrane-supported methanol, dimethylether and dimethylcarbonate synthesis, Microporous and Mesoporous Materials 207 (2015) 33-38.

[93] C.S.M. Pereira, A.E. Rodrigues, Process intensification: New technologies (SMBR and PermSMBR) for the synthesis of acetals, Catalysis Today 218-219 (2013) 148-152.
[94] V.M.T.M. Silva, C.S.M. Pereira, A.E. Rodrigues, PermSMBR — A New Hybrid Technology: Application on Green Solvent and Biofuel Production, AIChE Journal 57 (2011) 1840-1851.
[95] N. Diban, A.T. Aguayo, J. Bilbao, A. Urtiaga, I. Ortiz, Membrane Reactors for in Situ Water Removal: A Review of Applications, Industrial & Engineering Chemistry Research 52 (2013) 10342−10354.
[96] M. Bernal, E. Piera, J. Coronas, M. Menendez, J. Santamarıa, Mordenite and ZSM-5 hydrophilic tubular membranes for the separation of gas phase mixtures, Catalysis Today 56 (2000) 221-227.
[97] H. Wang, Y.S. Lin, Effects of Water Vapor on Gas Permeation and Separation Properties of MFI Zeolite Membranes at High Temperatures, AIChE Journal 58 (2012) 153-162.
[98] E. Piera, M. Salomon, J. Coronas, M. Menendez, J. Santamaria, Synthesis, characterization and separation properties of a composite mordenite/ZSM-5/chabazite hydrophilic membrane, Journal of Membrane Science 149 (1998) 99-114.
[99] S.A.S. Rezai, J. Lindmark, C. Andersson, F. Jareman, K. Möller, J. Hedlund, Water/hydrogen/hexane multicomponent selectivity of thin MFI membranes with different Si/Al ratios, Microporous and Mesoporous Materials 108 (2008) 136-142.
[100] K. Aoki, K. Kusakabe, S. Morooka, Gas permeation properties of A-type zeolite membrane formed on porous substrate by hydrothermal synthesis, Journal of Membrane Science 141 (1998) 197-205.
[101] K. Aoki, K. Kusakabe, S. Morooka, Separation of Gases with an A-Type Zeolite Membrane, Industrial & Engineering Chemistry Research 39 (2000) 2245-2251.
[102] B. Ilić, S.G. Wettstein, A review of adsorbate and temperature-induced zeolite framework flexibility, Microporous and Mesoporous Materials 239 (2017) 221-234.
[103] J. Caro, M. Noack, Zeolite membranes – Recent developments and progress, Microporous and Mesoporous Materials 115 (2008) 215-233.
[104] S.M. Lee, N. Xu, J.R. Grace, A. Li, C.J. Lim, S.S. Kim, F. Fotovat, A. Schaadt, R.J. White, Structure, stability and permeation properties of NaA zeolite membranes for H2O/H2 and CH3OH/H2 separations, Journal of the European Ceramic Society 38 (2018) 211-219.
[105] L.A. Bernstein, C.R.F. Lund, Membrane reactors for catalytic series and series- parallel reactions, Journal of Membrane Science 77 (1993) 155-164.
[106] J. Boon, H. Li, J.W. Dijkstra, J.A.Z. Pieterse, 2-dimensional membrane separator modelling: Mass transfer by convection and diffusion, Energy Procedia 4 (2011) 699-706.
[107] J. Boon, J.A.Z. Pieterse, J.W. Dijkstra, M.V.S. Annaland, Modelling and systematic experimental investigation of mass transfer in supported palladium-based membrane separators, International Journal of Greenhouse Gas Control 11 (2012) 122-129.

[108] S. Jadhav, P. Vaidya, B. Bhanage, J. Joshi, Chemical Engineering Research and Design Catalytic carbon dioxide hydrogenation to methanol : A review of recent studies, Chemical Engineering Research and Design 92 (2014) 2557-2567.
[109] S. Recker, M. Skiborowski, C. Redepenning, W. Marquardt, A unifying framework for optimization-based design of integrated reaction – separation processes, Computers and Chemical Engineering 81 (2015) 260-271.
[110] G. Schembecker, S. Tlatlik, Process synthesis for reactive separations, Chemical Engineering and Processing 42 (2003) 179-189.
[111] A. Stankiewicz, Reactive separations for process intensification: an industrial perspective, Chemical Engineering & Processing 42 (2003) 137-144.
[112] J.P.M. Sanders, J.H. Clark, G.J. Harmsen, H.J. Heeres, J.J. Heijnen, S.R.A. Kersten, W.P.M.V. Swaaij, J.A. Moulijn, Chemical Engineering and Processing : Process Intensification Process intensification in the future production of base chemicals from biomass, Chemical Engineering & Processing: Process Intensification 51 (2012) 117-136.
[113] W. Seider, J. Seader, D. Lewin, S. Widagdo, Process Design Principles, third ed., Wiley, 2009.
[114] G.J. Harmsen, Industrial best practices of conceptual process design, Chemical Engineering and Processing 43 (2004) 677-681.
[115] J.C. Abanades, E.S. Rubin, M. Mazzotti, H.J. Herzog, On the climate change mitigation potential of CO_2 conversion to fuels, Energy & Environmental Science 10 (2017) 2491-2499.
[116] H.S. Fogler, Elements of Chemical Reaction Engineering, Prentice Hall PTR, 2006.
[117] A. Zachopoulos, E. Heracleous, Overcoming the equilibrium barriers of CO_2 hydrogenation to methanol via water sorption: A thermodynamic analysis, Journal of CO_2 Utilization 21 (2017) 360-367.
[118] A. Cybulski, J. Moulijn, Structured Catalysts and Reactors, second ed., CRC, 2005.
[119] T.A. Peters, J. Fontalvo, M.A.G. Vorstman, J.T.F. Keurentjes, Design directions for composite catalytic hollow fibre membranes for condensation reactions, Chemical Engineering Research and Design 82 (2004) 220-228.
[120] A. Rodrigues, Simulating moving bed: Design concepts and applications, OSPT-post-graduate course “Adsorption Processes” (2005).
[121] A.N. Antzara, A. Arregi, E. Heracleous, A.A. Lemonidou, In-depth evaluation of a ZrO_2 promoted CaO-based CO_2 sorbent in fl uidized bed reactor tests, Chemical Engineering Journal 333 (2018) 697-711.
[122] L. Di Felice, V. Middelkoop, V. Anzoletti, F. Snijkers, M. van Sint Annaland, F. Gallucci, New high temperature sealing technique and permeability data for hollow fiber BSCF perovskite membranes, Chemical Engineering and Processing: Process Intensification 107 (2016) 206-219.

Chapter 3. Sorption enhanced dimethyl ether synthesis model development and analysis

Abstract

The sorption enhanced DME synthesis process is a promising intensification, already achieving over 80% single-pass CO_2 conversion for a non-optimized system. The increased single-pass conversion requires less downstream separation and smaller recycle streams, especially for a CO_2-rich feed. A key optimization parameter for the process performance is the working capacity of the system. This capacity can be improved by optimizing the reactive adsorption conditions and the regeneration procedure. In this chapter, a detailed modelling study is performed to investigate the impact of various process parameters on the operating window and the interaction between different steps in a complete sorption enhanced DME synthesis cycle, and to compare its performance to other direct DME synthesis processes. The development of sorption enhanced DME synthesis, with its high efficiency carbon conversion, could play a significant role in the energy transition in which the carbon conversion will become leading.

This chapter is based on published work:

J. van Kampen et al., Sorption enhanced dimethyl ether synthesis for high efficiency carbon conversion: Modelling and cycle design, Journal of CO_2 Utilization 37 (2020) 295–308.

S. Guffanti et al., Reactor modelling and design for sorption enhanced dimethyl ether synthesis, Chemical Engineering Journal 404 (2021) 126573-126585.

3.1. Introduction

Dimethyl ether (DME) is projected to play an important role in the energy transition [1]. As explained in Chapter 1, indirect DME production is a two-step process. Intermediate methanol is synthesized from syngas, subsequently followed by the dehydration of methanol to DME in a separate reactor. The following equilibrium reactions are involved in DME synthesis:

Methanol synthesis:

$$CO_2 + 3\,H_2 \rightleftharpoons CH_3OH + H_2O \qquad \Delta H^0 = -49\ kJ/mol \qquad (1)$$

$$CO + 2\,H_2 \rightleftharpoons CH_3OH \qquad \Delta H^0 = -90\ kJ/mol \qquad (2)$$

Water-gas shift:

$$CO + H_2O \rightleftharpoons CO_2 + H_2 \qquad \Delta H^0 = -41\ kJ/mol \qquad (3)$$

Methanol dehydration:

$$2\,CH_3OH \rightleftharpoons CH_3OCH_3 + H_2O \qquad \Delta H^0 = -24\ kJ/mol \qquad (4)$$

Direct DME synthesis (from CO):

$$3\,CO + 3\,H_2 \rightleftharpoons CH_3OCH_3 + CO_2 \qquad \Delta H^0 = -245\ kJ/mol \qquad (5)$$

Sorption enhanced direct DME synthesis (from CO_2):

$$2\,CO_2 + 6\,H_2 \rightleftharpoons CH_3OCH_3 + 3\,H_2O \qquad \Delta H^0 = -122\ kJ/mol \qquad (6)$$

Both the methanol synthesis (Equations 1 and 2) and its subsequent dehydration (Equation 4) are thermodynamically limited, resulting in limited yield, extensive separations and large recycles. In recent years a lot of attention is going to the direct production of DME in a single-step process [2-15]. An advantage to operate methanol synthesis and methanol dehydration in one single step is that the subsequent dehydration of methanol removes it from the reaction medium and thereby shifts the reaction equilibrium for the methanol synthesis reaction. Direct DME synthesis (from CO and H_2) (Equation 5) reduces the extent of necessary process steps and allows for an increased overall DME yield. However, separation and recycling remain necessary.

Sorption enhanced DME synthesis (SEDMES) (Equation 6) is a novel process for the production of DME from synthesis gas [16, 17], in which water is removed in situ by the use of a solid adsorbent, typically a LTA zeolite [18, 19]. The concept is based on Le Chatelier's principle stating that reactant conversion to products in an equilibrium limited reaction is increased by selectively removing reaction products, which is utilized for various processes and products mainly considering CO_2 separation [20, 21]. By the removal of H_2O as reaction product, the oxygen surplus of the feed no longer ends up in CO_2, as is the case for direct DME synthesis. As a result, CO_2 can be used as feed, rather than being the main byproduct. In a sorption enhanced system, as the SEDMES process, the periodic regeneration of the saturated adsorbent is typically done by pressure swing, temperature swing,

purge/concentration swing or combinations of these methods. While the different regeneration procedures have their own typical duration (timings), the timing of adsorption and regeneration have to be carefully tuned. The simplest case would be a two-reactor column system, in which one column is producing the sorption enhanced product, while the other column is regenerating. However, the regeneration procedure typically consists of multiple steps and in general requires more time than the reactive adsorption. Therefore, multicolumn systems are usually designed for sorption enhanced processes. Figure 3-1 provides a schematic overview of the SEDMES process and the involved consecutive steps that a reactor column goes through during one full SEDMES cycle: one reactor is fed with syngas and produces DME during reactive adsorption, while the other reactors are regenerated by feeding a purge gas, are repressurized/depressurized for a pressure swing cycle, or heated/cooled for a temperature swing regeneration. Each of the columns continuously goes through the different steps of the SEDMES cycle consecutively. This relatively simple three-column SEDMES process is used as a base for the model study in this work and is shown in Figure 3-2.

This contribution presents an elaborate model study on the SEDMES process, investigating in detail the impact of various process parameters on the operating window, as well as the interaction of different cycle steps. Finally, the performance of the SEDMES process is compared to other direct DME synthesis processes at demonstration scale.

This chapter first introduces an elaborate model description, followed by a comparison of the model with experimental results. A full SEDMES cycle is described, and its performance is extensively studied. Finally, a comparison of SEDMES and direct DME synthesis is made.

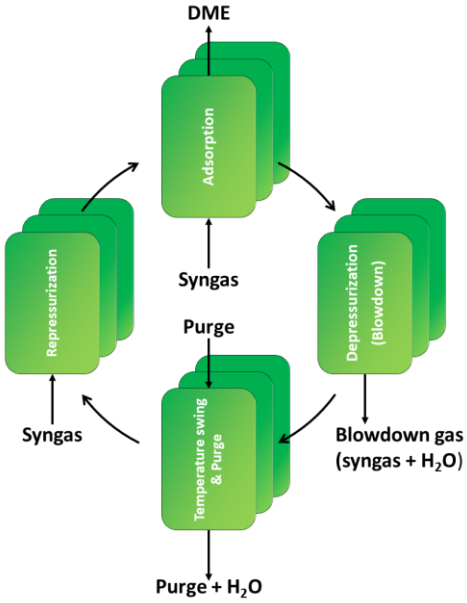

FIGURE 3-1: SCHEMATIC OVERVIEW OF THE SEDMES PROCESS STEPS (FOUR STEP TPSA CYCLE).

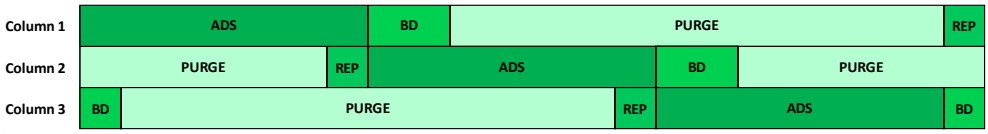

FIGURE 3-2: 3-COLUMN CYCLE DESIGN FOR A 4-STEP SEDMES PROCESS (ADS=ADSORPTION STEP, BD=BLOWDOWN STEP, PURGE=PURGE STEP, REP=REPRESSURIZATION STEP).

3.2. Model

To analyze the sorption enhanced DME synthesis process a cyclic one-dimensional, dynamic reactor model was developed, based on previous modelling experience for the sorption enhanced water-gas shift process [22, 23]. The cyclic model solves the consecutive steps in the cycle using a fixed-bed pseudo-homogeneous reactor model, assuming a homogeneous mixture of direct DME synthesis catalyst and LTA zeolite particles. The different aspects of the model, viz. the conservation equations on the reactor and particle scale, reaction kinetics and adsorption isotherms and the model parameters and numerical solution strategy, are shortly outlined in the next sections.

3.2.1. Mass, momentum and energy conservation for gas and particle phase

For the description of the fluid flow and mass transfer, the 1D non-steady non-isothermal differential mass and momentum balances are solved. The total mass and momentum balances, component material balances and overall energy balance are given in Table 3-1. Constitutive equations have been taken from the literature [24-28].

TABLE 3-1: REACTOR MODEL EQUATIONS.

Continuity	$\frac{\partial \rho}{\partial t} = -\frac{\partial \rho v}{\partial z} - \frac{1-\varepsilon_b}{\varepsilon_b} a_p \sum M_i N_i$	(7)
Momentum	$\frac{\partial \rho v}{\partial t} = -\frac{\partial \rho v^2}{\partial z} - \frac{\partial P}{\partial z} - G\frac{\rho \lvert u \rvert u}{d_p}$	(8)
Species mass balance	$\frac{\partial \rho \omega_i}{\partial t} = -\frac{\partial \rho v \omega_i}{\partial z} + \frac{\partial}{\partial z}\left(D_z \rho \frac{\partial \omega_i}{\partial z}\right) - \frac{1-\varepsilon_b}{\varepsilon_b} a_p M_i N_i$	(9)
Overall energy balance	$(\varepsilon_b \rho Cp + (1-\varepsilon_b)\rho_p Cp_p)\frac{\partial T}{\partial t} = -\rho Cpu\frac{\partial T}{\partial z} + \frac{\partial}{\partial z}\left(\lambda \frac{\partial T}{\partial z}\right) + \frac{4U(T_w - T)}{d_r} + (1-\varepsilon_b)\rho_p\left(\sum -\Delta H_{r,i} r_i + \sum -\Delta H_{ads,i}\frac{\partial \overline{q_i}}{\partial t}\right)$	(10)
Equation of state	$PM = \rho RT$	(11)

Particle-scale model

To account for intraparticle species concentration profiles inside both the catalyst and the adsorbent particles a linear driving force (LDF) approximation is used (Table 3-2), thus accounting for intraparticle transport (expressed by the flux N_i), reaction and adsorption (Equation 12), and intracrystalline transport and adsorption (Equation 13). Glueckauf has shown that when the conditions are close enough to equilibrium ($D_e t/R_p^2 > 0.1$) a LDF approximation holds [26]. In these equations $\bar{c}$ is the average concentration in the particle, whereas $\bar{q}$ is the average amount adsorbed in the adsorbent particles, and q^* is the amount adsorbed in equilibrium with the (bulk) concentration, which is given by the adsorption isotherm of steam on the zeolite adsorbent (see section 3.2.3). The equations for the intraparticle model are derived from the common linear driving force approximation for porous spherical particles, including the effective macro- and micropore diffusion (D_p, D_c) [24].

TABLE 3-2: INTRAPARTICLE EQUATIONS.

Intraparticle mass balance	$\frac{\partial \bar{c}_i}{\partial t} = k_{LDF,1}\left(\frac{\rho\omega_i}{M_i} - \bar{c}_i\right) + f_{cat}\frac{\rho_p}{\varepsilon_p} r_i - (1 - f_{cat})\frac{\rho_p}{\varepsilon_p}\frac{\partial \bar{q}_i}{\partial t}$	(12)
Intracrystalline mass balance	$\frac{\partial \bar{q}_i}{\partial t} = k_{LDF,2}(q_i^* - \bar{q}_i)$	(13)
Mass transfer coefficients	$k_{LDF,1} = \frac{15 D_p}{r_p^2}$	(14)
	$k_{LDF,2} = \frac{15 D_c}{r_c^2}$	(15)

3.2.2. Reaction kinetics

The direct DME synthesis catalyst is a bifunctional catalyst [17, 29], which is considered to be a mixture of a methanol synthesis catalyst ($Cu/ZnO/Al_2O_3$) and a methanol dehydration catalyst (γ-Al_2O_3, [18]). For the methanol synthesis (1,2) and the water-gas shift reaction (3) the kinetic expressions by Graaf et al. and Vanden Bussche et al. are used [14, 30, 31] (Table 3-3). Although the expressions allow using partial fugacities, initially partial pressures are used according to the equation of state. In Table 3-4 the kinetic and adsorption constants are defined according to Van 't Hoff relations [14, 30]. The equilibrium constants are taken from Graaf et al. (1986) [32]. For the methanol dehydration reaction (Equation 4) the kinetic expression by Berčič et al. (1992) is used [18, 33]. The kinetic and adsorption constants by Ng et al. (1999) (adapted from Berčič et al.) are again defined according to Van 't Hoff relations [14]. The equilibrium constant is given by Zhiliang et al. (2004), from Hu et al. (1990) [34].

TABLE 3-3: REACTION RATE EQUATIONS FOR METHANOL SYNTHESIS AND METHANOL DEHYDRATION.

Methanol synthesis from CO (Graaf et al. [30])	$r_{CH3OH,1} = \frac{k_1 K_{CO}\left[\varphi_{CO}\varphi_{H2}^{3/2} - \varphi_{CH3OH}/\left(\varphi_{H2}^{1/2} K_{p1}\right)\right]}{(1+K_{CO}\varphi_{CO}+K_{CO2}\varphi_{CO2})\left[\varphi_{H2}^{1/2}+\left(K_{H2O}/K_{H2}^{1/2}\right)\varphi_{H2O}\right]}$	(16)
Water-gas shift (Graaf et al. [30])	$r_{CO} = \frac{k_2 K_{CO2}\left[\varphi_{CO2}\varphi_{H2} - \varphi_{H2O}\varphi_{CO}/K_{p2}\right]}{(1+K_{CO}\varphi_{CO}+K_{CO2}\varphi_{CO2})\left[\varphi_{H2}^{1/2}+\left(K_{H2O}/K_{H2}^{1/2}\right)\varphi_{H2O}\right]}$	(17)
Methanol synthesis from CO_2 (Graaf et al. [30])	$r_{CH3OH,2} = \frac{k_3 K_{CO2}\left[\varphi_{CO2}\varphi_{H2}^{3/2} - \varphi_{CH3OH}\varphi_{H2O}/\left(\varphi_{H2}^{3/2} K_{p3}\right)\right]}{(1+K_{CO}\varphi_{CO}+K_{CO2}\varphi_{CO2})\left[\varphi_{H2}^{1/2}+\left(K_{H2O}/K_{H2}^{1/2}\right)\varphi_{H2O}\right]}$	(18)
Water-gas shift (Vanden Bussche et al. [31])	$r_{RWGS} = \frac{k'_2\varphi_{CO2}\left[1-(1/K_{p2})(\varphi_{H2O}\varphi_{CO})/(\varphi_{CO2}\varphi_{H2})\right]}{\left(1+K_2(\varphi_{H2O}/\varphi_{H2})+\sqrt{K_3\varphi_{H2}}+K_4\varphi_{H2O}\right)}$	(19)
Methanol synthesis from CO_2 (Vanden Bussche et al. [31])	$r_{MeOH} = \frac{k'_3\varphi_{H2}\varphi_{CO2}\left[1-(1/K_{p3})(\varphi_{CH3OH}\varphi_{H2O})/(\varphi_{CO2}\varphi_{H2}{}^3)\right]}{\left(1+K_2(\varphi_{H2O}/\varphi_{H2})+\sqrt{K_3\varphi_{H2}}+K_4\varphi_{H2O}\right)^3}$	(20)
Methanol dehydration (Berčič et al. [33])	$r_{DME} = \frac{k_4 K_{CH3OH}^2\left[C_{CH3OH}^2 - C_{H2O}C_{DME}/K_{p4}\right]}{\left[1+2(K_{CH3OH}C_{CH3OH})^{1/2}+K_{H2O}C_{H2O}\right]^4}$	(21)

TABLE 3-4: KINETIC, ADSORPTION AND EQUILIBRIUM CONSTANTS FOR METHANOL SYNTHESIS AND METHANOL DEHYDRATION.

$k_1 = 2.69 \cdot 10^7 \exp\left(\frac{-109900}{RT}\right)$	(22)
$k_2 = 7.31 \cdot 10^8 \exp\left(\frac{-123400}{RT}\right)$	(23)
$k_3 = 4.36 \cdot 10^2 \exp\left(\frac{-65200}{RT}\right)$	(24)
$K_{CO} = 7.99 \cdot 10^{-7} \exp\left(\frac{58100}{RT}\right)$	(25)
$K_{CO2} = 1.02 \cdot 10^{-7} \exp\left(\frac{67400}{RT}\right)$	(26)
$K_{H2O}/K_{H2}^{\frac{1}{2}} = 4.13 \cdot 10^{-11} \exp\left(\frac{104500}{RT}\right)$	(27)
$k'_2 = 1.09 \cdot 10^{10} \exp\left(\frac{-94765}{RT}\right)$	(28)
$k'_3 = 1.65 \cdot \exp\left(\frac{-36696}{RT}\right)$	(29)
$K_2 = 3.61 \cdot 10^3$	(30)
$K_3 = 0.37 \cdot \exp\left(\frac{17197}{RT}\right)$	(31)
$K_4 = 7.14 \cdot 10^{-11} \exp\left(\frac{124119}{RT}\right)$	(32)
$\log_{10} K_{p1} = \frac{5139}{T} - 12.621$	(33)
$\log_{10} K_{p2} = \frac{-2073}{T} + 2.029$	(34)
$k_4 = 3.7 \cdot 10^{10} \exp\left(\frac{-105000}{RT}\right)$	(35)

$$K_{CH3OH} = 7.9 \cdot 10^{-4} \exp\left(\frac{70500}{RT}\right) \quad (36)$$

$$K_{H2O} = 0.84 \cdot 10^{-1} \exp\left(\frac{41100}{RT}\right) \quad (37)$$

$$\ln K_{p4} = \frac{4019}{T} + 3.707 \ln T - 2.783 \cdot 10^{-3} T + 3.8 \cdot 10^{-7} T^2 - 6.561 \cdot 10^4 / T^2 - 26.64 \quad (38)$$

Because equation (18) (reaction rate expression for the methanol synthesis from CO_2) can be written as the stoichiometric sum of equations (16) and (17), K_{p3} can be calculated as:

$$K_{p3} = K_{p1} \cdot K_{p2} \quad (39)$$

And thus:

$$\log_{10} K_{p3} = \frac{3066}{T} - 10.592 \quad (40)$$

3.2.3. Adsorption isotherm and kinetics

The direct DME synthesis catalyst is mixed homogeneously with a LTA zeolite adsorbent. Steam is considered to be the only adsorbed component, due to the high affinity for its adsorption by the zeolite adsorbent. Gabruś et al. (2015) derived a Langmuir-Freundlich isotherm model for zeolite 3A from adsorption equilibrium data at elevated temperatures (up to 250 °C) [35], which is shown in Table 3-5. In these equations q is the adsorbent loading (mol kg^{-1}), q_s is the saturation loading (mol kg^{-1}), p is the partial pressure of the adsorbate (Pa), and T is the temperature (K). The values for the isotherm constants can be found in Table 3-6.

TABLE 3-5: ISOTHERM MODEL [35].

$$q = q_s \frac{bp^n}{1+bp^n} \quad (41)$$

$$q_s = a_0 + \frac{a_1}{T} + \frac{a_2}{T^2} \quad (42)$$

$$b = exp\left(b_0 + \frac{b_1}{T} + \frac{b_2}{T^2}\right) \quad (43)$$

$$n = n_0 + \frac{n_1}{T} \quad (44)$$

TABLE 3-6: LANGMUIR-FREUNDLICH ADSORPTION ISOTHERM CONSTANTS ACCORDING TO GABRUŚ ET AL. (2015) [35].

Isotherm parameters	Value
a_0 (mol kg^{-1})	0.24486
a_1 (mol kg^{-1} K)	-29.161
a_2 (mol kg^{-1} K^2)	743.36
b_0 (Pa^{-1})	-10.659
b_1 (Pa^{-1} K)	1969.4
b_2 (Pa^{-1} K^2)	933.58

n_0 (-)	-0.09294
n_1 (K)	340.56

3.2.4. Model parameters

The pressure drop in a packed bed with porous particles is given by the Ergun equation [36]. The Ergun parameter *G* in Equation (8) is defined as given in Table 3-7. As mentioned above, both for the particle concentrations and the adsorbent species concentrations a double linear driving force (LDF) approximation is used. The LDF rate constants are given in Table 3-2. The effective diffusivities are given by the micropore (intracrystalline) D_c and macropore (intercrystalline) diffusivity D_p respectively. Since the adsorption of gases occurs in the zeolite crystals, where diffusion is slow, intracrystalline diffusion has an important or even rate limiting role in the adsorption and desorption [26]. The molecular gas diffusivity D_m was calculated using Blanc's law [27] and the binary diffusion coefficients are predicted according to Fuller and Poling [27, 37]. Axial dispersion is evaluated according to Wakao (for a rectangular isotherm), which is recommended for strongly adsorbed components under laminar flow conditions [24].

TABLE 3-7: MODEL PARAMETERS.

Ergun constant	$G = \frac{1-\varepsilon_b}{\varepsilon_b^3}\left(\frac{150(1-\varepsilon_b)}{Re_p} + 1.75\right)$	(45)
Reynolds number	$Re_p = \frac{\varepsilon_b \rho v d_p}{\mu}$	(46)
Macropore diffusivity	$D_p = \frac{\varepsilon_p D_m}{1.5} = \frac{\varepsilon_p D_m \sigma}{\tau}$	(47)
Molecular gas diffusivity	$D_{i,m} = \left(\sum_{\substack{j=1 \\ j\neq i}}^{n} \frac{x_j}{D_{i,j}}\right)^{-1}$	(48)
Binary diffusion coefficients	$D_{AB} = \frac{0.00143T^{1.75}}{PM_{AB}^{\frac{1}{2}}((\Sigma_A v_i)^{\frac{1}{3}}+(\Sigma_B v_i)^{\frac{1}{3}})^2}$	(49)
Axial dispersion	$D_z = \frac{20D_m}{\varepsilon_b} + \frac{v d_p}{2}$	(50)

All parameters in the energy balance (10) can be found in Table 3-8. The heat capacity of the individual gases and the mixture are calculated according to Poling et al. [27, 37]. The heat capacity of the solid phase is fixed at 960 J kg^{-1} K^{-1} [38]. The axial thermal conductivity is calculated according to Westerterp et al. [25]. The heat of reaction is evaluated using Kirschhoff's law and the heat of adsorption is fixed at -45.95 kJ mol^{-1} [35].

TABLE 3-8: ENERGY BALANCE PARAMETERS.

Gas heat capacity	$Cp_i = a + a_1 T + a_2 T^2 + a_3 T^3 + a_4 T^4$	(51)
Particle heat capacity	960	(52)

Axial thermal conductivity	$\lambda = \lambda_0 + \lambda_{t'}$	(53)
	$\lambda_{t'} = \frac{\rho c_p d_p u}{8 \cdot \left[2 - \left(1 - \frac{2d_p}{d_t}\right)^2\right]}$	(54)
	$\frac{\lambda_0}{\lambda_G} = 0.67\varepsilon + (1-\varepsilon)^{0.5} \cdot A$	(55)
	$C = 1.25$	(56)
	$B = C\left(\frac{1-\varepsilon}{\varepsilon}\right)^{1.11}$	(57)
	$A = \frac{2}{\left(1-\frac{\lambda_G B}{\lambda_S}\right)}\left[\frac{\left(1-\frac{\lambda_G}{\lambda_S}\right)B}{\left(1-\frac{\lambda_G B}{\lambda_S}\right)^2} ln\left[\frac{\lambda_S}{B\lambda_G}\right] - \frac{B+1}{2} - \frac{B-1}{\left(1-\frac{\lambda_G B}{\lambda_S}\right)}\right]$	(58)
Heat of reaction	$\Delta H_{r,i}(T_2) = \Delta H_{r,i}(T_1) + \Delta C_p \Delta T$	(59)
Heat of adsorption	-45.95 kJ mol^{-1}	(60)

3.2.5. Method of solution

The obtained system of partial differential equations is solved in Matlab as a set of ordinary differential equations following the Method of Lines. A method for stiff differential equations is used with Matlab built-in variable-step, variable-order solver ode15s after uniform spatial discretization in 30 finite differences, using a Barton flux delimited second-order upwind approximation for the convective terms. The feed flow rate and temperature are specified at the reactor inlet, the pressure at the reactor outlet. Danckwerts' boundary conditions are used at the inlet for the heat and mass balances and zero gradient boundary conditions at the outlet. Simulations are run until cyclic steady state is achieved, meaning that the results for each consecutive cycle are equal in terms of DME yield (relative tolerance 10^{-3}).

TABLE 3-9: REACTOR OPERATING CONDITIONS, BASE CASE SCENARIO.

Operating conditions	Value
Bed length (m)	0.2
Reactor diameter (m)	0.02
Bed voidage (-)	0.372
Particle diameter (m)	$318 \cdot 10^{-6}$
Particle (bulk) density (kg m^{-3})	1194
Particle porosity (-)	0.662
Crystal diameter (m)	$1 \cdot 10^{-6}$
Reactor temperature (K)	548.15

Reactor pressure (bara)	30
Regeneration temperature (K)	673.15
Regeneration pressure (bara)	3
GHSV (m^3_{syngas} hr^{-1} m^{-3}_{cat})	760

3.3. Results and discussion

To investigate the SEDMES process and determine its possible operation window, the effects of various process parameters on the sorption enhanced DME synthesis process was studied first using the developed model. The SEDMES process was considered as a three-column continuous system. While one column is operated in the reactive adsorption step, the other two columns are regenerating. The regeneration steps consist of a blowdown step (for pressure swing), a purge step including heating and cooling for temperature swing operation and a repressurization step (for pressure swing). The base case operating conditions are given in Table 3-9.

3.3.1. Sorption enhanced DME synthesis: experimental (breakthrough)

To validate the developed cyclic model, it was first used to predict the performance of sorption enhanced DME synthesis in a laboratory scale reactor (Table 3-9). Figure 3-3 and Figure 3-4 show a typical breakthrough experiment for sorption enhanced DME synthesis, as measured by van Kampen et al. [29]. During the first transient period, before steam breakthrough, DME is the major product together with some unconverted CO. After breakthrough of steam (inset Figure 3-3), the DME concentration drops combined with a breakthrough of CO_2 and methanol. In the steady state, when the adsorbent is fully saturated, the equilibrium for direct DME synthesis is obtained. As can be seen from Figure 3-3, the model with the kinetics taken from Graaf et al. [30] describes this experimentally observed behavior quite reasonably. In contrast to the model predictions using the kinetics from Vanden Bussche and Froment [31], which seem not to be able to describe the SEDMES process adequately due to the faster conversion of CO_2 and the lack of CO conversion in the absence of steam (Figure 3-4). In the next sections the kinetics from Graaf et al. will therefore be used to investigate the performance of a continuous SEDMES process rather than breakthrough experiments.

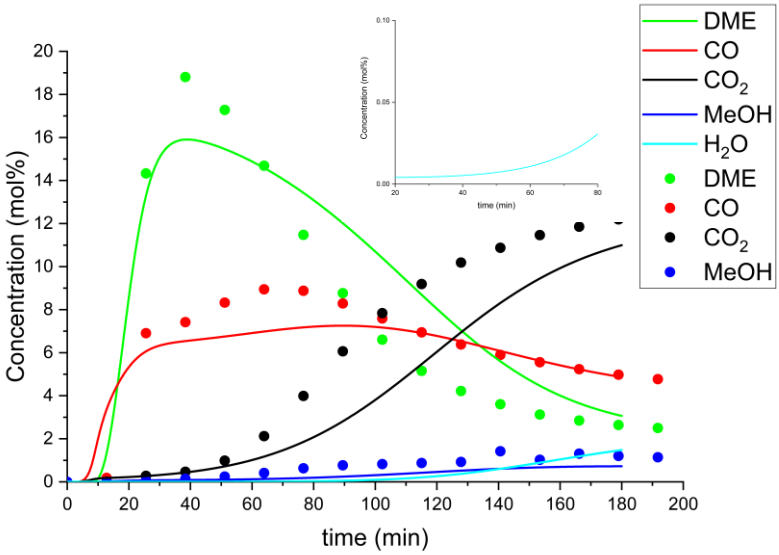

FIGURE 3-3: BREAKTHROUGH EXPERIMENT (POINTS) AND MODEL PREDICTION (LINES) WITH CZA KINETICS FROM GRAAF ET AL. [30] AT 40 BAR(A), 275 °C, FEED H_2:CO:CO_2 = 8:1:2 INCLUDING 30 VOL.% INERT (REGENERATION AT 3 BAR(A) AND 400 °C); EXPERIMENTAL DATA TAKEN FROM VAN KAMPEN ET AL. [29]. INSET SHOWS STEAM BREAKTHROUGH FROM 20 TO 80 MINUTES.

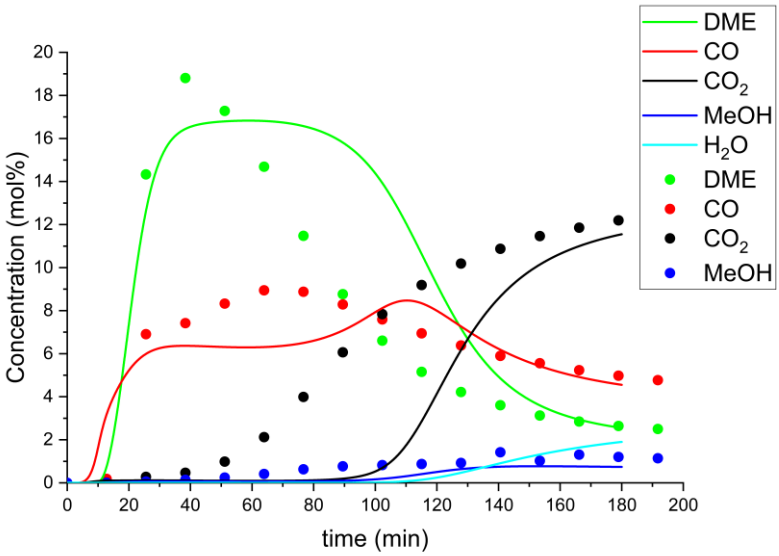

FIGURE 3-4: BREAKTHROUGH EXPERIMENT (POINTS) AND MODEL PREDICTION (LINES) WITH CZA KINETICS FROM VANDEN BUSSCHE AND FROMENT [31] AT 40 BAR(A), 275 °C, FEED H_2:CO:CO_2 = 8:1:2 INCLUDING 30 VOL.% INERT (REGENERATION AT 3 BAR(A) AND 400 °C); EXPERIMENTAL DATA TAKEN FROM VAN KAMPEN ET AL. [29].

3.3.2. Sorption enhanced DME synthesis: continuous process

A temperature swing (TSA) to 400 °C is considered for the regeneration in the SEDMES process, and a realistic duration of 1 hour heating and 2 hours of cooling during the purge step is selected. Together with the blowdown/depressurization (30 min) and the repressurization (15 min), this results in a total regeneration time of 3.75 hour (225 min). If the adsorption step is operated for half this time, 112.5 minutes, a three-column system can assure continuous production of DME, where one reactor column produces DME, while the other two columns are regenerating.

To investigate the effect of various process parameters on the performance of the SEDMES process some key performance indicators have to be addressed. The cyclic process has two input streams, the syngas feed and a purge gas, and three output streams, the DME product stream during the reactive adsorption step, a blowdown stream (containing syngas, some product and initially desorbed steam), and a purge gas stream containing desorbed steam. Time integration of the input and output streams gives an overall yield and selectivity for the cyclic steady state of the SEDMES process.

3.3.3. Base case

In the reactive adsorption step a syngas stream is fed to the SEDMES system and a DME enriched product stream is produced. In the base case, the syngas feed consists of a stoichiometric amount of H_2 to CO_x ($M = \frac{([H_2]-[CO_2])}{([CO]+[CO_2])} = 2$) and a CO_2 to CO ratio of 2. The DME product stream contains, besides DME, unreacted syngas and small amounts of methanol, inert gas (originating from the purge step), and steam slip (Figure 3-6). Although the conversion is already 64% (where the thermodynamic equilibrium without adsorption would yield 26% conversion for the current feed gas composition), a significant fraction of the product stream remains unconverted syngas due to the net moles consuming reaction. The yield towards DME is limited by the slip level of steam in the system. This remaining amount of steam can be affected by various process parameters, as discussed below.

The transient behavior of the system can be explained by the moving concentration fronts through the reactor bed, as shown in Figure 3-5. These figures show the gas phase concentration (wt.%) as a function of the axial coordinate in the reactor at the end of the repressurization, adsorption, blowdown and purge steps (equal to the beginning of the next step). For the reactive adsorption step and the purge step, profiles during the steps are shown as well. Figure 3-5a clearly shows the reaction front present in the reactor column, characterized by a high conversion towards DME. It can also be observed that nitrogen is present at the end of the reactor. This nitrogen is a remainder of the purge step. Nitrogen is still present in the reactor column at the end of the purge step (the column has been repressurized by syngas). During the first period of the adsorption step this leftover nitrogen is flushed out of the column, in Figure 3-5b showing the composition profile during the

adsorption step, the nitrogen is therefore totally gone. While undesirable for the SEDMES process, this inert N_2 purge clearly shows the effect of the purge gas on the adsorption step. This leftover N_2 can be prevented by the choice of a different purge gas and/or the addition of an extra step to the process. In the meantime, it can be observed that the water content starts increasing in the upstream half of the reactor, which results mainly in an increase in the CO_2 concentration and a decrease in the DME concentration (Figure 3-5b). This behavior continues until the end of the adsorption step. The nearly flat axial profile at the end of the adsorption step (Figure 3-5c) also confirms that the feed flow rate during the adsorption step is rather high, leading to water breakthrough. Hence, the column is not able to maintain sorption enhancement during the entire adsorption step. After the adsorption step the column is depressurized in the blowdown step. Figure 3-6 shows that the product from this step mainly consists of unconverted syngas and an initial part (about 2%) of the desorbed water. This initial desorption of water can also be observed from the axial profiles at the end of the adsorption, and therefore beginning of the blowdown step and at the end of the blowdown step (Figure 3-5c and d). As the blowdown product consists mainly of syngas, it could be considered to recycle this stream to the feed of the adsorption step (after repressurization and possibly drying). During the purge the remaining water (98% of the amount adsorbed) is desorbed to regenerate the adsorptive capacity of the adsorbent material. In Figure 3-6 it can be seen that the purge product primarily consists of the purge gas and desorbed steam. This high purge product purity allows knocking out H_2O from the purge stream and recycling the N_2 as purge gas. Figure 3-5e and f show that at the end of the three-hour purge period almost no water is removed from the column anymore. This indicates that the purge, and therefore total regeneration time, could be somewhat reduced, provided that the TSA regeneration would allow for faster heating and cooling of the reactor column. Figure 3-7 also shows that the adsorbent is regenerated almost completely after the purge. The axial profile of the water loading of the adsorbent material at the end of the purge step shows a small linear decrease due to the countercurrent operation of the regeneration. At the start of the adsorption step the axial loading profile shows a linear decrease over the length of the column due to the co-current repressurization with syngas, in which the sorption enhanced reaction starts to occur. At the end of the adsorption step the loading is in equilibrium with the water content in the gas phase (Figure 3-5c), defined by the adsorption isotherm.

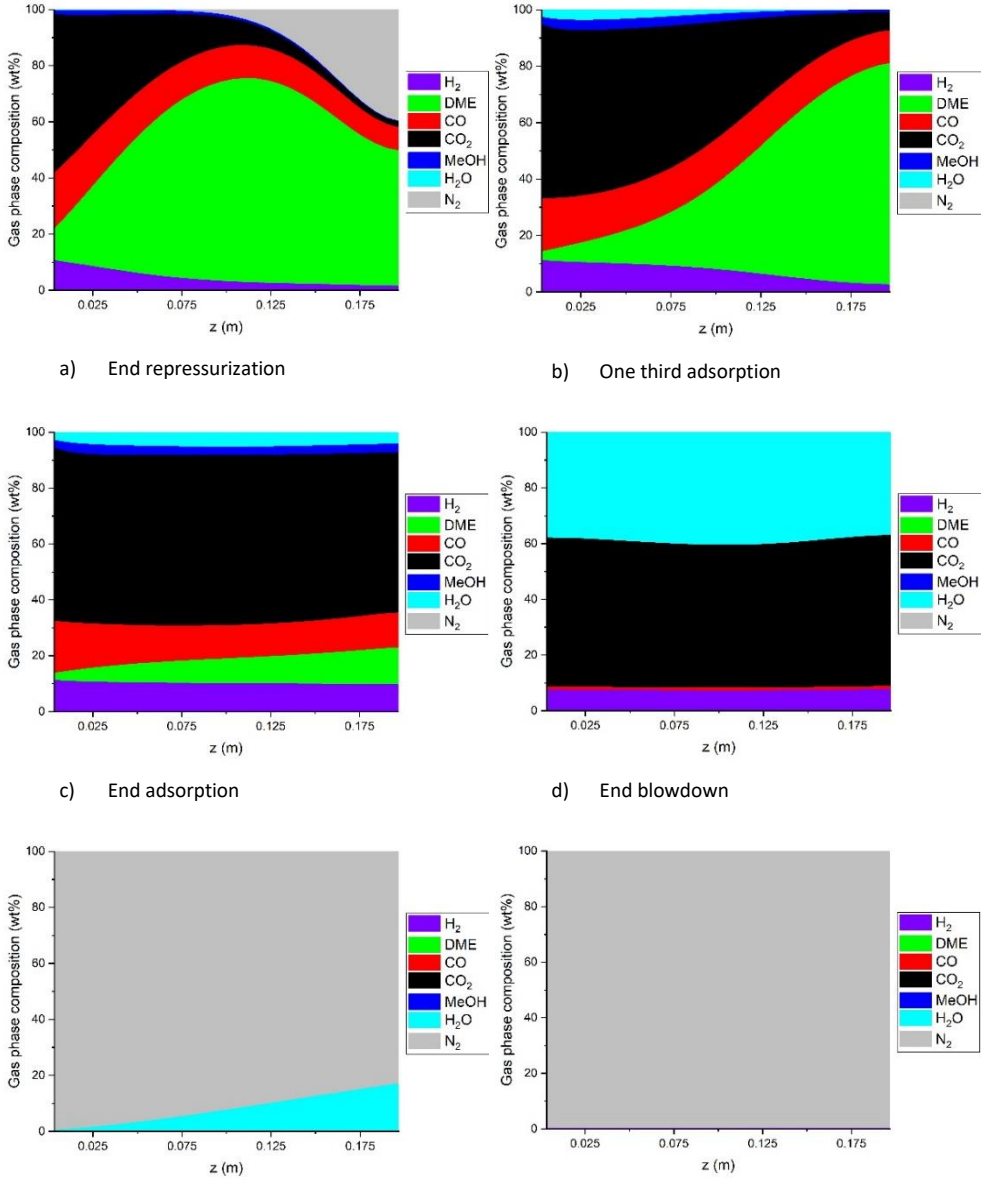

a) End repressurization

b) One third adsorption

c) End adsorption

d) End blowdown

e) One sixth purge

f) End purge

FIGURE 3-5: GAS PHASE CONCENTRATIONS VERSUS AXIAL COORDINATE AT THE END OF, AND DURING, THE VARIOUS STEPS IN A CYCLE FOR THE BASE CASE.

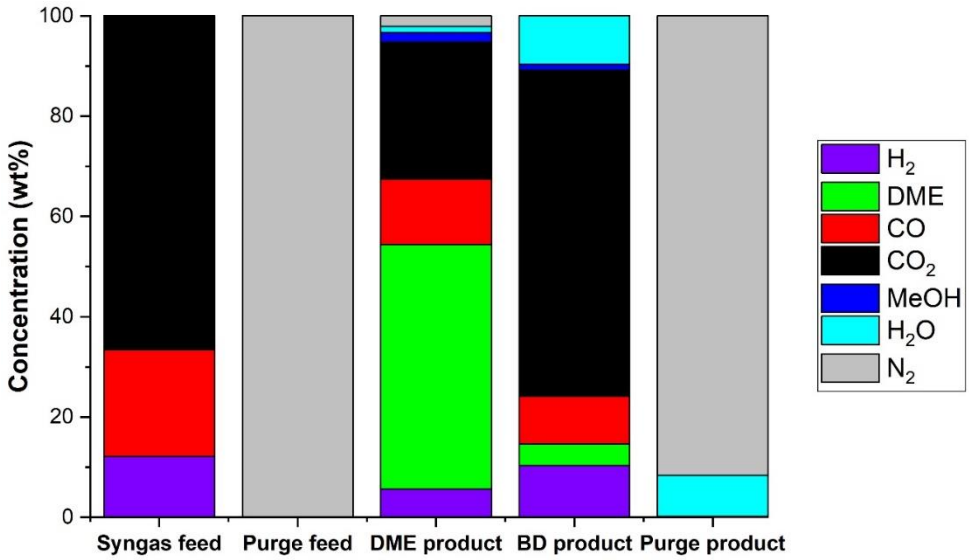

FIGURE 3-6: OVERVIEW OF THE CYCLIC STEADY-STATE COMPOSITION (WT.%) OF THE FEED AND PRODUCT STREAMS FOR THE BASE CASE SEDMES SCENARIO.

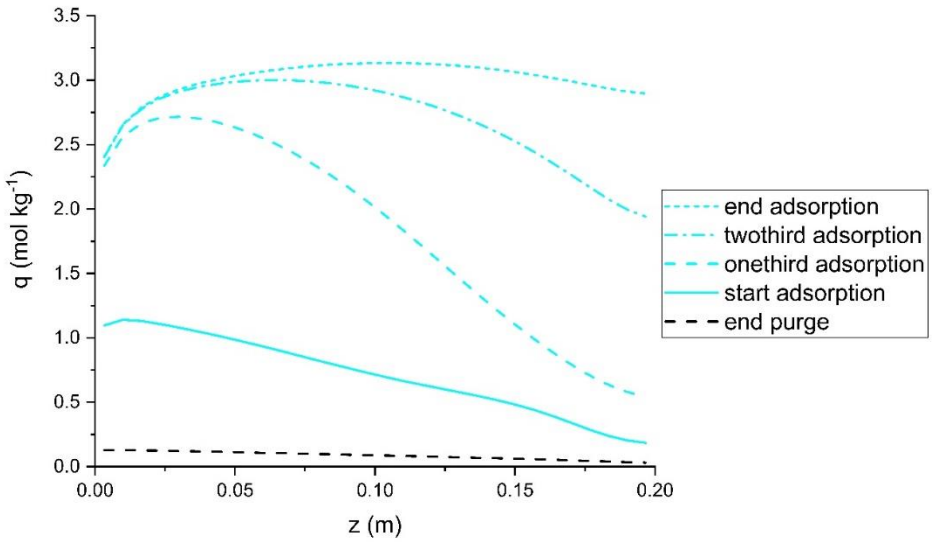

FIGURE 3-7: ADSORBENT LOADING OVER THE LENGTH OF THE REACTOR DURING THE ADSORPTION STEP (START: SOLID LINE, ONE THIRD: LONG DASHED, TWO THIRD: LONG DASH DOT, END: DASHED LINE) AND AT THE END OF THE PURGE (DASHED BLACK).

3.3.4. Working capacity

The key parameter in the development of sorption enhanced processes is the cyclic working capacity of the adsorbent that can be reached for the given reactor and operating conditions. The working capacity is defined as the difference in average loading of the adsorbent bed at the end of the regeneration and the end of the adsorption steps. From Figure 3-7, the working capacity for the base case can be determined at 2.83 mol kg^{-1}. Complete conversion, in which all produced steam is adsorbed, would require an almost 37% higher working capacity. However, as discussed below, a trade-off exists between the yield and the productivity, defined as the amount of DME produced per unit of time per unit of bed volume. This clearly indicates that optimizing the working capacity together with the productivity of the system is crucial for the system performance.

The working capacity can be influenced by many parameters, both during the reactive adsorption step and during the inherent regeneration of the system. These are discussed in the next sections.

3.3.5. Adsorption

Catalyst to adsorbent ratio

For all reactive adsorption processes an optimum catalyst to sorbent ratio exists, balancing the reaction rate and the steam/(by-)product adsorption. This ratio defines the fraction of the direct DME synthesis catalyst and the adsorbent material, which are homogeneously mixed and distributed along the reactor. Figure 3-8 shows the carbon selectivity in the product stream for four different catalyst to adsorbent ratios, varying from 1:16 to 1:2. Going from 1:2 down to 1:8, the lower ratios clearly result in the highest percentage of DME and the least amount of CO_2 in the product. Conversely, a ratio of 1:2 results in the highest maximum DME concentration.

For the chosen adsorption time and feed flow rate, an increasing amount of adsorbent will benefit the overall DME production rate during the adsorption step due to the limiting adsorption capacity in this scenario. However, to increase the amount of adsorbent, the amount of catalyst cannot be reduced without a cost. For a ratio of 1:16 the amount of catalyst becomes limiting and both the DME selectivity and the maximum DME concentration decrease. For the investigated scenario, the optimal ratio of catalyst to adsorbent appears to be between 1:8 and 1:4 (Figure 3-8).

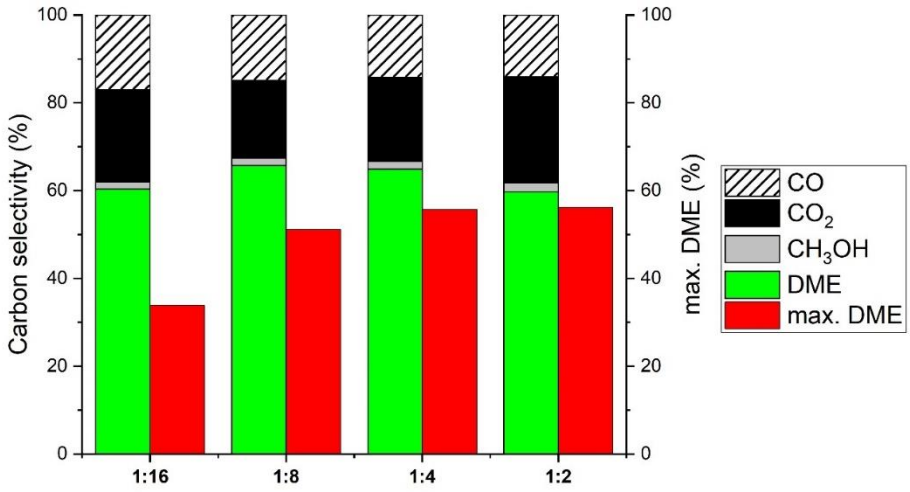

FIGURE 3-8: THE CARBON SELECTIVITY OF THE ADSORPTION PRODUCT STREAM, AND THE MAXIMUM DME CONCENTRATION FOR FOUR DIFFERENT CATALYST TO ADSORBENT RATIO'S: 1:16, 1:8, 1:4, AND 1:2.

Syngas feed rate

By lowering the gas hourly space velocity (GHSV) the residence time of the reactants in the SEDMES reactor increases, and vice versa. Additionally, the amount of water, produced in a given period, relative to the amount of adsorbent changes. Figure 3-9 shows that a lower GHSV during the reactive adsorption step leads to a higher conversion towards DME. As mentioned in Section 3.3.4, considering the base case working capacity of the adsorbent, not enough material is present to adsorb all steam produced for 100% conversion to DME. Lowering the space velocity, although the conversion is increased, leads to a decrease in the amount of steam produced. Therefore, a larger part of the steam produced can be adsorbed, resulting in less steam slip at the end of the reactor and therefore in an enhanced conversion.

Regarding this, the optimal GHSV would be as low as possible from a selectivity point-of-view. However, the low GHSV (in combination with the limited size of a lab-scale reactor) results in a large impact of dispersive transport on the behavior of a process. The Péclet number (Pe) is defined as the ratio of convective transport over dispersive transport. A Pe of zero describes the limiting situation of a fully mixed system and an ideal PFR can be described with an infinite Péclet number. With a maximum Péclet number of 11 for the base case, clearly dispersive transport has a large contribution compared to convective transport for the lab-scale SEDMES process. For lower GHSV this contribution becomes dominant, eventually effecting the selectivity as well. In contrast to the selectivity, the productivity

drops significantly for lower space velocities (Figure 3-9). Process design for a specific case therefore needs to balance selectivity and productivity.

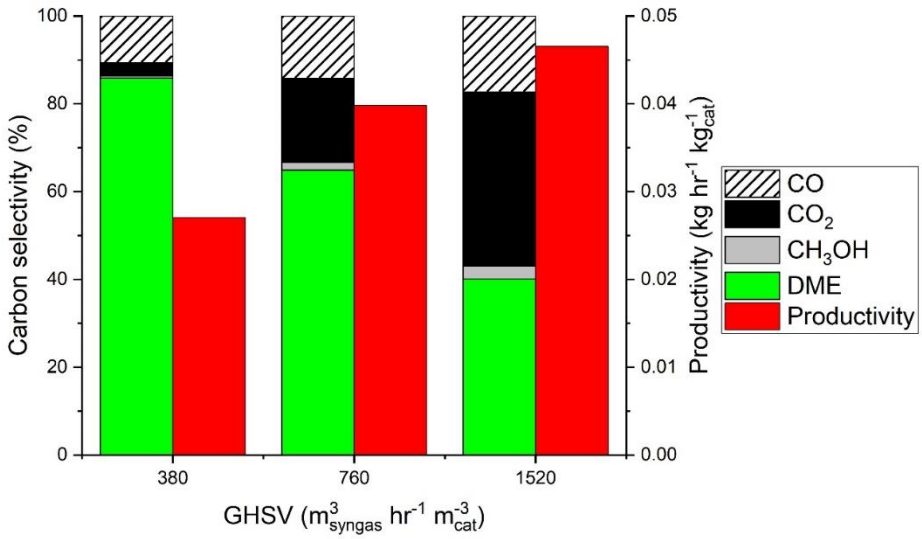

FIGURE 3-9: CARBON SELECTIVITY OF ADSORPTION PRODUCT AND THE DME PRODUCTIVITY FOR THREE DIFFERENT SYNGAS FEED FLOW RATES: 380, 760, AND 1520 M_{SYNGAS}^3 HR^{-1} M_{CAT}^{-3}.

Temperature and pressure

Other parameters affecting the total adsorption capacity of the system are the temperature and pressure during the reactive adsorption step. The choice of total pressure in the adsorption step has three important implications for the performance of the SEDMES cycle: (1) the thermodynamic equilibrium (excluding the effect of water adsorption) changes, (2) an increase in steam partial pressure increases the equilibrium amount of water adsorbed, and (3) more gas is required for column repressurization.

Whereas the methanol synthesis reactions (1) and (2) are shrinking reactions, increasing the reaction pressure enhances the production of methanol and its subsequent conversion towards DME. As can be observed in Figure 3-10 a higher adsorption pressure results indeed in a higher methanol and especially DME yield for the SEDMES process. Interestingly, the conversion of CO increases more with increasing pressure than the conversion of CO_2. At an adsorption pressure of 10 bar even more CO is formed due to the reverse-WGS than is converted towards methanol and DME. The conversion of CO to methanol does not result in H_2O by-product formation and is therefore not directly enhanced by steam adsorption, whereas the conversion of CO_2 is. As a result of the less enhanced CO conversion, the pressure effect (due to negative gas expansion coefficient) has a larger effect on this conversion than on the conversion of CO_2. However, the conversion of CO_2 is enhanced as

well. This is caused by the higher working capacity of the adsorbent, since not only the reactions are enhanced by increasing pressure, also the adsorption capacity is increased. Although the adsorbent is less dry at the beginning of the adsorption step for higher pressures, due to more reaction and adsorption during the repressurization step, the end loading increases with increasing pressure. Whereas the loading after regeneration is similar for all pressures, the working capacity increases with increasing pressure (Figure 3-10). Even though operation at elevated pressure results in a higher conversion and therefore a higher steam content, the improved loading (due to the higher steam partial pressure) results in an increased sorption enhancement. Due to the repressurization with syngas, more syngas is fed to the system at 50 bar adsorption pressure compared to 10 bar adsorption pressure. The effective GHSV (considering both repressurization and adsorption steps) is therefore respectively 16% more for 50 bar, and 15% lower for 10 bar than the base case scenario (30 bar). Although an increased GHSV results in a lower conversion towards DME (Figure 3-9), the positive effect of the pressure on reaction and adsorption is more pronounced than the small increase in space velocity with increasing syngas repressurization.

Clearly, operation at elevated pressure has a positive effect on the performance of the SEDMES process, since it improves the thermodynamics of the system, the reaction kinetics and the adsorption capacity. At 30 bar already 64.9% DME selectivity is achieved, which further improves to 76.7% at 50 bar operating pressure. Eventually, the optimal pressure has to be determined by a full process techno-economic evaluation in which the benefits (DME yield) and costs (of compression) are determined.

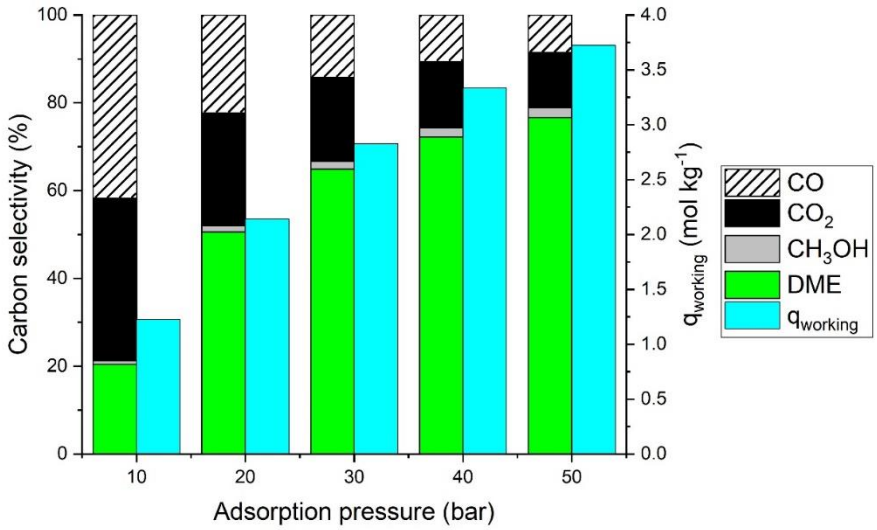

FIGURE 3-10: CARBON SELECTIVITY OF ADSORPTION PRODUCT FOR VARIOUS ADSORPTION PRESSURES AND THE CYCLIC WORKING CAPACITY OF THE ADSORBENT MATERIAL AS A FUNCTION OF THE TOTAL PRESSURE.

Not only the pressure affects the reaction and adsorption behavior, also the adsorption temperature has a significant effect. Methanol synthesis is thermodynamically favored at lower temperatures, yet high catalyst activity requires methanol synthesis temperatures of around 250 °C. Despite the fact that the temperature for methanol dehydration is generally higher, around 300 °C [33], direct DME synthesis is often performed at temperatures of around 250 °C [6, 9, 13-15], not only because the methanol synthesis is considered to be the rate determining step in direct DME synthesis, but also to prevent deactivation of the CZA catalyst at temperatures above 300 °C. Figure 3-11 shows this behavior for the kinetically determined carbon selectivity in direct DME synthesis based on the kinetics used in this study, Equations (16) – (38). Although the thermodynamic equilibrium for the direct synthesis of DME is favored at lower temperatures, the faster reaction kinetics at higher temperatures result in an optimum DME yield between 250 and 275 °C.

From the adsorption isotherm (Equations 41-44) it can be seen that the higher the temperature the lower the equilibrium loading on the zeolite material (Figure 3-13). This effect is also exploited in temperature swing regeneration. During the adsorption however, a lower temperature results in a higher working capacity of the material. Whereas the system is limited by the adsorption capacity, the SEDMES process benefits from operation at lower temperatures due to an increased adsorption capacity. Figure 3-12 shows the DME carbon selectivity as a function of the working capacities obtained from the loading at the end of the purge and the end of the adsorption step for the four studied temperatures.

When decreasing the operating temperature from 300 to 250 °C the working capacity is increased, corresponding to the higher isotherm capacity and DME yield with decreasing temperature. At 225 °C the working capacity is lower than at 250 °C, despite the higher isotherm capacity. The catalytic activity limits the conversion at 225 °C and therefore a lower working capacity is obtained, resulting in the V-shaped curve (Figure 3-12).
Although the adsorption capacity benefits from operation at lower temperatures, lower temperatures decrease the catalyst activity. For the case studied, clearly an optimum is found at a temperature of around 250 °C. At this temperature a DME yield of more than 79% is obtained, a 14% increase compared to the base case scenario.

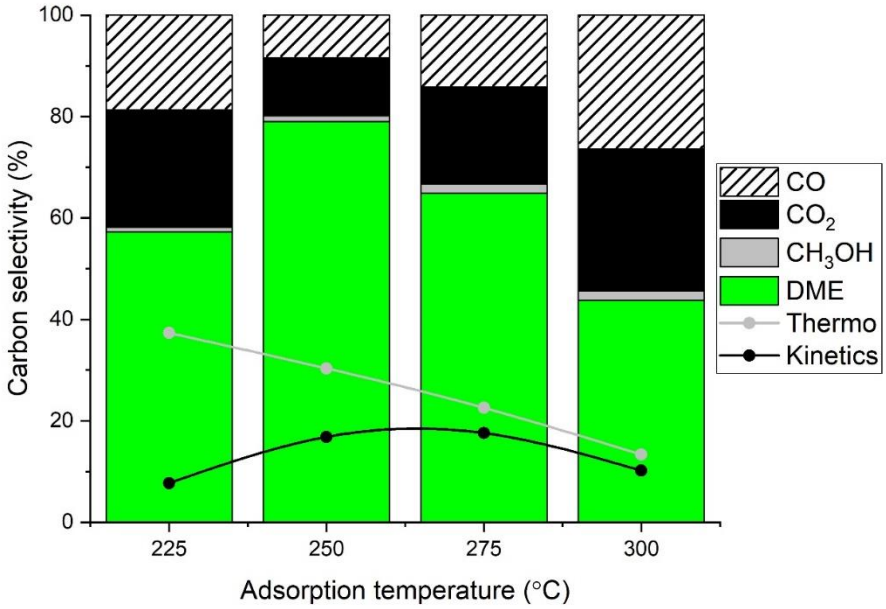

FIGURE 3-11: CARBON SELECTIVITY OF ADSORPTION PRODUCT FOR VARIOUS ADSORPTION TEMPERATURES. CARBON SELECTIVITY/YIELD TOWARDS DME AS A FUNCTION OF REACTION TEMPERATURE. BOTH THE YIELD OF THE KINETIC MODEL (SAME FEED FLOW RATE AND CATALYST AMOUNT AS FOR SEDMES) AND THE THERMODYNAMIC EQUILIBRIUM ARE GIVEN FOR DIRECT DME SYNTHESIS IN ABSENCE OF WATER ADSORPTION (LINES ARE GIVEN AS A GUIDE TO THE EYE).

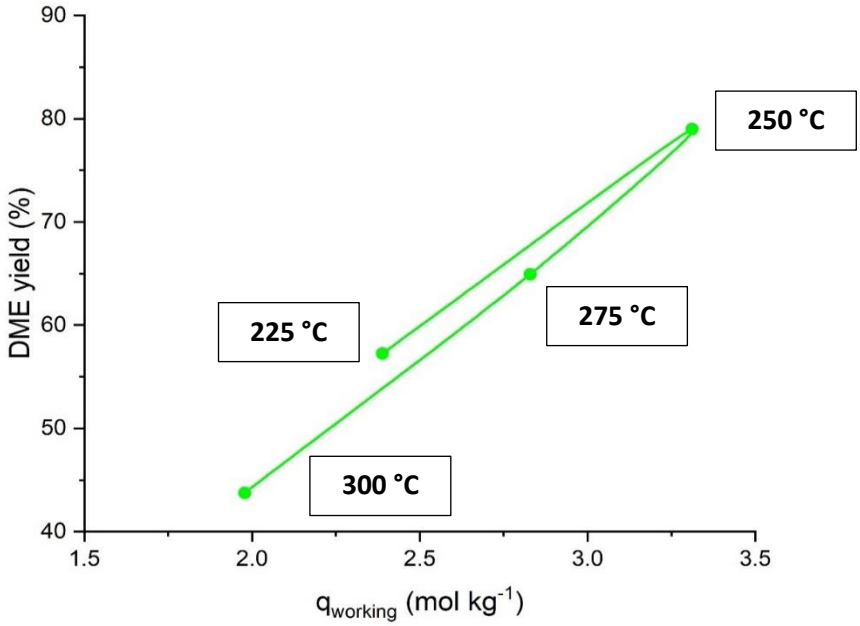

FIGURE 3-12: DME YIELD AS FUNCTION OF THE WORKING CAPACITY FOR DIFFERENT ADSORPTION TEMPERATURES.

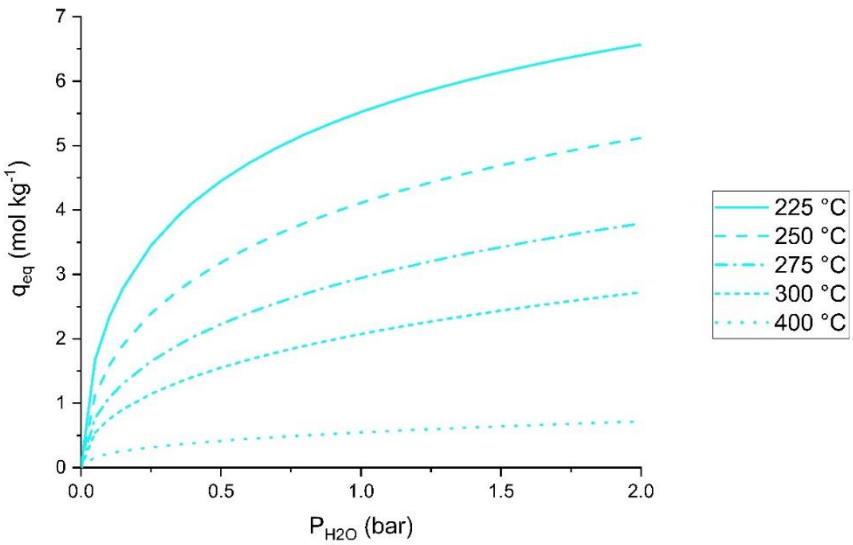

FIGURE 3-13: ADSORPTION ISOTHERM UP TO 2 BAR PARTIAL PRESSURE OF WATER AT 225, 250, 275, 300 AND 400 °C.

3.3.6. Regeneration

Besides tuning the parameters of the reactive adsorption step, the conditions for the regeneration step can be optimized as well. The regeneration step is particularly important, because it partly determines the working capacity of the adsorbent. In the next sections the influence of the regeneration step conditions on the performance of the SEDMES process is discussed.

Regeneration mode

In the base case scenario the columns are regenerated by a combined temperature and pressure swing (TPSA), following experimental practice [29]. First the reactor column is depressurized, resulting in a blowdown product stream. Next, the column is fed with a(n) (inert) purge gas at low pressure combined with a temperature increase (1 hour) and decrease (2 hours) to further regenerate the system. After this regeneration the column is repressurized again to the adsorption pressure (30 bar in the base case). Alternative possibilities for the regeneration procedure would be a temperature swing or a pressure swing only. With only a temperature swing the system would not be exposed to alternating pressures (at elevated temperature), relieving some design constraints on such a system and allowing for recovery of purge gas at higher pressure. If a pressure swing system is feasible, no relatively time-consuming heating and cooling is required during the regeneration step, making the regeneration (and therefore total cycle) time possibly shorter and the productivity potentially higher.

Figure 3-14 shows the carbon selectivity for the product stream during the adsorption step. The syngas feed is adjusted in the TSA case to account for the repressurization with syngas in the case of (T)PSA. In Section 3.3.5 it is discussed that a higher space velocity results in a decreased carbon selectivity (Figure 3-9). From Figure 3-14 it can be seen that either a TSA (with an increased, so equal to PSA, syngas feed) or PSA does not perform as well as the base case TPSA regeneration. As a result, TPSA gives the highest DME yield and productivity due to the better regeneration of the adsorbent material (Figure 3-15).

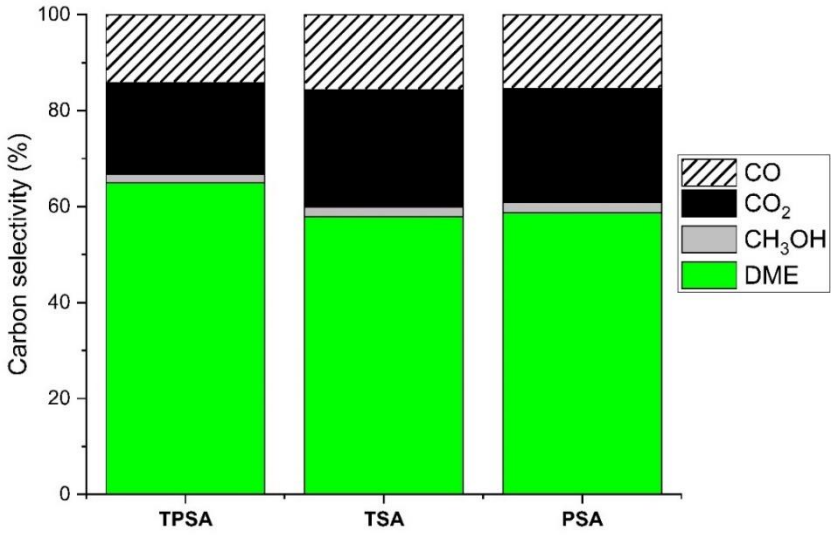

FIGURE 3-14: CARBON SELECTIVITY OF ADSORPTION PRODUCT FOR TPSA, TSA AND PSA REGENERATION.

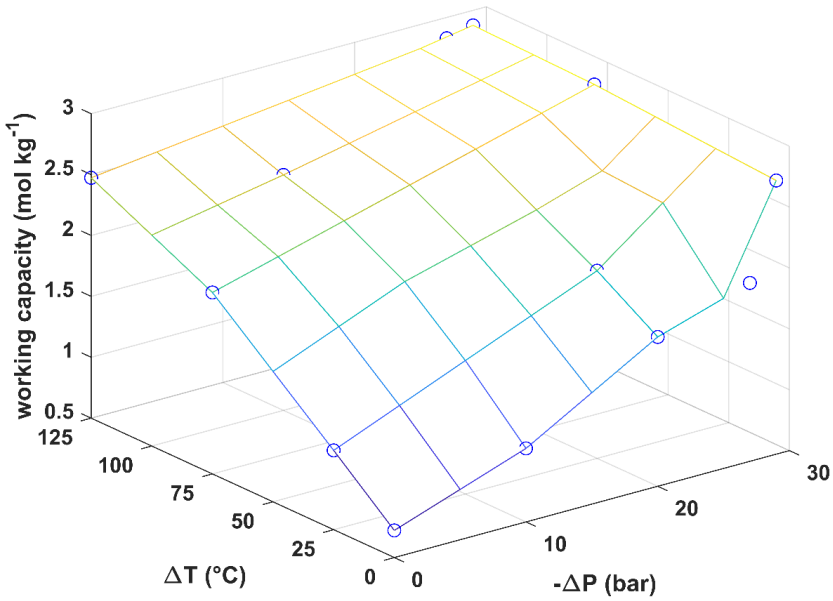

FIGURE 3-15: SURFACE RESPONSE PLOT FOR THE EFFECT OF TEMPERATURE AND PRESSURE SWING ON THE WORKING CAPACITY, BASE CASE CONDITIONS. LINES ARE A GUIDE FOR THE EYE BETWEEN THE STUDIED CASES (O).

In Figure 3-15 the effect of the pressure swing and the temperature swing on the working capacity of the adsorbent material is shown. The studied cases are operated at the same base case conditions, such as adsorption at 275°C and 30 bar(a). Moreover, all cycle times are kept the same, only the extent of pressure reduction and/or temperature increase is varied. The GHSV is adjusted, so each case has the same amount of syngas fed during the combined repressurization and adsorption steps.

A first aspect to be noticed is the regeneration by purging alone: without temperature increase or depressurization a working capacity of 0.72 mol kg^{-1} is already obtained. Increasing the temperature or reducing the pressure during regeneration increases the working capacity. However, with increasing temperature swing the gained extra working capacity becomes less compared to increasing the pressure with a pressure swing, where the working capacity is still improved significantly between 27 and 29 bar pressure difference. This behavior can be related to the shape of the isotherm (Figure 3-13), which is steep for low partial pressures and flattens for higher partial pressures of steam.

Although a combined temperature and pressure swing regeneration results in the highest working capacity, and also the current experimental work on sorption enhanced DME synthesis shows the best performance with a TPSA, the studied regeneration response behavior indicates that both TSA and PSA alone could be an option in the SEDMES process development. This is generally preferred in the design of a process and the possibly shorter regeneration (and therefore total cycle) times which could potentially increase the productivity.

Purge: composition and flow rate

An important aspect for the SEDMES process is the regeneration during the purge step, in which most of the sorbent regeneration occurs. Typically, more than 99% of the purge product consist of the purge N_2 itself and desorbed H_2O (Figure 3-6) allowing easy recycle of the N_2 as purge gas.

By increasing the purge gas flow rate, the reactor bed is regenerated slightly better, resulting in an increased DME yield and selectivity. However, a limited amount of steam is still desorbed at the end of the purge step as is shown for the base case scenario (Figure 3-5f). By increasing the purge gas flow rate even further the regeneration, and therefore the DME yield, is only slightly improved. Figure 3-16 shows the direct link between the working capacity of the system and the DME yield. Whereas other performance parameters remain (relatively) unaffected, an increase in the working capacity by increasing the purge flow rate results in a linear increase in the DME yield.

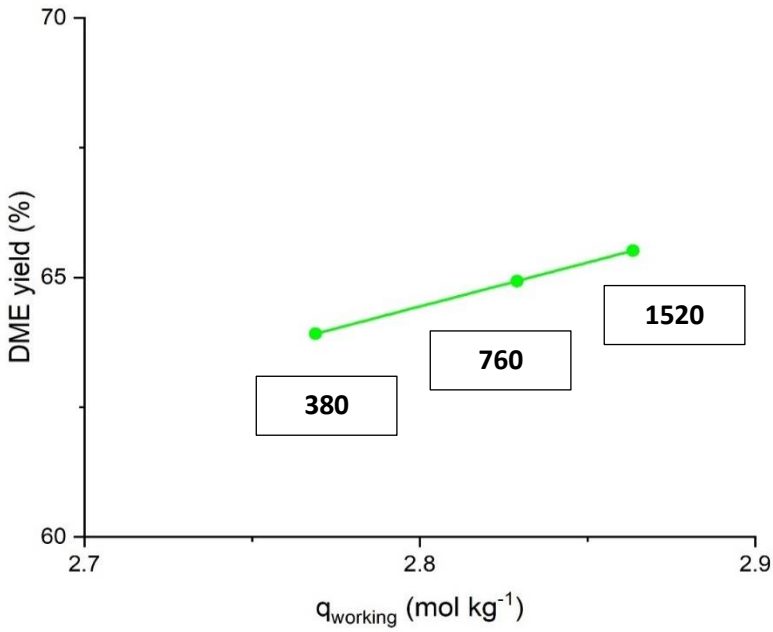

FIGURE 3-16: DME YIELD AS FUNCTION OF THE WORKING CAPACITY FOR THE DIFFERENT PURGE FLOW RATES (M_{SYNGAS}^3 HR^{-1} M_{CAT}^{-3}).

As mentioned before (in Section 3.3.3) for the base case, some purge gas ends up in the DME product, so preferably either reactants or products already present in the process are used as purge gas, viz. syngas, CO_2, or H_2. A possible purge stream which is available, is the syngas feed stream. As shown in Figure 3-17, using syngas as purge gas results in a lower DME yield (and productivity) compared to the nitrogen purge. Although no methanol is formed at the regeneration conditions (low pressure, high temperature), and subsequently also no DME is produced, still the reverse-WGS reaction occurs. This is evidenced by the purge product enrichment in CO (compared to CO_2). As a result of the formed and adsorbed H_2O the adsorbent is regenerated to a lesser extent when using syngas as purge gas compared to an inert purge gas (Figure 3-18). Therefore, the DME yield in the SEDMES cycle is evidently lower compared to a cycle with an inert N_2 purge. Another possible purge gas would be CO_2. In comparison, for CO_2 adsorption processes, such as the SEWGS process, often steam is used as a purge gas. Although CO_2 purge performs better than the syngas feed in regenerating the adsorptive capacity of the system, it still performs considerably less than an inert (N_2) purge stream (Figure 3-17, Figure 3-18). Finally, H_2 is considered as a purge gas. A H_2 purge performs equally well as the N_2 purge, as can be seen from the loading after the purge in Figure 3-18. Due to the slight excess of H_2 remaining after the purge, more reaction occurs during the repressurization. This results in a slightly higher adsorbent

loading at the start of the adsorption step itself. This higher adsorbent loading balances the higher conversion during repressurization, resulting in a performance which is similar to the base case.

The purge product composition has to be compared as well. In the case of N_2 purge gas more than 99% of the purge product consists of N_2 and desorbed H_2O. This would allow reusing this stream as purge feed gas after removal of H_2O, so a limited amount of make-up purge gas is required. For a syngas purge system, the purge product is enriched in CO. After removal of steam and compression the purge product could be used as syngas feed to the adsorption step. Whereas the regeneration is less extensive with syngas as the purge gas (Figure 3-18), the working capacity of the system is reduced by 13% compared to N_2 purge (Figure 3-19). However, the enrichment in CO of the syngas adsorption feed would also reduce the required working capacity for the system, making a syngas purge interesting for a process with low pressure syngas available.

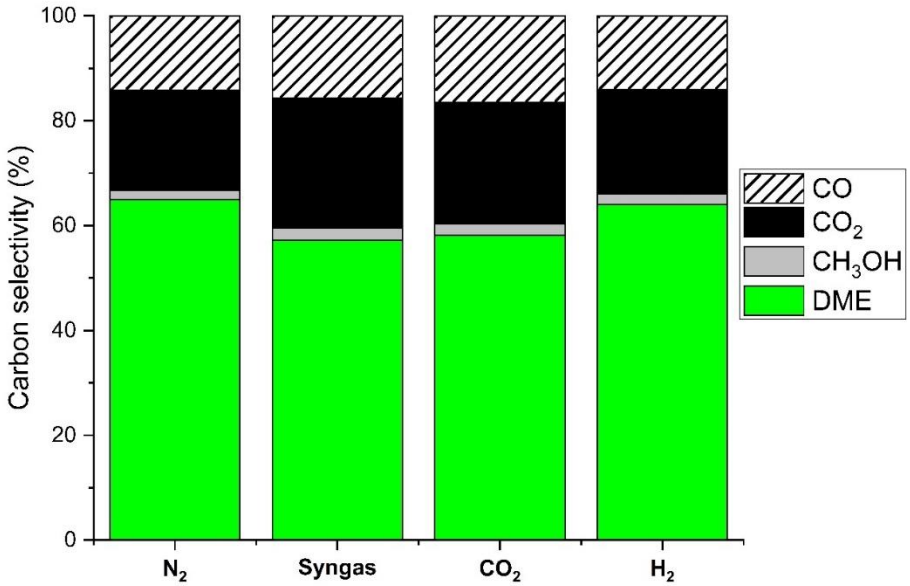

FIGURE 3-17: CARBON SELECTIVITY OF ADSORPTION PRODUCT FOR NITROGEN, SYNGAS, CO_2 AND H_2 PURGE DURING TPSA REGENERATION.

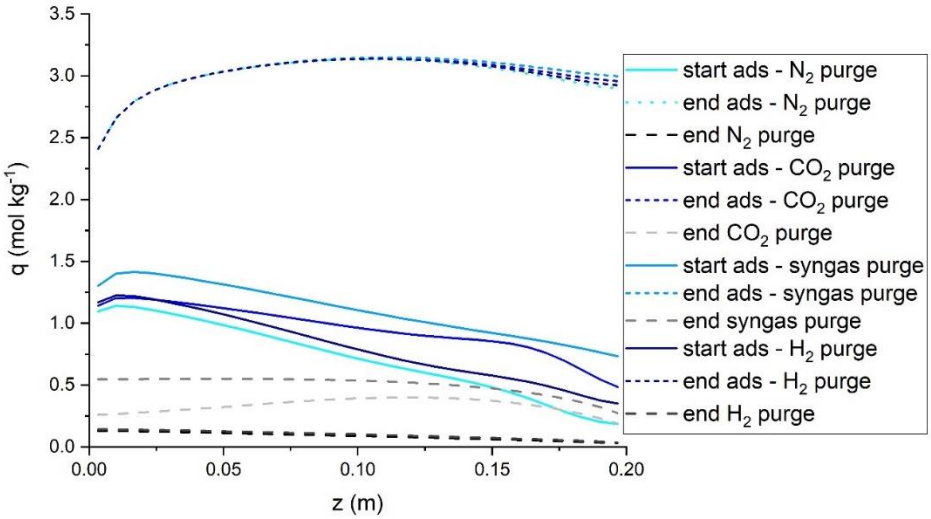

FIGURE 3-18: ADSORBENT LOADING OVER THE LENGTH OF THE REACTOR AT THE START OF THE ADSORPTION STEP (SOLID LINE), AT THE END OF THE ADSORPTION STEP (DASHED LINE), AND AT THE END OF THE PURGE STEP (DOTTED LINE) FOR NITROGEN, SYNGAS, CO_2 AND H_2 PURGE.

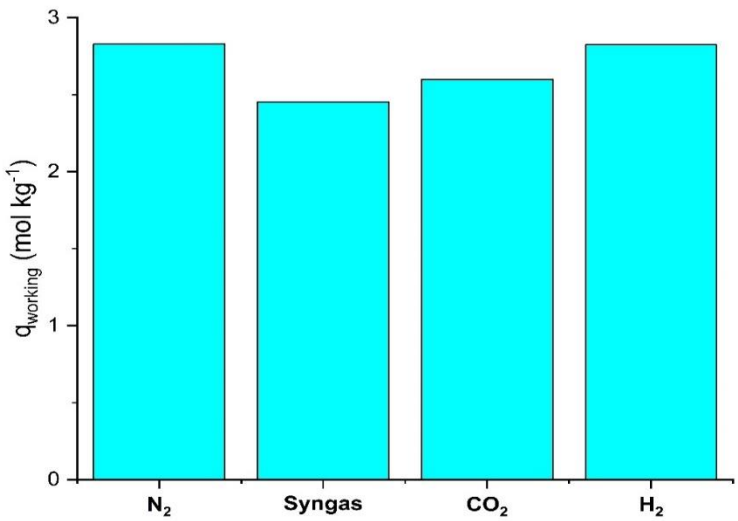

FIGURE 3-19: WORKING CAPACITY FOR NITROGEN, SYNGAS, CO_2 AND H_2 PURGE DURING TPSA REGENERATION.

Repressurization

Also in the repressurization step of the column from a low regeneration pressure to the adsorption pressure several choices can be made for the gas stream to be used. Here, the syngas feed and the DME product have been considered. In the base case scenario, the syngas feed of the adsorption step is also used for repressurization of the reactor column. This reactant stream is available upstream of the reactor and therefore the column can be repressurized co-currently with syngas, avoiding dilution by another stream as seen for N_2 purge. Alternatively, the reactor can be repressurized with the DME-rich product, available downstream of the reactor. Therefore, product repressurization is done in counter-current operation compared to reactant repressurization and this results in an opposite axial profile compared to syngas repressurization (Figure 3-5), where the remaining N_2 from the purge is now present at the beginning of the reactor column rather than at the end. Therefore, the remaining purge gas ends up in the DME product stream after the column is totally flushed compared to the first minutes for co-current repressurization. An advantage of counter-current repressurization is that the adsorbent is completely dry at the end of the column (Figure 3-21) and the initial product composition is almost pure DME. Consequently, the carbon selectivity for DME in the adsorption product stream is the highest for repressurization with DME product (Figure 3-20). Although more DME is present in the product composition for a repressurization with DME, the amount of DME necessary to repressurize has to be subtracted from the adsorption product. This results in less DME formed for DME repressurization compared to syngas repressurization. However, the effective productivity for repressurization with DME is higher, i.e. more DME is produced per amount of syngas fed. Repressurization with product is interesting due to the high purity of the product initially obtained in the adsorption step. Although the loss of product can be costly, a trade-off needs to be found between using syngas feed or DME product as repressurization gas.

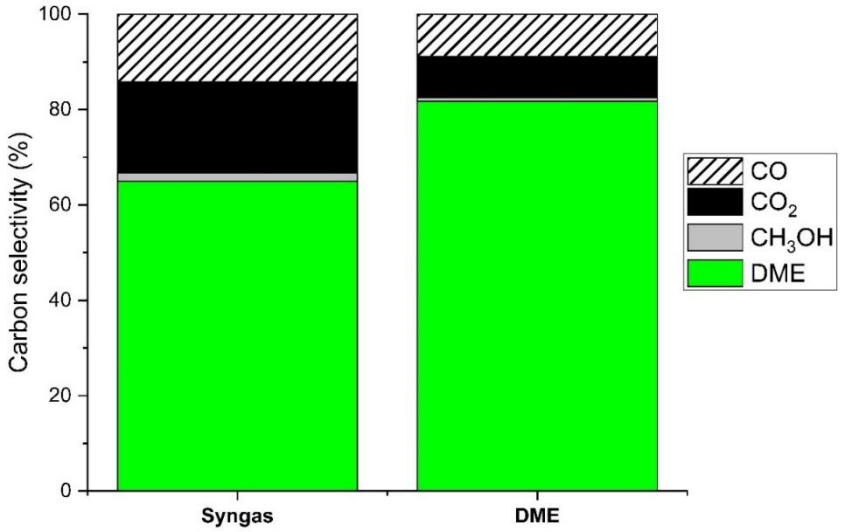

FIGURE 3-20: CARBON SELECTIVITY OF ADSORPTION PRODUCT FOR THE DIFFERENT REPRESSURIZATION GASES.

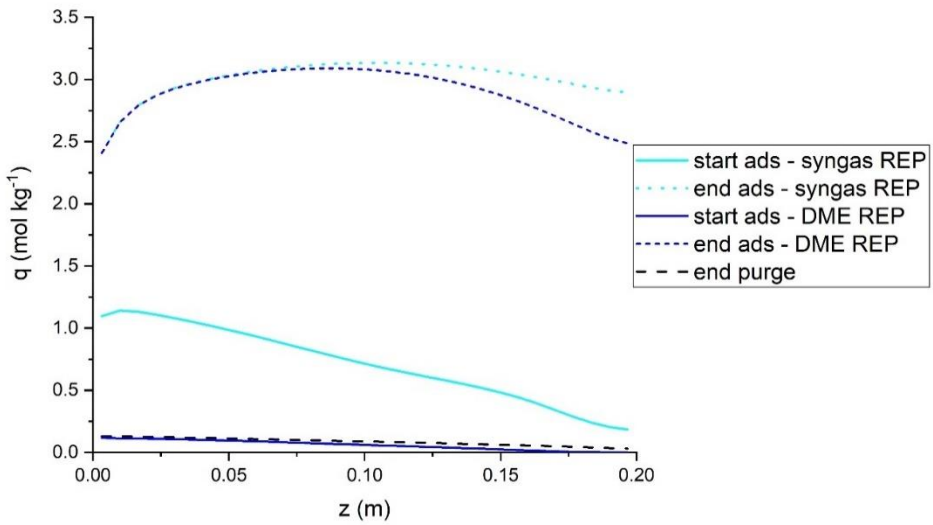

FIGURE 3-21: ADSORBENT LOADING OVER THE LENGTH OF THE REACTOR AT THE START OF THE ADSORPTION STEP (SOLID LINE) AND AT THE END OF THE ADSORPTION STEP (DASHED LINE), GIVEN FOR THE REPRESSURIZATION CASES. THE LOADING AT THE END OF THE PURGE STEP (DOTTED LINE) IS SIMILAR FOR BOTH CASES.

3.3.7. Heat management

Direct DME synthesis is an overall exothermic process (Equations 5-6), since both methanol synthesis (Equations 1-2) and its subsequent dehydration are exothermic (Equation 4). In addition, the adsorption of steam is also exothermic (ΔH_{ads} ≈ -45 kJ mol^{-1}). Thus, heat management is an important aspect of the process.

By operating the reactors adiabatically rather than isothermally the heat of reaction and heat of adsorption affect the adsorption step, and the heat of desorption affects the regeneration. Due to the exothermic nature of both the reaction and adsorption, the temperature in the reactor rises significantly (Figure 3-24). As a result, the adsorbent loading, limited by the temperature dependent isotherm, almost halves to 1.48 mol kg^{-1} (Figure 3-23). The reduced working capacity results in a tremendous drop in performance if the reactors are operated adiabatically compared to the isothermal case, as is shown in Figure 3-22. Whereas the adsorption of steam is exothermic, its desorption is endothermic. The inherent cooling of the reactor limits the desorption due to the isotherm displacement (Figure 3-23, Figure 3-24). Therefore, in temperature swing regeneration heat is supplied to improve the desorption. The current TPSA conditions require to go towards isothermal operation of the reactive adsorption step, rather than an adiabatic system.

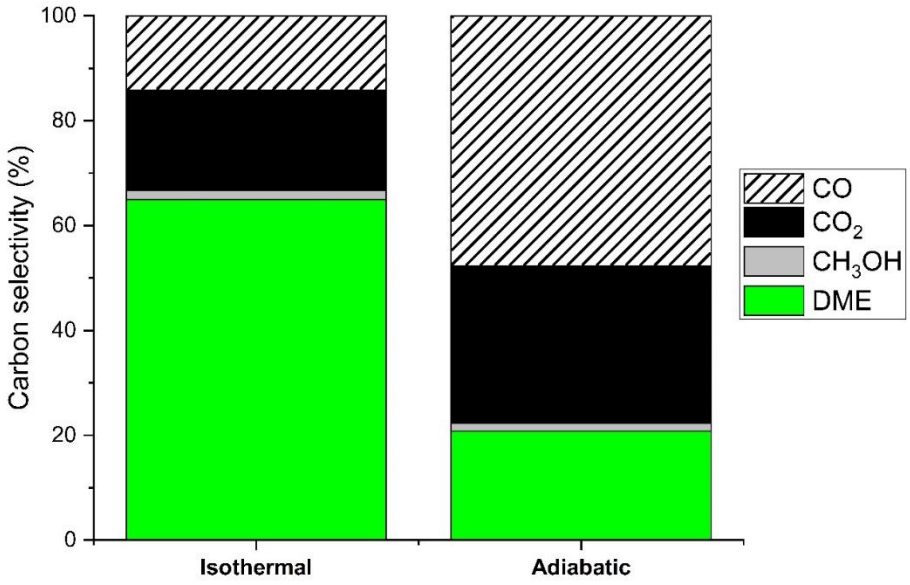

FIGURE 3-22: CARBON SELECTIVITY OF ADSORPTION PRODUCT FOR AN ISOTHERMAL AND AN ADIABATIC REACTOR.

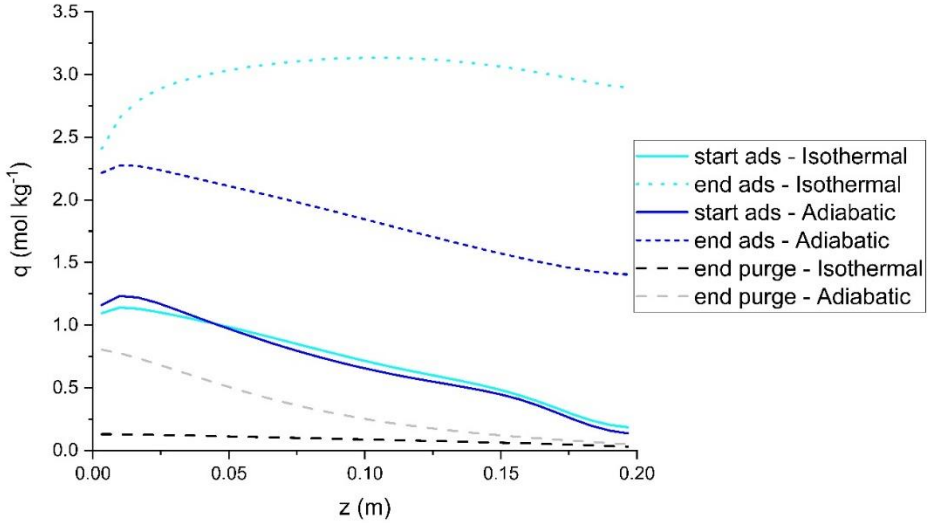

FIGURE 3-23: ADSORBENT LOADING OVER THE LENGTH OF THE REACTOR AT THE START OF THE ADSORPTION STEP (SOLID LINE), AT THE END OF THE ADSORPTION STEP (DASHED LINE) AND AT THE END OF THE PURGE STEP (DOTTED LINE), GIVEN FOR THE ISOTHERMAL AND ADIABATIC REACTOR CASES.

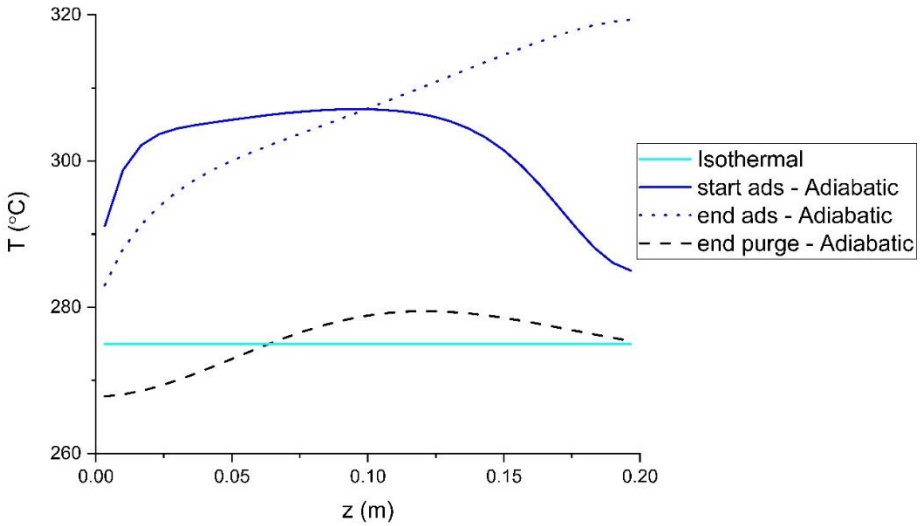

FIGURE 3-24: TEMPERATURE PROFILE OVER THE LENGTH OF THE REACTOR AT THE START OF THE ADSORPTION STEP (SOLID LINE), AT THE END OF THE ADSORPTION STEP (DASHED LINE) AND AT THE END OF THE PURGE STEP (DOTTED LINE) FOR THE ADIABATIC REACTOR.

3.3.8. Temperature control

The isothermal operation is envisioned in an externally cooled multi-tubular fixed bed reactor, similar to conventional methanol and direct DME synthesis. The effect of the tube diameter is investigated by more detailed 2D modelling considering tubes with internal diameters equal to 25.6 mm, 38 mm and 46.6 mm [39]. The other parameters are given in Table 3-10, with an intermediate feed composition (CO/CO_2=1, stoichiometric H_2 and 6.3% inert).

TABLE 3-10: REACTOR OPERATING CONDITIONS FOR MULTI-TUBULAR FIXED BED.

Operating conditions	Value
Bed length (m)	6
Adsorbent particle diameter (m)	$3.2 \cdot 10^{-3}$
Catalyst particle diameter (m)	$3 \cdot 10^{-3}$
Bed density (kg m^{-3})	800
Reactor temperature (K)	523
Reactor pressure (bara)	25
GHSV (hr^{-1})	140

The calculated maximum temperature profile envelopes in the cross-section centerline are reported in Figure 3-25. As expected, temperature control is much easier with smaller tubes that can exchange better the heat generated by reaction and adsorption: it is straightforward that the larger the tubes are, the higher are the maximum temperatures. However, it is important to notice that, thanks to the dilution of the catalyst by the sorbent, the differences among the three simulated profiles are not so drastic, and even with the largest diameter (46.6 mm) temperature control is not a critical issue (less than 10 K difference at any position along the axial coordinate, with a maximum temperature of 553 K). This is a key difference with the conventional direct DME synthesis, which usually requires tubes with smaller internal diameters (3 cm diameter in [40]) to avoid hot-spots exceeding the catalyst temperature limit.

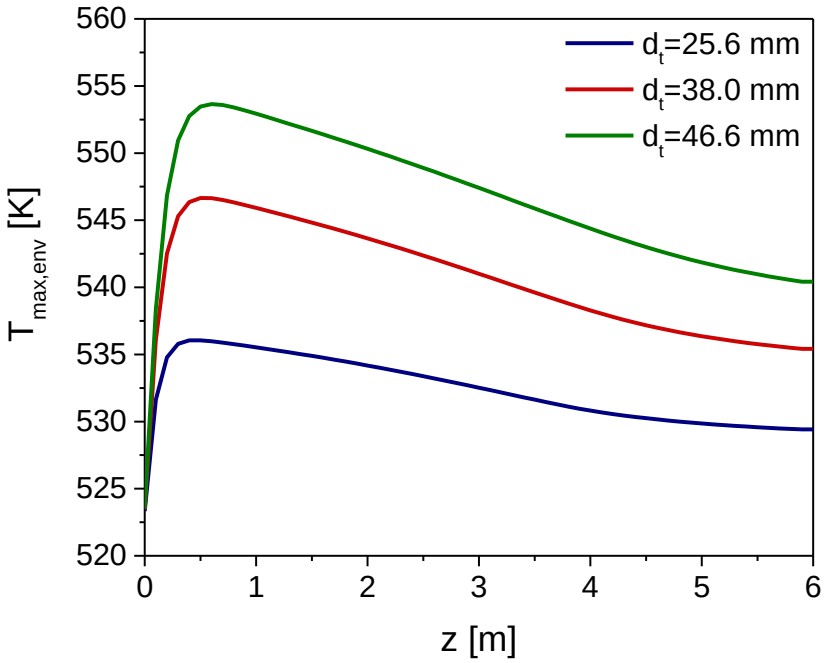

FIGURE 3-25: AXIAL PROFILE OF MAXIMUM GAS CENTERLINE LOCAL TEMPERATURES WITH DIFFERENT TUBE DIAMETERS.

The temperature difference has no strong effect on the DME production, as shown in Figure 3-26 where the specific outlet flow rates of DME have been plotted. Only a slightly higher peak in the DME flow rate is observed when using larger diameters just after the breakthrough at ~500 s, while the opposite situation is observed on the long term (after ~1100 s), when the production of DME is higher with a smaller tube diameter. This is a consequence of the temperature effect on the reaction kinetics and water adsorption equilibria, respectively. Just after the DME breakthrough the higher temperature in the larger tubes enhances the reaction kinetics, increasing the reactant conversion to DME; afterwards the lower temperature allowed by smaller diameter tubes becomes progressively beneficial due to its positive effect on the water adsorption equilibrium with a consequent improvement in the DME production rate. As a result, the DME carbon yield decreases less than 2.5% passing from an internal diameter of 25.6 mm to 46.6 mm. The small yield improvement obtained using smaller tubes is given by the thermodynamic increase in the water adsorption capacity, leading to an increase in the DME production capacity.

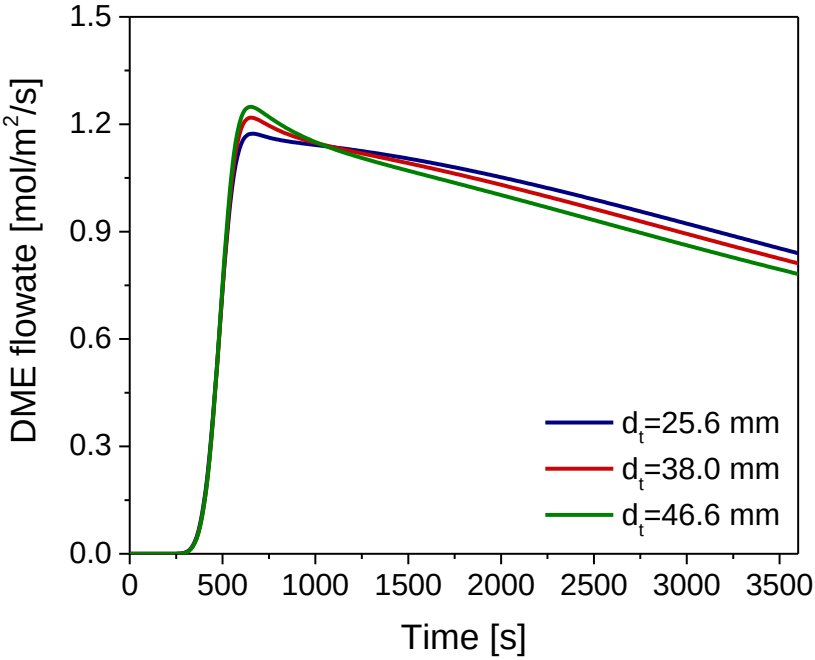

FIGURE 3-26: TIME EVOLUTION OF OUTLET DME FLOW RATE PER UNIT AREA WITH DIFFERENT TUBE DIAMETERS.

3.3.9. SEDMES vs. direct DME

In direct DME synthesis CO is converted to DME with CO_2 as the major by-product. With increasing CO_2 content in the feed both the conversion and the selectivity towards DME decrease significantly, as shown in Figure 3-27. KOGAS has developed a direct DME synthesis process in which natural gas is reformed (with CO_2) to a CO-rich syngas, which is subsequently converted to DME and CO_2. With an average DME production of 8 tons per day, a CO conversion of around 80% is achieved with a maximum DME selectivity of 67% [12]. A carbon-selectivity of 67% to DME would mean full (100%) conversion of CO towards DME and CO_2 for a CO feed (Equation 5). Figure 3-27 shows that for an increasing CO_2 content in the feed both the conversion of the carbon feed and the selectivity to DME drop to far lower values for the direct DME synthesis. This is, however, not the case for sorption enhanced DME synthesis. One of the major advantages of SEDMES is the highly selective direct conversion of CO_2 to DME. As a result, both the carbon conversion and the DME selectivity are much higher for the SEDMES process compared to the direct DME synthesis, especially for a CO_2-rich feed (Figure 3-27).

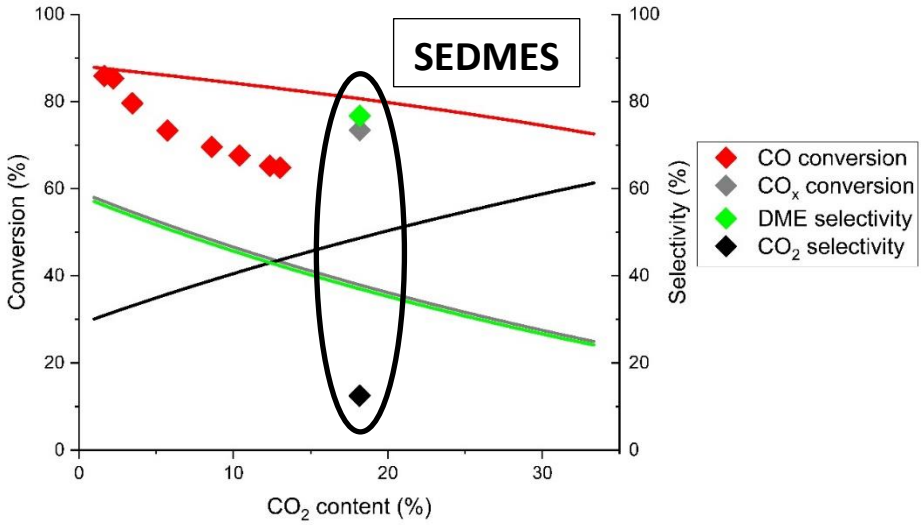

FIGURE 3-27: CO CONVERSION (RED DIAMONDS) AS A FUNCTION OF THE CO_2 CONTENT IN THE FEED OF THE KOGAS DIRECT DME PROCESS, AS REPORTED BY [12, 41]. LINES REPRESENT CO (RED), CO_x (GRAY) CONVERSION AND DME (GREEN) AND CO_2 (BLACK) SELECTIVITY BY THERMODYNAMIC CALCULATION AS A FUNCTION OF THE CO_2 CONTENT IN THE FEED; H_2/CO=1, 50 BAR(A) AND 260 °C. SEDMES CO_x CONVERSION (GRAY DIAMOND), DME SELECTIVITY (GREEN DIAMOND) AND CO_2 SELECTIVITY (BLACK DIAMOND) ARE GIVEN FOR SIMULATION AT 50 BAR(A).

3.4. Conclusion

Sorption enhanced DME synthesis (SEDMES) is studied as a full cyclic process of adsorption and inherent regeneration. Reaction kinetics derived for methanol synthesis and methanol dehydration, and a water adsorption isotherm for LTA zeolite 3A describe experimental data for the SEDMES process reasonably well.

The SEDMES process is a promising process intensification, already achieving over 80% single-pass CO_2 conversion and more than 70% single-pass DME (carbon) yield for a non-optimized three-reactor column system. The increased single-pass conversion reduces downstream separation units and smaller recycle streams, especially for a CO_2-rich feed.

A key parameter for optimizing the SEDMES process is the working adsorption capacity of the system. Improving this capacity could be done by optimizing the reactive adsorption conditions and by optimizing the regeneration method. The results described in this work show, supported by experimental work, that a typical window for the SEDMES process includes adsorption temperatures between 250 and 275 °C and pressures of 20 bar or above.

The regeneration, inherent to a reactive adsorption process, has a large influence on the working adsorption capacity of the system. A combination of temperature and pressure

swing regeneration results in the best system performance regarding the DME yield and CO_2 conversion, which is also supported by experimental findings in the literature. However, this study indicates that both TSA and PSA alone could also be an option for the SEDMES process. Especially, PSA is generally preferred for its facilitated design and possibly improved productivity.

Finally, under the current TPSA conditions, cooled reactor operation of the reactive adsorption step is required to achieve high performance of the system. SEDMES temperature control in a multi-tubular fixed bed reactor, however, is not a critical issue. The maximum bed temperature stays well below the limits reported in the literature (300 °C) to preserve the CZA catalyst stability. Accordingly, larger tube diameters (up to 46.6 mm) can be adopted compared to conventional direct DME synthesis, with less than 2.5% loss in DME yield.

Nomenclature

a_p	Particle interfacial area (m^2 m^{-3})
c_i	Concentration of component i (mol m^{-3})
Cp	Gas thermal conductivity (J kg^{-1} K^{-1})
Cp_p	Particle thermal conductivity (J kg^{-1} K^{-1})
d_c	Crystal diameter (m)
d_p	Particle diameter (m)
D_c	Micropore diffusion coefficient (m^2 s^{-1})
D_k	Knudsen diffusion coefficient (m^2 s^{-1})
D_m	Molecular diffusion coefficient (m^2 s^{-1})
D_p	Macropore diffusion coefficient (m^2 s^{-1})
D_z	Axial dispersion coefficient (m^2 s^{-1})
f_{ads}	Fraction adsorbent (-)
f_{cat}	Fraction catalyst (-)
G	Ergun constant (-)
ΔH_{ads}	Adsorption enthalpy (J mol^{-1})
$\Delta H_{r,i}$	Reaction enthalpy (J mol^{-1})
k	Reaction rate constant (mol s^{-1} kg^{-1} bar^{-1}) or (kmol kg^{-1} hr^{-1})
k_{LDF}	Linear driving force rate constant (s^{-1})
K_i	Adsorption equilibrium constant of component i (bar^{-1}) or (m^3 $kmol^{-3}$)
K_p	Equilibrium constant (based on partial pressure) (-)
M_i	Molecular weight of component i (kg mol^{-1})
N_i	Mole flux of component i (mol m^{-2} s^{-1})
P	Reactor pressure (bara)
P_i	Partial pressure of component i (bara)

Pe	Péclet number (-)
q_i	Adsorbent loading (mol kg^{-1})
r_i	Reaction rate of component i (mol m^{-3} s^{-1}) or (mol kg^{-1} s^{-1}) or (kmol kg^{-1} hr^{-1})
R	Ideal gas constant (J mol^{-1} K^{-1})
Re_p	Particle Reynolds number (-)
t	Time (s)
T	Temperature (K)
u	Superficial gas velocity (m s^{-1})
U	Overall heat transfer coefficient (W m^{-2} K^{-1})
v	Interstitial gas velocity (m s^{-1})
z	axial coordinate (m)

Greek letters

ε_b	Bed voidage (-)
ε_p	Particle porosity (-)
λ	Axial thermal conductivity (W m^{-1} K^{-1})
ρ	Density (kg m^{-3})
ρ_p	Particle (bulk) density (kg m^{-3})
ϕ	Partial fugacity of component i (bara)
ω_i	Weight fraction of component i (-)

Abbreviations

ADS	Adsorption step
BD	Blowdown/depressurization step
CCUS	Carbon capture, utilization and storage
CZA	Copper/Zinc Oxide/Alumina
DMC	Dimethyl carbonate
DME	Dimethyl ether
EOS	Equation of state
LTA	Linde Type A
PSA	Pressure swing adsorption
REP	Repressurization step
rWGS	Reverse water-gas shift
SEDMES	Sorption enhanced DME synthesis
TSA	Temperature swing adsorption
WGS	Water-gas shift

Bibliography

[1] T.A. Semelsberger, R.L. Borup, H.L. Greene, Dimethyl ether (DME) as an alternative fuel, Journal of Power Sources 156 (2006) 497-511.

[2] G. Bonura, M. Cordaro, C. Cannilla, A. Mezzapica, L. Spadaro, F. Arena, F. Frusteri, Catalytic behaviour of a bifunctional system for the one step synthesis of DME by CO_2 hydrogenation, Catalysis Today 228 (2014) 51-57.

[3] M. Cai, A. Palčić, V. Subramanian, S. Moldovan, O. Ersen, V. Valtchev, V.V. Ordomsky, A.Y. Khodakov, Direct dimethyl ether synthesis from syngas on copper-zeolite hybrid catalysts with a wide range of zeolite particle sizes, Journal of Catalysis 338 (2016) 227-238.

[4] E. Catizzone, A. Aloise, M. Migliori, G. Giordano, Dimethyl ether synthesis via methanol dehydration: Effect of zeolite structure, Applied Catalysis A: General 502 (2015) 215-220.

[5] W.H. Chen, C.L. Hsu, X.D. Wang, Thermodynamic approach and comparison of two-step and single step DME (dimethyl ether) syntheses with carbon dioxide utilization, Energy 109 (2016) 326-340.

[6] F. Dadgar, R. Myrstad, P. Pfeifer, A. Holmen, H.J. Venvik, Catalyst Deactivation During One-Step Dimethyl Ether Synthesis from Synthesis Gas, Catalysis Letters 147 (2017) 865-879.

[7] M.D. Falco, M. Capocelli, A. Basile, Selective membrane application for the industrial one-step DME production process fed by CO_2 rich streams: Modeling and simulation, International Journal of Hydrogen Energy (2017) 6771-6786.

[8] F. Frusteri, M. Migliori, C. Cannilla, L. Frusteri, E. Catizzone, A. Aloise, G. Giordano, G. Bonura, Direct CO_2-to-DME hydrogenation reaction: New evidences of a superior behaviour of FER-based hybrid systems to obtain high DME yield, Journal of CO_2 Utilization 18 (2017) 353-361.

[9] A. García-Trenco, A. Martínez, The influence of zeolite surface-aluminum species on the deactivation of CuZnAl/zeolite hybrid catalysts for the direct DME synthesis, Catalysis Today 227 (2014) 144-153.

[10] I.A. Kurzina, S.I. Reshetnikov, N.I. Karakchieva, L.N. Kurina, Direct synthesis of dimethyl ether from synthesis gas: Experimental study and mathematical modeling, Chemical Engineering Journal 329 (2017) 135-141.

[11] Y. Li, T. Wang, X. Yin, C. Wu, L. Ma, H. Li, X. Zhang, Y. Lv, Pilot-scale tests of direct dimethyl ether synthesis from biomass-derived syngas, Asia-Pacific Power and Energy Engineering Conference (APPEEC)Wuhan, 2009.

[12] S.-H. Lee, W. Cho, T. Song, Y.-J. Ra, Scale up study of DME direct synthesis technology, Proceedings of World gas conference, 2009.

[13] S.P. Naik, T. Ryu, V. Bui, J.D. Miller, N.B. Drinnan, W. Zmierczak, Synthesis of DME from CO_2/H_2 gas mixture, Chemical Engineering Journal 167 (2011) 362-368.

[14] K.L. Ng, D. Chadwick, B.A. Toseland, Kinetics and modelling of dimethyl ether synthesis from synthesis gas, Chemical Engineering Science 54 (1999) 3587-3592.
[15] V.M. Lebarbier, R.A. Dagle, L. Kovarik, J.A. Lizarazo-Adarme, D.L. King, D.R. Palo, Synthesis of methanol and dimethyl ether from syngas over Pd/ZnO/Al2O3 catalysts, Catalysis Science & Technology 2 (2012) 2116–2127.
[16] I. Iliuta, M.C. Iliuta, F. Larachi, Sorption-enhanced dimethyl ether synthesis — Multiscale reactor modeling, Chemical Engineering Science 66 (2011) 2241-2251.
[17] J. Boon, F. van Berkel, H. van Dijk, J. Vente, Separation enhanced dimethyl ether synthesis, 5th TMFB International Conference, Aachen, 2017.
[18] J. Boon, J. van Kampen, R. Hoogendoorn, S. Tanase, F.P.F. van Berkel, M. van Sint Annaland, Reversible deactivation of γ-alumina by steam in the gas-phase dehydration of methanol to dimethyl ether, Catalysis Communications 119 (2019) 22-27.
[19] J. van Kampen, J. Boon, F. van Berkel, J. Vente, M. van Sint Annaland, Steam separation enhanced reactions: Review and outlook, Chemical Engineering Journal 374 (2019) 1286–1303.
[20] A.E. Rodrigues, L.M. Madeira, Y.-J. Wu, R. Faria, Sorption Enhanced Reaction Processes, World Scientific, 2017.
[21] J.C. Abanades, J. Boon, P. Cobden, K. Coenen, D.S.M. Constantino, R.P.V. Faria, J.R. Fernández, F. Gallucci, M.C. Iliuta, A.E. Rodrigues, E. van Dijk, M. van Sint Annaland, Sorption Enhancement of Chemical Processes, 1 ed., Academic Press, 2017.
[22] J. Boon, P.D. Cobden, H.A.J. van Dijk, C. Hoogland, E.R. van Selow, M. van Sint Annaland, Isotherm model for high-temperature, high-pressure adsorption of and on K-promoted hydrotalcite, Chemical Engineering Journal 248 (2014) 406-414.
[23] J. Boon, P.D. Cobden, H.A.J. van Dijk, M. van Sint Annaland, High-temperature pressure swing adsorption cycle design for sorption-enhanced water–gas shift, Chemical Engineering Science 122 (2015) 219-231.
[24] D.M. Ruthven, Principles of Adsorption and Adsorption Processes, Wiley, 1984.
[25] K.R. Westerterp, W.P.M. van Swaaij, A.A.C.M. Beenackers, Chemical Reactor Design and Operation, second ed., Wiley. 1984.
[26] R.T. Yang, Gas Separation by Adsorption Processes, Imperial College Press, 1997.
[27] B.E. Poling, J.M. Prausnitz, J.P. O'Connell, The properties of gases and liquids, McGraw-Hill, 2001.
[28] R.B. Bird, W.E. Stewart, E.N. Lightfoot, Transport Phenomena, Wiley, New York, 1960.
[29] J. van Kampen, J. Boon, F. van Berkel, H. van Dijk, J. Vente, M. van Sint Annaland, Regeneration conditions as the key to sorption enhanced dimethyl ether synthesis, 25th International Symposium on Chemical Reaction Engineering, Florence, 2018.
[30] H. Graaf, E.J. Stamhuis, A.A.C.M. Beenackers, Kinetics of low-pressure methanol synthesis, Chemical Engineering Science 43 (1988) 3185-3195.

[31] K.M. Vanden Bussche, G.F. Froment, A Steady-State Kinetic Model for Methanol Synthesis and the Water Gas Shift Reaction on a Commercial $Cu/ZnO/Al_2O_3$ Catalyst, Journal of Catalysis 161 (1996) 1-10.
[32] G.H. Graaf, P.J.J.M. Sijtsema, E.J. Stamhuis, G.E.H. Joostes, Chemical equilibria in methanol synthesis, Chemical Engineering Science 41 (1986) 2883-2890.
[33] G. Berčič, J. Levec, Intrinsic and Global Reaction Rate of Methanol Dehydration Over γ-Al_2O_3 Pellets, Industrial & Engineering Chemistry Research 31 (1992) 1035-1040.
[34] Z. Wang, J. Wang, F. Ren, M. Han, Y. Jin, Thermodynamics of the Single-Step Synthesis of Dimethyl Ether from Syngas, Tsinghua Science and Technology 9 (2004) 168-176.
[35] E. Gabruś, J. Nastaj, P. Tabero, T. Aleksandrzak, Experimental studies on 3A and 4A zeolite molecular sieves regeneration in TSA process: Aliphatic alcohols dewatering-water desorption, Chemical Engineering Journal 259 (2015) 232-242.
[36] H.S. Fogler, Elements of Chemical Reaction Engineering, Prentice Hall PTR, 2006.
[37] E.N. Fuller, P.D. Schettler, J.C. Giddings, A new method for prediction of binary gas-phase diffusion coefficients, Industrial and Engineering Chemistry 58 (1966) 19-27.
[38] M. Gwadera, K. Kupiec, J. Rakoczy, Investigation of thermal effects of water vapor adsorption on zeolites, Technical Transactions: Mechanics (2012) 88-94.
[39] S. Guffanti, C.G. Visconti, J. van Kampen, J. Boon, G. Groppi, Reactor modelling and design for sorption enhanced dimethyl ether synthesis, Chemical Engineering Journal 404 (2021) 126573-126585.
[40] D. Song, W. Cho, G. Lee, D.K. Park, E.S. Yoon, Numerical Analysis of a Pilot-Scale Fixed-Bed Reactor for Dimethyl Ether (DME) Synthesis, Ind. Eng. Chem. Res. 47 (2008) 4553–4559.
[41] DME Handbook Supplement, Japan DME Forum, Tokyo, 2011.

Chapter 4. Steam adsorption on molecular sieve 3A for sorption enhanced reaction processes

Abstract

Steam adsorption enhanced reaction processes, such as sorption enhanced DME synthesis, are a promising process intensification for many types of reactions, where water is formed as a byproduct. To assess the potential of these processes, adequate models are required that accurately describe water adsorption, particularly under the desired elevated temperatures and pressures. In this chapter, an adsorption isotherm is presented for H_2O adsorption at 200-350 °C and 0.05-4.5 bar partial pressure on molecular sieve (LTA) 3A. The isotherm has been developed on the basis of experimental data obtained from a thermogravimetric analysis and integrated breakthrough curves. The experimental data at lower steam partial pressures can be described with a Generalized Statistical Thermodynamic Adsorption (GSTA) isotherm, whereas at higher steam partial pressures the experimental data can be adequately captured by capillary condensation. Based on the characteristics of the adsorbent particles, a linear driving force relation has been derived for the adsorption mass transfer rate and the apparent micropore diffusivity is determined. The isotherm and mass transport model presented here prove to be adequate for modelling and improved evaluation of steam adsorption enhanced reaction processes.

This chapter is based on published work:

J. van Kampen et al., Steam adsorption on molecular sieve 3A for sorption enhanced reaction processes, Adsorption (2020).

4.1. Introduction

Steam separation enhanced reaction processes show great potential as process intensification for many types of reactions, in which water is formed as a byproduct [1]. Even so, the production and efficient handling of steam remains a major bottleneck for industrial CO_2 utilization [2-4]. In this context, several groups have experimentally demonstrated the benefit of sorption enhancement in terms of product yield that exceeds the thermodynamic equilibrium in absence of steam adsorption [1, 5-12]. In parallel, modelling studies on sorption enhanced reactions have sought to conceptually understand sorption enhancement and focus on process design [13-18]. This work strongly relies on the understanding of the interaction of steam and the adsorbent under relevant conditions.

In contrast to typical conditions for water adsorption, sorption enhanced DME synthesis requires good sorbent material performance at elevated temperature and pressure [1]. Based on available open literature, selected adsorbents were tested [1, 6, 19-44]. Next to the physically adsorbing zeolite Type A and Faujasite samples, three chemical adsorbents were also tested: LHMC, HHMC, and hydrotalcite. Their performance in terms of the cyclic working capacity for steam adsorption was rather disappointing (~1 mol/kg), therefore they have been disregarded for sorption enhanced DME synthesis.

The majority of the experimental work on reactive steam adsorption also uses Linde Type A (LTA) and Faujasite (Linde 13X) zeolite materials for water adsorption [1]. Indeed, under the required operating conditions these materials show sufficient hydrothermal stability, possess adequate adsorption capacity, and adequate regeneration properties compared to other materials, such as typical chemisorbents [1, 23]. Where zeolites 13X, 5A and to lesser extent 4A are also used for CO_2 adsorption applications and potentially adsorb reaction products [7, 29-31, 36, 45, 46], zeolite 3A is highly selective for water due to size exclusion by its limited pore size (Figure 4-1). Due to this high selectivity for water adsorption, zeolite 3A seems promising as adsorbent in sorption enhanced reactions for CO_2 conversion.

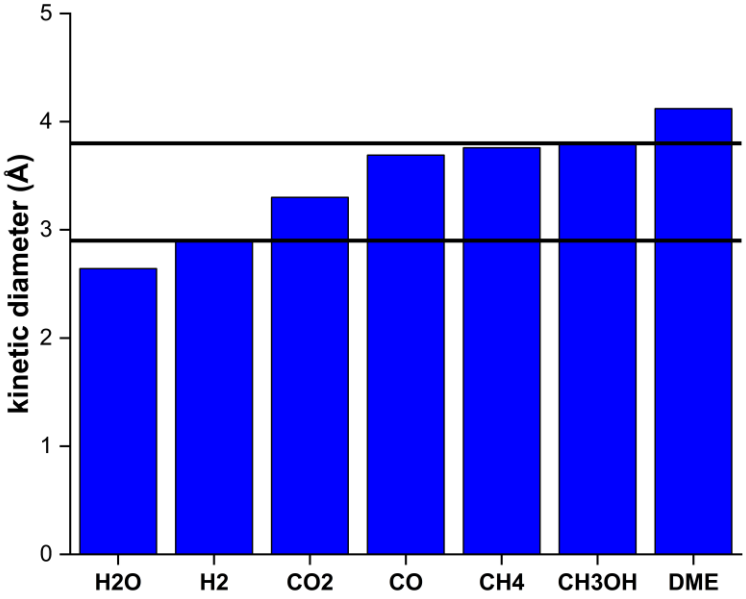

FIGURE 4-1: KINETIC DIAMETER OF VARIOUS COMPONENTS PRESENT IN SORPTION ENHANCED REACTIONS, COMPARED TO THE PORE SIZES OF ZEOLITES 3A (2.9 Å) AND 4A (3.8 Å) RESPECTIVELY [43, 46].

Extensive research has been carried out on the development, characterization and improvement of these materials for various applications [43, 46-49]. Although the heterogeneity of the adsorbent is often well described in a limited range by a semi-empirical isotherm correlation, such as the Sips and Toth isotherms [21, 24], Llano-Restrepo et al. (2009) have shown that traditional adsorption models are not able to describe water vapor adsorption in zeolite 3A (Grace Davison) over a wide range of temperatures (-20 to 100 °C) and 8 orders of magnitude water vapor partial pressure (0.01 Pa up to 1 bar) [35]. They derived a Generalized Statistical Thermodynamic Adsorption (GSTA) model from Hill's statistical thermodynamic adsorption model, which is shown to be able to describe the water vapor adsorption correctly with seven statistical subsystems. With this model they provide a physical meaning to the statistical subsystems, and the site specific (event) enthalpy and entropy could be obtained. In parallel to its thermodynamic derivation, the GSTA model can be seen as a multi-site Langmuir model in which the contribution to the capacity is equal for all sites [50]. The difference is in the energy attributed to a specific site for the heterogeneous Langmuir model compared to the energy attributed to the event of *n* molecules adsorbing for the GSTA model. In support of this, Wang (2020) recently showed

that the same dataset can be described by a triple-Langmuir model using the same number of fitting parameters [51]. Nonetheless, the adjustable number of equilibrium parameters makes the GSTA model flexible and capable of describing water adsorption (as well as other components) on molecular sieves [50]. However, the more parameters (*m*+2 for the GSTA model) a model contains, typically the better the data description will be, as demonstrated by the recent results from Wang (2020).

In memory of Dr. Shivaji Sircar's extensive and groundbreaking work, we benefit from following it with respect to sorption enhanced reactions, adsorption equilibria, and mass transfer in adsorption. This article studies molecular sieve zeolite 3A under relevant conditions for the sorption enhanced CO_2 conversion by a combined experimental and modelling approach. Quantitative data for water adsorption at elevated temperature (200-350 °C) and partial pressure (0.05-4.5 bar) allows evaluation of a suitable adsorption isotherm under these conditions. Besides the adsorption capacity, the kinetics of adsorption are essential the for modelling and evaluation of applications of the adsorbent in sorption enhanced reaction processes [1, 52]. However, often the kinetics of adsorption is actually a mislabeling and the adsorbate mass transfer rate is measured and described [53]. Therefore, a kinetic description of water adsorption is developed by means of a mass transfer rate model.

First, the material and its characterization for model parameter determination is reported, followed by the experimental procedure and model interpretation. The results and discussion section starts with the adsorption capacity and isotherm determination, followed by the kinetic description of water adsorption on zeolite 3A. Finally, the conclusions are summarized.

4.2. Materials and methods

4.2.1. Materials

Experiments were performed with molecular sieve type 3A, purchased as 1.6 mm pellets (UOP Molecular Sieves, Advanced Specialty Gas Equipment, USA), using the 1.6 mm pellets or a 212–425 µm sieve fraction. The material was analyzed by scanning electronic macroscopy (SEM) to determine the crystal and macropore size, which are used for the kinetic description of water adsorption on the material (Table 4-1). In Figure 4-2 the cubical zeolite crystals can be clearly observed with an average (spherical) crystal diameter of 4 µm. Also, large macropores (1 µm) are present between the zeolite crystals.

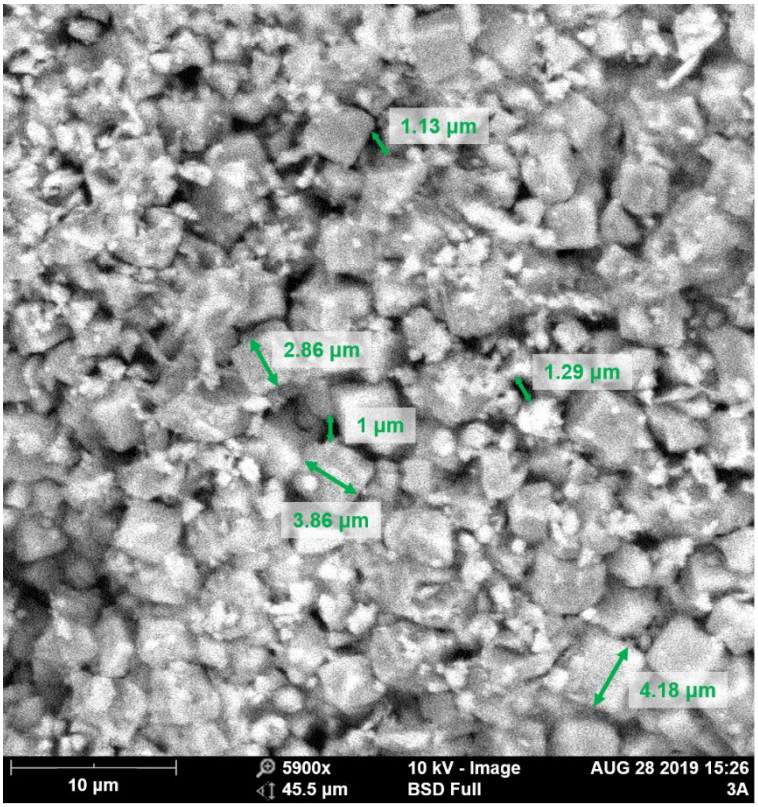

FIGURE 4-2: SEM PICTURE FROM CROSS-SECTIONAL CUT OF A 3A PELLET.

4.2.2. Thermogravimetric analysis

Thermogravimetric analysis (TGA) was performed at Eindhoven University of Technology (TU/e) on an in-house designed setup for operation up to 10 bar (HP-TGA, Figure 4-3). A microbalance (Sartorius M25DD), with an operating range of 200 mg and a sensitivity of 1 µg, is used. The current experiments are performed in the range of 200-400 °C. A nitrogen stream is used to purge the balance and the reactor heating elements protecting them from contamination. The gas feeding system is equipped with Bronkhorst mass flow controllers (MFC) to produce different gas mixtures, and a Bronkhorst controlled evaporation mixing (CEM) system is installed to produce the desired quantities of steam with N_2 as carrier gas. All lines are traced and can be uniformly heated up to 450 °C to avoid steam condensation at elevated pressures. A porous ceramic basket was used with 50-100 mg of sample mass for each experiment. The gas flow rate was such that mass transfer limitations due to the reduced volumetric flow rate in the reactor are avoided, which was verified by flow rate variation.

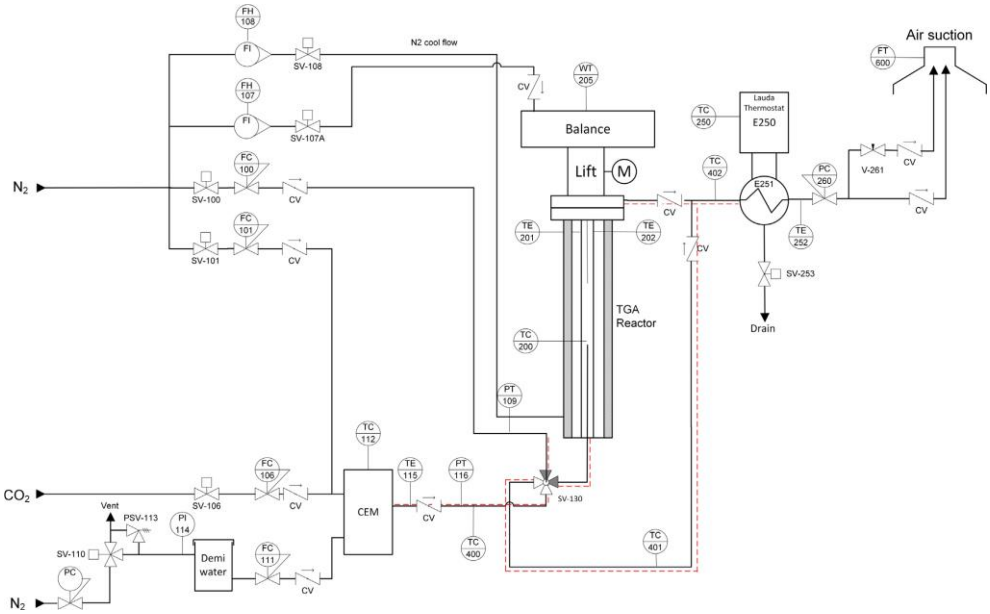

FIGURE 4-3: P&ID OF THE HP-TGA SETUP.

4.2.3. Breakthrough experiments

Experimental breakthrough runs were performed at TNO (Petten) on the 'Microflow 5' test-rig for atmospheric pressure experiments (Figure 4-4). A quartz reactor with an internal diameter of 10 mm was filled with 2 gram of sorbent resulting in a typical bed height of about 40 mm. During adsorption 100 ml_N min^{-1} was fed to the reactor at 200-250 °C. The gas mixture contained 5-40 mol% H_2O, 5% CH_4 as tracer and balance N_2. Regeneration is performed by switching the gas flow to 100 mol% N_2, in some cases with increasing the temperature to 350 °C for 5 minutes. Off-gas analysis was performed continuously by a Perkin Elmer Frontier FTIR with heated Pike 2.4 m gas cell. After the experiment (regeneration step), the final mass of the sorbent is determined, and this value is used for the adsorption capacity calculations of each cycle. Experimental runs at high pressure were performed similarly, but were conducted on the high-pressure multi-column 'Spider' test-rig (Figure 4-4). The reactors of 9.2 mm internal diameter, filled with 5 g sample, are electrically heated and can be run at pressure. During adsorption, the reactors were each fed with 150 ml_N min^{-1} of gas mixtures at 200-250 °C and 5-30 bar(a) pressure. The gas mixtures consisted of 10-15 mol% water and 5 mol% argon as tracer in balance N_2. Adsorbent regeneration always consisted of periodically switching off the water supply, followed by decreasing the pressure. In some cases, the regeneration procedure included raising the temperature to 250-400 °C. Gas analysis was performed by a mass spectrometer (MS) measuring hydrogen (m/z=2), water (m/z=18), carbon monoxide/nitrogen (m/z=28), argon (m/z=40), and carbon dioxide (m/z=44).

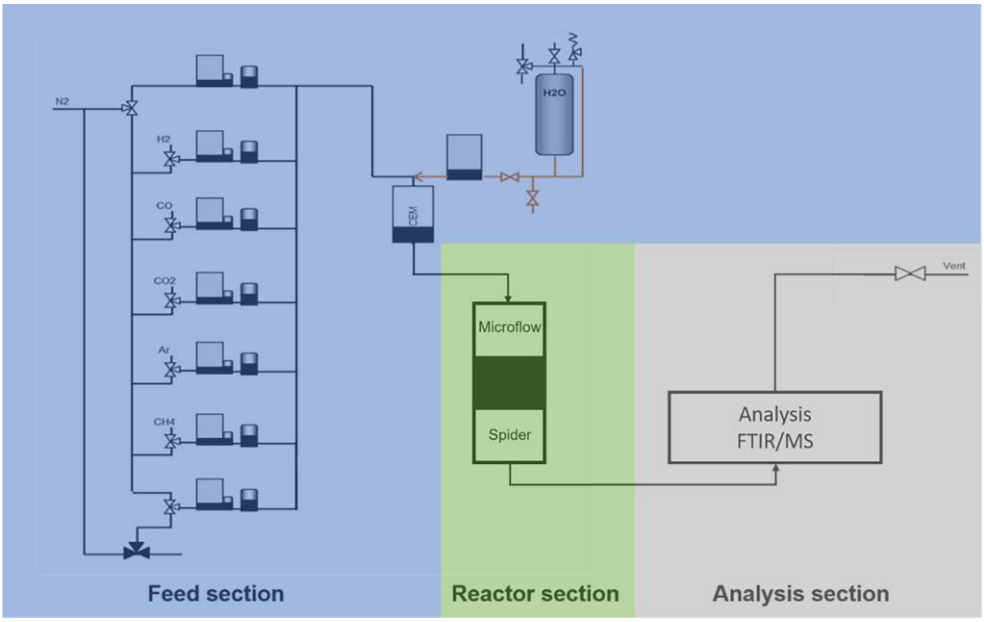

FIGURE 4-4: SCHEMATIC PRESENTATION OF THE BREAKTHROUGH TESTING UNITS 'MICROFLOW 5' AND 'SPIDER'.

4.2.4. Data interpretation and model development

Data interpretation

In the TGA experiments a weight change is obtained, which can be used directly to study the cyclic sorption capacity. For the breakthrough experiments, however, this is not the case. Setting up a material balance for component *i* over the reactor column, accumulation of component *i* between *t=0* and complete breakthrough ($t=t_{end}$) must equal to the difference between the molar inflow and outflow rates.

$$\frac{y_i(t_{end})pV_g}{RT} + q_i(t_{end})m_{ads} - \frac{y_i(0)pV_g}{RT} - q_i(0)m_{ads} = t_{end}F_{i,in} - \int_{t=0}^{t_{end}}(y_iF)_{out}\,dt \qquad (1)$$

The trapezoidal rule has been used for approximating the integral by a summation over discrete measurement data. The breakthrough of tracer (q_{tracer}=0), prior to breakthrough of H_2O, is integrated to obtain V_g, the total interparticle and intraparticle gas volume, according to the Gibbsian surface excess concept [53, 54]. After breakthrough, the tracer signal is used to quantify the outlet flow rate prior to and during breakthrough and Equation 1 can then be used to compute the water loading (q).

In Figure 4-5 an overlay of breakthrough experiments is shown. Both the breakthrough of tracer and water can be seen clearly. The comparable breakthrough signals also show that the experiments can be reproduced with sufficient accuracy. The cyclic stability of the

material is confirmed, as shown in Figure 4-6. In addition, the size exclusion mechanism of zeolite 3A is confirmed as well. The water adsorption capacity does not alter under the studied conditions with H_2, CO and/or CO_2 present in the feed gas mixture.

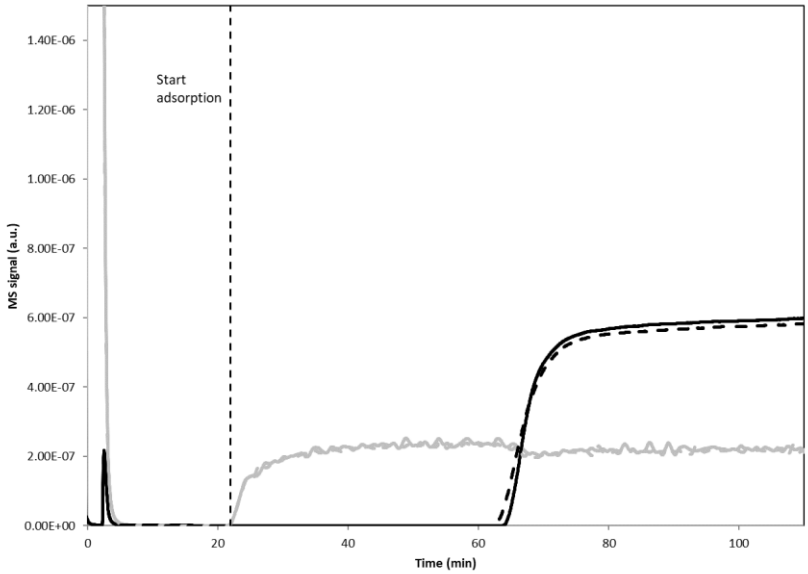

FIGURE 4-5: OVERLAY OF SEVERAL BREAKTHROUGH EXPERIMENTS WITH ZEOLITE 3A AT 250 °C ADSORPTION TEMPERATURE AND 3 BAR PARTIAL PRESSURE: TRACER SIGNAL (GREY LINES), H_2O CYCLE 55 (BLACK SOLID LINE) AND H_2O CYCLE 58 (BLACK DASHED LINE).

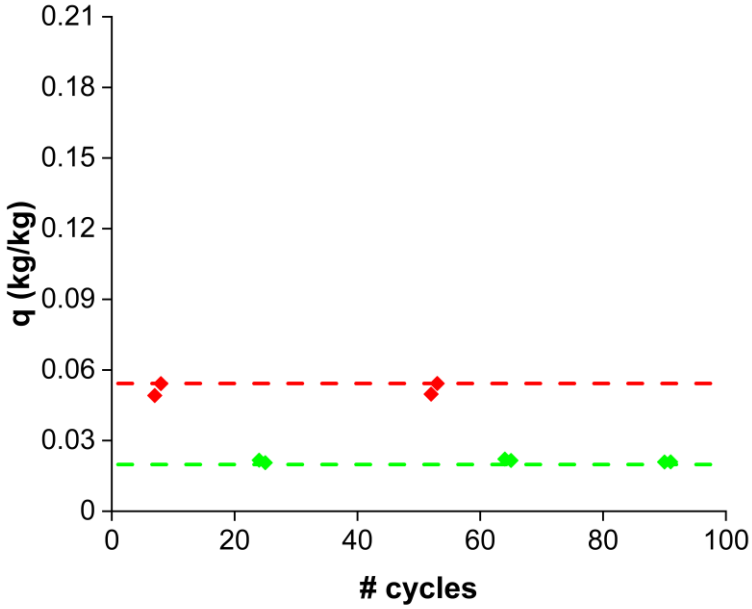

FIGURE 4-6: WATER LOADING OBSERVED DURING CYCLIC BREAKTHROUGH EXPERIMENTS WITH ZEOLITE 3A AT 0.1 BAR PARTIAL PRESSURE AND DIFFERENT TEMPERATURES (• 200 °C, • 250 °C). ISOTHERM PREDICTION IS SHOWN BY THE DASHED LINES.

Model development

The adsorption capacity and mass transfer for water adsorption are determined by model evaluation. The material parameters used for modelling are reported in Table 4-1.

TABLE 4-1: MATERIAL PARAMETERS USED FOR MODELLING.

$q_{s,crystal}$ (wt.%)	25.5	[55]
d_p (mm)	1.6	[55]
ρ_b (kg m^{-3})	640	[55]
ε_p (-)	0.662	[21]
ε_b (-)	0.372	[21]
d_m (µm)	1	This work
d_c (µm)	4	This work

Adsorption isotherm model

Adsorption isotherms are derived on the basis of the underlying physics of sorbent-sorbate interaction. The GSTA model derived by Llano-Restrepo et al. is highly flexible in fitting *m* event energies and is given below [35]:

$$q = \frac{q_{max}}{m} \frac{\sum_{n=1}^{m} nK_n^0 (\frac{P}{P^0})^n}{1+\sum_{n=1}^{m} K_n^0 (\frac{P}{P^0})^n} \quad (2)$$

$$\ln K_n^0 = -\frac{\Delta H_n^0}{RT} + \frac{\Delta S_n^0}{R} \quad (3)$$

Where q_{max} is the maximum (theoretical) adsorption capacity, m is the number of distinct adsorption sites (statistical subsystems), K^0_n is the dimensionless equilibrium constant with the standard-state pressure P^0 relative to the adsorption of n molecules in a given statistical subsystem, and the standard enthalpy and entropy of these subsystems are represented by ΔH^0_n and ΔS^0_n. The model contains m+2 fitting parameters, but in this work q_{max} is fixed as the maximum adsorption capacity given by the supplier.

As presented in the Introduction, the GSTA model can be seen as a special case of a multi-site Langmuir where the site contribution to the adsorption capacity is equal. The multi-site Langmuir model is given below:

$$q = \sum_{i=1}^{j} q_{s,i} \frac{K_{L,i}p}{1+K_{L,i}p} \quad (4)$$

$$K_{L,i} = b_i e^{-E_{a,i}/RT} \quad (5)$$

Here q_s is the saturation capacity of the specific site, j is the number of adsorption sites and K_L is the equilibrium constant of the Langmuir model. Each site has a different associated energy and is correlated with temperature according to the van 't Hoff equation (5).

Capillary condensation describes the condensation of vapor into capillaries or small pores at vapor pressures lower than the saturation vapor pressure of the liquid with a planar surface [56]. It is known to play a role in water adsorption on various porous adsorbents [43] and can be described using the Kelvin equation, presented here for a sphere-like volume of radius r_{pore} [56]:

$$\ln\left(\frac{p}{p_s}\right) = -\frac{2\gamma v_m}{RTr_{pore}} \quad (6)$$

where p_s is the saturation vapor pressure for a flat liquid surface, v_m is the molar volume of the liquid, γ is the surface tension and r_{pore} is the pore radius. Assuming the effective pore size is uniformly distributed (from 0 to r_{max}), one can derive the following equation [57]:

$$q = \frac{\mu}{RTln(\frac{p_s}{p})} \quad (7)$$

$$\mu = \frac{2\gamma V_{pore}}{r_{max}} \quad (8)$$

In literature, between 2 and 7 [21, 34, 35, 37, 50, 51] different energetic sites have been proposed for water adsorption on LTA zeolites. Clearly, the LTA framework consists of two

distinct cavities which are accessible to water, the α and β cages [48, 49]. It is shown that there are more adsorption sites, specifically related to the cation and its position in the α cage [34, 58]. However, the energies found for the different sites by other authors are very close [34, 35, 50]. Therefore, it is suggested here to consider three distinctive sites. These sites correspond to the α cage and the β cage in the micropore and a mesopore contribution. Recently, a similar approach was used to describe water adsorption on zeolites 3A and 4A with a triple Langmuir isotherm [51]. It has been shown that a triple-site Langmuir is able to describe the water adsorption in zeolite 3A (Grace Davison), similar compared to the seven-site GSTA model [35, 51]. This can be explained by the fact that the authors use the same number of fitting parameters (9). However, it shows the validity of a multi-site Langmuir approach, of which the GSTA model is a special case. It does not explain the multilayer adsorption observed in this work and by other authors [24, 43, 59], which does not occur in the micropores of the adsorbent, but rather in the mesopores [43, 60]. Therefore, the third site could be described by a multilayer isotherm such as generally used in the BET isotherm [43, 60, 61]. However, in a porous adsorbent multilayer formation will progress to capillary condensation, in which smaller pores are completely filled with water [43]. Taking this into account, the Kelvin equation can be used to describe multilayer formation and subsequent capillary condensation [43, 57, 59, 62, 63]. Based on these considerations, a dual-site GSTA isotherm (Equation 2 with m=2 or Equation 4 with j=2 and $q_{s,i}=q_{s,j}$) plus the Kelvin equation (Equation 7) are used to describe the water adsorption (Equation 9):

$$q = \frac{f q_s}{m}\left(\frac{\sum_{n=1}^{m} n K_n^0 (\frac{P}{P^0})^n}{1+\sum_{n=1}^{m} K_n^0 (\frac{P}{P^0})^n}\right) + \frac{\mu}{RTln(\frac{p_s}{p})} \tag{9}$$

The maximum capacity of the zeolite crystal is fixed at 25.5 wt.%, as given by the vendor and the pellet is considered to contain 20% binder (f=0.8) (Table 4-1).

Adsorption mass transfer model

In order to assess the adsorbate mass transport, the linear driving force (LDF) approximation is used [53, 64, 65]. The overall mass transfer coefficient (k_{LDF}) can be defined as a series of resistances, consisting of external film resistance, macropore resistance, and micropore resistance, respectively [43]. This approach is used to assess mass transfer limitations in one or more of the pores and the film layer, rather than describe the transport phenomenon. The transport through the pores of a practical porous adsorbent is a very complex phenomenon, mainly due to the heterogeneous pore structure.

$$\frac{1}{k_{LDF}} = \frac{R_p \Lambda}{3k_f} + \frac{{R_p}^2 \Lambda}{15\varepsilon_p D_p} + \frac{{R_c}^2}{15D_c} \tag{10}$$

$$\Lambda = \varepsilon_p + (1-\varepsilon_p)\rho_p \frac{\partial q}{\partial c} \tag{11}$$

The particle and crystal radius are given by R_p and R_c respectively. Similarly D_p and D_c are the macropore and micropore diffusivity. ε_p is the particle porosity and ρ_p its density. Λ is the partition ratio, describing the isotherm dependence. The film mass transfer coefficient (k_f) is estimated with the correlation by Wakao and Funazkri [43]:

$$Sh = 2 + 1.1Re^{0.6}Sc^{1/3} \quad (12)$$

The equations used for the macropore and micropore diffusion are given in Table 4-2 [43, 60, 66, 67].

TABLE 4-2: MACROPORE AND MICROPORE DIFFUSION EQUATIONS.

Macropore diffusivity	$D_p = \frac{\left(\frac{1}{D_m}+\frac{1}{D_K}\right)^{-1}}{\tau}$	(13)
Molecular gas diffusivity	$D_{i,m} = \left(\sum_{\substack{j=1 \\ j\neq i}}^{n} \frac{x_j}{D_{i,j}}\right)^{-1}$	(14)
Binary diffusion coefficients	$D_{AB} = \frac{0.00143T^{1.75}}{PM_{AB}^{\frac{1}{2}}((\Sigma_A v_i)^{\frac{1}{3}}+(\Sigma_B v_i)^{\frac{1}{3}})^2}$	(15)
Effective micropore diffusivity (Darken relation)	$D_c = D_c^* \frac{\partial ln\, p}{\partial lnq}$	(16)
Micropore diffusivity	$D_c^* = D_c^0 e^{-E_a/RT}$	(17)

4.3. Results and discussion

4.3.1. Adsorption capacity

Figure 4-7 shows the equilibrium data for water vapor adsorption on the zeolite 3A. The breakthrough data align well with the TGA data at lower pressures, confirming the experimental approach. Where the TGA data start to deviate at higher steam partial pressures due to experimental uncertainty, the breakthrough data at higher pressures show an increasing adsorption capacity, as is known for this type of material at low temperatures [24, 34, 35, 43].

In a porous adsorbent the observed multilayer formation will progress to capillary condensation [43]. Therefore, considering capillary condensation, a dual-site GSTA isotherm in combination with the Kelvin equation is used to describe the water adsorption (Equation 9).

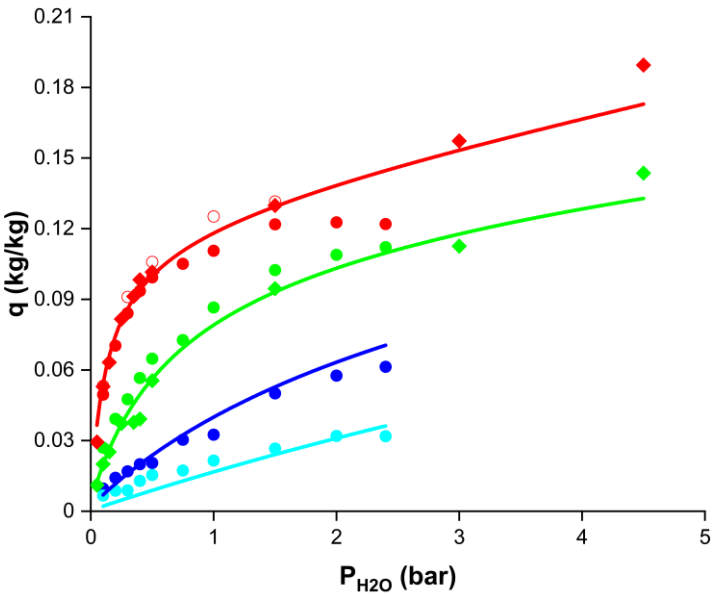

FIGURE 4-7: FIT OF THE DUAL-SITE GSTA CAPILLARY CONDENSATION MODEL TO THE ADSORPTION ISOTHERMS DATA POINTS OF WATER VAPOR IN ZEOLITE 3A AT DIFFERENT TEMPERATURES (• 200 °C, • 250 °C, • 300 °C, • 350 °C). CIRCLES: EXPERIMENTAL TGA DATA AND CRUSHED SAMPLE DUPLO (OPEN CIRCLES); DIAMONDS: EXPERIMENTAL BREAKTHROUGH DATA; SOLID LINES: ISOTHERM MODEL WITH PARAMETERS FROM TABLE 4-3. THEORETICAL MAXIMUM CAPACITY OF THE CRYSTALS IS FIXED AT 25.5 WT.%.

TABLE 4-3: PARAMETERS FOR THE DUAL-SITE GSTA ISOTHERM WITH CAPILLARY CONDENSATION ON WATER ADSORPTION DATA.

Fixed parameters		***Fitted parameters ± standard error***			
q_s (kg kg^{-1})	0.255	ΔH^0_1 (kJ mol^{-1})	-62.4 ± 3.1	ΔS^0_1 (J K^{-1} mol^{-1})	-115 ± 5
f (-)	0.8	ΔH^0_2 (kJ mol^{-1})	-75.1 ± 31.0	ΔS^0_2 (J K^{-1} mol^{-1})	-160 ± 52
m (-)	2				

As is shown in Figure 4-7 a good predictive quality is achieved for the experimental data. The good predictive capability of the observed loading is shown in Figure 4-8, where the average deviation is about 4%. The resulting regressed parameters (Table 4-3) show two distinctive sites for the micropore adsorption.

Despite the different physical interpretation, it can be observed that the first event energy (attributed here to the α cage) aligns well with the values reported in literature, which are very close for subsequent events [34, 35, 50]. The second event energy is significantly higher (less negative), which can be explained by the β cage contribution used here compared to the GSTA approach as used in literature. Whereas the GSTA model can be seen as a multi-

site Langmuir isotherm with equal site contribution to the adsorption capacity [50], the activation energies for the corresponding dual-site Langmuir can be determined. Although the experiments in this work are performed at elevated temperatures and pressures compared to previous works, the approximate energies found for the α and β cage, -70 and -10 kJ mol^{-1} respectively, are in agreement with the range reported in literature [21, 34, 35, 37, 50, 51, 68]. Note that the contribution to the total capacity is considered equal, as for the GSTA model. Considering the smaller uptake in the β cage (1/3) compared to the α cage (2/3) [34], the activation energies become respectively 37% smaller and 10% larger.

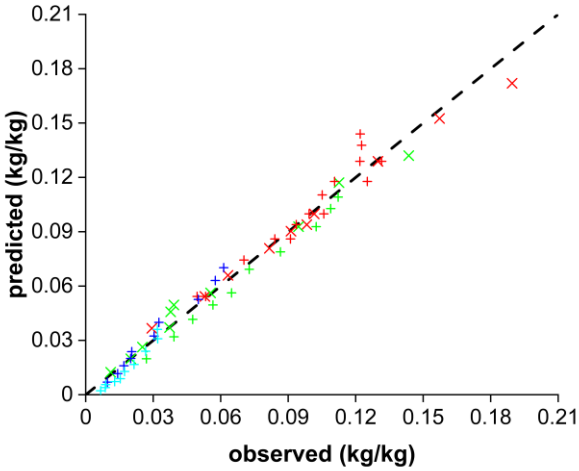

FIGURE 4-8: PARITY PLOT FOR THE DUAL-SITE GSTA ISOTHERM WITH CAPILLARY CONDENSATION AT THE DIFFERENT STUDIED TEMPERATURES (• 200 °C, • 250 °C, • 300 °C, • 350 °C).

The values found for capillary condensation are shown in Table 4-4. Taking the temperature dependence of the surface tension into consideration, the results are in the same order of magnitude with values reported in literature for alumina. The capillary condensation results also indicate that the condensation occurs in mesopores (20-500 Å) rather than actual larger macropores (>500 Å), which is typical for capillary condensation [56]. As shown in Figure 4-9 the model is able to describe low temperature data reported by other authors quite well, taking into account the model only uses two subsystems and capillary condensation [42]. The capillary condensation, based on a uniform pore distribution, however, does not have a finite limit and cannot describe a type 4 isotherm of the Brunauer's classification fully. This will cause an overprediction at low temperature outside the scope of this work and a pressure close the saturation pressure, which could be solved by including the maximum amount adsorbed in the mesopore, if known [57, 69]. Despite the improvement which could be made for the region close to the saturation pressure, the isotherm model is

able to describe the equilibrium data under sorption enhanced reaction temperatures and pressures well.

TABLE 4-4: PARAMETERS FOR CAPILLARY CONDENSATION FOUND FOR THE DUAL-SITE GSTA (THIS WORK) AND VALUES FOUND FOR CAPILLARY CONDENSATION ON DIFFERENT TYPES OF ALUMINA [57].

Temperature (K)	μ/RT (mol kg^{-1}) *This work*
473.15	*2.63*
523.15	*1.67*
573.15	*0.849*
623.15	*0.196*

Alumina	μ/RT (mol kg^{-1}) [57]
A1	0.975
AA300	5.76
Nakarai	5.44
F-200	9.57

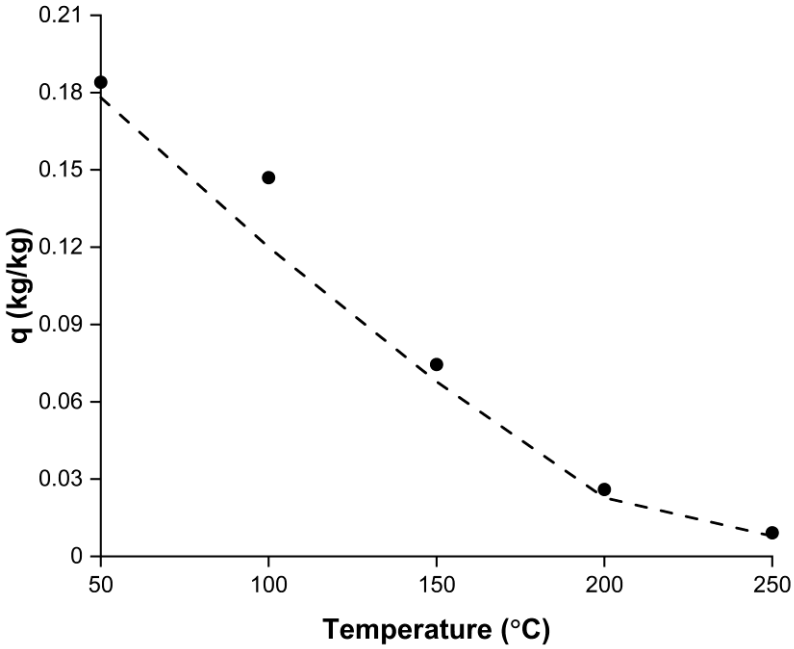

FIGURE 4-9: GSTA MODEL PREDICTION (LINE) FOR LOW TEMPERATURE DATA AT A PARTIAL PRESSURE OF 2.337 KPA FROM GHODHBENE ET AL. [42].

4.3.2. Adsorbate mass transfer

Besides the adsorption capacity at elevated temperatures, the kinetics of adsorption and the adsorbate mass transport are essential for the application of the adsorbent in a sorption

enhanced reaction process [1, 52]. Figure 4-10 shows that the experimental mass transfer rate can be described well with the linear driving force (LDF) approximation [64, 65], which can be explained by the parabolic concentration profiles in the adsorbent particle over long half-cycle times [70, 71]. This is observed for all partial pressures and temperatures (Figure 4-10).

The overall mass transfer coefficient can be defined as a series of resistances (Equation 10) to assess mass transfer limitations, contributed to by the external film resistance ($\frac{R_p \Lambda}{3k_f}$), macropore resistance ($\frac{{R_p}^2 \Lambda}{15\varepsilon_p D_p}$) and micropore resistance ($\frac{{R_c}^2}{15D_c}$), respectively [43, 53]. Other authors also confirmed the predictive capability of the LDF model for the water adsorption on zeolite 3A [68, 72]. The overall mass transfer resistance has been attributed to a combination of the external film resistance and the macropore resistance [72], or to a combination of the macropore and micropore resistances [68]. If we calculate the external mass transfer resistance and the macropore resistance according to Equations 10-15, we observe that the data presented here are solely limited by the micropore resistance (Figure 4-11, Figure 4-12). Even if the macropore diameter would be a factor ten smaller (0.1 µm), the micropore resistance would still make up more than 95% of the total mass transfer resistance. Also the practical adsorbent pellet size can vary, affecting the external film resistance and mainly the macropore resistance due to the quadratic dependence, which has been shown to influence the overall mass transfer coefficient significantly [68, 73]. Experiments with varying pellet size would clarify the relative contribution of the different mass transfer resistances. In addition, direct imaging could be a powerful technique to circumvent possible issues arising from this, and is a good addition to the existing experimental methods [73, 74]. As shown by the difference between the graphs in Figure 4-10, the overall mass transfer coefficient increases with increasing partial pressure of water. Although the micropore resistance is always rate determining, the contribution of the micropore resistance to the overall mass transfer resistance increases with increasing partial pressure (Figure 4-11). Despite the increasing micropore transfer rate at higher partial pressures, the decrease of the partition ratio (Equation 11), and therefore the decrease in the macropore resistance, at higher partial pressures is larger. As expected, the increasing temperature also increases the overall mass transfer coefficient (Figure 4-10). Although all diffusion mechanisms are temperature dependent and the diffusivities increase with increasing temperature, the partition ratio decreases with temperature since the adsorption is favored at low temperature. As a result there is a small decrease (98% to 97.3%) of the relative micropore resistance from 200 to 250 °C, and an increase (to 98.4%) going towards 350 °C (Figure 4-12).

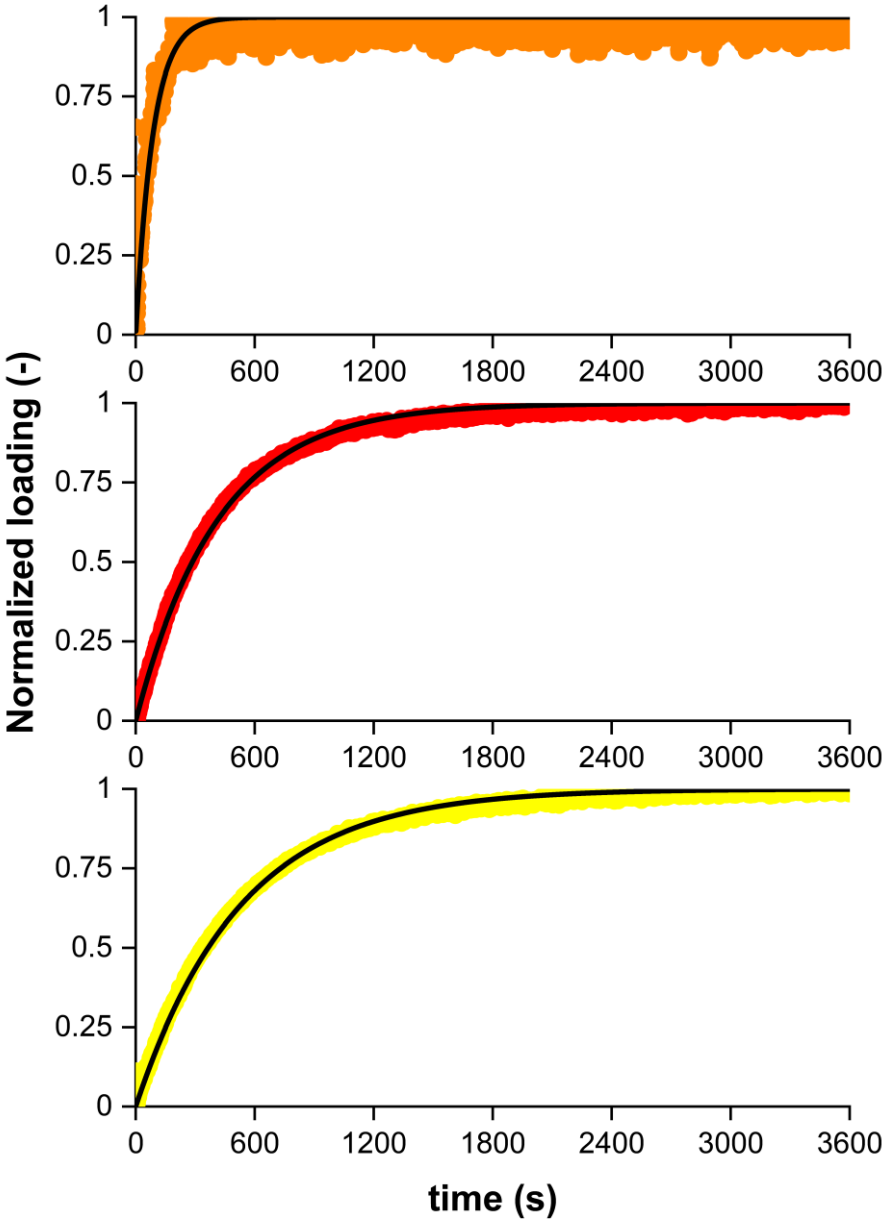

FIGURE 4-10: FIT OF LDF MASS TRANSFER RATE (BLACK LINES) AT 300 °C AND 0.5 BAR WATER PARTIAL PRESSURE (TOP), 200 °C AND 0.5 BAR WATER PARTIAL PRESSURE (MIDDLE) AND 200 °C AND 0.3 BAR WATER PARTIAL PRESSURE (BOTTOM).

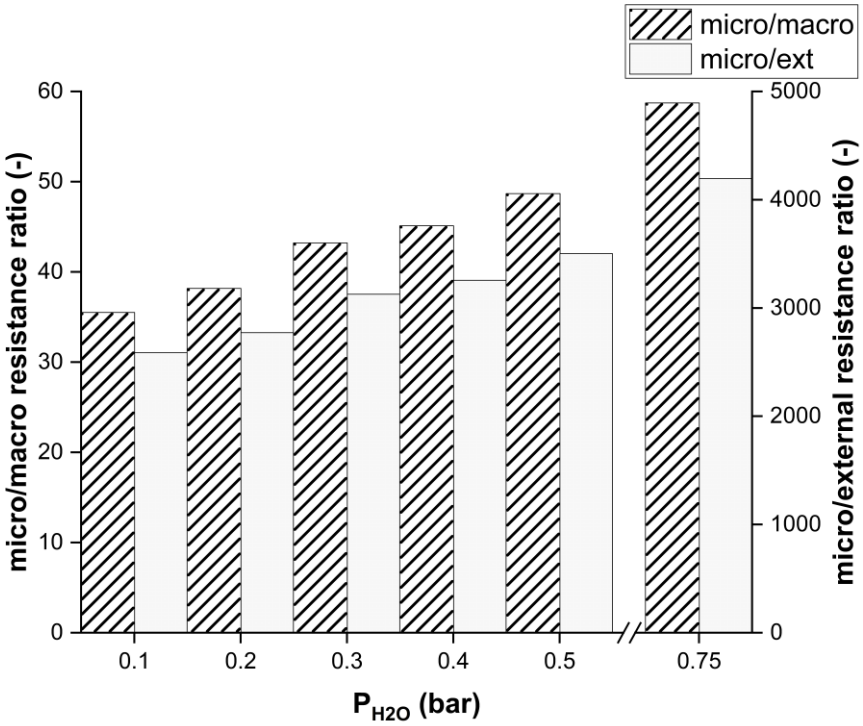

FIGURE 4-11: MASS TRANSFER RESISTANCES AS RATIO OF THE MICROPORE RESISTANCE TO THE MACROPORE RESISTANCE (LEFT AXIS) AND THE EXTERNAL FILM RESISTANCE (RIGHT AXIS) FOR ADSORPTION EXPERIMENTS AT 200 °C.

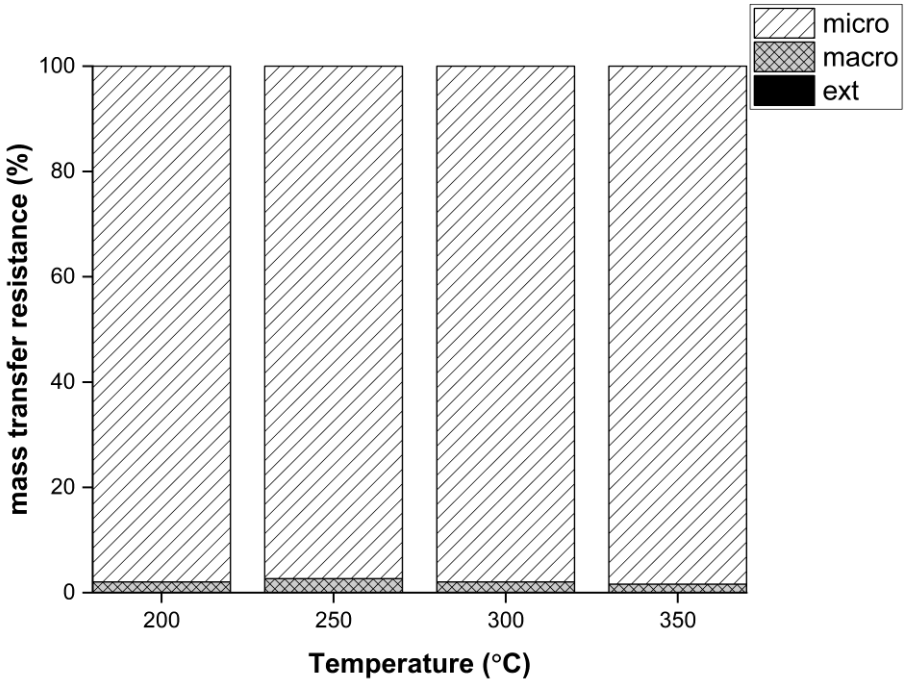

FIGURE 4-12: MASS TRANSFER RESISTANCES IN PERCENTAGE OF OVERALL RESISTANCE FOR ADSORPTION EXPERIMENTS AT 0.5 BAR PARTIAL PRESSURE.

Knowing the respective contributions of the mass transfer resistances to the overall mass transfer coefficient, the micropore diffusivity can be calculated. Due to the small aperture of the micropores, the intracrystalline diffusion is relatively slow and the diffusivity is usually concentration and temperature dependent, given by the Darken relation (Equation 16) [43, 60].

The values found for the micropore diffusivity are reported in Table 4-5. Relatively high indeed, the activation energy of 54.2 kJ mol^{-1} is in good agreement with values (of up to 60 kJ mol^{-1}) reported for zeolites A [43, 46, 68]. Clearly, the activation energy strongly depends on the sorbate diameter (Figure 4-1) relative to the micropore size. Therefore, one could also expect a high activation energy for the small pore molecular sieve 3A.

TABLE 4-5: PARAMETERS FOR THE MICROPORE DIFFUSIVITY (ACCORDING TO LDF MODEL).

D_c^0 (m^2 s^{-1})	1.87 10^{-10}
E_a (kJ mol^{-1})	54.2

As discussed for the adsorption capacity, there are multiple sites (α and β cage) for adsorption in zeolite 3A. Therefore multiple micropore diffusivities could be expected, in

agreement with some authors who show a single LDF model not being able to predict the adsorption rate [42]. Secondly, the LDF approximation is based on parabolic concentration profiles, which is known to be invalid for short cycle times [75-77]. Based on this a refinement of the current model could be made, but the experimental data show this is not required. Under the currently considered conditions, the adsorbate mass transfer described here proves to be sufficiently adequate for all modelling purposes. The LDF model has been verified experimentally for use in process modelling.

4.4. Conclusions

In conclusion, it is shown that molecular sieve (LTA) 3A has an adequate adsorption capacity at elevated temperatures, which increases rapidly at higher partial pressures of steam. This makes the LTA adsorbent suitable for sorption enhanced reaction processes, such as CO_2 conversion, enabling high yield condensation reaction products.

The water adsorption on the material can be described with a multi-site GSTA isotherm and additional capillary condensation. The multi-site isotherm can be best described as a dual-site GSTA isotherm (dual-Langmuir) corresponding to the respective α and β cages. Using a GSTA isotherm (or heterogeneous Langmuir) allows further flexibility in the number of distinct adsorption sites.

The adsorption mass transfer rate can be described by the linear driving force approximation, which is sufficiently accurate for all reactor and process modelling purposes. The mass transfer resistance during adsorption on zeolite 3A is shown to be dominantly determined by micropore resistance, due to the cage aperture.

Nomenclature

a_p	Particle interfacial area ($m^2\ m^{-3}$)
b	Isotherm equilibrium constant (bar^{-1})
d_c	Crystal diameter (m)
d_m	Macropore diameter (m)
d_p	Particle diameter (m)
D_c	Micropore diffusion coefficient ($m^2\ s^{-1}$)
D_k	Knudsen diffusion coefficient ($m^2\ s^{-1}$)
D_m	Molecular diffusion coefficient ($m^2\ s^{-1}$)
D_p	Macropore diffusion coefficient ($m^2\ s^{-1}$)
E_a	Activation energy ($kJ\ mol^{-1}$)
F_i	Molar flow of component i ($mol\ s^{-1}$)
k_f	External film mass transfer coefficient ($m\ s^{-1}$)
k_{LDF}	Linear driving force rate constant (s^{-1})
K_L	Equilibrium constant of the multi-site Langmuir model

K_n	Equilibrium constant of the GSTA model (-)
m	number of equilibrium parameters in the GSTA model
m_{ads}	mass of adsorbent (kg)
M_i	Molecular weight of component i (kg mol^{-1})
n	Index number of parameters and adsorption sites in the GSTA model
P	Pressure (bara)
P^0	Standard pressure (bara)
P_i	Partial pressure of component i (bara)
q_i	Adsorbent loading (mol kg^{-1}) or (kg kg^{-1})
q_{max}	Maximum adsorption capacity (kg kg^{-1})
q_s	Saturation capacity (kg kg^{-1})
R	Ideal gas constant (J mol^{-1} K^{-1})
R_c	Crystal radius (m)
R_p	Particle radius (m)
Re	Reynolds number (-)
Sc	Schmidt number (-)
Sh	Sherwood number (-)
t	Time (s)
T	Temperature (K)
u	Superficial gas velocity (m s^{-1})
v	Interstitial gas velocity (m s^{-1})
V_g	Gas volume (m^3)
y_i	Molar fraction of component i (-)

Greek letters

γ	surface tension (N m^{-1})
ΔH^0	Standard molar enthalpy (kJ mol^{-1})
ΔS^0	Standard molar entropy (J K^{-1} mol^{-1})
ε_b	Bed voidage (-)
ε_p	Particle porosity (-)
Λ	Partition function (-)
μ	Parameter corresponding to the adsorption potential (mol kg^{-1}) or (kg kg^{-1})
ρ	Density (kg m^{-3})
ρ_p	Particle density (kg m^{-3})
τ	Tortuosity (-)

Abbreviations

DME	Dimethyl ether
GSTA	Generalized Statistical Thermodynamic Adsorption

LTA Linde Type A
SEDMES Sorption enhanced DME synthesis
SEM Scanning electron microscopy
TGA Thermogravimetric analysis

Bibliography

[1] J. van Kampen, J. Boon, F. van Berkel, J. Vente, M. van Sint Annaland, Steam separation enhanced reactions: Review and outlook, Chemical Engineering Journal 374 (2019) 1286–1303.
[2] G. Centi, S. Perathoner, Opportunities and prospects in the chemical recycling of carbon dioxide to fuels, Catalysis Today 148 (2009) 191-205.
[3] Accelerating Breakthrough Innovation in Carbon Capture, Utilization, and Storage, Report of the Mission Innovation Carbon Capture, Utilization, and Storage Expert's Workshop, 2017.
[4] A. Katelhon, R. Meys, S. Deutz, S. Suh, A. Bardow, Climate change mitigation potential of carbon capture and utilization in the chemical industry, Proc Natl Acad Sci U S A 116 (2019) 11187-11194.
[5] H.-J. Kim, H. Jung, K.-Y. Lee, Effect of Water on Liquid Phase DME Synthesis from Syngas over Hybrid Catalysts Composed of Cu/ZnO/Al_2O_3 and γ-Al_2O_3, Korean Journal of Chemical Engineering 18 (2001) 838-841.
[6] B.T. Carvill, J.R. Hufton, M. Anand, S. Sircar, Sorption-enhanced reaction process, AIChE Journal 42 (1996) 2765-2772.
[7] A. Borgschulte, N. Gallandat, B. Probst, R. Suter, E. Callini, D. Ferri, Y. Arroyo, R. Erni, H. Geerlings, A. Züttel, Sorption enhanced CO_2 methanation, Physical Chemistry Chemical Physics 15 (2013) 9620-9620.
[8] S. Ressler, M. Elsner, C. Dittrich, D. Agar, S. Geisler, O. Hinrichsen, Reactive gas adsorption, Integrated Reaction and Separation Operations, Springer2006.
[9] J.-C. Choi, L.-N. He, H. Yasuda, T. Sakakura, Selective and high yield synthesis of dimethyl carbonate directly from carbon dioxide and methanol, Green Chemistry 4 (2002) 230-234.
[10] J. Boon, J. van Kampen, R. Hoogendoorn, S. Tanase, F.P.F. van Berkel, M. van Sint Annaland, Reversible deactivation of γ-alumina by steam in the gas-phase dehydration of methanol to dimethyl ether, Catalysis Communications 119 (2019) 22-27.
[11] J. van Kampen, S. Booneveld, J. Boon, J. Vente, M. van Sint Annaland, Experimental validation of pressure swing regeneration for faster cycling in sorption enhanced dimethyl ether synthesis, Chemical Communications 56 (2020) 13540-13542.
[12] D. Liuzzi, C. Peinado, M.A. Peña, J. van Kampen, J. Boon, S. Rojas, Increasing dimethyl ether production from biomass-derived syngas via sorption enhanced dimethyl ether synthesis, Sustainable Energy & Fuels 4 (2020) 5674-5681.

[13] J. van Kampen, J. Boon, J. Vente, M. van Sint Annaland, Sorption enhanced dimethyl ether synthesis for high efficiency carbon conversion: Modelling and cycle design, Journal of CO_2 Utilization 37 (2020) 295-308.
[14] I. Iliuta, M.C. Iliuta, F. Larachi, Sorption-enhanced dimethyl ether synthesis — Multiscale reactor modeling, Chemical Engineering Science 66 (2011) 2241-2251.
[15] A.A.M. Parra, C. Asmanoglo, D.W. Agar, Cyclic Steady-State Behavior of a Fixed-Bed Adsorptive Reactor for Reverse Water-Gas Shift Reaction, Chemical & Engineering Technology 40 (2017) 915-926.
[16] A.A.M. Parra, C. Asmanoglo, D.W. Agar, Modelling and optimization of a moving-bed adsorptive reactor for the reverse water-gas shift reaction, Computers and Chemical Engineering 109 (2018) 203-215.
[17] M. Bayat, M. Heravi, M.R. Rahimpour, Sorption enhanced process by integrated heat-exchanger reactor assisted by fluidization concept for methanol synthesis, Chemical Engineering and Processing: Process Intensification 110 (2016) 30-43.
[18] S. Guffanti, C.G. Visconti, J. van Kampen, J. Boon, G. Groppi, Reactor modelling and design for sorption enhanced dimethyl ether synthesis, Chemical Engineering Journal 404 (2021) 126573-126585.
[19] Y. Yuan, H. Zhang, F. Yang, N. Zhang, X. Cao, Inorganic composite sorbents for water vapor sorption: A research progress, Renewable and Sustainable Energy Reviews 54 (2016) 761-776.
[20] H. Li, C. Qiu, S. Ren, Q. Dong, S. Zhang, F. Zhou, X. Liang, J. Wang, S. Li, M. Yu, Na+-gated water-conducting nanochannels for boosting CO2 conversion to liquid fuels, Science Catalysis 367 (2020) 667–671.
[21] E. Gabruś, J. Nastaj, P. Tabero, T. Aleksandrzak, Experimental studies on 3A and 4A zeolite molecular sieves regeneration in TSA process: Aliphatic alcohols dewatering-water desorption, Chemical Engineering Journal 259 (2015) 232-242.
[22] Z. Pan, C.Y. Zhao, Dehydration/hydration of MgO/H_2O chemical thermal storage system, Energy 82 (2015) 611-618.
[23] A. Kohl, R. Nielsen, Gas Dehydration and Purification by Adsorption, Gas Purification, Gulf Publishing Company1997.
[24] K.-M. Kim, H.-T. Oh, S.-J. Lim, K. Ho, Y. Park, C.-H. Lee, Adsorption Equilibria of Water Vapor on Zeolite 3A, Zeolite 13X, and Dealuminated y Zeolite, Journal of Chemical and Engineering Data 61 (2016) 1547-1554.
[25] B. Dou, C. Wang, Y. Song, H. Chen, B. Jiang, M. Yang, Y. Xu, Solid sorbents for in-situ CO_2 removal during sorption-enhanced steam reforming process: A review, Renewable and Sustainable Energy Reviews 53 (2016) 536-546.
[26] A. Ignatchenko, D.G. Nealon, R. Dushane, K. Humphries, Interaction of water with titania and zirconia surfaces, Journal of Molecular Catalysis A: Chemical 256 (2006) 57-74.

[27] W. Zhu, L. Gora, A.W.C. van den Berg, F. Kapteijn, J.C. Jansen, J.A. Moulijn, Water vapour separation from permanent gases by a zeolite-4A membrane, Journal of Membrane Science 253 (2005) 57-66.
[28] S. Khajavi, J.C. Jansen, F. Kapteijn, Application of hydroxy sodalite films as novel water selective membranes, Journal of Membrane Science 326 (2009) 153-160.
[29] J. Terreni, M. Trottmann, T. Franken, A. Heel, A. Borgschulte, Sorption-Enhanced Methanol Synthesis, Energy Technology 7 (2019) 1801093-1801101.
[30] S. Walspurger, G.D. Elzinga, J.W. Dijkstra, M. Saric, W.G. Haije, Sorption enhanced methanation for substitute natural gas production: Experimental results and thermodynamic considerations, Chemical Engineering Journal 242 (2014) 379-386.
[31] J.B. Lad, Y.T. Makkawi, Adsorption of dimethyl ether (DME) on zeolite molecular sieves, Chemical Engineering Journal 256 (2014) 335-346.
[32] B.A.V. Santos, V.M.T.M. Silva, J.M. Loureiro, E. Rodrigues, Adsorption of H_2O and Dimethyl Carbonate at High Pressure over Zeolite 3A in Fixed Bed Column, Industrial & Engineering Chemistry Research 53 (2014) 2473−2483.
[33] B. Mette, H. Kerskes, H. Drück, H. Müller-Steinhagen, Experimental and numerical investigations on the water vapor adsorption isotherms and kinetics of binderless zeolite 13X, International Journal of Heat and Mass Transfer 71 (2014) 555-561.
[34] R. Lin, A. Ladshaw, Y. Nan, J. Liu, S. Yiacoumi, C. Tsouris, D.W. DePaoli, L.L. Tavlarides, Isotherms for Water Adsorption on Molecular Sieve 3A: Influence of Cation Composition, Industrial & Engineering Chemistry Research 54 (2015) 10442-10448.
[35] M. Llano-Restrepo, M.A. Mosquera, Accurate correlation, thermochemistry, and structural interpretation of equilibrium adsorption isotherms of water vapor in zeolite 3A by means of a generalized statistical thermodynamic adsorption model, Fluid Phase Equilibria 283 (2009) 73-88.
[36] Q.H. Dirar, K.F. Loughlin, Intrinsic adsorption properties of CO2 on 5A and 13X zeolite, Adsorption 19 (2013) 1149-1163.
[37] K.F. Loughlin, Water isotherm models for 4A (NaA) zeolite, Adsorption 15 (2009) 337-353.
[38] J. Boon, P.D. Cobden, H.A.J. van Dijk, C. Hoogland, E.R. van Selow, M. van Sint Annaland, Isotherm model for high-temperature, high-pressure adsorption of and on K-promoted hydrotalcite, Chemical Engineering Journal 248 (2014) 406-414.
[39] A. Borgschulte, E. Callini, N. Stadie, Y. Arroyo, M.D. Rossell, R. Erni, H. Geerlings, A. Züttel, D. Ferri, Manipulating the reaction path of the CO_2 hydrogenation reaction in molecular sieves, Catalysis Science & Technology 5 (2015) 4613-4621.
[40] R. Delmelle, J. Terreni, A. Remhof, A. Heel, J. Proost, A. Borgschulte, Evolution of Water Diffusion in a Sorption-Enhanced Methanation Catalyst, Catalysts 8 (2018) 341-355.
[41] H. Sun, D. Wu, X. Guo, B. Shen, a. Navrotsky, Energetics of sodium–calcium exchanged zeolite A, Phys. Chem. Chem. Phys. 17 (2015) 11198-11203.

[42] M. Ghodhbene, F. Bougie, P. Fongarland, M.C. Iliuta, Hydrophilic zeolite sorbents for in-situ water removal in high temperature processes, The Canadian Journal of Chemical Engineering 95 (2017) 1842-1849.
[43] D.M. Ruthven, Principles of Adsorption and Adsorption Processes, Wiley, 1984.
[44] R. Plessius, R. Kromhout, L. Dantas, M. Ferbinteanu, M.C. Mittelmeijer-hazeleger, R. Krishna, G. Rothenberg, S. Tanase, Highly Selective Water Adsorption in a Lanthanum Metal – Organic Framework, Chem. Eur. J. 20 (2014) 7922-7925.
[45] K.N. Son, G.E. Cmarik, J.C. Knox, J.A. Weibel, S.V. Garimella, Measurement and Prediction of the Heat of Adsorption and Equilibrium Concentration of CO2on Zeolite 13X, Journal of Chemical & Engineering Data 63 (2018) 1663-1674.
[46] S. Sircar, A. Myers, Gas Separation by Zeolites, Handbook of Zeolite Science and Technology, CRC, 2003.
[47] W. Gren, S.C. Parker, B. Slater, D.W. Lewis, Structure of Zeolite A (LTA) Surfaces and the Zeolite A/Water Interface, J. Phys. Chem. C 114 (2010) 9739-9747.
[48] D.W. Breck, W.G. Eversole, R.M. Milton, T.B. Reed, T.L. Thomas, Crystalline Zeolites. I. The Properties of a New Synthetic Zeolite, Type A, Journal of the American Chemical Society 78 (1956) 5963-5971.
[49] T.B. Reed, D.W. Breck, Crystalline Zeolites. II. Crystal Structure Synthetic Zeolite, Type A, Journal of the American Chemical Society 78 (1956) 5972-5977.
[50] A. Ladshaw, S. Yiacoumi, C. Tsouris, D. DePaoli, Generalized gas–solid adsorption modeling: Single-component equilibria, Fluid Phase Equilibria 388 (2015) 169-181.
[51] Y. Wang, Measurements and Modeling of Water Adsorption Isotherms of Zeolite Linde-Type A Crystals, Industrial & Engineering Chemistry Research 59 (2020) 8304-8314.
[52] S. Sircar, Basic Research Needs for Design of Adsorptive Gas Separation Processes, Ind. Eng. Chem. Res. 45 (2006) 5435-5448.
[53] S. Sircar, Adsorbate mass transfer into porous adsorbents – A practical viewpoint, Separation and Purification Technology 192 (2018) 383-400.
[54] O. Talu, Measurement and Analysis of Mixture Adsorption Equilibrium in Porous Solids, Chemie Ingenieur Technik 83 (2011) 67-82.
[55] Advanced Specialty Gas Equipment, New Jersey, USA.
[56] H.-J. Butt, K. Graf, M. Kappl, Physics abnd Chemistry of Interfaces, second ed., Wiley-VCH, Weinheim, 2006.
[57] X.J. Liu, Y.F. Shi, M.A. Kalbassi, R. Underwood, Y.S. Liu, Water vapor adsorption isotherm expressions based on capillary condensation, Separation and Purification Technology 116 (2013) 95-100.
[58] A. Zhang, W. Zeng, T.M. Niemczyk, M.R. Keenan, D.M. Haaland, Multivariate Analysis of Infrared Spectra for Monitoring and Understanding the Kinetics and Mechanisms of Adsorption Processes, Applied Spectroscopy 59 (2005) 47-55.

[59] H. Ahn, C.-H. Lee, Effects of capillary condensation on adsorption and thermal desorption dynamics of water in zeolite 13X and layered beds, Chemical Engineering Science 59 (2004) 2727-2743.
[60] D.D. Do, Adsorption Analysis: Equilibria and Kinetics, Imperial College Press, 1998.
[61] G.L. Aranovich, M.D. Donohue, A New Approach to Analysis of Multilayer Adsorption, Journal of Colloid and Interface Science 173 (1995) 515-520.
[62] S. Sircar, New adsorption-condensation theory for adsorption of vapors on porous activated carbons, Carbon 25 (1987) 39-48.
[63] S. Sircar, M.B. Rao, T.C. Golden, Drying of gases and liquids by activated alumina, in: A. Dabrowski, V.A. Tertykh (Eds.) Adsorption on New and Modified Inorganic Sorbents, Elsevier Science, 1996.
[64] E. Glueckauf, J.I. Coates, Theory of chromatography. Part IV. The influence of incomplete equilibrium on the front boundary of chromatograms and on the effectiveness of separation, Journal of the Chemical Society (1947) 1315-1321.
[65] E. Glueckauf, Theory of chromatography. Part 10.—Formulae for diffusion into spheres and their application to chromatography, Transactions of the Faraday Society 51 (1955) 1540-1551.
[66] B.E. Poling, J.M. Prausnitz, J.P. O'Connell, The properties of gases and liquids, McGraw-Hill, 2001.
[67] E.N. Fuller, P.D. Schettler, J.C. Giddings, A new method for prediction of binary gas-phase diffusion coefficients, Industrial and Engineering Chemistry 58 (1966) 19-27.
[68] M. Simo, S. Sivashanmugam, C.J. Brown, V. Hlavacek, Adsorption/Desorption of Water and Ethanol on 3A Zeolite in Near-Adiabatic Fixed Bed, Industrial & Engineering Chemistry Research 48 (2009) 9247–9260.
[69] X.J. Liu, Y.F. Shi, M.A. Kalbassi, R. Underwood, Y.S. Liu, A comprehensive description of water vapor equilibriums on alumina F-200: Adsorption, desorption, and H2O/CO2 binary adsorption, Separation and Purification Technology 133 (2014) 276-281.
[70] S. Sircar, J.R. Hufton, Why Does the Linear Driving Force Model for Adsorption Kinetics Work?, Adsorption 6 (2000) 137–147.
[71] S. Sircar, J.R. Hufton, Intraparticle Adsorbate Concentration Profile for LDF Model, AIChE Journal 46 (2000) 659-660.
[72] R. Lin, J. Liu, Y. Nan, D.W. DePaoli, L.L. Tavlarides, Kinetics of Water Vapor Adsorption on Single-Layer Molecular Sieve 3A: Experiments and Modeling, Industrial & Engineering Chemistry Research 53 (2014) 16015-16024.
[73] J. Terreni, M. Trottmann, R. Delmelle, A. Heel, P. Trtik, E.H. Lehmann, A. Borgschulte, Observing Chemical Reactions by Time-Resolved High-Resolution Neutron Imaging, The Journal of Physical Chemistry C 122 (2018) 23574-23581.
[74] S. Sircar, Recent Developments in Macroscopic Measurement of Multicomponent Gas Adsorption Equilibria, Kinetics, and Heats, Ind. Eng. Chem. Res. 46 (2007) 2917-2927.

[75] E. Alpay, D.M. Scott, The linear driving force model for fast-cycle adsorption and desorption in a spherical particle, Chemical Engineering Science 47 (1992) 499-502.
[76] G. Carta, The linear driving force approximation for cyclic mass transfer in spherical particles, Chemical Engineering Science 48 (1993) 622-625.
[77] A.E. Rodrigues, M.M. Dias, Linear driving force approximation in cyclic adsorption processes: Simple results from system dynamics based on frequency response analysis, Chemical Engineering and Processing 37 (1998) 489–502.

Chapter 5. Proof-of-concept for sorption enhanced dimethyl ether synthesis

Abstract

In this chapter a proof-of-concept for sorption enhanced dimethyl ether synthesis (SEDMES) is demonstrated with commercial and novel materials.

The direct synthesis of dimethyl ether (DME) takes place in one reactor combining two catalytic functions, Cu-ZnO-Al_2O_3 (CZA) for the synthesis of methanol and an acid catalyst (typically γ-Al_2O_3) for methanol dehydration to DME. However, the catalytic performance of those catalysts is negatively affected by the high CO_2/CO ratio in biobased syngas, resulting in low methanol and DME production rates. In this chapter it is shown that promoters such as zirconium and gallium oxides increase the CO fraction in the syngas. However, the production of H_2O is also increased, leading to the deactivation of both CZA and γ-Al_2O_3. Acidic γ-Al_2O_3 is an active catalyst for the dehydration of methanol to dimethyl ether (DME). However, the produced steam reduces the activity. Therefore, the influence of the exposure of γ-Al_2O_3 to steam on the catalytic activity for methanol dehydration has been determined. At 250 °C and increasing stream partial pressure the conversion of γ-Al_2O_3 into γ-AlO(OH) is observed at a p(H_2O) of 13-14 bar. As a consequence, the catalytic activity decreases, reducing the rate of methanol dehydration to around 25%. However, this conversion is reversible and under reaction conditions γ-AlO(OH) converts back to γ-Al_2O_3, recovering its catalytic activity. Finally, the reaction kinetics for the commercial catalysts (CZA and γ-Al_2O_3) are determined for model validation purposes.

This chapter is based on published work:

J. Boon et al., Reversible deactivation of γ-alumina by steam in the gas-phase dehydration of methanol to dimethyl ether, Catalysis Communications 119 (2019) 22–27.

D. Liuzzi et al., Increasing dimethyl ether production from biomass-derived syngas via sorption enhanced dimethyl ether synthesis, Sustainable Energy Fuel 4 (2020) 5674-5681.

J. van Kampen et al., Sorption enhanced dimethyl ether synthesis under industrially relevant conditions: Experimental validation of pressure swing regeneration, Reaction Chemistry & Engineering 6 (2021) 244-257.

5.1. Introduction

In this chapter a proof-of-concept for sorption enhanced dimethyl ether synthesis (SEDMES) is given with commercial and novel materials. The production of DME from syngas proceeds via a number of steps and reactions. First, methanol is produced from syngas:

$$CO + 2H_2 \rightleftharpoons CH_3OH \quad (1)$$

$$CO_2 + 3H_2 \rightleftharpoons CH_3OH + H_2O \quad (2)$$

involving also the water-gas shift (WGS) equilibrium:

$$CO + H_2O \rightleftharpoons CO_2 + H_2 \quad (3)$$

as the produced H_2O can react with CO to form CO_2 and H_2. In a last step, DME is produced from methanol through dehydration:

$$2CH_3OH \rightleftharpoons CH_3OCH_3 + H_2O \quad (4)$$

In the previous chapters, the major benefits of SEDMES over conventional DME synthesis have been discussed. The use of a solid steam sorbent forces the excess oxygen to form steam rather than CO_2, thereby increasing the overall carbon efficiency of the process. According to Le Chatelier's principle, the removal of one of the products will shift the equilibrium-limited conversion to the product side.

The direct synthesis of DME (DDMES), with or without sorption enhancement, entails the use of two different catalytic phases, one for the synthesis of methanol from syngas and one for the subsequent dehydration to DME. Cu-ZnO-Al_2O_3 (CZA) materials are the benchmark catalysts for the synthesis of methanol from syngas [1-3], whereas acidic solids such as γ-Al_2O_3 [2, 4], zeolites [5, 6], acidic oxides [7] or heteropoly acids [8-11] are the most active catalysts for the methanol dehydration.

Cu^0, or more likely the Cu/ZnO interphase is considered as the active site for the methanol production [12, 13]. The dependence of the activity on the morphology and size of copper particles [12, 14] and the effect of promoters such as Mn [6, 15], Zr [4, 15, 16], or Ga [16], have been discussed thoroughly in the literature. The main carbon source for methanol, either CO or CO_2, is also a recurring topic in the literature. Although there is seemingly an agreement that methanol is mostly produced from CO_2 (Equation 1) [13, 16, 17], other authors claim that the relative hydrogenation rate of CO and CO_2 depends on the conditions and the CO_2/CO ratio of the syngas [18, 19]. Partly, the lack of consensus arises from the interconversion between CO and CO_2 during methanol (and direct DME) synthesis through the WGS reaction (Equation 3). Regardless of the actual source of methanol, it is well admitted that methanol production rates from CO_2-rich syngas are slower than from CO rich ones. On the one hand, the presence of a small amount of CO_2 in the syngas is beneficial for the synthesis of methanol because it promotes the partial oxidation of metallic Cu into Cu^+, which increases methanol production rates. On the other hand, CO_2 has an inhibitory effect since it adsorbs strongly on the active sites thus poisoning the catalyst [20, 21]. In addition, the presence of CO_2 in the syngas results in the production of H_2O in the reaction medium

via the reverse water gas shift and methanol synthesis reactions (Equations 2 and 3, respectively). Water is a major source of catalyst deactivation, causing the agglomeration of the Cu particles in CZA and the deactivation of γ-Al_2O_3. Moreover, since H_2O is produced along with methanol and DME, a high partial pressure of H_2O in the reaction medium also inhibits methanol and DME production [22]. Martin et al. reported that the optimum CO_2 content for the methanol synthesis is 2.4 vol.% [23]. Unfortunately, the CO_2 content of biomass-derived syngas is usually well above this optimum value [24, 25]. From a catalytic point of view, it has been reported that the use of promoters such as Zr or Ga oxides can increase conversion rates of CO_2-rich syngas mixtures over CZA [26, 27]. However, this strategy also results in a high production rate of H_2O, which has to be removed from the reaction medium, as is the case in sorption enhanced DME synthesis.

γ-Al_2O_3 as a solid acid remains the catalyst of choice for the industrial production of DME, due to its low cost, high surface area, good thermal and mechanical stability, and high selectivity to DME because its relatively weak Lewis acid sites do not promote side reactions [28]. In fact, the reduced water content in SEDMES will likely promote coking of more acidic catalysts such as zeolites [29, 30]. As SEDMES also requires a water adsorbent, typically an LTA zeolite, it also requires periodic regeneration by a temperature or pressure swing [31]. The catalytic activity for the methanol dehydration reaction can be significantly enhanced by regeneration at relatively high temperatures of 400 °C [31], which has prompted an exploration of the interaction of water with γ-Al_2O_3 and the ensuing activity for the methanol dehydration reaction (4). The Al_2O_3-H_2O phase diagram has been extensively studied in the liquid phase with the pH as parameter [32]. The phase transformation of γ-Al_2O_3 into boehmite under hydrothermal conditions has been reported by Koichumanova et al. [33], who were able to measure the water induced phase transformation of γ-Al_2O_3 into boehmite. However, remarkably little is known about this system at elevated temperatures.

While Brønsted acidity of alumina may be inferred from the presence of surface hydroxyl groups, the Lewis acid sites on γ-Al_2O_3 catalyze dehydration reactions of simple alcohols [34, 35]. The presence of water formed in the reaction inhibits the catalytically active sites, in two distinctly different ways. Deactivation can be caused by the adsorption of dimers, trimers, or even larger alcohol-water clusters, which is in competition with the desired adsorption of alcohol dimers for the formation of ether [35-37]. (Similar phenomena have been reported in dehydration over H-ZSM-5 [38].) Consequently, prevailing kinetics for methanol dehydration over γ-Al_2O_3 feature a reduction of the rate of reaction by the adsorption of water on the surface [39, 40].

$$-r_{\mathrm{MeOH}} = \frac{kK_{\mathrm{MeOH}}^2\left([\mathrm{MeOH}]^2 - \frac{[\mathrm{H_2O}][\mathrm{DME}]}{K}\right)}{\left(1+2\sqrt{K_{\mathrm{MeOH}}[\mathrm{MeOH}]}+K_{\mathrm{H_2O}}[\mathrm{H_2O}]\right)^4} \quad (5)$$

Conversely, deactivation may also occur due to the irreversible deactivation of γ-Al_2O_3 which has been reported at higher partial pressures of steam [41] and has been attributed to the formation of (surface) boehmite (aluminium oxide hydroxide, γ-AlO(OH)):

$$\gamma\text{-}Al_2O_3 + H_2O \rightleftharpoons 2\gamma\text{-}AlO(OH) \qquad \Delta H^0 = 12.7\ \text{kJ mol}^{-1} \qquad (6)$$

In particular, this may occur in slurry reactors where the rate of water removal might be low [42] and may be particularly relevant in case of the direct synthesis of DME from H_2 and CO_2 [28]. The formation of boehmite under these conditions is not unexpected, since the transition between γ-AlO(OH) and γ-Al_2O_3 also occurs in the range of 300-500 °C [43], but the exact nature of the deactivation of γ-Al_2O_3 and the in situ formation of boehmite and its reversibility have not been reported in literature.

Ideally, the rate of the methanol dehydration reaction is interpreted in terms of the chemical composition of the alumina surface involved in the reaction, being γ-Al_2O_3, γ-AlO(OH), or an intermediate species. Thus, a comprehensive understanding of the interaction of water with γ-Al_2O_3 is required to explain the observed negative reaction order for water at more conventional reaction conditions, as well as understanding of the effect of unconventional reactor conditions (i.e., H_2/CO_2 feed or frequent regeneration) on the reversibility of this deactivation. In this work, the transition between boehmite and γ-Al_2O_3 has been studied with the aim to relate the methanol dehydration reaction rate to the state of the alumina catalyst.

This chapter presents a proof-of-concept for the sorption enhanced DME synthesis. The effect of CZA catalysts doped with ZrO_2 and Ga_2O_3, known to promote the r-WGS reaction, is studied in the synthesis of methanol, the direct synthesis of DME and the sorption enhanced DME synthesis using CO_2-rich syngas (composition similar to that obtained from biomass-derived syngas). In addition, an investigation of the boehmite to γ-Al_2O_3 phase transition in the range of 250-400 °C and steam partial pressures up to 15 bar is presented. Subsequently, results are reported of methanol dehydration experiments over γ-Al_2O_3 and hydrated γ-Al_2O_3. Finally, the reaction kinetics for the commercial materials (CZA and γ-Al_2O_3) are determined for model validation purposes.

5.2. Experimental

A proof-of-concept for sorption enhanced DME synthesis was performed using (a homogeneous physical mixture of) commercially available catalyst and adsorbent: CZA catalyst, γ-Al_2O_3 (assay>98%, Riogen NJ, USA), obtained as 3 mm pellets, and molecular sieve type 3A, purchased as 1.6 mm pellets (UOP Molecular Sieves, Advanced Specialty Gas Equipment, USA), all ground to a 212 to 425 µm sieve fraction. All experiments were performed using the 212-425 µm sieve fraction, unless stated otherwise. The synthesis and

characterization of the novel, doped CZA catalysts is described in more detail in the joint publication by CSIC and TNO [44].

The surface area of γ-Al_2O_3 was measured on a Thermo Scientific Surfer instrument at 77 K, using vacuum dried samples (200 °C, 3 h). Thermodynamic equilibria under the tested conditions were calculated using HSC Chemistry 5.11. Powder X-ray diffraction (PXRD) patterns were obtained from 5 to 80° 2θ with a MiniFlex II diffractometer using Ni-filtered Cu-Kα radiation, at 30 kV and 15 mA. Thermogravimetric analysis (TGA) and differential scanning calorimetry (DSC) were performed on a Netzch Jupiter STA 449F3 instrument in the temperature range 30–700 °C and, using a 1:1 argon/air mixture (20 mL min^{-1}) and a heating rate of 5 K min^{-1}.

5.2.1. Characterization of the copper catalysts

Specific surface areas and pore size distribution were determined from the N_2 adsorption-desorption isotherms collected in an Asap2020 Micromeritics at -196 °C after degasification at 140 °C.

X-ray diffractograms were obtained in a polycrystal X-ray X´Pert Pro PANalytical with a configuration θ-2θ, using CuKα radiation (wavelength of 0.15418 nm), and an Anton Paar XRK900 was used for the pre-treatment of the samples under reductive atmosphere. The size of the Cu crystallites (d_{Cu}) was calculated with the Scherrer equation (equation 7).

$$d_{Cu} = \frac{K\lambda}{\beta \cos\theta} \quad (7)$$

where K is the Scherrer constant, 0.94 for spherical crystals with cubic symmetry, and λ represents the wavelength of the incident radiation. β and θ are the full width at half maximum (FWHM) and the position of the diffraction peak, respectively. Based on the calculated d_{Cu}, the surface area of the reduced copper particles (S_{Cu}, m^2_{Cu}/g_{cat}) was calculated with equation 8, in which ρ_{Cu} is the density of copper (8.92 g cm^{-3}) and Cu content is the mass fraction of copper in the catalyst.

$$S_{Cu}(XRD) = {6000 \cdot Cu\ content}/{\rho_{Cu} \cdot d_{Cu}} \quad (8)$$

The chemical composition of the catalysts was analyzed in an inducted coupled plasma-optical emission spectroscope PlasmaQuant PQ 9000 Analytik Jena, after proper digestion of the solid.

Cu dispersion and Cu surface area were determined from N_2O chemisorption. First, a temperature-programmed reduction (TPR-t) was performed by subjecting the catalyst under study to a thermal treatment between 25 to 280 °C at a rate of 2 °C/min, under a gas flow of H_2/N_2 (20/80 v/v). The temperature was decreased to 30 °C, and N_2O was flown through the reactor at 30 °C during 15 min. Once the chemisorption ended, non-chemisorbed N_2O was flushed under flowing He during 30 minutes. In this step, surface Cu

species are selectively oxidized to Cu_2O. Next, a second TPR (TPR-s) was performed from 30 to 280 °C, with a heating rate of 10 °C/min under a H_2/N_2 20/80 flow. The hydrogen consumed in TPR-t stands for the totality of the copper in the catalyst. The hydrogen consumed in TPR-s accounts to the reduction of surface cupper species (Cu_2O) oxidized during the N_2O chemisorption step. Cu dispersion (D_{Cu}) was calculated from equation 9.

$$D_{Cu}(\%) = 2 \cdot area\ TPR - s / area\ TPR - t \cdot 100 \quad (9)$$

and the surface area of copper (S_{Cu}, in $m^2_{Cu}\ g_{cat}^{-1}$) was calculated with equation 10.

$$S_{Cu}(chem\ N_2O) = a_{m,Cu} \frac{N_A D_{Cu} Cu\ content}{M_{Cu} \cdot 100} \quad (10)$$

The value of the surface area occupied by an atom of Cu in a polycrystalline surface, $a_{m,Cu}$, is 6.85 m^2 atom of Cu^{-1}. N_A is the Avogadro number and M_{Cu} is the atomic mass of Cu (63.55 g/mol). For the number of copper sites per gram of catalyst, equation 11 was used.

$$Cu\ sites_{cat\ i} = S_{Cu}(chem\ N_2O) \cdot \rho_{S,Cu} / N_A \quad (11)$$

Where Cu $sites_{cat\ i}$ is the number of copper sites in catalysts i, in moles of copper/g, and $\rho_{S,Cu}$ is de surface density of copper, which is $1{,}47 \cdot 10^{19}$ atoms/m^2.

Table 5-1 displays the specific surface areas, pore diameters, elemental composition, and results of RXD and N_2O chemisorption of the CZA catalysts studied in this work. As shown in Table 5-1, all catalysts have similar Cu loading of 60-67 wt.%. The commercial CZA catalyst (CZA_comm) displays the largest specific surface area in the series. Its homemade analogue (CZA) displays a lower surface area due to the lower content of Al_2O_3. The addition of ZrO_2 (CZAZ) increases the surface area of the material. On the other hand, the catalyst with gallium presents the lowest surface area of the series. The CZA_comm shows a narrow distribution of the pore sizes, while the rest of the catalysts present a bimodal distribution or a very wide range in the diameter of their pores, which are larger than in the commercial catalyst.

TABLE 5-1: TEXTURAL PROPERTIES AND COMPOSITIONS OF THE SYNTHESIZED AND COMMERCIAL CATALYSTS. PARTICLE SIZE (D_{Cu}), DISPERSION (D_{Cu}) AND CU SURFACE AREA (S_{Cu}).

Catalyst	Surface area	Pore diameter	Composition (wt. %)						d_{Cu}	S_{Cu} (XRD)	D_{Cu}	S_{Cu} (chem N_2O)
	$m^2\ g^{-1}$	nm	Cu	ZnO	Al_2O_3	ZrO_2	Ga_2O_3	MgO	nm	$m^2_{Cu}\ g_{cat}^{-1}$	%	$m^2_{Cu}\ g_{cat}^{-1}$
CZA	38	12; 36	67	29	5	-	-	-	11	41	7.8	34
CZAZ	88	6; 48	67	10	15	8	-	-	8	56	5.8	25
CZAZGa	28	13-50	63	16	13	6	1	-	9	47	-	-
CZA_comm	97	7	59	27	11	-	-	2	6	66	13.7	52

The X-ray diffractograms for the catalysts reduced in H_2/N_2 at 250 °C (heating rate 2 °C/min) are shown in Figure 5-1. All diffractograms display the characteristic diffraction lines for metallic Cu, with peaks at 43, 50, 74°and ZnO at 32, 35, 37 and 57°. The absence of diffraction peaks for Al_2O_3, ZrO_2 or Ga_2O_3 indicates that these phases are amorphous or highly dispersed on the solid surface.

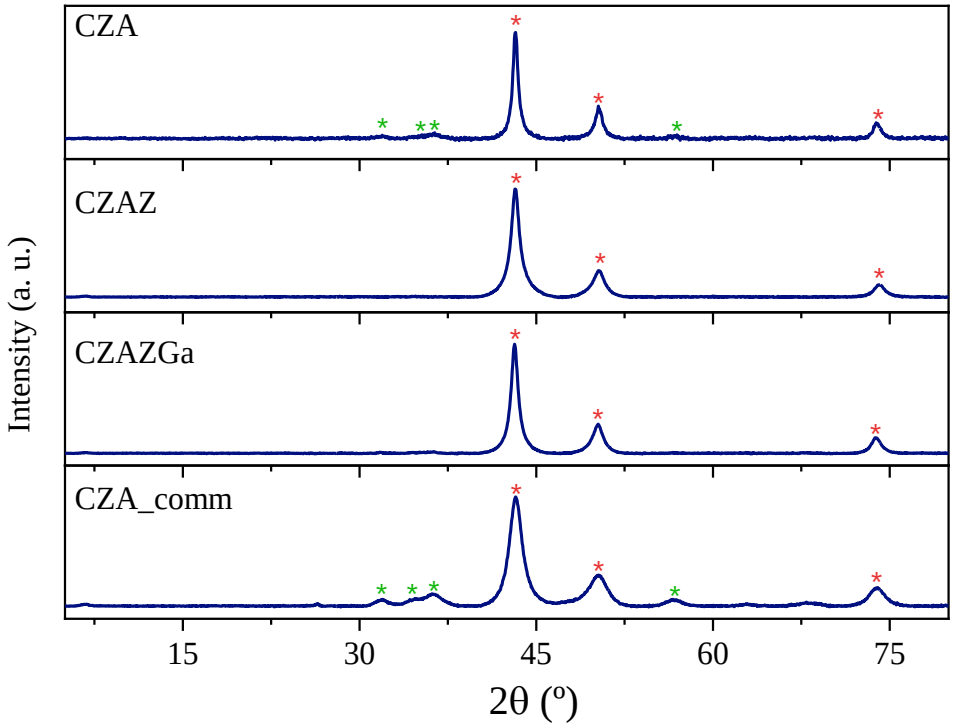

FIGURE 5-1: X-RAY DIFFRACTOGRAMS OF THE CATALYSTS AFTER REDUCTION AT 250 °C. *CU0, *ZNO.

Table 5-1 reports the Cu dispersion and surface areas of the catalysts as determined from N_2O chemisorption. Unfortunately, it was not possible to conduct an N_2O chemisorption experiment with the Ga-doped sample, CZAZGa, because Ga_2O_3 reduction overlaps with the reduction of Cu [45], invalidating the assumption that hydrogen consumption during the experiment accounts only to the reduction of copper. Therefore, we also calculated the Cu dispersion and surface area of all catalysts from the particle sizes obtained from the XRD results using equations 5 and 6. The N_2O chemisorption results reveal that CZA_comm displays the highest Cu surface area in the series, followed by CZA and CZAZ. The same trend is obtained when using the particle sizes obtained from XRD, with CZAZGa displaying the lowest Cu surface area of the series.

5.2.2. Methanol synthesis

The catalytic tests for methanol synthesis were performed in a fixed-bed stainless-steel reactor with a diameter of 0.9 cm. The catalytic bed consisted of 200 mg of catalysts sieved at 250-300 µm fraction and diluted in SiC to avoid hot spots. The catalysts were pre-treated in situ with a H_2/N_2 20/80 vol. flow at 250 °C during 2.5 h. Afterwards, the reactor was cooled to 100 °C in N_2 and then pressurized to 25 bar with a syngas, similar to biomass-derived syngas, with a $CO/CO_2/H_2/N_2$ volumetric composition of 1/1.9/7.7/1.18 (Air Liquid), so that the M module ($[H_2-CO_2]/[CO+CO_2]$) is 2. Once this pressure was reached, the reactor was heated to 270 °C and the proper flow rate of syngas to get a GHSV= 7500 h^{-1} was set. Reactor outlet gases were analyzed with an on-line Varian CP-3800 gas chromatograph equipped with a Hayesep Q packed column connected to a thermal conductivity detector (TCD) and a Rtx-1 capillary column connected to a flame ionization detector (FID). N_2 was used as intern patron for the calculations of CO and CO_2 conversions. The methanol produced was calculated taking into account that it was the only product, since no other compound different to the ones in the feed was observed. The activity of each catalyst was measured for at least 5 hours. The composition of the outlet gases was analyzed three times and the values reported in this work are the averaged values.
The CO and CO_2 conversions were calculated as indicated in equation 12.

$$X_i = \frac{mole\ flow_{i,in} - mole\ flow_{i,out}}{mole\ flow_{i,in}} \quad (12)$$

where X_i represents the conversion of compound i (CO or CO_2), and mole $flow_{i,in}$ and mole $flow_{i,out}$ are the inlet and outlet molar flow rates of compound i, respectively, in moles/s. For the turnover frequency numbers (TOF, in s^{-1}), equations 13 and 14 and were used.

$$Methanol\ production\ (MeS)\ = \sum mole\ flow_{i,in} \cdot X_i \quad (13)$$

$$TOF = Methanol\ production\ (MeS) \cdot Cu\ sites\ \cdot g_{cat} \quad (14)$$

Methanol production (MeS) is expressed in moles/s, and g_{cat} represents the grams of catalyst loaded into the reactor. Since methanol is the only product detected, the methanol production was calculated with equation 13.

5.2.3. Direct synthesis of DME and sorption enhanced DME synthesis

The metallic and acidic catalyst were crushed to powder, mixed in a 1:1 weight ratio, pelletized, and finally crushed and sieved to 212-425 µm. The adsorbent zeolite 3A was also crushed and sieved to the same fraction. The catalytic bed was prepared mixing the

catalysts and the zeolite in a ratio 1:4 (weight basis) and diluted with SiC in order to avoid the hot spots formed during the reaction.
The experiments were conducted on the high-pressure multi-column rig ('Spider', Figure 5-2), with 8 reactors of 20 mm internal diameter. 5.3 g of a 1:1 catalyst mixture of the Cu-based and acid catalyst plus 21 g of 3A zeolite was loaded in each reactor. A flow rate of 90 NmL min^{-1} of simulated syngas ($CO_2/CO=2$, and $M=(H_2-CO_2)/(CO+CO_2)=2$) was fed to each reactor at 275 °C, 25 bar. The catalytic mixture was activated under a H_2/N_2 flow (20/80 v/v) at 250 °C and 1 bar during 2.5 h. Product analysis was performed by gas chromatography (GC, equipped with a TCD and a FID detector) and mass spectrometry, by monitoring the following species; hydrogen (m/z=2), water (m/z=18), carbon monoxide/nitrogen (m/z=28), argon (m/z=40), carbon dioxide (m/z=44) and DME (m/z=46). Traces of C_2H_4 (m/z=28) were detected, but due to the extremely low intensity of the signal, it was not considered. C_2H_4 comes from the further dehydration of DME in the presence of an acid catalyst [46, 47], so the assumption that CO and CO_2 are converted only to form methanol is still valid for these experiments. All experiments were performed in triplicate. The first was always discarded, the second and third obtained very similar results.
The data for the SEDMES regime were those collected during the early stages of the reaction, in the transient state (ca. 50 minutes), when the adsorbent zeolite was still dry. The data collected once the zeolite was saturated, at steady state, represent the DDMES (after ca. 100 minutes). The adsorption capacity of the zeolite was regenerated in situ. The regeneration protocol consisted of periodic switching to dry nitrogen, followed by decreasing the pressure to 3 bar and increasing the temperature to 400 °C. For every setting, the reaction and the regeneration were measured for every sample.

5.2.4. Boehmite – γ-Al_2O_3 equilibrium

A batch of reference boehmite was prepared by treating 12.0 g of γ-Al_2O_3 pellets in 50 mL of water at 200 °C for 15 hours inside a hydrothermal synthesis reactor equipped with a 100 mL Teflon liner. The γ-Al_2O_3 to boehmite phase transition was studied in a batch autoclave. To study the boehmite to γ-Al_2O_3 interconversion, γ-Al_2O_3 (0.125 g, 1.223 mmol) was transferred to a ceramic crucible which was placed into a 50 mL stainless steel autoclave. Specific volumes of water (see legend in Figure 5-6 for details) were added avoiding direct contact with the γ-Al_2O_3. The vessel was sealed and heated to 250 °C under autogenic pressure for a set period of time. After cooling to room temperature, the sample was transferred to an oven and dried at 120 °C.

5.2.5. Catalytic activity of γ-Al_2O_3 for methanol dehydration

The catalytic activity of the sample was tested in a fixed bed reactor with a diameter of 20 mm and a bed height of 170 mm, equipped with an axially fitted thermocouple. Analysis

was performed by a Thermo Scientific TRACE 1300 gas chromatograph equipped with a TCD detector calibrated for CO, CO_2, H_2, O_2, and N_2 and an FID detector calibrated for DME, MeOH, EtOH, ethylene, ethane and methane. The reactor was filled with a homogeneous mixture of 5.26 g 212-425 µm sieve fraction γ-Al_2O_3 and 100.03 g of 600-1180 µm sieve fraction SiC, resulting in a total bed volume of 60 cm^3. The reactor was fed with a mixture of 90% N_2 and 10% vapor feed (methanol, steam) at a total volumetric gas flow rate of 889 ml min^{-1}. The liquid feed of methanol (anhydrous 99.8%, Sigma Aldrich) was introduced by a Scientific Systems, Inc. Series 1500 dual piston pump, before controlled evaporative mixing. Both pressure and temperature cycles have been performed. A pressure cycle consisted of a 3 hour feeding period at a specific pressure with 0.5 hour intervals for changing pressure. Consecutive pressures were 40, 35, 25, 15, and 5 bar(a), controlled with a margin of ± 0.05 bar. The temperature was maintained at 250 ± 1 °C. A temperature cycle consists of 2 hour measurements at a specified temperature with 0.5 hour intervals for changing temperature. The temperature range was 250-350-250 °C with intermittent ramping of 25 °C. The pressure would be maintained at 25 bar(a). During any interval where the pressure or temperature was changed, the liquid feed would be interrupted, and the N_2 flow rate was set to 100 ml min^{-1}. The carbon atom balance typically closed within ± 10%, data with a carbon balance error of more than ± 20% have been omitted. The carbon selectivity towards DME (*S*) was calculated according to Equation 15, the methanol conversion (*X*) according to Equation 16, all based on measured outlet concentrations.

$$S = 100\frac{2[\mathrm{DME}]}{2[\mathrm{DME}]+[\mathrm{MeOH}]+[\mathrm{CO}]+[\mathrm{CO_2}]+[\mathrm{CH_4}]+2[\mathrm{EtOH}]+2[\mathrm{C_2H_4}]+2[\mathrm{C_2H_6}]} \quad (15)$$

$$X = 100\left(1-\frac{[\mathrm{MeOH}]}{2[\mathrm{DME}]+[\mathrm{MeOH}]+[\mathrm{CO}]+[\mathrm{CO_2}]+[\mathrm{CH_4}]+2[\mathrm{EtOH}]+2[\mathrm{C_2H_4}]+2[\mathrm{C_2H_6}]}\right) \quad (16)$$

Typical reproducibility of the measured conversion was within ± 3%. Overall, it was noticed that the γ-Al_2O_3 is highly selective. Throughout the experiments the selectivity towards DME was generally 99.9%, and never below 99.2%. After testing the catalytic activity, the in situ formation of boehmite was performed by subjecting the material present in the reactor to a p(H_2O) of 14 bar for 40 hours at 250 °C. The reactor was fed with a N_2 / H_2O feed in a ratio 1:1 at a total gas flow rate of 400 ml min^1. The total pressure was kept at 28 bar(a). Temperature profile experiments were performed, similar to those for the initial γ-Al_2O_3. Finally, the PXRD pattern of the spent catalysts was recorded using the before mentioned apparatus.

5.2.6. Catalytic activity of CZA

CZA catalyst testing at high pressure was performed similarly, but was conducted on the high-pressure multi-column rig ('Spider', Figure 5-2). Samples of initially 0.5 gram catalyst were tested. The reactors of 9.2 mm internal diameter were electrically heated and were run at elevated pressure. During adsorption and/or reaction, the reactors were each fed

with 100-150 ml_N min^{-1} of gas mixtures at 200-300 °C and 5-30 bar(a) pressure. The gas mixtures consisted of various syngas ratios for catalyst testing and 5 mol% argon as tracer in balance nitrogen. Gas analysis was performed by a gas chromatograph (GC, equipped with a TCD and a FID detector) and a mass spectrometer (MS) measuring hydrogen (m/z=2), water (m/z=18), carbon monoxide/nitrogen (m/z=28), argon (m/z=40), carbon dioxide (m/z=44) and DME (m/z=46).

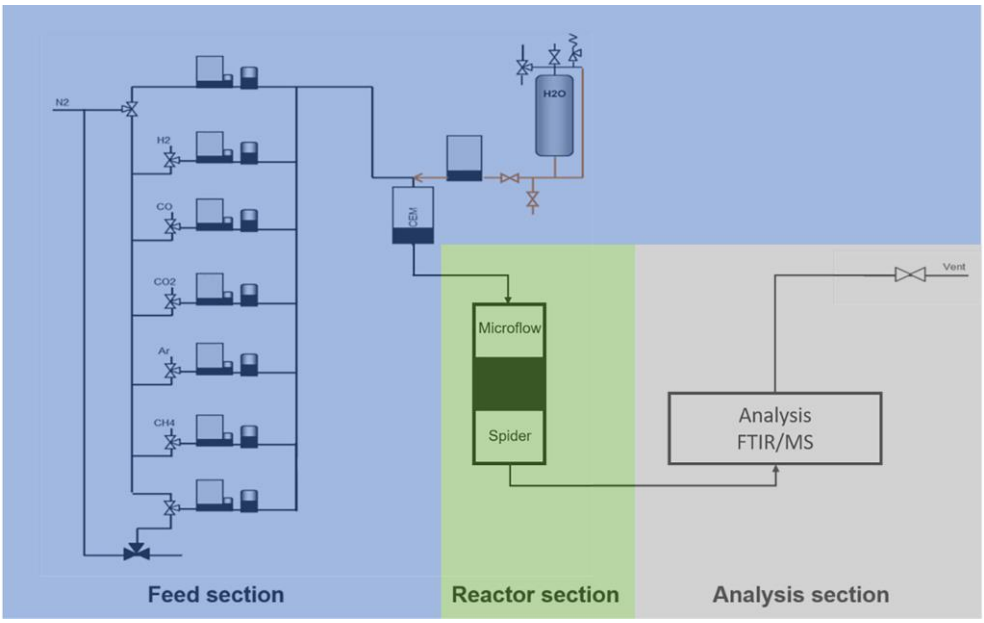

FIGURE 5-2: SCHEMATIC PRESENTATION OF THE ATMOSPHERIC AND HIGH-PRESSURE REACTOR UNITS 'MICROFLOW 5' AND 'SPIDER'.

5.3. Results and discussion

Three different reactions were studied in the first part of this chapter, namely the synthesis of methanol (MeS), the direct synthesis of DME (DDMES) and the sorption enhanced DME synthesis (SEDMES). The MeS experiments were performed as steady-state experiment, and the SEDMES and DDMES experiments were performed in a transient mode, see Figure 5-3. The final steady-state conversion level, after complete saturation of the zeolite adsorbent, was taken as the DDMES experiment. The pre-breakthrough part of the experiment corresponds to the SEDMES. As an example, Figure 5-3 shows the transient response for the CZA catalyst, identifying regions considered for reporting the performances of the SEDMES and DDMES modes. Although water is not removed prior to product analysis, the product selectivity is reported on dry basis.

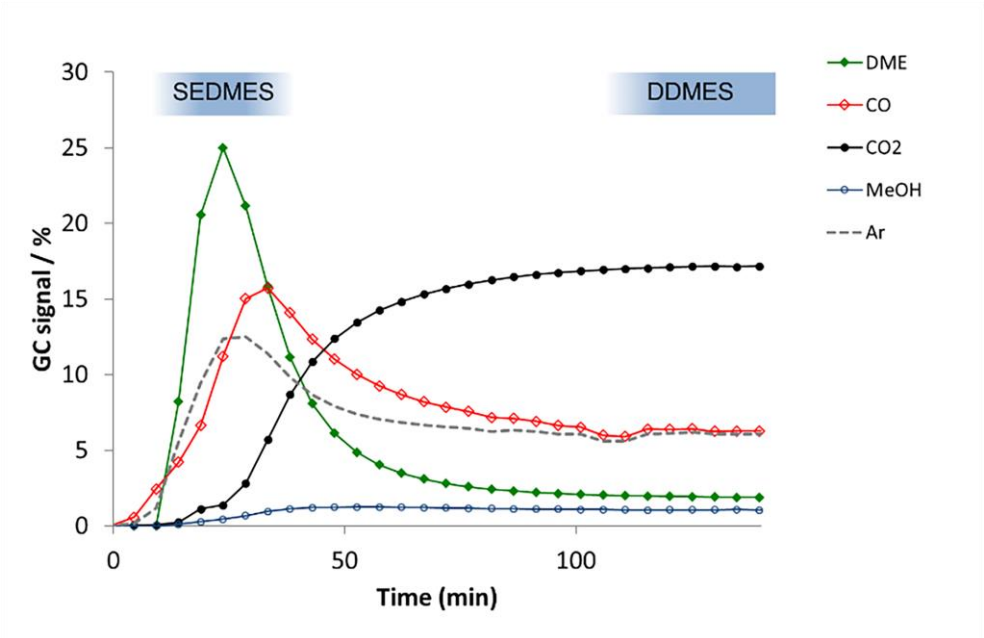

FIGURE 5-3: OUTLET COMPOSITIONS FOR DDMES AND SEDMES EXPERIMENT: 275 °C, 25 BAR, 1080 H^{-1}, CO_2/CO=2.

5.3.1. Synthesis of methanol

As shown in Figure 5-4a, both CZA_comm and CZA record the highest CO and CO_2 conversions of ca. 7.6 and 9.9%, respectively. These conversions are close to the equilibrium conversion values. Doping the catalysts with ZrO_2 decreases the CO conversion to ca. 1.6%, without affecting the CO_2 conversion. CZAZGa displays the lowest CO and CO_2 conversions in the series, with a negative CO conversion of -10.6%, indicating that the content of CO in the outlet is higher than in the inlet. Negative conversion values indicate that CO is formed during the process via the r-WGS reaction, which is promoted by the addition of ZrO_2 and especially Ga_2O_3 to CZA. Figure 5-4b shows the outlet concentrations of CO_2, CO and methanol for all catalysts. All catalysts show a similar CO_2 outlet concentration of around 57% mole (the equilibrium value is 58.7% mole), but the concentration of CO increases in the order CZA_comm (32.2% mole) < CZA (34.4% mole) < CZAZ (36.8% mole) < CZAZGa (39.8% mole) (the value at equilibrium is 32.2% mole), confirming the higher activity of CZAZ and CZAZGa for the r-WGS reaction. The methanol production is higher over the unpromoted catalysts, *i.e.*, CZA_comm (9.9% mole) and CZA (8.5% mole), decreasing over CZAZ (5.9% mole) and CZAZGa (3.1% mole) (9.1% mole at the equilibrium). A direct relationship between the outlet concentration of methanol and the Cu surface area of the catalysts obtained through N_2O chemisorption can be observed (CZA_comm > CZA > CZAZ, see Table 5-1). This direct relationship between methanol production and the Cu surface area also has been reported by other authors [13]. In terms of TOF, a similar value of around

$2 \cdot 10^{-3}$ s^{-1} was obtained for these three catalysts. On the other hand, the activity trends shown in Figure 5-4a and b reveal that even if the addition of ZrO_2 and Ga_2O_3 increases the CO/CO_2 ratio in the reactor, it does not result in a higher methanol production. Perez Ramírez et al. studied the synthesis of methanol over CZA commercial catalysts using different syngas compositions and concluded that a CO_2 concentration of ca. 2.4% in the syngas is optimal for the synthesis of methanol [23]. The presence of a small amount of CO_2 suffices to form methanol and water. The H_2O formed activates the WGS reaction to produce more CO_2, which is converted into methanol. In this way, the production and consumption of H_2O (Equations 2 and 3, respectively) are balanced in the overall process, favoring the production of methanol while avoiding catalyst deactivation via Cu sintering. However, when the syngas contains a high concentration of CO_2, such as that used in this work, methanol production is not optimal with CZA catalysts. In principle it is possible to adjust the CO_2/CO ratio in the syngas via the WGS reaction. The addition of Zr and Ga promoters to CZA catalysts improves the CO_2 adsorption on the catalyst and favors the reverse WGS reaction thus increasing the CH_3OH production from CO_2 [4, 15, 16]. Faen Song et al. found that a Zr loading of approximate 3 mol% improves the dispersion of Cu and the adsorption of CO_x on the surface of the CZA, stating that higher values result in the sintering of Cu particles, and therefore a decrease in the catalyst activity [4]. W. J. Lee et al. studied the addition of Zr, Mg and Ga to a commercial CZA catalyst and concluded that Zr favors the methanol production, but lowers the CO_2 conversion [48].

As shown in this chapter, doping CZA with Zr or Ga oxides promotes the r-WGS, thus increasing the CO/CO_2 ratio in the reactor. However, this effect does not lead to a higher methanol production with the doped catalysts. This can be explained by taking into account that the CO_2 transformation into CO via the r-WGS reaction results in the production of H_2O (Equation 3). The presence of H_2O in the reaction medium is detrimental for the production of methanol from CO_2 (Equation 2) because it displaces the equilibrium towards the reactants. The outlet gas composition of the experiments with CZA_comm and CZA is close to the equilibrium composition (9.2% of CH_3OH). However, a methanol concentration below the equilibrium value is obtained with the doped catalysts, 5.9% with CZAZ and 3.1% with CZAZ-Ga. As shown above, CZAZ and CZAZGa display the lowest ZnO content in the series (see Table 5-1). ZnO plays a very important role in the performance of CZA catalysts as a structural promoter of the active phase [49-51]. The presence of ZnO promotes the formation of small and stable Cu crystals on the catalyst, improves its dispersion and even promotes H_2 dissociation under conditions of deficient adsorption of H_2 on Cu particles, followed by H_2 spillover to Cu [49]. The N_2O chemisorption data reveal that the catalysts with the highest ZnO loadings (CZA_comm and CZA) display the highest Cu surface areas (see Table 5-1), therefore showing the highest methanol production rates. Conversely, CZAZ and CZAZGa display the lowest Cu surface areas in the series, and consequently the lowest methanol production rates. In addition, it is possible that by promoting the r-WGS reaction

Cu particles in the latter samples tend to agglomerate due to the excess of H_2O in the reaction medium.

Since CO_2 is the source for both methanol (Equation 2) and CO (Equation 3), the CH_3OH to CO ratio can be taken as a good descriptor for the preferential reaction pathway on each catalyst. Thus, high CH_3OH/CO ratios indicate that the catalyst is more active to methanol production than to the r-WGS reaction. Conversely, lower CH_3OH/CO ratios indicate that the catalyst is more active to the r-WGSR. As shown in Figure 5-4a, the CH_3OH/CO-ratio decreases in the order CZA_comm > CZA > CZAZ > CZAZGa, confirming the promotional effect of ZrO_2 and Ga_2O_3 towards the r-WGS reaction.

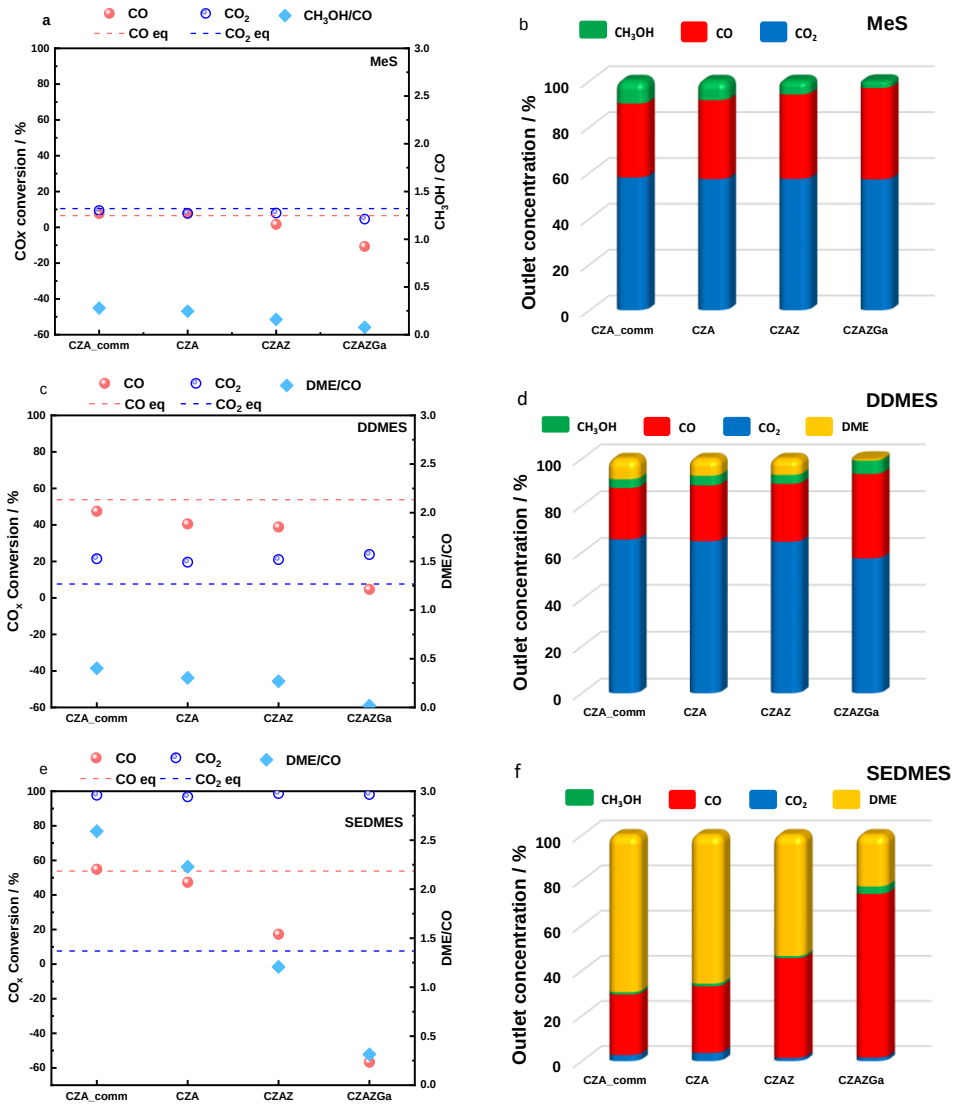

FIGURE 5-4: CO_2 AND CO CONVERSIONS, CH_3OH/CO OR DME/CO-RATIOS AND OUTLET MOLE CONCENTRATIONS OF METHANOL (GREEN BAR), CO (RED BAR), CO_2 (BLUE BAR) AND DME (YELLOW BAR), RECORDED DURING THE MES (A AND B), DDMES (C AND D) AND SEDMES (E AND F) PROCESSES UNDER THE FOLLOWING CONDITIONS: DDMES AND SEDMES: 275 °C, 25 BAR, 1080 H^{-1}, CO_2/CO=2; MES: 270 °C, 25 BAR, 7500 H^{-1}, CO_2/CO=1.9.

5.3.2. Direct dimethyl ether synthesis

As shown in Figure 5-4c, the CO_2 and CO conversions obtained in the DDMES are higher than during the MeS with all catalysts. This observation indicates that the production of DME from methanol (Equation 4) shifts the syngas to methanol reactions (Equations 1 and 2) towards the formation of CH_3OH. All catalysts show similar CO_2 conversions, ca. 20%, with CZAZGa showing a slightly higher conversion of 23%. These conversion values appear to be above the equilibrium values, but it must be noticed that the equilibrium calculations have been carried out considering only CO, CO_2, H_2, H_2O, methanol and DME in the system. As stated before, traces of C_2H_4 have been observed in both DDMES and SEDMES experiments. If ethylene is included among the products, CO and CO_2 equilibrium conversions rise to ca. 100% and above 50%, respectively. This effect of the presence of C_2H_4 in the reacting system on the thermodynamics can explain why the outlet concentration of CO_2 surpasses the theoretical value. On the other hand, CO conversions below the equilibrium value (54%) are observed. Again, CZA_comm shows the highest CO conversion of 47.5% followed by CZA (40.5%), CZAZ (38.8%), and CZAZGa (4.7%). These results do not reflect the promoting effect of the Zr addition that has been reported recently for CO_2-containing syngas [4, 52]. However, in the mentioned studies, the copper dispersion was increased in the Zr-doped catalysts, unlike what has been observed in this work, and the CO_2 content in the syngas was much lower. The product selectivity is shown in Figure 5-4d. As observed, methanol and DME are produced over all catalysts, with CZA_comm, CZA, and CZAZ reaching DME outlet concentrations of 8.7% mole, 7.2% mole, and 6.8% mole. Note that these values are slightly below the DME equilibrium concentration of 10.9% mole at the conditions studied in this work. CZAZGa produced a very low amount of DME, with an outlet concentration of ca. 0.8% mole, but shows the highest concentration of methanol of 5.7% mole *vs* ca. 4% mole shown by the other catalysts (the equilibrium value for methanol composition is 3.8% mole). Note that the combined production of methanol and DME with CZAZGa is the lowest in the series. The lower activity towards the production of methanol and DME in the catalytic bed with CZAZGa /γ-Al_2O_3 can be explained by the very high activity of CZAZGa for the r-WGS reaction, which results in a high content of H_2O in the reaction medium, which is known to deactivate both methanol production over CZA catalysts and methanol dehydration over γ-Al_2O_3. As explained above, we used the DME/CO outlet ratio as a descriptor of the preferential reaction pathway, DME production versus r-WGS reaction, with the catalysts under study during the DDMES. In line with the trend observed above for the synthesis of methanol MeS, all catalysts show a similar trend of DME/CO ratios of ca. between 0.4 (CZA_comm) and 0.3 (CZAZ), with CZAZGa showing the smallest ratio of 0.02, indicating a high r-WGS activity of this catalyst hence a higher CO selectivity.

5.3.3. Sorption enhanced DME synthesis

As shown in Figure 5-4e, the SEDMES process results in significantly higher CO_2 conversions, ca. 100%, irrespectively of the catalyst under study. The CO conversions with the CZA catalysts (CZA_comm 55% and CZA 47%) are higher than in the other process, but the ones recorded with CZAZ (17%) and CZAZGa (-56%), especially the latter, are lower than the ones recorded during the DDMES and MeS. DME and methanol are produced with all catalysts. DME production is significantly higher than that obtained in the DDMES process, with outlet concentration values of 70%, 66%, 54%, and 23% for CZA_comm, CZA, CZAZ, and CZAZGa, respectively (Figure 5-4f). All of these values are well above the aforementioned DME equilibrium concentration of 10.9 %. The significantly higher CO and CO_2 conversions (above equilibrium) and DME production reveal the promotional effect of water removal with zeolite 3A during the direct DME synthesis from syngas.

The *in situ* removal of H_2O during the SEDMES process exacerbates the different performances between the catalysts with a high activity for the production of methanol (CZA_comm and CZA) and the ones with a high activity for the r-WGS reaction (CZAZ and CZAZGa). DME production is favored over CZA and CZA_comm, indicating the higher catalytic activity of these catalysts for the reactions in which methanol and DME are produced, Equations 2 and 4, respectively. On the other hand, since the r-WGS reaction (Equation 3) is faster than the methanol production over CZAZGa, water removal promotes further the production of CO from CO_2, resulting in negative CO conversion values, which is an indication that the rate of methanol production from CO (Equation 1) is very slow.

Finally, it is worth mentioning that the CO_2 concentration in the products in SEDMES is very low (<4%) for all catalysts, which is very important for the DME/CO_2 separation process downstream. These low CO_2 outlet concentrations suggest that the SEDMES process could be applied also to the DME production from captured CO_2, improving the C conversion in this process. It has been demonstrated that the direct synthesis of DME achieves lower C conversions as the feed is switched to CO_2-H_2 over different catalytic mixtures [15], and the results in this work indicate that the CO_2 conversion might increase considerably if a sorbent were used to remove water from this reacting system.

5.3.4. Reversible deactivation

To investigate the interaction of water with γ-Al_2O_3 and the ensuing activity for the methanol dehydration reaction, the purchased γ-Al_2O_3 was characterized by PXRD and nitrogen adsorption studies. The PXRD pattern of the catalyst (Figure 5-5) showed a well-defined γ-Al_2O_3 structure with characteristic broad Bragg reflections at 46 and 67° 2θ [53], which also contains traces of an amorphous AlO_x phase (broad peak around 2θ = 38°) [54]. Nitrogen adsorption showed typical Type II isotherm behavior according to the Brunauer classification, resulting in a Brunauer-Emmett-Teller (BET) specific surface area of 192 $m^2\ g^{-1}$

with an average pore diameter of 8.98 nm, both of which are well within typical ranges reported for this type of material [55].

5.3.5. Boehmite – γ-Al_2O_3 equilibrium

The phase transition between boehmite and γ-Al_2O_3 has been monitored using PXRD analysis for the detection of γ-AlO(OH) and TGA/DSC experiments for studying the subsequent decomposition to γ-Al_2O_3. As discussed in the introduction, the transition from γ-Al_2O_3 to γ-AlO(OH) by steam is not yet understood. Thus, the initial focus in this section is on the transformation of γ-Al_2O_3 to γ-AlO(OH) in the presence of steam. Section 5.3.6 discusses the catalytic activity of the steam-exposed sample in comparison to that of the original γ-Al_2O_3.

Two sets of experiments were employed to study the transition of γ-Al_2O_3 to boehmite. The first set (Figure 5-5) consisted of exposure to a fixed water concentration for different time spans, while the second set (Figure 5-6) consisted of equal times of exposure to different water concentrations. The main conclusion drawn from the individual steam exposure experiments is that at 250 °C, a steam partial pressure of at least 13 bar is required to convert γ-Al_2O_3 to crystalline γ-AlO(OH) (Figure 5-6). Furthermore, the phase transformation of γ-Al_2O_3 to boehmite by steam is unlikely to be complete in less than 66 h at 14 bar of H_2O and 250 °C.

From the PXRD studies, γ-Al_2O_3 can easily be identified by the characteristic broad peaks at 46° and 67°, while boehmite can be identified by the sharp peaks at 14.55° and 28.25°. Therefore, the PXRD patterns from the first set of experiments show that the crystalline boehmite phase is already present after one hour of steam exposure (Figure 5-5). However, at this stage the original crystalline γ-Al_2O_3 phase is still present. More boehmite is formed when prolonging the exposure. Even after 66 hours of exposure the γ-Al_2O_3 peaks could still be recognized in the PXRD. Furthermore, in the PXRD pattern of the reference boehmite, prepared hydrothermally, the peaks at 46° and 67° corresponding to the γ-Al_2O_3 phase are noticeably smaller compared to the sample exposed for 66 hours. We therefore conclude that the steam exposure for 66 hours does not fully convert the γ-Al_2O_3 to boehmite under the employed conditions.

As shown in Figure 5-6, after subjecting the γ-Al_2O_3 catalyst to 13-14 bar of steam partial pressure, the characteristic peaks of boehmite are clearly visible in the PXRD, albeit they are less pronounced than for the sample exposed to 15 bar. Conversely, no boehmite formation was observed after subjecting the material to 12.5 bar and lower partial pressures of steam. Also, for duplications of the experiment at 13 bar steam no significant boehmite formation could be detected by PXRD. Therefore, the required steam pressure to induce the phase transition from γ-Al_2O_3 to γ-AlO(OH) at 250 °C appears to be between 13 and 14 bar.

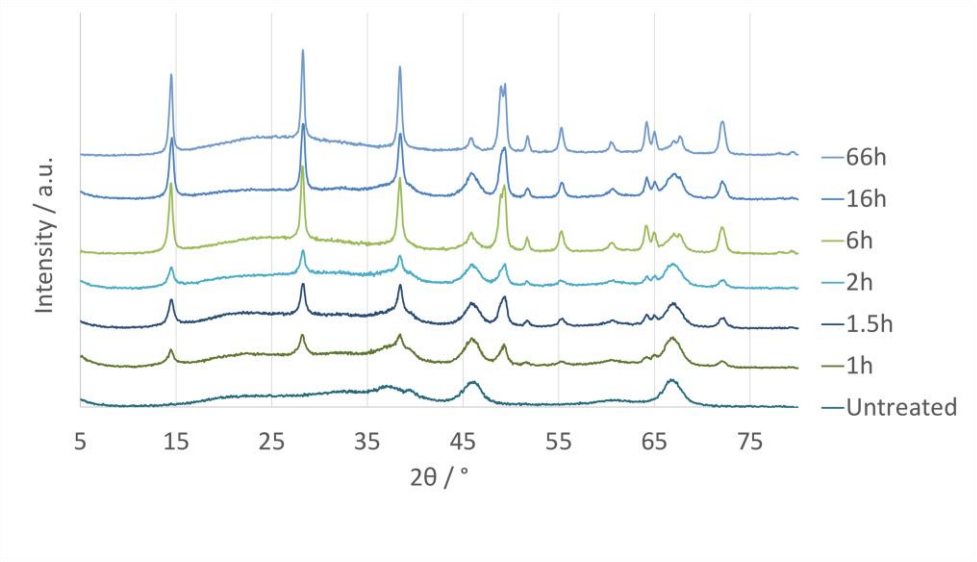

FIGURE 5-5: PXRD MEASUREMENTS OF GAMMA-AL_2O_3 AFTER DIFFERENT EXPOSURE TIMES TO 250 °C, 14 BAR H_2O.

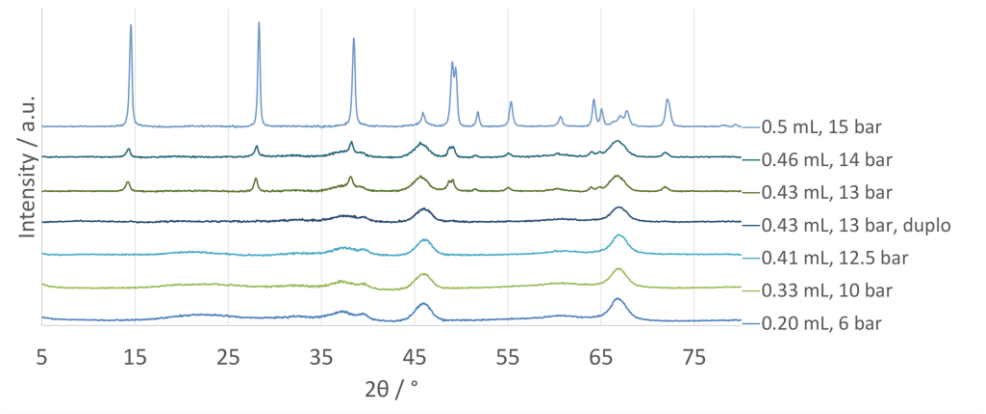

FIGURE 5-6: PXRD MEASUREMENTS OF GAMMA-AL_2O_3 AFTER 18.5 HOURS EXPOSURE TO 250 °C, 6-15 BAR H_2O.

A typical TGA response of the dehydration of the formed γ-AlO(OH) back to γ-Al_2O_3 is shown in Figure 5-7. From 120 °C upwards, a progressive loss of mass is observed, corresponding to the dehydration of the sample. A minimum in differential (DTG) is observed at temperatures in the range of 450-490 °C, depending on the preceding exposure to steam. The observed mass loss relates to the extent to which the sample had been converted to γ-AlO(OH) during steam exposure (note the theoretical maximum weight loss for full

conversion according to Equation 6 equals 15%). Sanchez Escribano et al. [56] have shown that free active hydroxyl groups on the surface of γ-Al_2O_3 gradually disappear with increasing temperatures in the range of 200-400 °C and Krokidis et al. [14] have theoretically shown that several steps and transition states occur in the transformation of γ-AlO(OH) to γ-Al_2O_3, leading to a stepwise dehydration in the temperature range of 320-540 °C. This is very much in line with the TGA data presented here. The observed weight loss in the range of 120-320 °C may be attributed to the loss of surface adsorbed water and hydroxyl groups, in line with the classical Peri model of the surface of γ-Al_2O_3 [57]. Clearly, the bulk of the material is converted back to γ-Al_2O_3 in the temperature range of 450-490 °C (Table 5-2), but significant additional dehydration can be observed from 500 °C upwards (Figure 5-7). The data shown in Table 5-2 indicate that the activation energies for the dehydration of boehmite to γ-Al_2O_3 range from ca. 16 to 340 J/g. However, there is no uniform variation of the activation energies for the conversion of boehmite to γ-Al_2O_3 for the different steam exposure times. This is likely due to several factors involved during the experimental procedures, including the synthetic conditions of boehmite, its structural and morphological properties as well as the steam exposure conditions. Generally, it has been observed that large crystallites lead to large activation energies [58]. Several studies reported that the thermal transformation of boehmite to γ-Al_2O_3 is a complex process involving at least four steps [58-60]. The first step corresponds to the desorption of the physisorbed water, which is a reversible process. The second step involves the desorption of the chemisorbed water, followed by the decomposition of boehmite into transition phase alumina. The last step is the dehydroxylation of the transition phase alumina to γ-Al_2O_3.

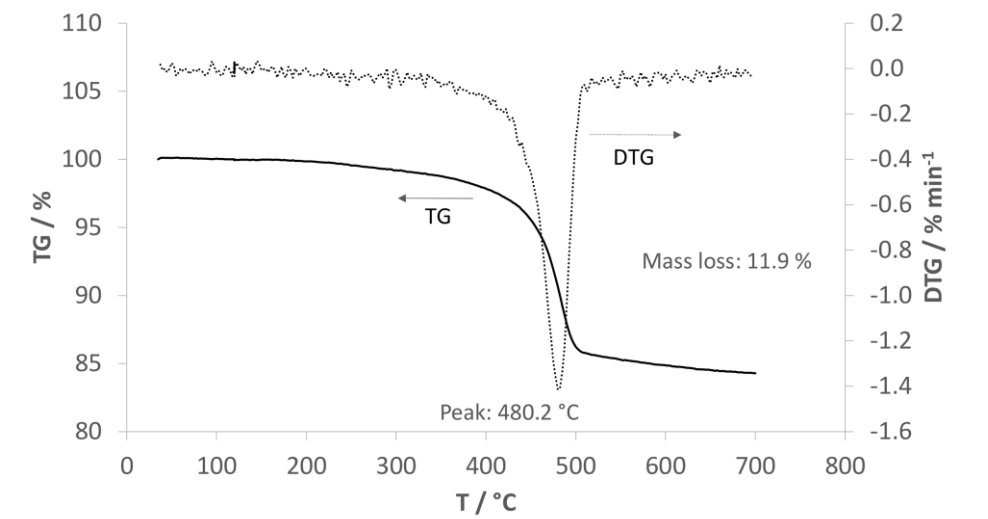

FIGURE 5-7: THE TGA CURVE OF THE GAMMA-AL_2O_3 SAMPLE EXPOSED TO STEAM AT 14 BAR FOR 6 H.

TABLE 5-2: TGA RESULTS FOR STEAM-EXPOSED GAMMA-AL_2O_3.

Entry	Exposure time (h)	Mass loss 120 – 700 °C (%)	DTG minimum (°C)	DSC area 1 (J g^{-1})	DSC area 2 (J g^{-1})
1	0	4	-	29.98	-15.9
2	1	7.3	453	75.56	-40.29
3	1.5	8.4	471.8	43.31	-66.19
4	2	7.8	472.6	22.82	-47.71
5	3	10.4	473.6	47.66	-121.6
6	6	11.9	480.2	110	-159.8
7	16	9.6	480.5	67.88	-81.24
8	66	13.5	488.9	132.3	-278.9
10	Hydrothermal	15.7	479.6	80.62	-339.1

Based on the combined experimental results described above, we can conclude that a reversible conversion between γ-AlO(OH) and γ-Al_2O_3 occurs in the range of 200-500 °C which depends on the partial pressure of steam. In Section 5.3.6, the state of the alumina will be related to the catalytic activity for the methanol dehydration reaction.

The Lewis acid sites at the surface of γ-Al_2O_3 are due to the coordinatively unsaturated aluminium cations which are formed as a result of dehydroxylation of hydrated oxide surface. A simple dehydroxylation reaction involves two neighboring hydroxyl groups, leaving coordinatively unsaturated electron-deficient surface aluminium ions without rearrangement of the surface structure. It is known that eliminating >75% surface hydroxyl

groups leads to the rearrangement of oxygen ions and vacancies in the surface layers, whilst a removal of >90% surface hydroxyl groups results in a migration of the ions at the surface [61, 62]. Therefore, the mechanism involved in the formation of Lewis acid sites takes into account both the dehydroxylation and deoxygenation reactions at the surface. The generally accepted model is: $2Al\text{-}OH^- \rightarrow H_2O + AlO^- + Al^+$. In this model, Al^+ is a surface oxygen vacancy creating a low-coordinated Lewis acid site. Considering that the transition of γ-Al_2O_3 to boehmite results in a higher concentration of surface hydroxyl groups, this scenario implies that the surface acidity of restored γ-Al_2O_3 is highly dependent on its exposure on stream. Consequently, the acidity of restored alumina is expected to increase with the time exposed to steam.

5.3.6. Catalytic activity of γ-alumina for methanol dehydration

To investigate the implications of the observed reversible transition between γ-Al_2O_3 and γ-AlO(OH) for the catalytic activity for methanol dehydration, several catalyst tests have been performed. Initially, the methanol conversion was measured as a function of the reactor pressure as shown in Figure 5-8. Under these conditions, based on Equation 5, the surface adsorption of the produced steam is expected to have a negative impact on the observed methanol conversion as determined by the work of Berčič and Levec [40]. The reaction rate has a negative order dependence on the steam partial pressure and a positive (less than first) order in methanol partial pressure, which has been widely reported in literature for this and similar alcohol dehydration reactions over γ-Al_2O_3 [35, 37, 40, 63]. Indeed, this is reflected in the experimental results (Figure 5-8). Note that the steam adsorption is clearly reversible as the experiments were performed in the order of decreasing reactor pressure. Under these conditions, the maximum applied steam partial pressure is about 2.4 bar which cannot induce the formation of γ-AlO(OH), as shown above in Section 5.3.5. In conclusion, the surface adsorption of water is reversible under these conditions.

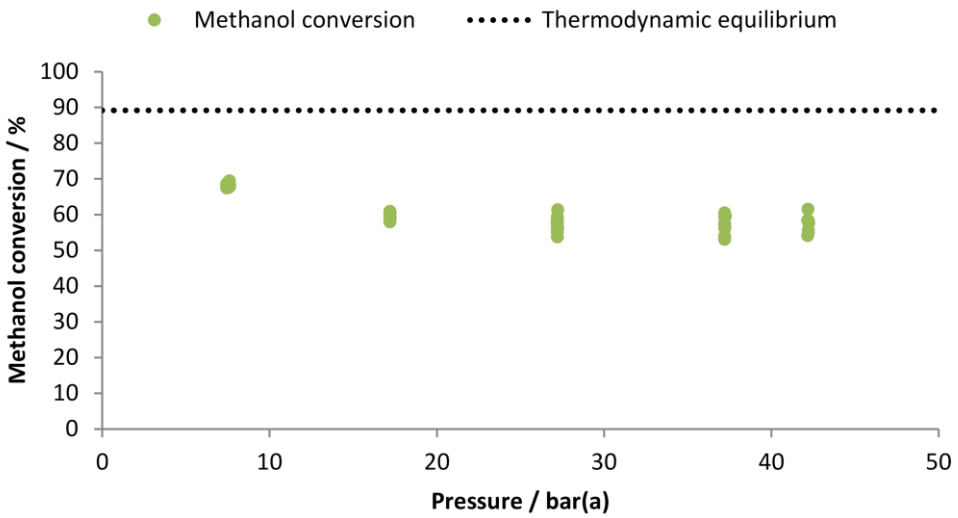

FIGURE 5-8: METHANOL CONVERSION OVER GAMMA-AL_2O_3 AT 250 °C, 7-42 BAR(A), 10% METHANOL IN NITROGEN, FEED FLOW RATE 889 ML_N MIN^{-1}.

The second experimental campaign involved high steam pressures, which were applied in between catalytic tests. Figure 5-9 shows the methanol conversion as a function of time at 250 °C. (Data at higher temperatures have been omitted for clarity.) Three tests can be discerned: (i) the initial test with γ-Al_2O_3 for the first 120 minutes, (ii) testing after exposure to 14 bar of steam at 250 °C for 40 hours, and (iii) testing of the sample after a temperature program to 350 °C.

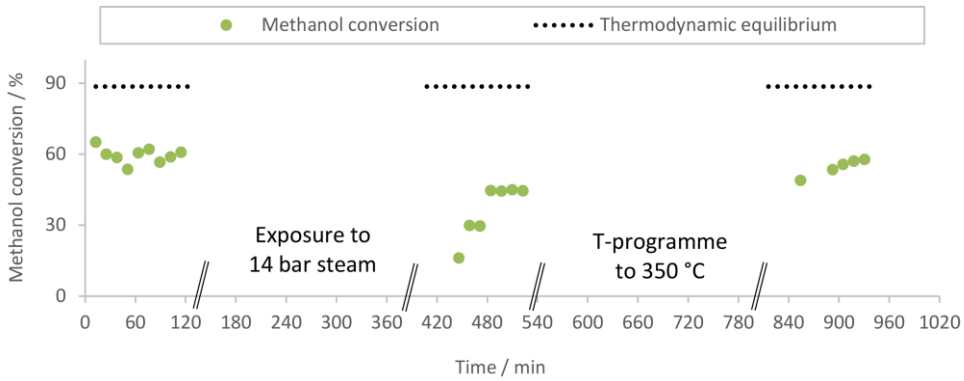

FIGURE 5-9: METHANOL CONVERSION OVER GAMMA-AL_2O_3 AT 250 °C, 25 BAR(A), 10% METHANOL IN NITROGEN, FEED FLOW RATE 889 ML_N MIN^{-1}.

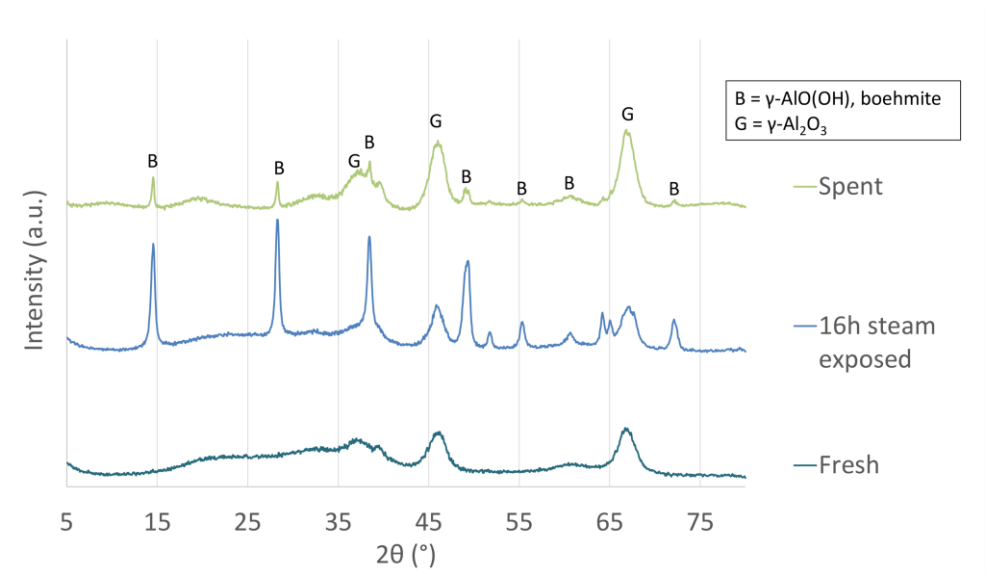

FIGURE 5-10: PXRD PATTERNS FOR THE SPENT CATALYST, STEAM-EXPOSED GAMMA-AL_2O_3 (14 BAR STEAM, 250 °C, 40 HOURS), AND FRESH GAMMA-AL_2O_3.

As discussed above, the exposure to 14 bar steam is expected to convert the γ-Al_2O_3 catalyst into γ-AlO(OH), not only on the surface but also in the bulk of the material. The high surface coverage by adsorbed water and hydroxyl groups is expected to have a strong impact on the catalytic activity of the sample by preventing the adsorption of methanol [64]. Indeed, the catalytic activity appears to be strongly affected as the measured methanol conversion starts significantly lower (at around 446 minutes on stream). This can be attributed to the conversion of γ-Al_2O_3 to γ-AlO(OH) which has been discussed above. Takagi et al. [65] have shown that the concentration of weak Lewis acids sites, that catalyze the methanol dehydration reaction, increases by more than a factor 4 when γ-AlO(OH) is calcined to γ-Al_2O_3. A similar restoration can be observed in the following data points, which show an in situ restoration, i.e. in the presence of produced steam, as the activity for methanol dehydration reaches a constant 45% conversion after 485 minutes on stream. The temperature of 250 °C is too low to completely restore the γ-Al_2O_3 phase as shown in Section 5.3.5, yet sufficient to largely restore the Lewis acid surface sites and hence the catalytic activity of the surface. In addition, the temperature program to 350 °C further restores the activity to the range of the original catalytic activity of the γ-Al_2O_3 sample. At this temperature, a significant part of the sample will remain as γ-AlO(OH), as observed in the XRD pattern of the spent catalyst (Figure 5-10). It can be concluded that, whereas γ-AlO(OH) remains after testing at 350 °C, this does not affect the catalytic activity for methanol dehydration and the deactivation by formation of γ-AlO(OH) is reversible in practice.

5.3.7. Catalytic activity of Copper-Zinc Oxide-Alumina

The copper-zinc oxide-alumina (CZA) methanol synthesis catalyst is tested separately, and in combination with the methanol dehydration catalyst γ-alumina. As shown in Figure 5-11, clearly the DME production is far from equilibrium under direct DME synthesis conditions, whereas the methanol production is close to equilibrium for methanol synthesis (greater than equilibrium in DME synthesis) at temperatures over 250 °C. The optimum temperature for methanol synthesis shifts by dilution of the CZA catalyst from 230 to 250 °C, which is well aligned with temperatures reported for methanol and direct DME synthesis in literature [22, 39, 66-76]. DME synthesis, however, is far from equilibrium for all catalyst compositions and the DME yield keeps increasing with temperature [22, 77]. Despite the fact that the temperature for methanol dehydration is generally higher [78-81], direct DME synthesis is often performed at temperatures of around 250 °C [22, 39, 66-70], not only because the methanol synthesis is considered to be the rate determining step in direct DME synthesis, but also to prevent deactivation of the CZA catalyst at temperatures above 300 °C. In literature methanol to acidic catalyst ratios of 1:1 up to 8:1 can be found [22, 39, 68, 82-86]. The rate limiting methanol synthesis is the reason to choose higher amounts of methanol synthesis catalyst. However, Figure 5-11 shows the limited dehydration in the

direct synthesis from CO_2. It is well known that a small amount of CO_2 in the synthesis gas enhances methanol synthesis kinetics [20], which is not the case with CO_2 as the feed. The additional water present due to CO_2 conversion (Equation 2), which cannot be converted in the WGS reaction (Equation 3) due to the absence of CO, limits the dehydration of methanol over γ-alumina.

As discussed in the previous section, the performance of γ-alumina is studied under typical methanol dehydration and SEDMES conditions. Despite the large attention for more active low-temperature methanol dehydration catalysts [15, 22, 66, 79, 81, 83, 85-105], γ-Al_2O_3 remains the catalyst of choice for industrial DME production, due to its low cost, high surface area, good thermal and mechanical stability, and high selectivity to DME because its relatively weak Lewis acid sites do not promote side reactions [81, 82, 106, 107]. In contrast to direct DME synthesis, SEDMES offers two specific advantages for the (γ-Al_2O_3) catalyst: the system is operated at low steam pressures and is periodically regenerated due to its adsorptive nature. In fact, the reduced steam content will likely promote deactivation (coking) of other, more acidic, dehydration catalysts [66, 87].

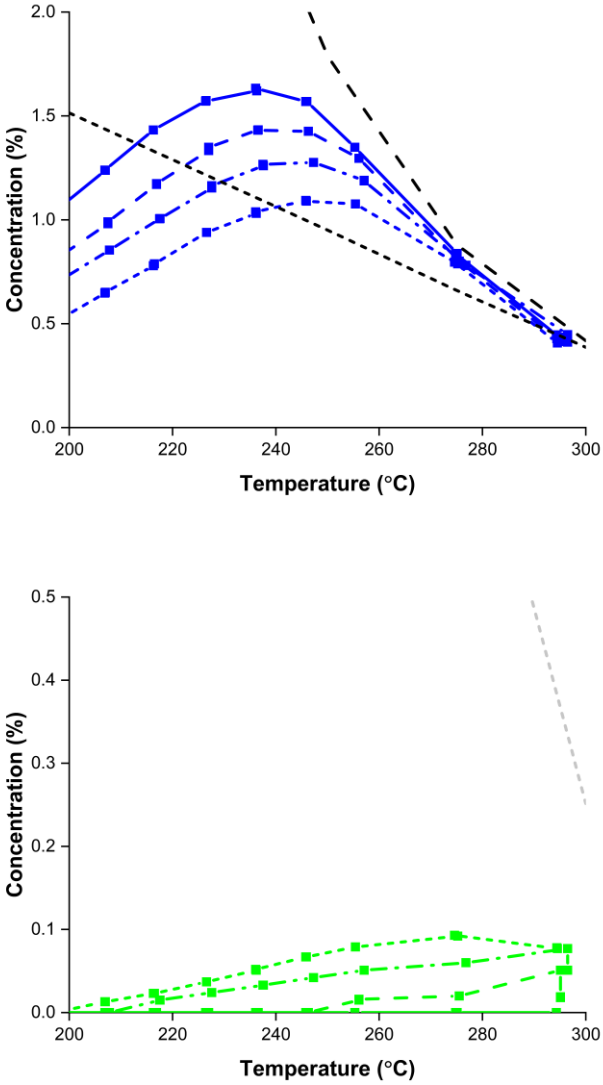

FIGURE 5-11: METHANOL (TOP, BLUE) AND DME (BOTTOM, GREEN) CONCENTRATION IN DIRECT SYNTHESIS FOR CO_2 FEED AT 25 BAR AND 200-300 °C. THE CATALYST RATIO CZA:ALUMINA IS 1:0 (SOLID), 4:1 (LONG DASH), 2:1 (DASH DOT) AND 1:1 (SHORT DASH). METHANOL EQUILIBRIUM (BLACK) AND DME EQUILIBRIUM (GREY) VALUES IN METHANOL SYNTHESIS (DASH) AND DIRECT DME SYNTHESIS (SHORT DASH).

Reaction kinetics for the used materials are determined by fitting the parameters in the methanol synthesis and dehydration reaction models from Graaf et al. (1988) and Berčič et al. (1992) respectively [67, 71, 78]. The new parameters are given in Table 5-3 and their good predictive capability of the observed concentrations is shown in Figure 5-12. For

methanol synthesis the average deviation is less than 5%, which is similar for the DME concentration. Only the methanol concentration in the dehydration experiments shows a higher deviation (11%) due to increased experimental error by feeding liquid methanol at varying conditions [80]. The activation energies determined for the methanol synthesis kinetics are lower than the values originally reported, especially considering the conversion of CO, resulting from a higher activity catalyst [71]. This corresponds with activity factors larger than one reported for present-day methanol synthesis catalysis [76, 108]. Also a difference in catalyst activity for methanol dehydration is observed, where the activation energy is changed 24% compared to the original value [78]. The altered value aligns well with modifications of the methanol dehydration kinetics reported for direct DME synthesis in the open literature [39].

TABLE 5-3: MODEL PARAMETERS FOR METHANOL SYNTHESIS AND DEHYDRATION REACTION KINETICS [67].

Parameter	Value (kJ mol^{-1})	Deviation from original
E_a (k1)	68.1	-38 %
E_a (k2)	107	-13 %
E_a (k3)	54.3	-17 %
ΔH (K_{CO})	-15.7	-73 %
ΔH (K_{CO2})	-56.0	-17 %
ΔH ($K_{H2O}/K_{H2}^{1/2}$)	-107	+2.4 %
E_a (k4)	109	-24 %
ΔH (K_{CH3OH})	-69.6	-1.3 %
ΔH (K_{H2O})	-39.3	-4.4 %

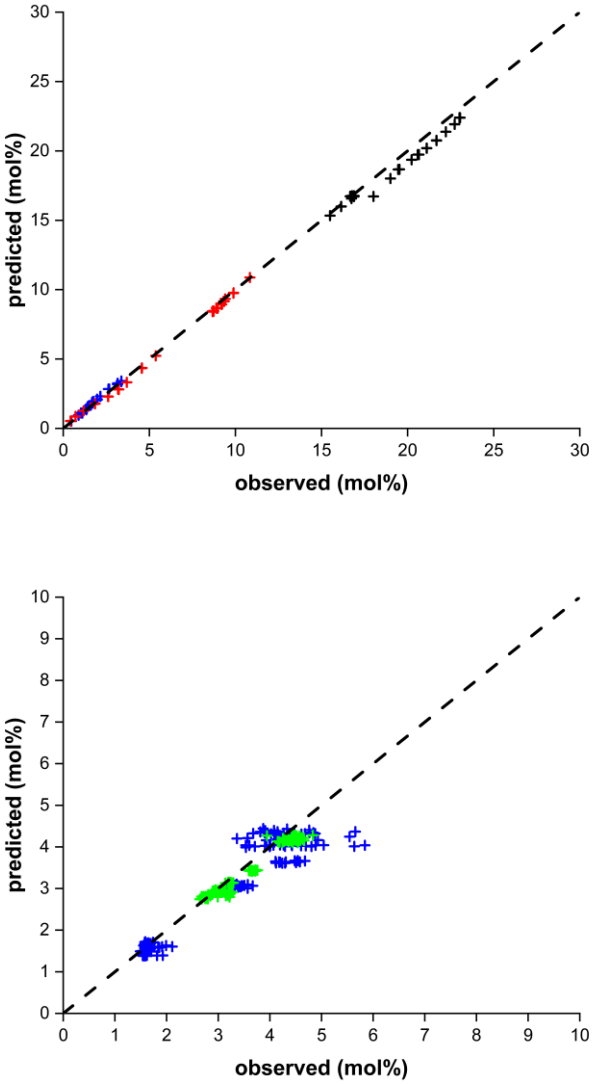

FIGURE 5-12: PARITY PLOT FOR A) METHANOL SYNTHESIS AND B) METHANOL DEHYDRATION. METHANOL (BLUE), DME (GREEN), CO (RED) AND CO_2 (BLACK).

5.4. Conclusions

In this chapter, a proof-of-concept for sorption enhanced DME, with commercial and novel materials, is shown and discussed. The performance of several CZA catalysts for the synthesis of methanol and the direct synthesis of DME (using additional γ-Al_2O_3 as acid catalyst) from a CO_2-rich syngas, akin to that obtained from the gasification of biomass, is studied. In order to adjust the CO_2/CO ratio within the reactor, CZA has been doped with Zr and Ga oxides. This strategy allows to increase the CO/CO_2 product ratio, but it fails to increase the methanol production rate. This is probably due to the higher activity of the doped catalysts for the r-WGS reaction and the concomitant production of H_2O, which results in a loss of activity of the doped CZA for the production of methanol from syngas. In addition, the presence of water in the reaction medium prevents the production of methanol from syngas and the production of DME from methanol. In order to remove H_2O during the direct synthesis of DME from CO_2-rich syngas a solid H_2O adsorbent, zeolite 3A, is added to the system. This strategy, referred to as sorption enhanced DME synthesis (SEDMES), allows to shift the equilibria to the product side, thus resulting in higher carbon conversions and DME productions. In fact, a proof-of-concept was demonstrated with DME concentrations of ca. 70%, well above the equilibrium value, for the undoped CZA catalysts, which show the highest production rate of methanol from CO_2-rich syngas. On the other hand, water removal during SEDMES with the Zr and Ga doped catalysts lead to a high production rate of CO.

The activity and stability of the acid catalyst, γ-Al_2O_3, for the methanol dehydration reaction has been investigated. It was found that γ-Al_2O_3 has a high activity and selectivity for the production of DME from methanol at 250 °C. Adsorbed steam, however, reduces the catalytic activity of γ- Al_2O_3. At 250 °C and steam partial pressures of 14 bar and higher, the conversion to crystalline boehmite has been confirmed through PXRD measurements. While crystalline boehmite remained present after testing methanol dehydration at 350 °C, it was shown that the activity for methanol dehydration is restored in situ at 250 °C. This confirms that the deactivation by steam is reversible under DME synthesis conditions.

Reaction kinetics for the commercial materials have been determined by fitting the parameters in the methanol synthesis and dehydration reaction models from Graaf et al. (1988) and Berčič et al. (1992), respectively, to the reported experimental data. The activation energies determined for both the methanol synthesis and methanol dehydration kinetics are lower than the values originally reported, attributed to the higher activity of present-day catalysts. Next to the study of the adsorbent material, this investigation of the catalysts, and the combination of all materials involved results in a validated dynamic reactor model, which will allow adequate upscaling of the SEDMES technology and predictions of large scale DME synthesis.

Nomenclature

a_p	Particle interfacial area (m^2 m^{-3})
b	Isotherm equilibrium constant (bar^{-1})
c_i	Concentration of component i (mol m^{-3})
Cp	Gas thermal conductivity (J kg^{-1} K^{-1})
Cp_p	Particle thermal conductivity (J kg^{-1} K^{-1})
d_p	Particle diameter (m)
D_z	Axial dispersion coefficient (m^2 s^{-1})
E_a	Activation energy (kJ mol^{-1})
G	Ergun constant (-)
ΔH_{ads}	Adsorption enthalpy (J mol^{-1})
$\Delta H_{r,i}$	Reaction enthalpy (J mol^{-1})
k	Reaction rate constant (mol s^{-1} kg^{-1} bar^{-1}) or (kmol kg^{-1} hr^{-1})
K_i	Adsorption equilibrium constant of component i (bar^{-1}) or (m^3 $kmol^{-3}$)
K_p	Equilibrium constant (based on partial pressure) (-)
M_i	Molecular weight of component i (kg mol^{-1})
N_i	Mole flux of component i (mol m^{-2} s^{-1})
P	Reactor pressure (bara)
P_i	Partial pressure of component i (bara)
q_i	Adsorbent loading (mol kg^{-1})
q_s	Saturation capacity (kg kg^{-1})
r_i	Reaction rate of component i (mol m^{-3} s^{-1}) or (mol kg^{-1} s^{-1}) or (kmol kg^{-1} hr^{-1})
R	Ideal gas constant (J mol^{-1} K^{-1})
t	Time (s)
T	Temperature (K)
u	Superficial gas velocity (m s^{-1})
U	Overall heat transfer coefficient (W m^{-2} K^{-1})
v	Interstitial gas velocity (m s^{-1})
z	axial coordinate (m)

Greek letters

ε_b	Bed voidage (-)
λ	Axial thermal conductivity (W m^{-1} K^{-1})
ρ	Density (kg m^{-3})
ρ_p	Particle density (kg m^{-3})
ϕ_i	Partial fugacity of component i (bara)
ω_i	Weight fraction of component i (-)

Bibliography

[1] R. Khoshbin, M. Haghighi, Direct conversion of syngas to dimethyl ether as a green fuel over ultrasound-assisted synthesized CuO–ZnO–Al2O3/HZSM-5 nanocatalyst: effect of active phase ratio on physicochemical and catalytic properties at different process conditions, Catal. Sci. Technol. 4 (2014) 1779-1792.

[2] R. Peláez, P. Marín, S. Ordóñez, Direct synthesis of dimethyl ether from syngas over mechanical mixtures of CuO/ZnO/Al2O3 and γ-Al2O3: Process optimization and kinetic modelling, Fuel Processing Technology 168 (2017) 40-49.

[3] C. Baltes, S. Vukojevic, F. Schuth, Correlations between synthesis, precursor, and catalyst structure and activity of a large set of CuO/ZnO/Al2O3 catalysts for methanol synthesis, Journal of Catalysis 258 (2008) 334-344.

[4] F. Song, Y. Tan, H. Xie, Q. Zhang, Y. Han, Direct synthesis of dimethyl ether from biomass-derived syngas over Cu–ZnO–Al2O3–ZrO2(x)/γ-Al2O3 bifunctional catalysts: Effect of Zr-loading, Fuel Processing Technology 126 (2014) 88-94.

[5] D. Mao, X. Guo, Dimethyl Ether Synthesis from Syngas over the Admixed Cu/ZnO/Al2O3Catalyst and Alkaline Earth Oxide-Modified HZSM-5 Zeolite, Energy Technology 2 (2014) 882-888.

[6] X.-J. Tang, J.-H. Fei, Z.-Y. Hou, X.-M. Zheng, H. Lou, Characterization of Cu−Mn/Zeolite-Y Catalyst for One-Step Synthesis of Dimethyl Ether from CO−H2, Energy & Fuels 22 (2008) 2877–2884.

[7] R. Ladera, E. Finocchio, S. Rojas, J.L.G. Fierro, M. Ojeda, Supported niobium catalysts for methanol dehydration to dimethyl ether: FTIR studies of acid properties, Catalysis Today 192 (2012) 136-143.

[8] R.M. Ladera, J.L.G. Fierro, M. Ojeda, S. Rojas, TiO2-supported heteropoly acids for low-temperature synthesis of dimethyl ether from methanol, Journal of Catalysis 312 (2014) 195-203.

[9] R.M. Ladera, M. Ojeda, J.L.G. Fierro, S. Rojas, TiO2-supported heteropoly acid catalysts for dehydration of methanol to dimethyl ether: relevance of dispersion and support interaction, Catalysis Science & Technology 5 (2015) 484-491.

[10] A. Kornas, M. Śliwa, M. Ruggiero-Mikołajczyk, K. Samson, J. Podobiński, R. Karcz, D. Duraczyńska, D. Rutkowska-Zbik, R. Grabowski, Direct hydrogenation of CO2 to dimethyl ether (DME) over hybrid catalysts containing CuO/ZrO2 as a metallic function and heteropolyacids as an acidic function, Reaction Kinetics, Mechanisms and Catalysis 130 (2020) 179-194.

[11] C. Peinado, D. Liuzzi, R.M. Ladera-Gallardo, M. Retuerto, M. Ojeda, M.A. Pena, S. Rojas, Effects of support and reaction pressure for the synthesis of dimethyl ether over heteropolyacid catalysts, Sci Rep 10 (2020) 8551.

[12] A.A. Khassin, T.P. Minyukova, T.M. Yurieva, Genesis of catalysts for methanol synthesis, Mendeleev Communications 24 (2014) 67-74.
[13] K.C. Waugh, Methanol Synthesis, Catalysis Letters 142 (2012) 1153-1166.
[14] J. Yoshihara, C.T. Campbell, Methanol Synthesis and Reverse Water–Gas Shift Kinetics over Cu(110) Model Catalysts: Structural Sensitivity, Journal of Catalysis 161 (1996) 776–782.
[15] A. Ateka, I. Sierra, J. Ereña, J. Bilbao, A.T. Aguayo, Performance of CuO–ZnO–ZrO2and CuO–ZnO–MnO as metallic functions and SAPO-18 as acid function of the catalyst for the synthesis of DME co-feeding CO2, Fuel Processing Technology 152 (2016) 34-45.
[16] H. Ham, S.W. Baek, C.-H. Shin, J.W. Bae, Roles of Structural Promoters for Direct CO2 Hydrogenation to Dimethyl Ether over Ordered Mesoporous Bifunctional Cu/M–Al2O3 (M = Ga or Zn), ACS Catalysis 9 (2019) 679-690.
[17] M. Muhler, E. Törnqvist, L.P. Nielsen, B.S. Clausen, H. Topsøe, On the role of adsorbed atomic oxygen and CO2 in copper based methanol synthesis catalysts, Catalysis Letters 25 (1994) 1-10.
[18] L.C. Grabow, M. Mavrikakis, Mechanism of Methanol Synthesis on Cu through CO2 and CO Hydrogenation, ACS Catalysis 1 (2011) 365-384.
[19] Y. Yang, C.A. Mims, D.H. Mei, C.H.F. Peden, C.T. Campbell, Mechanistic studies of methanol synthesis over Cu from CO/CO2/H2/H2O mixtures: The source of C in methanol and the role of water, Journal of Catalysis 298 (2013) 10-17.
[20] K. Klier, V. Chatikavanij, R.G. Herman, G.W. Simmons, Catalytic synthesis of methanol from CO/H_2, Journal of Catalysis 74 (1982) 343-360.
[21] J.B. Hansen, P.E.H. Nielsen, Methanol Synthesis, Handbook of Heterogeneous Catalysis, Wiley-VCH Verlag, 2008.
[22] F. Dadgar, R. Myrstad, P. Pfeifer, A. Holmen, H.J. Venvik, Direct dimethyl ether synthesis from synthesis gas: The influence of methanol dehydration on methanol synthesis reaction, Catalysis Today 270 (2016) 76-84.
[23] O. Martin, A.J. Martín, C. Mondelli, S. Mitchell, T.F. Segawa, R. Hauert, C. Drouilly, D. Curulla-Ferré, J. Pérez-Ramírez, Indium Oxide as a Superior Catalyst for Methanol Synthesis by CO_2 Hydrogenation, Angewandte Chemie International Edition 55 (2016) 6261-6265.
[24] A. Molino, V. Larocca, S. Chianese, D. Musmarra, Biofuels Production by Biomass Gasification: A Review, Energies 11 (2018) 811-841.
[25] I. Martínez, V. Kulakova, G. Grasa, R. Murillo, Experimental investigation on sorption enhanced gasification (SEG) of biomass in a fluidized bed reactor for producing a tailored syngas, Fuel 259 (2020) 116252-116259.
[26] S.-H. Kang, J.W. Bae, K.W. Jun, K.-S. Min, S.-L. Song, S.-H. Jeong, Catalyst for synthesizing methanol from synthesis gas and the preparation method thereof, United States of America, 2014.

[27] R. Ladera, F.J. Pérez-Alonso, J.M. González-Carballo, M. Ojeda, S. Rojas, J.L.G. Fierro, Catalytic valorization of CO2 via methanol synthesis with Ga-promoted Cu–ZnO–ZrO2 catalysts, Applied Catalysis B: Environmental 142-143 (2013) 241-248.
[28] E. Catizzone, G. Bonura, M. Migliori, F. Frusteri, G. Giordano, CO2 Recycling to Dimethyl Ether: State-of-the-Art and Perspectives, Molecules 23 (2017) 31.
[29] E. Catizzone, M. Migliori, A. Purita, G. Giordano, Ferrierite vs. γ-Al2O3: The superiority of zeolites in terms of water-resistance in vapour-phase dehydration of methanol to dimethyl ether, Journal of Energy Chemistry (2018).
[30] F. Dadgar, R. Myrstad, P. Pfeifer, A. Holmen, H.J. Venvik, Catalyst Deactivation During One-Step Dimethyl Ether Synthesis from Synthesis Gas, Catalysis Letters 147 (2017) 865-879.
[31] J. van Kampen, S. Booneveld, J. Boon, M. van Sint Annaland, Catalytic Aspects of Sorption-Enhanced DME Synthesis, CHAINS 2017 Chemistry for the Future, NWO, Veldhoven, the Netherlands, 2017.
[32] P. Patnaik, Handbook of inorganic chemicals, McGraw-Hill New York, 2003.
[33] K. Koichumanova, K.B. Sai Sankar Gupta, L. Lefferts, B.L. Mojet, K. Seshan, An in situ ATR-IR spectroscopy study of aluminas under aqueous phase reforming conditions, Physical Chemistry Chemical Physics 17 (2015) 23795-23804.
[34] S. Roy, G. Mpourmpakis, D.-Y. Hong, D.G. Vlachos, A. Bhan, R.J. Gorte, Mechanistic Study of Alcohol Dehydration on γ-Al_2O_3, ACS Catalysis 2 (2012) 1846-1853.
[35] J.F. DeWilde, H. Chiang, D.A. Hickman, C.R. Ho, A. Bhan, Kinetics and Mechanism of Ethanol Dehydration on γ-Al2O3: The Critical Role of Dimer Inhibition, ACS Catalysis 3 (2013) 798-807.
[36] A. Mandal, M. Prakash, R.M. Kumar, R. Parthasarathi, V. Subramanian, Ab Initio and DFT Studies on Methanol–Water Clusters, The Journal of Physical Chemistry A 114 (2010) 2250-2258.
[37] M. Kang, J.F. DeWilde, A. Bhan, Kinetics and mechanism of alcohol dehydration on γ-Al2O3: effects of carbon chain length and substitution, ACS Catalysis 5 (2014) 602-612.
[38] Y. Zhi, H. Shi, L. Mu, Y. Liu, D. Mei, D.M. Camaioni, J.A. Lercher, Dehydration Pathways of 1-Propanol on HZSM-5 in the Presence and Absence of Water, Journal of the American Chemical Society 137 (2015) 15781-15794.
[39] K.L. Ng, D. Chadwick, B.A. Toseland, Kinetics and modelling of dimethyl ether synthesis from synthesis gas, Chemical Engineering Science 54 (1999) 3587-3592.
[40] G. Berčič, J. Levec, Intrinsic and global reaction rate of methanol dehydration over γ-alumina pellets, Industrial & Engineering Chemistry Research 31 (1992) 1035-1040.
[41] K. Larmier, A. Nicolle, C. Chizallet, N. Cadran, S. Maury, A.-F. Lamic-Humblot, E. Marceau, H. Lauron-Pernot, Influence of Coadsorbed Water and Alcohol Molecules on Isopropyl Alcohol Dehydration on γ-Alumina: Multiscale Modeling of Experimental Kinetic Profiles, ACS Catalysis 6 (2016) 1905-1920.

[42] S.P. Naik, T. Ryu, V. Bui, J.D. Miller, N.B. Drinnan, W. Zmierczak, Synthesis of DME from CO_2/H_2 gas mixture, Chemical Engineering Journal 167 (2011) 362-368.
[43] I. Levin, D. Brandon, Metastable Alumina Polymorphs: Crystal Structures and Transition Sequences, Journal of the American Ceramic Society 81 (1998) 1995-2012.
[44] D. Liuzzi, C. Peinado, M.A. Peña, J. van Kampen, J. Boon, S. Rojas, Increasing dimethyl ether production from biomass-derived syngas via sorption enhanced dimethyl ether synthesis, Sustainable Energy & Fuels 4 (2020) 5674-5681.
[45] T.A. Zepeda, B. Pawelec, A. Infantes-Molina, R.I. Yocupicio, G. Alonso-Núñez, S. Fuentes, J.N. Diaz de León, J.L.G. Fierro, Ortho-xylene hydroisomerization under pressure on HMS-Ti mesoporous silica decorated with Ga2O3 nanoparticles, Fuel 158 (2015) 405-415.
[46] S.N. Khadzhiev, N.V. Kolesnichenko, N.N. Ezhova, Manufacturing of lower olefins from natural gas through methanol and its derivatives (review), Petroleum Chemistry 48 (2008) 325-334.
[47] M. Stöcker, Methanol-to-hydrocarbons: catalytic materials and their behavior, Microporous and Mesoporous Materials 29 (1999) 3-48.
[48] W.J. Lee, A. Bordoloi, J. Patel, T. Bhatelia, The effect of metal additives in Cu/Zn/Al2O3 as a catalyst for low-pressure methanol synthesis in an oil-cooled annulus reactor, Catalysis Today 343 (2020) 183-190.
[49] M.S. Spencer, The role of zinc oxide in Cu/ZnO catalysts for methanol synthesis and the water–gas shift reaction, Topics in Catalysis 8 (1999) 259–266.
[50] F. Li, M. Ao, G.H. Pham, J. Sunarso, Y. Chen, J. Liu, K. Wang, S. Liu, Cu/ZnO Catalysts Derived from Bimetallic Metal-Organic Framework for Dimethyl Ether Synthesis from Syngas with Enhanced Selectivity and Stability, Small 16 (2020) 1906276-1906283.
[51] M.R. Gogate, Methanol synthesis revisited: The nature of the active site of Cu in industrial Cu/ZnO/Al2O3 catalyst and Cu-Zn synergy, Petroleum Science and Technology 37 (2019) 671-678.
[52] M. Sánchez-Contador, A. Ateka, P. Rodriguez-Vega, J. Bilbao, A.T. Aguayo, Optimization of the Zr Content in the CuO-ZnO-ZrO2/SAPO-11 Catalyst for the Selective Hydrogenation of CO+CO2 Mixtures in the Direct Synthesis of Dimethyl Ether, Industrial & Engineering Chemistry Research 57 (2018) 1169-1178.
[53] A. Boumaza, L. Favaro, J. Ledion, G. Sattonnay, J.B. Brubach, P. Berthet, A.M. Huntz, P. Roy, R. Tetot, Transition alumina phases induced by heat treatment of boehmite: An X-ray diffraction and infrared spectroscopy study, J. Solid State Chem. 182 (2009) 1171-1176.
[54] D.J. Suh, T.-J. Park, J.-H. Kim, K.-L. Kim, Fast Sol–Gel Synthetic Route to High-Surface-Area Alumina Aerogels, Chemistry of Materials 9 (1997) 1903-1905.
[55] T.K. Phung, C. Herrera, M.Á. Larrubia, M. García-Diéguez, E. Finocchio, L.J. Alemany, G. Busca, Surface and catalytic properties of some γ-Al_2O_3 powders, Applied Catalysis A: General 483 (2014) 41-51.

[56] V. Sanchez Escribano, G. Garbarino, E. Finocchio, G. Busca, γ-Alumina and Amorphous Silica–Alumina: Structural Features, Acid Sites and the Role of Adsorbed Water, Topics in Catalysis 60 (2017) 1554-1564.
[57] J.B. Peri, A Model for the Surface of γ-Alumina, The Journal of Physical Chemistry 69 (1965) 220-230.
[58] B. Xu, P. Smith, Dehydration kinetics of boehmite in the temperature range 723–873K, Thermochimica Acta 531 (2012) 46-53.
[59] F. Karouia, M. Boualleg, M. Digne, P. Alphonse, The impact of nanocrystallite size and shape on phase transformation: Application to the boehmite/alumina transformation, Advanced Powder Technology 27 (2016) 1814-1820.
[60] T. Tsukada, H. Segawa, A. Yasumori, K. Okada, Crystallinity of boehmite and its effect on the phase transition temperature of alumina, Journal of Materials Chemistry 9 (1999) 549-553.
[61] R. Vidruk, M.V. Landau, M. Herskowitz, V. Ezersky, A. Goldbourt, Control of surface acidity and catalytic activity of γ-Al2O3 by adjusting the nanocrystalline contact interface, Journal of Catalysis 282 (2011) 215-227.
[62] H. Knözinger, P. Ratnasamy, Catalytic Aluminas: Surface Models and Characterization of Surface Sites, Catalysis Reviews 17 (1978) 31-70.
[63] M. Migliori, A. Aloise, E. Catizzone, G. Giordano, Kinetic Analysis of Methanol to Dimethyl Ether Reaction over H-MFI Catalyst, Industrial & Engineering Chemistry Research 53 (2014) 14885-14891.
[64] R.S. Schiffino, R.P. Merrill, A mechanistic study of the methanol dehydration reaction on γ-alumina catalyst, The Journal of Physical Chemistry 97 (1993) 6425-6435.
[65] A. Takagaki, J.C. Jung, S. Hayashi, Solid Lewis acidity of boehmite γ-AlO(OH) and its catalytic activity for transformation of sugars in water, RSC Advances 4 (2014) 43785-43791.
[66] F. Dadgar, R. Myrstad, P. Pfeifer, A. Holmen, H.J. Venvik, Catalyst Deactivation During One-Step Dimethyl Ether Synthesis from Synthesis Gas, Catalysis Letters 147 (2017) 865-879.
[67] J. van Kampen, J. Boon, J. Vente, M. van Sint Annaland, Sorption enhanced dimethyl ether synthesis for high efficiency carbon conversion: Modelling and cycle design, Journal of CO_2 Utilization 37 (2020) 295-308.
[68] A. García-Trenco, A. Martínez, The influence of zeolite surface-aluminum species on the deactivation of CuZnAl/zeolite hybrid catalysts for the direct DME synthesis, Catalysis Today 227 (2014) 144-153.
[69] S.P. Naik, T. Ryu, V. Bui, J.D. Miller, N.B. Drinnan, W. Zmierczak, Synthesis of DME from CO_2/H_2 gas mixture, Chemical Engineering Journal 167 (2011) 362-368.
[70] V.M. Lebarbier, R.A. Dagle, L. Kovarik, J.A. Lizarazo-Adarme, D.L. King, D.R. Palo, Synthesis of methanol and dimethyl ether from syngas over Pd/ZnO/Al2O3 catalysts, Catalysis Science & Technology 2 (2012) 2116–2127.

[71] H. Graaf, E.J. Stamhuis, A.A.C.M. Beenackers, Kinetics of low-pressure methanol synthesis, Chemical Engineering Science 43 (1988) 3185-3195.
[72] S. Dang, H. Yang, P. Gao, H. Wang, X. Li, W. Wei, Y. Sun, A review of research progress on heterogeneous catalysts for methanol synthesis from carbon dioxide hydrogenation, Catalysis Today 330 (2018) 61-75.
[73] S. Jadhav, P. Vaidya, B. Bhanage, J. Joshi, Chemical Engineering Research and Design Catalytic carbon dioxide hydrogenation to methanol : A review of recent studies, Chemical Engineering Research and Design 92 (2014) 2557-2567.
[74] H.J. Venvik, J. Yang, Catalysis in microstructured reactors: Short review on small-scale syngas production and further conversion into methanol, DME and Fischer-Tropsch products, Catalysis Today 285 (2017) 135-146.
[75] X. Jiang, X. Nie, X. Guo, C. Song, J.G. Chen, Recent Advances in Carbon Dioxide Hydrogenation to Methanol via Heterogeneous Catalysis, Chemical Reviews 120 (2020) 7984-8034.
[76] A. Montebelli, C.G. Visconti, G. Groppi, E. Tronconi, C. Ferreira, S. Kohler, Enabling small-scale methanol synthesis reactors through the adoption of highly conductive structured catalysts, Catalysis Today 215 (2013) 176-185.
[77] I.A. Kurzina, S.I. Reshetnikov, N.I. Karakchieva, L.N. Kurina, Direct synthesis of dimethyl ether from synthesis gas: Experimental study and mathematical modeling, Chemical Engineering Journal 329 (2017) 135-141.
[78] G. Berčič, J. Levec, Intrinsic and Global Reaction Rate of Methanol Dehydration Over γ-Al_2O_3 Pellets, Industrial & Engineering Chemistry Research 31 (1992) 1035-1040.
[79] H. Bateni, C. Able, Development of Heterogeneous Catalysts for Dehydration of Methanol to Dimethyl Ether: A Review, Catalysis in Industry 11 (2019) 7-33.
[80] J. Boon, J. van Kampen, R. Hoogendoorn, S. Tanase, F.P.F. van Berkel, M. van Sint Annaland, Reversible deactivation of γ-alumina by steam in the gas-phase dehydration of methanol to dimethyl ether, Catalysis Communications 119 (2019) 22-27.
[81] U. Mondal, G.D. Yadav, Perspective of dimethyl ether as fuel: Part I. Catalysis, Journal of CO2 Utilization 32 (2019) 299-320.
[82] M. Stiefel, R. Ahmad, U. Arnold, M. Döring, Direct synthesis of dimethyl ether from carbon-monoxide-rich synthesis gas : In fl uence of dehydration catalysts and operating conditions, Fuel Processing Technology 92 (2011) 1466-1474.
[83] A. García-Trenco, S. Valencia, A. Martínez, The impact of zeolite pore structure on the catalytic behavior of CuZnAl/zeolite hybrid catalysts for the direct DME synthesis, Applied Catalysis A: General 468 (2013) 102-111.
[84] A.T. Aguayo, J. Erena, D. Mier, J.M. Arandes, M. Olazar, J. Bilbao, Kinetic Modeling of Dimethyl Ether Synthesis in a Single Step on a CuO−ZnO−Al2O3/γ-Al2O3 Catalyst, Industrial & Engineering Chemistry Research 46 (2007) 5522-5530.

[85] G. Bonura, M. Cordaro, C. Cannilla, A. Mezzapica, L. Spadaro, F. Arena, F. Frusteri, Catalytic behaviour of a bifunctional system for the one step synthesis of DME by CO_2 hydrogenation, Catalysis Today 228 (2014) 51-57.
[86] F. Frusteri, M. Migliori, C. Cannilla, L. Frusteri, E. Catizzone, A. Aloise, G. Giordano, G. Bonura, Direct CO_2-to-DME hydrogenation reaction: New evidences of a superior behaviour of FER-based hybrid systems to obtain high DME yield, Journal of CO_2 Utilization 18 (2017) 353-361.
[87] E. Catizzone, M. Migliori, A. Purita, G. Giordano, Ferrierite vs. γ-Al2O3: The superiority of zeolites in terms of water-resistance in vapour-phase dehydration of methanol to dimethyl ether, Journal of Energy Chemistry 30 (2019) 162-169.
[88] E. Catizzone, S.V. Daele, M. Bianco, A. Di Michele, A. Aloise, M. Migliori, V. Valtchev, G. Giordano, Catalytic application of ferrierite nanocrystals in vapour-phase dehydration of methanol to dimethyl ether, Applied Catalysis B: Environmental 243 (2019) 273-282.
[89] E. Catizzone, A. Aloise, M. Migliori, G. Giordano, From 1-D to 3-D zeolite structures: performance assessment in catalysis of vapour-phase methanol dehydration to DME, Microporous and Mesoporous Materials 243 (2017) 102-111.
[90] E. Catizzone, A. Aloise, M. Migliori, G. Giordano, Dimethyl ether synthesis via methanol dehydration: Effect of zeolite structure, Applied Catalysis A: General 502 (2015) 215-220.
[91] V. Barbarossa, R. Viscardi, G. Maestri, R. Maggi, D. Mirabile Gattia, E. Paris, Sulfonated catalysts for methanol dehydration to dimethyl ether (DME), Materials Research Bulletin 113 (2019) 64-69.
[92] G. Baracchini, A.G.F. Machoke, M. Klumpp, R. Wen, P. Arnold, W. Schwieger, R. Dittmeyer, Structured catalysts for the direct synthesis of dimethyl ether from synthesis gas: A comparison of core@shell versus hybrid catalyst configuration, Catalysis Today 342 (2020) 46-58.
[93] S. Baier, C.D. Damsgaard, M. Klumpp, J. Reinhardt, T. Sheppard, Z. Balogh, T. Kasama, F. Benzi, J.B. Wagner, W. Schwieger, C.G. Schroer, J.D. Grunwaldt, Stability of a Bifunctional Cu-Based Core@Zeolite Shell Catalyst for Dimethyl Ether Synthesis Under Redox Conditions Studied by Environmental Transmission Electron Microscopy and In Situ X-Ray Ptychography, Microsc Microanal 23 (2017) 501-512.
[94] S. Ren, W.R. Shoemaker, X. Wang, Z. Shang, N. Klinghoffer, S. Li, M. Yu, X. He, T.A. White, X. Liang, Highly active and selective Cu-ZnO based catalyst for methanol and dimethyl ether synthesis via CO2 hydrogenation, Fuel 239 (2019) 1125-1133.
[95] T.A. Semelsberger, K.C. Ott, R.L. Borup, H.L. Greene, Role of acidity on the hydrolysis of dimethyl ether (DME) to methanol, Applied Catalysis B: Environmental 61 (2005) 281-287.
[96] M. Cai, A. Palčić, V. Subramanian, S. Moldovan, O. Ersen, V. Valtchev, V.V. Ordomsky, A.Y. Khodakov, Direct dimethyl ether synthesis from syngas on copper-zeolite hybrid catalysts with a wide range of zeolite particle sizes, Journal of Catalysis 338 (2016) 227-238.

[97] A. Ateka, P. Pérez-Uriarte, I. Sierra, J. Ereña, J. Bilbao, A.T. Aguayo, Regenerability of the CuO–ZnO–MnO/SAPO-18 catalyst used in the synthesis of dimethyl ether in a single step, Reaction Kinetics, Mechanisms and Catalysis 119 (2016) 655-670.
[98] A. Ateka, M. Sánchez-Contador, J. Ereña, A.T. Aguayo, J. Bilbao, Catalyst configuration for the direct synthesis of dimethyl ether from CO and CO2 hydrogenation on CuO–ZnO–MnO/SAPO-18 catalysts, Reaction Kinetics, Mechanisms and Catalysis 124 (2018) 401-418.
[99] Y. Wang, W.-l. Wang, Y.-x. Chen, J.-j. Zheng, R.-f. Li, Synthesis of dimethyl ether from syngas using a hierarchically porous composite zeolite as the methanol dehydration catalyst, Journal of Fuel Chemistry and Technology 41 (2013) 873-880.
[100] A.E.A.A. Said, M.M. Abd El-Wahab, M.A. El-Aal, The catalytic performance of sulfated zirconia in the dehydration of methanol to dimethyl ether, Journal of Molecular Catalysis A: Chemical 394 (2014) 40-47.
[101] M. Rutkowska, D. Macina, N. Mirocha-Kubień, Z. Piwowarska, L. Chmielarz, Hierarchically structured ZSM-5 obtained by desilication as new catalyst for DME synthesis from methanol, Applied Catalysis B: Environmental 174-175 (2015) 336-343.
[102] M.H. Huang, H.M. Lee, K.C. Liang, C.C. Tzeng, W.H. Chen, An experimental study on single-step dimethyl ether (DME) synthesis from hydrogen and carbon monoxide under various catalysts, International Journal of Hydrogen Energy 40 (2015) 13583-13593.
[103] Y. Hua, X. Guo, D. Mao, G. Lu, G.L. Rempel, F.T.T. Ng, Single-step synthesis of dimethyl ether from biomass-derived syngas over CuO-ZnO-MO x (M = Zr, Al, Cr, Ti)/HZSM-5 hybrid catalyst: Effects of MO x, Applied Catalysis A: General 540 (2017) 68-74.
[104] R. Dębek, M.F.G. Ribeiro, A. Fernandes, M. Motak, Dehydration of methanol to dimethyl ether over modified vermiculites, Comptes Rendus Chimie 18 (2015) 1211-1222.
[105] M. Xu, D.W. Goodman, A. Bhattacharyya, Catalytic dehydration of methanol to dimethyl ether (DME) over Pd / Cab-O-Sil catalysts, Applied Catalysis A: General 149 (1997) 303-309.
[106] E. Catizzone, G. Bonura, M. Migliori, F. Frusteri, G. Giordano, CO_2 Recycling to Dimethyl Ether: State-of-the-Art and Perspectives, Molecules 23 (2018) 31-59.
[107] J. Sun, G. Yang, Y. Yoneyama, N. Tsubaki, Catalysis Chemistry of Dimethyl Ether Synthesis, ACS Catalysis 4 (2014) 3346−3356.
[108] S. Guffanti, C.G. Visconti, J. van Kampen, J. Boon, G. Groppi, Reactor modelling and design for sorption enhanced dimethyl ether synthesis, Chemical Engineering Journal 404 (2021) 126573-126585.

Chapter 6. Experimental validation of pressure swing regeneration in sorption enhanced dimethyl ether synthesis

Abstract

In this chapter, SEDMES is demonstrated experimentally on a bench-scale reactor with pressure swing regeneration. Pressure swing regeneration, rather than the time and energy intensive temperature swing regeneration, shows high performance with over 80% single-pass carbon selectivity to DME. This already allows for a factor four increase in productivity, with further optimization still possible. With the proposed isotherm for the water adsorbent, and the methanol synthesis and dehydration kinetics, the validated dynamic cycle model adequately describes the SEDMES bench-scale data.

Applying shorter cycle times, made possible by pressure swing regeneration, allows optimization of the DME productivity while maintaining the high single-pass yield typical for SEDMES. The experimental confirmation shown in this paper unlocks the full potential of the high efficiency carbon and hydrogen utilization by SEDMES technology.

This chapter is based on published work:

J. van Kampen et al., Experimental validation of pressure swing regeneration for faster cycling in sorption enhanced dimethyl ether synthesis, Chemical Communications 56 (2020) 13540-13542.

J. van Kampen et al., Sorption enhanced dimethyl ether synthesis under industrially relevant conditions: Experimental validation of pressure swing regeneration, Reaction Chemistry & Engineering 6 (2021) 244-257.

6.1. Introduction

Sorption enhanced DME synthesis is a promising process intensification strategy for the direct production of DME from CO_2 [1-6]. While enabling increased single-pass conversion and selectivity, experimental studies have indicated that time and energy intensive temperature swing regeneration would be required for adsorbent regeneration [1, 4]. Pressure swing regeneration is faster and more energy efficient as indicated in a previous SEDMES modelling study and discussed in Chapter 3 [4].

In this chapter the results of an experimental investigation into the bench-scale sorption enhanced production of DME are elaborated, including model validation. The materials involved in SEDMES have been tested separately under relevant conditions and combined for sorption enhanced DME production. As in the direct synthesis of DME, a copper-zinc oxide-alumina (CZA) methanol synthesis catalyst is used in combination with methanol dehydration catalyst γ-alumina. These materials have been elaborately discussed in the previous chapter. In addition, a solid steam adsorbent, LTA zeolite, is required, which is investigated in Chapter 4. Validation of sorption enhanced DME synthesis technology is shown with the best (commercially available) materials, model development and validation under industrially relevant conditions (TRL4) are performed. Special attention is being paid to the mode of regeneration, as the key to an economically attractive process.

In the next section, the used materials, the experimental procedures and model interpretation are reported. In the results and discussion section, firstly, the SEDMES testing is discussed. This is followed by model validation and prediction. Finally, the conclusions are summarized.

6.2. Experimental

6.2.1. Materials

Experimental validation of sorption enhanced DME synthesis was performed using (a homogeneous mixture of) commercially available catalyst and adsorbent: CZA catalyst, γ-Al_2O_3 (assay>98%, Riogen NJ, USA), obtained as 3 mm pellets, and molecular sieve type 3A, purchased as 1.6 mm pellets (UOP Molecular Sieves, Advanced Specialty Gas Equipment, USA).

6.2.2. Methods

A combination of commercially obtained CZA catalyst, γ-Al_2O_3 catalyst and zeolite 3A adsorbent were used for the experimental demonstration of direct DME synthesis from $CO/CO_2/H_2$-mixtures.

The experimental runs were conducted on a bench-scale high-pressure reactor setup (Figure 6-1), allowing tests up to 2 liters of sample, typically consisting of a 1:4 ratio (weight

basis) catalyst to sorbent. The ratio between catalyst and sorbent was not further optimized in this work. Adsorption was performed with different (stoichiometric) feed gas compositions, using 68.6-72.7 vol.% of hydrogen, 0-9.1 vol.% of carbon monoxide, 17.1-23.6 vol.% of carbon dioxide and inert argon, nitrogen or methane, at 25 bar(a) and a temperature range of 250-300 °C. The inert balance was used in order to keep the overall pressure stable, considering the nett mole consumption by the reaction and the adsorption of water. Regeneration was done by depressurization to 1-3 bar(a) for PSA regeneration, switching to dry, inert gas, and eventual heating to 400 °C for TSA regeneration. Finally, either the inert purge gas or the reactive feed gas is used for repressurization. Transient gas analysis was performed by micro-GC (measuring methane, CO, CO_2, nitrogen, argon, methanol and DME) and mass spectrometry measuring hydrogen (m/z=2), methane (m/z=15), water (m/z=18), carbon monoxide/nitrogen (m/z=28), methanol (m/z=31), carbon dioxide (m/z=44) and DME (m/z=45).

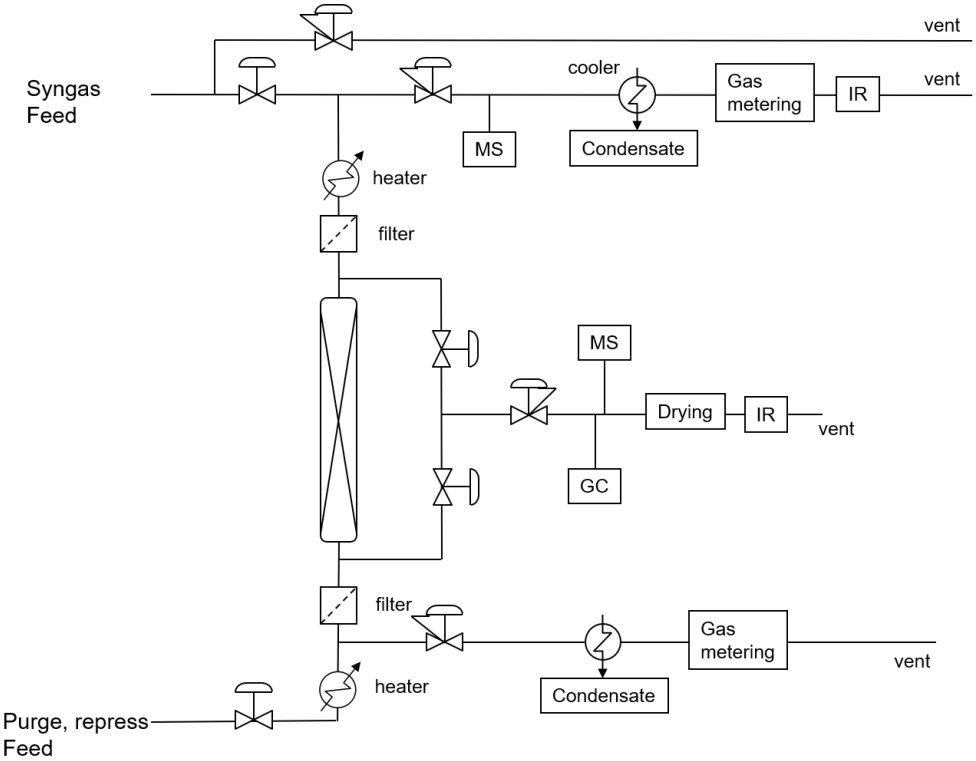

FIGURE 6-1: SCHEMATIC OF THE BENCH-SCALE REACTOR.

6.2.3. Data interpretation

In order to facilitate data interpretation, several key metrics have been defined to be able to quantify the SEDMES performance. The most important metric, the carbon selectivity *S(i)*, used here is defined as follows,

$$S(i) = \frac{ny(C_nH_mO_p)}{\sum_i n_i y(i)} \quad (1)$$

The carbon selectivities were calculated as molar concentration-based selectivities for each of the carbon containing species, *y(i)*. For example, the selectivity towards DME can be calculated as

$$S(DME) = \frac{2y(DME)}{y(CO)+y(CO_2)+2y(DME)+y(MeOH)+y(CH_4)} \quad (2)$$

Time integration (in the interval *t*: 0-t_{CO2}, where t_{CO2} is the (interpolated) point in time where the CO_2 outlet concentration reaches a level of 5 vol.%) of the streams gives an overall yield and selectivity for the cyclic (steady state) performance of the SEDMES process.

6.2.4. Model

A one-dimensional pseudo-homogeneous dynamic reactor model was developed in Matlab, verified and validated [4]. For the description of the fluid flow and mass transfer, the 1D non-steady differential mass and momentum balances are solved. The total mass, momentum, component and overall energy balances are given in Table 6-1. As described in Chapter 5, the reaction kinetics have been determined for the used catalyst materials by fitting the parameters in the models of Graaf et al. (1988) and Berčič et al. (1992) for the methanol synthesis and methanol dehydration respectively, shown in Table 6-2 [3, 7-9]. The steam adsorption isotherm of the LTA zeolite adsorbent is determined under the high pressure and temperature working conditions of the SEDMES process in Chapter 4 [10]. Full details of the different aspects of the model can be found in Chapter 3 [4].

TABLE 6-1: REACTOR MODEL EQUATIONS.

Overall mass balance	$\frac{\partial \rho}{\partial t} = -\frac{\partial \rho v}{\partial z} - \frac{1-\varepsilon_b}{\varepsilon_b} a_p \sum M_i N_i$	(3)
Momentum balance	$\frac{\partial \rho v}{\partial t} = -\frac{\partial \rho v^2}{\partial z} - \frac{\partial P}{\partial z} - G\frac{\rho \lvert u \rvert u}{d_p}$	(4)
Species mass balance	$\frac{\partial \rho \omega_i}{\partial t} = -\frac{\partial \rho v \omega_i}{\partial z} + \frac{\partial}{\partial z}\left(D_z \rho \frac{\partial \omega_i}{\partial z}\right) - \frac{1-\varepsilon_b}{\varepsilon_b} a_p M_i N_i$	(5)
Overall energy balance	$(\varepsilon_b \rho Cp + (1-\varepsilon_b)\rho_p Cp_p)\frac{\partial T}{\partial t} = -\rho Cpu\frac{\partial T}{\partial z} + \frac{\partial}{\partial z}\left(\lambda \frac{\partial T}{\partial z}\right) + \frac{4U(T_w - T)}{d_r}$	(6)

	$+(1-\varepsilon_b)\rho_p\left(\sum -\Delta H_{r,i} r_i + \sum -\Delta H_{ads,i}\frac{\partial \overline{q_i}}{\partial t}\right)$	
Equation of state	$PM = \rho RT$	(7)

TABLE 6-2: REACTION RATE EQUATIONS.

Methanol synthesis from CO (Graaf et al. [7])	$r_{CH3OH,1} = \frac{k_1 K_{CO}\left[\varphi_{CO}\varphi_{H2}^{3/2} - \varphi_{CH3OH}/\left(\varphi_{H2}^{1/2}K_{p1}\right)\right]}{(1+K_{CO}\varphi_{CO}+K_{CO2}\varphi_{CO2})\left[\varphi_{H2}^{1/2}+\left(K_{H2O}/K_{H2}^{1/2}\right)\varphi_{H2O}\right]}$	(8)
Water-gas shift (Graaf et al. [7])	$r_{CO} = \frac{k_2 K_{CO2}\left[\varphi_{CO2}\varphi_{H2} - \varphi_{H2O}\varphi_{CO}/K_{p2}\right]}{(1+K_{CO}\varphi_{CO}+K_{CO2}\varphi_{CO2})\left[\varphi_{H2}^{1/2}+\left(K_{H2O}/K_{H2}^{1/2}\right)\varphi_{H2O}\right]}$	(9)
Methanol synthesis from CO_2 (Graaf et al. [7])	$r_{CH3OH,2} = \frac{k_3 K_{CO2}\left[\varphi_{CO2}\varphi_{H2}^{3/2} - \varphi_{CH3OH}\varphi_{H2O}/\left(\varphi_{H2}^{3/2}K_{p3}\right)\right]}{(1+K_{CO}\varphi_{CO}+K_{CO2}\varphi_{CO2})\left[\varphi_{H2}^{1/2}+\left(K_{H2O}/K_{H2}^{1/2}\right)\varphi_{H2O}\right]}$	(10)
Methanol dehydration (Berčič et al. [8])	$r_{DME} = \frac{k_4 K_{CH3OH}^2\left[C_{CH3OH}^2 - C_{H2O}C_{DME}/K_{p4}\right]}{\left[1+2(K_{CH3OH}C_{CH3OH})^{1/2}+K_{H2O}C_{H2O}\right]^4}$	(11)

6.3. Results and discussion

To investigate the sorption enhanced DME synthesis process further, firstly the adsorption capacity at elevated temperature and pressure was studied in Chapter 4. This was followed by a performance study of the catalyst materials used in SEDMES (Chapter 5). In this chapter, a proof-of-concept for sorption enhanced DME synthesis at bench-scale is demonstrated experimentally and the cycle design is discussed as the way forward to enhance productivity and carbon selectivity.

6.3.1. Sorption enhanced DME synthesis

Sorption enhanced DME synthesis is demonstrated experimentally at a 2 liter bench-scale reactor (TRL4), already a large step forward in the development of the SEDMES process [1]. Figure 6-2 shows a representative breakthrough experiment of sorption enhanced DME synthesis. Prior to steam breakthrough, DME and unconverted CO are the primary products. After steam breakthrough the concentration of DME drops, accompanied by the breakthrough of CO_2 and methanol indicating saturation of the adsorbent. As can be seen in Figure 6-2 as well, the dynamic cycle model, using the reaction kinetics and water adsorption isotherm as determined in the previous chapters, describes the experimentally determined concentration and dynamic behavior well. Although not measured, the model prediction of the hydrogen concentration also accurately captures the experimental balance concentration (except for the first point, determined by product breakthrough). Based on previous modelling work [4], it was concluded that pressure swing regeneration rather than the so-far required time and energy intensive temperature swing regeneration

would be effective. Evaluation of regeneration strategies including pressure swing was therefore among the aims of testing under industrially relevant conditions. The testing under industrially relevant conditions performed in this work indeed proves high performance with pressure swing regeneration, demonstrating over 80% integral carbon selectivity towards DME when using pressure swing regeneration, without the need for a temperature swing (Figure 6-2). In Figure 6-3 the experimental carbon distribution for SEDMES at 275 °C is shown, indicating the single-pass conversion increase from 18% for conventional synthesis (represented as the thermodynamic equilibrium) to 68%. Crucially, the experiment serves to show how a similar conversion and selectivity is obtained with pressure swing regeneration (PSA) in comparison with previously reported experiments with a combined temperature and pressure swing regeneration (TPSA). As no time is required for heating and cooling, the adsorbent regeneration time can be reduced from 360 minutes to 60 minutes under the current conditions. As a result, the faster pressure swing regeneration already increases the DME productivity by a factor four, with even further optimization possible [11].

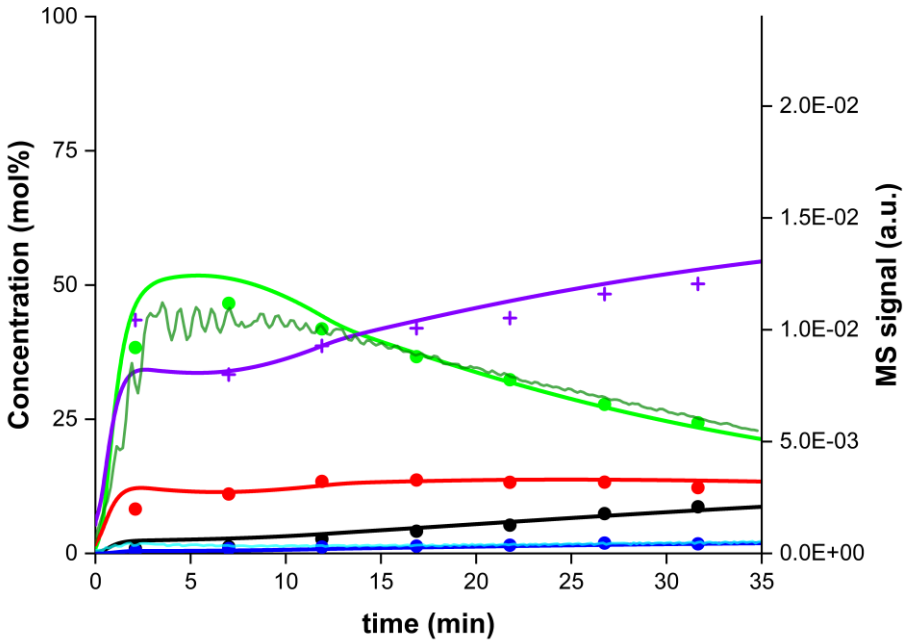

FIGURE 6-2: EXPERIMENTAL DATA AT 250 °C AND 25 BAR(A) FOR A CO_2:CO=2:1 FEED WITH STOICHIOMETRIC HYDROGEN, WITHOUT INERT (DOTS; DME (GREEN), CO (RED), CO_2 (BLACK), METHANOL (BLUE)), BALANCE CONCENTRATION (PURPLE CROSS) AND MODEL PREDICTION (LINES; HYDROGEN (PURPLE)). MS BREAKTHROUGH PROFILE OF DME (DARK GREEN LINE) AND H_2O (LIGHT BLUE LINE) SHOWN ON SECONDARY AXIS (A.U.).

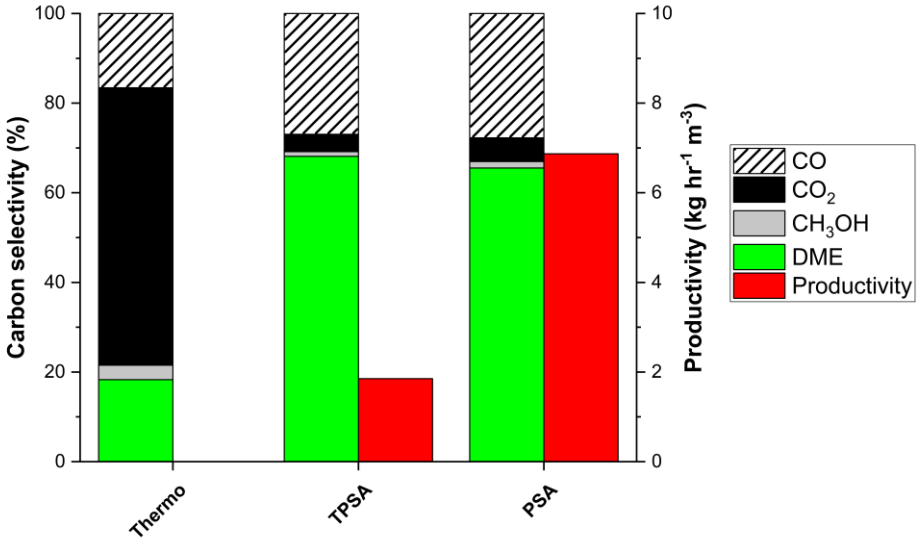

FIGURE 6-3: THERMODYNAMIC (MAXIMALLY POSSIBLE) CARBON DISTRIBUTION WITHOUT SORPTION ENHANCEMENT VERSUS EXPERIMENTALLY OBTAINED TPSA AND PSA RESULTS FOR SORPTION ENHANCED DME SYNTHESIS. CONDITIONS: 275 °C AND 25 BAR(A) FOR A CO_2:CO=2:1 FEED WITH STOICHIOMETRIC HYDROGEN AND CH_4 TRACER. TPSA: REGENERATION INCLUDED HEATING UP TO 400 °C.

One of the optimization parameters is the carbon selectivity towards DME. Thermodynamically the carbon selectivity to DME is unfavorable and CO_2 will be the main carbon containing product (Figure 6-4). However, sorption enhanced DME synthesis allows for a high single-pass carbon conversion to DME irrespective of the carbon source (CO or CO_2), 80% shown here. The model prediction for a CO_2:CO feed of 2:1 is very good (Figure 6-4, top), and despite a small overprediction for a CO_2 feed (Figure 6-4, bottom), the model prediction is still adequate. This overprediction is caused by an apparent catalyst deactivation during the initial part of the experimental campaign, which stabilizes over the full length of the campaign, as shown in Figure 6-5. It is well known that especially the CZA catalyst is prone to deactivation under more severe hydrothermal conditions. An advantage of the sorption enhanced reaction conditions include the extremely low water concentration, protecting the catalyst from hydrothermal sintering [12, 13]. However, water has also shown to have a positive influence in catalyst deactivation (by coking) for a CO-rich feed. The cause of the observed small decrease in catalyst activity is subject of follow-up work.

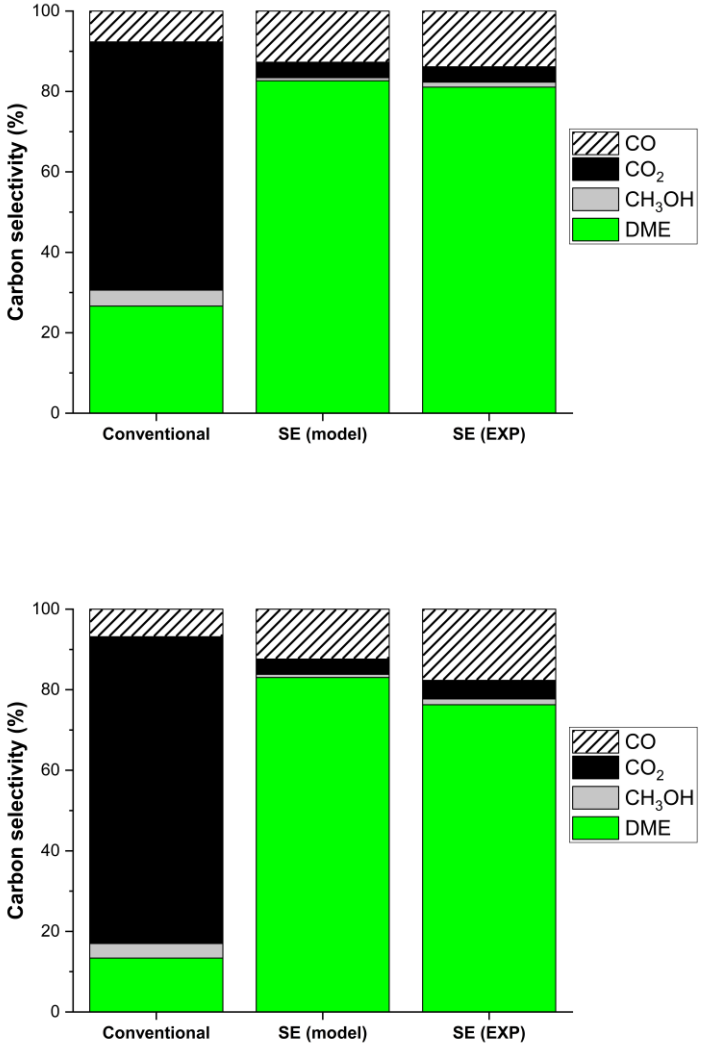

FIGURE 6-4: CARBON SELECTIVITY FOR CONVENTIONAL DIRECT DME SYNTHESIS (THERMODYNAMIC EQUILIBRIUM), FOR SORPTION ENHANCED DME SYNTHESIS MODEL PREDICTION AND EXPERIMENTAL SORPTION ENHANCED DME RESULTS AT 25 BAR(A) AND 250 °C FOR FEED: CO_2:CO=2:1 WITH STOICHIOMETRIC HYDROGEN & CH_4 TRACER (TOP) AND FEED: CO_2 WITH STOICHIOMETRIC HYDROGEN & CH_4 TRACER (BOTTOM).

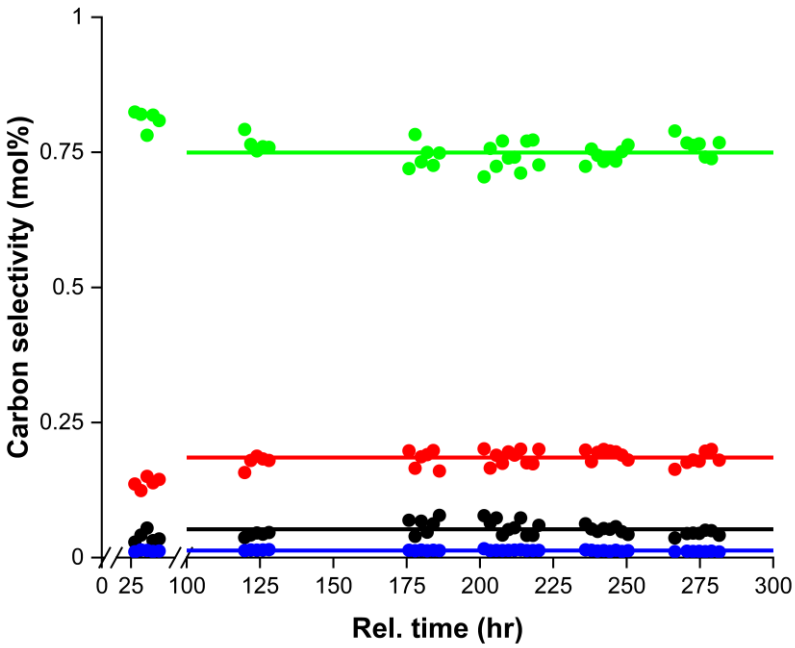

FIGURE 6-5: APPARENT CATALYST DEACTIVATION, SHOWN BY THE CARBON SELECTIVITY TO DME (GREEN), CO (RED), CO_2 (BLACK) AND METHANOL (BLUE) WITH RESPECT TO THE RELATIVE TIME (HOURS).

6.3.2. Carbon selectivity and productivity

Rather than just a given value, the carbon selectivity can be chosen and optimized by determining the relative time of the reactive adsorption step due to the dynamic nature of sorption enhanced processes. Figure 6-6 shows the change in carbon selectivity for the carbon containing species with respect to the adsorption time. Besides optimization by operating conditions as for conventional processes, the dynamic nature of SEDMES allows extra degrees of freedom and therefore, additional flexibility. Experimental carbon selectivity is reported (in other figures) as the integrated selectivity until 5% CO_2 is observed, loosely based on the desired high single-pass conversion of SEDMES and the reduced downstream purification requirements.

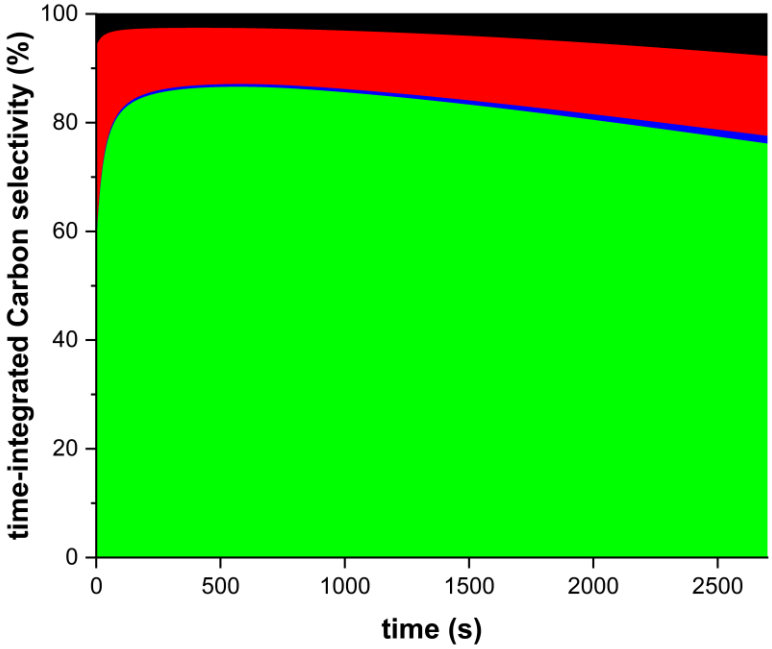

FIGURE 6-6: INTEGRATED CUMULATIVE CARBON SELECTIVITY TO DME (GREEN), CO (RED), CO_2 (BLACK) AND METHANOL (BLUE) WITH RESPECT TO THE RELATIVE TIME (MODEL PREDICTION FOR A CO_2:CO=2:1 FEED AT 25 BAR(A) AND 250 °C).

The gas hourly space velocity (GHSV) of the feed imposes a trade-off between productivity and selectivity, which is shown in Figure 6-7. Regarding this trade-off, the optimal GHSV would be as low as possible from a selectivity point-of-view. Although mass and heat transport eventually would affect the selectivity as well [4]. With increasing GHSV the productivity increases with a loss in selectivity, until the selectivity loss becomes dominant and the productivity will drop as well. In contrast to conventional “steady-state” reaction conditions, the SEDMES process has extra degrees of freedom to optimize the GHSV in combination with the cycle design and timing of the sorption enhanced reaction steps. The selectivity and productivity need to be balanced in the process design and techno-economic evaluation for a specific case.

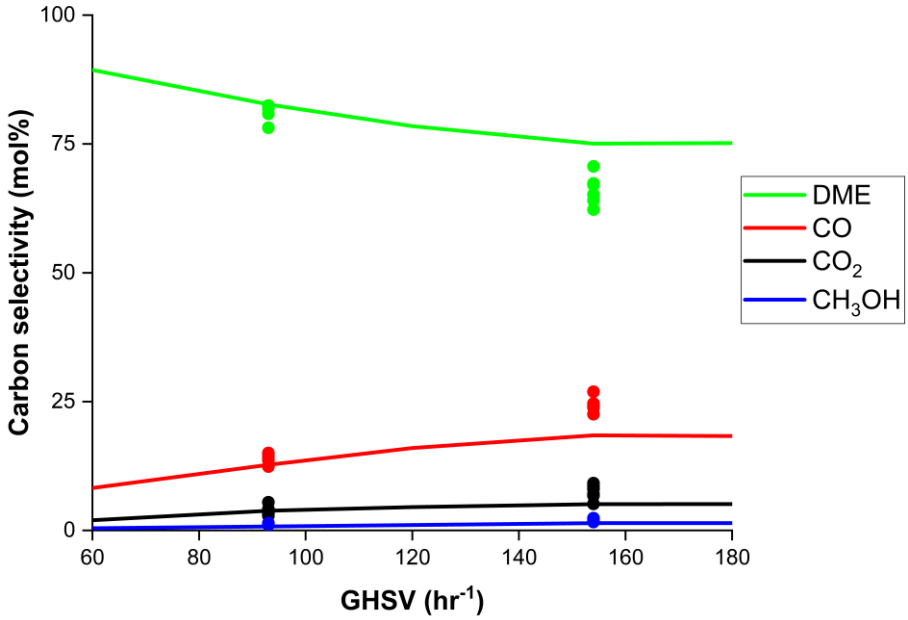

FIGURE 6-7: EXPERIMENTAL CARBON SELECTIVITY (DOTS) TO DME (GREEN), CO (RED), CO_2 (BLACK) AND METHANOL (BLUE) AND MODEL PREDICTION (LINES) AS FUNCTION OF FEED GAS HOURLY SPACE VELOCITY (HR^{-1}).

The duration of the regenerative purge step is one of these additional parameters. A longer purge time results in better regeneration of the system and therefor a higher DME selectivity (Figure 6-8), as seen experimentally and well predicted by the model. A longer purge time relative to the adsorption time, however, would require a cycle design with more columns, resulting in a lower overall specific productivity (kg hr^{-1} m^{-3}). To decrease the inventory (m^3) and therefore increase the overall productivity a short purge time would be desired. Figure 6-8 shows a small discrepancy between the experimental results for a 30 minute purge time. This can be explained by the notion that the experimental data points show a decreasing trend (rather than a spread as is the case for the other data) towards the modelled selectivity. The model with the GSTA isotherm, as determined in Chapter 4, gives improved predictions for a short purge time compared to previous reported predictions [14].

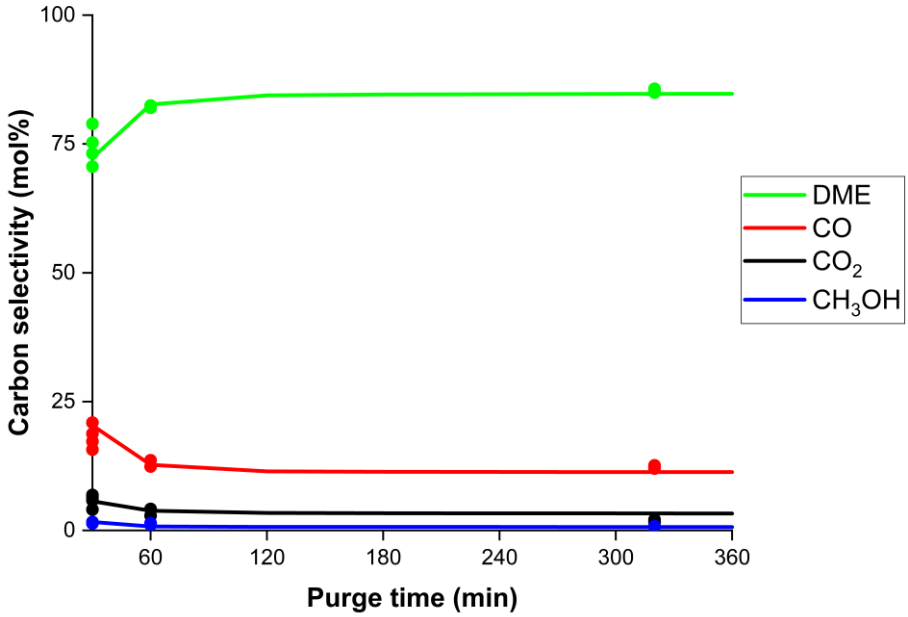

FIGURE 6-8: EXPERIMENTAL CARBON SELECTIVITY (DOTS) TO DME (GREEN), CO (RED), CO_2 (BLACK) AND METHANOL (BLUE) AND MODEL PREDICTION (LINES) AS FUNCTION OF PURGE DURATION (MIN).

Figure 6-9 shows the experimental results and model predictions accordingly for various combinations of the adsorption and regeneration time. It must be noted that the experimental results are based on 2-4 point integration for short timings. Nonetheless, the model predicts the experimental results well for lowering the adsorption and purge time to 20/30 and 10/20 minutes respectively. While the model previously predicted a significant drop in selectivity for 10/10 minutes due to a decreasing working capacity of the adsorbent [14], the experimental results show a significantly smaller drop which is described correctly with the GSTA isotherm.

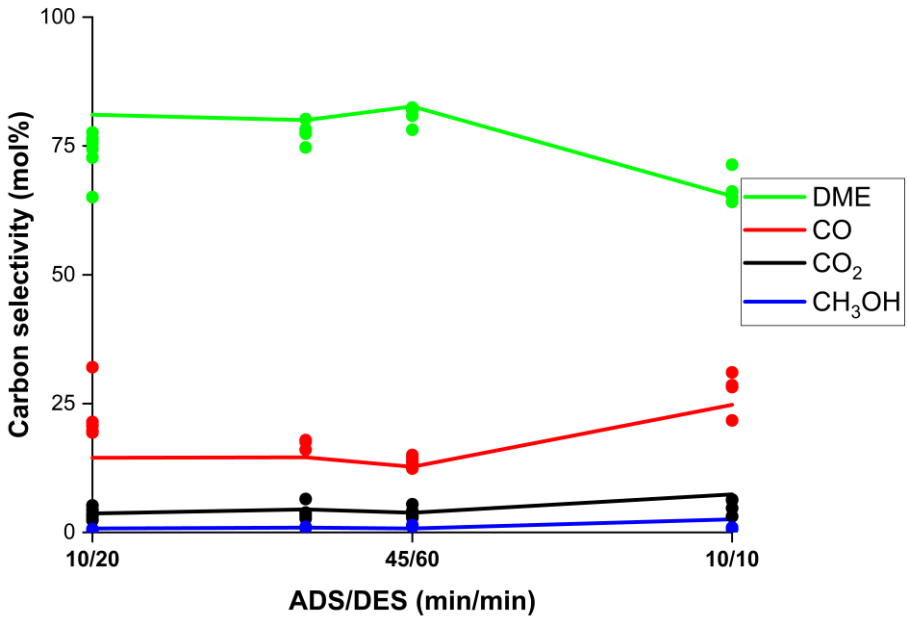

FIGURE 6-9: EXPERIMENTAL CARBON SELECTIVITY (DOTS) TO DME (GREEN), CO (RED), CO_2 (BLACK) AND METHANOL (BLUE) AND MODEL PREDICTION (LINES) AS FUNCTION OF ADS/DES RATIO (MIN/MIN).

The combination of the adsorption duration (ADS) and regeneration time (DES) allows optimizing the trade-off for DME selectivity and productivity, as shown in Figure 6-10. Shorter adsorption times potentially result in an increased production rate. The larger reactor column requirement when the purge time does not decrease with the adsorption time, however, results in a drop in cyclic productivity (kg hr^{-1} m^{-3}). Looking at the minimum number of columns required for any given adsorption and purge time, the productivity could be significantly boosted for shorter cycle times with the highest ADS/DES ratio (red bars in Figure 6-10). The promising experimental results indicate that a minor loss in selectivity could still result in increased productivity for faster cycling. The productivities reported in Figure 6-10 correspond to 0.04-0.06 kg hr^{-1} kg_{cat}^{-1}. This is a major improvement to the previously reported TPSA cycle and close to direct DME pilot plant productivity for CO to DME, which would strongly deteriorate for a CO_2-rich feed [4].

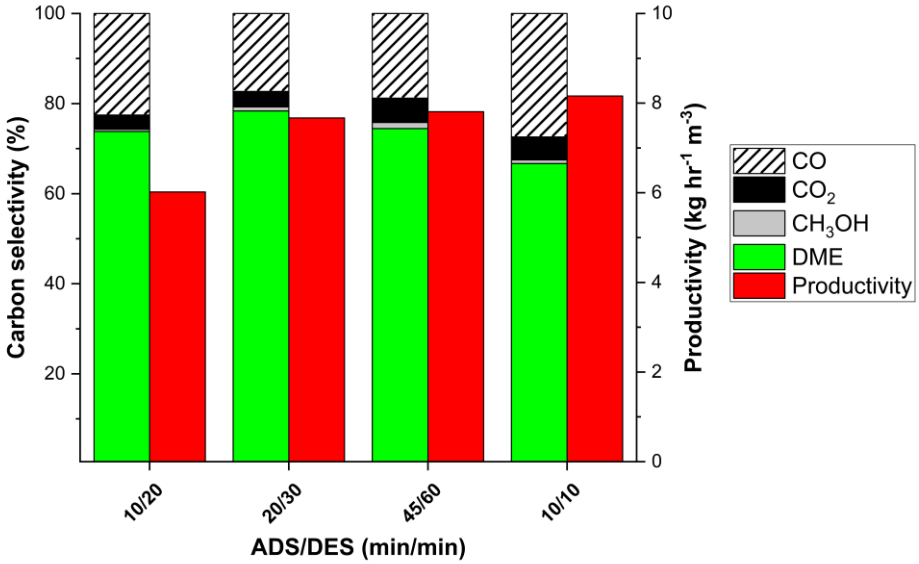

FIGURE 6-10: EXPERIMENTAL CARBON SELECTIVITY AND THE PRODUCTIVITY FOR THE MINIMUM NUMBER OF COLUMNS (ADSORPTION + PURGE TIME; RED BARS) AS FUNCTION OF ADS/DES RATIO; INTEGRATION UNTIL 5% CO_2 BREAKTHROUGH. CONDITIONS: 250 °C AND 25 BAR(A) FOR A CO_2:CO=2:1 FEED WITH STOICHIOMETRIC HYDROGEN AND CH_4 TRACER.

This increase in productivity shows the impact of the demonstrated PSA regeneration on the SEDMES process performance and thus on the carbon utilization potential. Benefiting from this work, the cycle design by means of modelling and experimental validation should further unlock the potential of the SEDMES technology as efficient carbon utilization technology. Followed by techno-economic and life cycles analyses, also the economic and carbon mitigating benefits of SEDMES over conventional DME synthesis technology should be addressed.

6.4. Conclusions

For the first time, a validated pressure swing regeneration cycle for sorption enhanced DME synthesis (SEDMES) is demonstrated under industrially relevant conditions. SEDMES is again demonstrated to be a highly flexible process for converting CO_2-rich (bio-based) syngas and CO_2 directly to DME with a high single-pass conversion, reducing or even eliminating the conventional large recycles and downstream purification sections. The industrially relevant testing performed in this chapter indeed proves this significant performance, 80% single-pass carbon selectivity to DME demonstrated with pressure swing regeneration, which

already allows for a factor four increase in productivity with further optimization still possible.

The study of the adsorbent material, the catalysts, and the combination of all materials involved, described in previous chapters, resulted in an improved validated dynamic reactor model, which allows adequate upscaling of the SEDMES technology and predictions of large scale DME synthesis for which faster cycling seems promising to further enhance productivity. Techno-economic and life cycle analyses have to be performed to investigate the economic and carbon mitigating benefits of the high efficiency carbon and hydrogen utilization by the SEDMES technology.

Nomenclature

a_p	Particle interfacial area (m^2 m^{-3})
b	Isotherm equilibrium constant (bar^{-1})
c_i	Concentration of component i (mol m^{-3})
Cp	Gas thermal conductivity (J kg^{-1} K^{-1})
Cp_p	Particle thermal conductivity (J kg^{-1} K^{-1})
d_p	Particle diameter (m)
D_z	Axial dispersion coefficient (m^2 s^{-1})
E_a	Activation energy (kJ mol^{-1})
G	Ergun constant (-)
ΔH_{ads}	Adsorption enthalpy (J mol^{-1})
$\Delta H_{r,i}$	Reaction enthalpy (J mol^{-1})
k	Reaction rate constant (mol s^{-1} kg^{-1} bar^{-1}) or (kmol kg^{-1} hr^{-1})
K_i	Adsorption equilibrium constant of component i (bar^{-1}) or (m^3 $kmol^{-3}$)
K_p	Equilibrium constant (based on partial pressure) (-)
M_i	Molecular weight of component i (kg mol^{-1})
N_i	Mole flux of component i (mol m^{-2} s^{-1})
P	Reactor pressure (bara)
P_i	Partial pressure of component i (bara)
q_i	Adsorbent loading (mol kg^{-1})
q_s	Saturation capacity (kg kg^{-1})
r_i	Reaction rate of component i (mol m^{-3} s^{-1}) or (mol kg^{-1} s^{-1}) or (kmol kg^{-1} hr^{-1})
R	Ideal gas constant (J mol^{-1} K^{-1})
t	Time (s)
T	Temperature (K)
u	Superficial gas velocity (m s^{-1})
U	Overall heat transfer coefficient (W m^{-2} K^{-1})

v	Interstitial gas velocity (m s^{-1})
z	axial coordinate (m)

Greek letters

ε_b	Bed voidage (-)
λ	Axial thermal conductivity (W m^{-1} K^{-1})
ρ	Density (kg m^{-3})
ρ_p	Particle density (kg m^{-3})
ϕ_i	Partial fugacity of component i (bara)
ω_i	Weight fraction of component i (-)

Bibliography

[1] J. van Kampen, J. Boon, F. van Berkel, J. Vente, M. van Sint Annaland, Steam separation enhanced reactions: Review and outlook, Chemical Engineering Journal 374 (2019) 1286–1303.

[2] I. Iliuta, M.C. Iliuta, F. Larachi, Sorption-enhanced dimethyl ether synthesis — Multiscale reactor modeling, Chemical Engineering Science 66 (2011) 2241-2251.

[3] J. Boon, J. van Kampen, R. Hoogendoorn, S. Tanase, F.P.F. van Berkel, M. van Sint Annaland, Reversible deactivation of γ-alumina by steam in the gas-phase dehydration of methanol to dimethyl ether, Catalysis Communications 119 (2019) 22-27.

[4] J. van Kampen, J. Boon, J. Vente, M. van Sint Annaland, Sorption enhanced dimethyl ether synthesis for high efficiency carbon conversion: Modelling and cycle design, Journal of CO_2 Utilization 37 (2020) 295-308.

[5] D. Liuzzi, C. Peinado, M.A. Peña, J. van Kampen, J. Boon, S. Rojas, Increasing dimethyl ether production from biomass-derived syngas via sorption enhanced dimethyl ether synthesis, Sustainable Energy & Fuels 4 (2020) 5674-5681.

[6] S. Guffanti, C.G. Visconti, J. van Kampen, J. Boon, G. Groppi, Reactor modelling and design for sorption enhanced dimethyl ether synthesis, Chemical Engineering Journal 404 (2021) 126573-126585.

[7] H. Graaf, E.J. Stamhuis, A.A.C.M. Beenackers, Kinetics of low-pressure methanol synthesis, Chemical Engineering Science 43 (1988) 3185-3195.

[8] G. Berčič, J. Levec, Intrinsic and Global Reaction Rate of Methanol Dehydration Over γ-Al_2O_3 Pellets, Industrial & Engineering Chemistry Research 31 (1992) 1035-1040.

[9] K.L. Ng, D. Chadwick, B.A. Toseland, Kinetics and modelling of dimethyl ether synthesis from synthesis gas, Chemical Engineering Science 54 (1999) 3587-3592.

[10] J. van Kampen, J. Boon, M. van Sint Annaland, Steam adsorption on molecular sieve 3A for sorption enhanced reaction processes, Adsorption (2020).

[11] J. van Kampen, S. Booneveld, J. Boon, J. Vente, M. van Sint Annaland, Experimental validation of pressure swing regeneration for faster cycling in sorption enhanced dimethyl ether synthesis, Chemical Communications 56 (2020) 13540-13542.
[12] M. Stiefel, R. Ahmad, U. Arnold, M. Döring, Direct synthesis of dimethyl ether from carbon-monoxide-rich synthesis gas : In fl uence of dehydration catalysts and operating conditions, Fuel Processing Technology 92 (2011) 1466-1474.
[13] F. Dadgar, R. Myrstad, P. Pfeifer, A. Holmen, H.J. Venvik, Catalyst Deactivation During One-Step Dimethyl Ether Synthesis from Synthesis Gas, Catalysis Letters 147 (2017) 865-879.
[14] J. van Kampen, J. Boon, J. Vente, M. van Sint Annaland, Sorption enhanced dimethyl ether synthesis under industrially relevant conditions: Experimental validation of pressure swing regeneration, Reaction Chemistry & Engineering Advanced Article (2020).

Chapter 7. Continuous multi-column sorption enhanced dimethyl ether synthesis: Dynamic operation and cycle design

Abstract

In this chapter, SEDMES technology is validated experimentally on a multi-column test-rig under industrially relevant conditions. Here the continuous production of DME by sorption enhancement is demonstrated for the first time in open literature. The essential pressure swing regeneration, as discussed in the previous chapter, is confirmed as the mode of regeneration.

In contrast to conventional processes, SEDMES is a transient and dynamic process, resulting in many degrees of freedom. SEDMES cycle design gives direction for further process systems engineering and techno-economic analysis. A preliminary cycle design, including 1 pressure equalization step, requires 6 columns to provide continuous feed and products streams. However, further development of the cycle design aims to reduce the number of columns and include separation units and recycles. Close integration of SEDMES cycle design, the overall process and its techno-economics are required, because combined they can be optimized and address the economic and carbon mitigating benefits of SEDMES over conventional DME synthesis technology.

The SEDMES reactor model does not only describe the transient behavior in the cyclic steady-state well, but also the dynamic approach to the cyclic steady-state is modelled well. The multi-column experiments have demonstrated that SEDMES can be operated at even lower temperatures (220 °C) than previously reported. Operation at lower temperatures would allow for a higher maximum temperature rise. Therefore, it would make higher conversions possible and it would allow even larger tube diameters for a multi-tubular reactor. Whereas the anticipated multi-tubular reactor concept is a complex and costly part of the SEDMES process, possible use of larger reactors could benefit the economic valorization.

Publications in preparation.

7.1. Introduction

Sorption enhanced DME synthesis is a multi-column process due to the inherent adsorbent regeneration [1, 2]. Traditional single column reactor setups therefore do not allow demonstration and testing of continuous DME production. In this chapter, SEDMES technology is validated experimentally on a multi-column test-rig under industrially relevant conditions. For the larger scale, continuous production of DME, and confirmation of the improved pressure swing regeneration, as shown in the previous chapter [3, 4], is sought.

Sorption enhancement results in transient and dynamic processes [5-8]. In contrast to conventional processes, which operate at steady-state, there is a cyclic steady-state (CSS). As shown in the previous chapters, the transient behavior at cyclic steady-state is investigated in detail and the SEDMES reactor model describes this behavior well. Process flexibility, where the feedstock and operating conditions could change, such as for Power-to-X (PtX) systems, could require dynamic operation [9-11]. Therefore, the dynamic operation is of particular interest for the multi-column experiments.

Cycle design is an important aspect for sorption enhanced processes, which entails many degrees of freedom [8]. Although the SEDMES cycle design should be closely integrated with the overall process design, the impact of a preliminary cycle design is investigated in more detail. Eventually, the combined cycle and flowsheet optimization by techno-economic analysis can address the economic and carbon mitigating benefits of SEDMES over conventional DME synthesis technology.

In this chapter the results of an experimental investigation into the multi-column sorption enhanced production of DME are discussed, including the SEDMES reactor model for data interpretation. Attention is paid to the confirmation of PSA regeneration during the continuous production of DME. Additionally, the dynamic operation is studied in more detail, including lower temperatures than previously reported for SEDMES. After experimental validation, the cycle design is studied by modelling to give direction for further process systems engineering and techno-economic analysis.

In the next section, the used materials, the experimental procedures and model interpretation are reported. In the results and discussion section, firstly, the experimental validation is discussed with model interpretation. This is followed by a modelling study of the SEDMES cycle design. Finally, the main conclusions are summarized.

7.2. Experimental

7.2.1. Materials

Experimental validation of sorption enhanced DME synthesis under industrially relevant conditions was performed using a homogeneous physical mixture of commercially available catalyst and adsorbent: CZA catalyst, γ-Al_2O_3 (assay>98%, Riogen NJ, USA), obtained as 3 mm pellets, and molecular sieve type 3A, purchased as 1.6 mm pellets (UOP Molecular Sieves, Obermeier, DE).

7.2.2. Methods

A combination of commercially obtained CZA catalyst, γ-Al_2O_3 catalyst and zeolite 3A adsorbent was used for the experimental demonstration of the direct DME synthesis from CO_2 with stoichiometric H_2. The experimental runs were conducted on a multi-column high-pressure reactor setup (Figure 7-1), allowing continuous production with 36 liters (divided over 6 columns) of sample, consisting of a 1:4 ratio (weight basis) catalyst to sorbent. The ratio between catalyst and sorbent was not further optimized in this work. Adsorption was performed at 25 bar(a) in a temperature range of 220-250 °C with argon as tracer. The inert balance was used to keep the overall pressure stable, considering the nett mole consumption by the reaction and the adsorption of water. Regeneration was done by depressurization to 1-3 bar(a) and switching to dry, inert gas (nitrogen) for the purge step. Finally, either the inert purge gas or the reactive feed gas was used for repressurization. During depressurization and repressurization two columns can be physically connected, resulting in partial repressurization of one column by the depressurization gas from another column, called pressure equalization. Transient gas analysis was performed by micro-GC (measuring methane, CO, CO_2, nitrogen, argon, methanol and DME) and mass spectrometry measuring hydrogen (m/z=2), methane (m/z=15), water (m/z=18), carbon monoxide/nitrogen (m/z=28), methanol (m/z=31), carbon dioxide (m/z=44) and DME (m/z=45) for the outlet gas stream from reactor column 6.

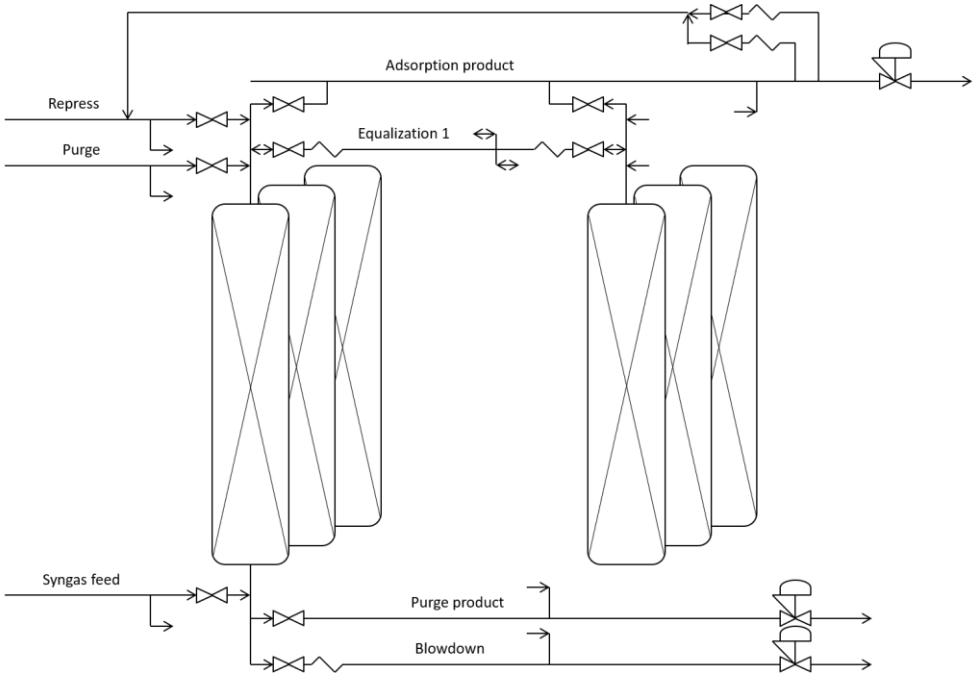

FIGURE 7-1: SCHEMATIC OF 2 INTERCONNECT REACTOR COLUMNS, INCLUDING THE VARIOUS FEED AND PRODUCT STREAMS. THE CONNECTIONS SHOWN FOR 1 REACTOR COLUMN ARE IDENTICAL FOR ALL 6 COLUMNS IN THE MULTI-COLUMN TEST-RIG.

7.2.3. Data interpretation

In order to facilitate data interpretation, several key metrics have been defined to be able to quantify the SEDMES performance. The most important metric, the carbon selectivity *S(i)*, used here is defined as follows,

$$S(i) = \frac{ny(C_nH_mO_p)}{\sum_i n_i y(i)} \quad (1)$$

The carbon selectivities were calculated as molar concentration-based selectivities for each of the carbon containing species, *y(i)*. For example, the selectivity towards DME can be calculated as

$$S(DME) = \frac{2y(DME)}{y(CO)+y(CO_2)+2y(DME)+y(MeOH)+y(CH_4)} \quad (2)$$

Time integration (over the duration of a step) of the streams gives an overall yield and selectivity for the cyclic (steady state) performance of the SEDMES process.

The second key performance indicator is the productivity (kg hr^{-1} m^{-3}) or production rate (kg hr^{-1}). Since the same reactor dimensions are used in all experiments, the production rate is used to assess the productivity of the system, which is defined as the mass of DME *m* collected during the adsorption step over the duration of this step τ per reactor tube:

$$Prod = \frac{m(DME)}{\tau(ADS)} \quad (3)$$

7.2.4. Model

A one-dimensional pseudo-homogeneous dynamic reactor model was developed in Matlab, verified and validated [2]. For the description of the fluid flow and mass transfer, the 1D non-steady differential mass and momentum balances are solved. The total mass, momentum, component mass and overall energy balances are given in Table 7-1. As described in Chapter 5, the reaction kinetics have been determined for the used catalyst materials by fitting the parameters in the kinetic models by Graaf et al. (1988) and Berčič et al. (1992) for the methanol synthesis and methanol dehydration respectively [12-15]. The steam adsorption isotherm of the LTA zeolite adsorbent is determined under the high pressure and temperature working conditions of the SEDMES process in Chapter 4 [16]. Numerically, a single reactor column is simulated in time following the consecutive steps in the cycle. Connecting (pressure equalization) steps in the multi-column system are temporarily stored. Full details of the different aspects of the model can be found in Chapter 3 [2].

TABLE 7-1: REACTOR MODEL EQUATIONS.

Overall mass balance	$\frac{\partial \rho}{\partial t} = -\frac{\partial \rho v}{\partial z} - \frac{1-\varepsilon_b}{\varepsilon_b} a_p \sum M_i N_i$	(4)
Momentum balance	$\frac{\partial \rho v}{\partial t} = -\frac{\partial \rho v^2}{\partial z} - \frac{\partial P}{\partial z} - G\frac{\rho \lvert u \rvert u}{d_p}$	(5)
Species mass balance	$\frac{\partial \rho \omega_i}{\partial t} = -\frac{\partial \rho v \omega_i}{\partial z} + \frac{\partial}{\partial z}\left(D_z \rho \frac{\partial \omega_i}{\partial z}\right) - \frac{1-\varepsilon_b}{\varepsilon_b} a_p M_i N_i$	(6)
Overall energy balance	$(\varepsilon_b \rho Cp + (1-\varepsilon_b)\rho_p Cp_p)\frac{\partial T}{\partial t} = -\rho Cpu\frac{\partial T}{\partial z} + \frac{\partial}{\partial z}\left(\lambda \frac{\partial T}{\partial z}\right) + \frac{4U(T_w - T)}{d_r} + (1-\varepsilon_b)\rho_p\left(\sum -\Delta H_{r,i} r_i + \sum -\Delta H_{ads,i}\frac{\partial \overline{q_i}}{\partial t}\right)$	(7)
Equation of state	$PM = \rho RT$	(8)

7.3. Results and discussion

To scale-up and investigate the sorption enhanced DME synthesis process even further, firstly the SEDMES technology is validated under industrially relevant conditions on a multi-column test rig, allowing for continuous DME production. The previously developed model (Chapter 3) is used for data interpretation. Finally, the cycle design is discussed and improvements are suggested as the way forward to enhance the productivity and carbon selectivity.

7.3.1. Continuous production

The demonstration of the SEDMES technology on a multi-column test rig allows for continuous production of DME by sorption enhancement, for the first time in the open literature. Figure 7-2 shows the continuous concentration profiles (balance unconverted H_2), collected as product during the reactive adsorption step. Whereas only the outlet concentrations of reactor column 6 are continuously monitored, these concentrations are extrapolated to the other reactor columns which show very similar behavior. In these experiments the nitrogen purge gas is used for repressurization, therefore initially nitrogen is flushed out. After this flush, a representative breakthrough profile of sorption enhanced DME synthesis is apparent from Figure 7-2. Prior to steam breakthrough, DME and unconverted CO are the primary products. After steam breakthrough the concentration of DME drops, accompanied by the breakthrough of CO_2 and methanol indicating saturation of the adsorbent. Although the conversion is still far higher than conventional conversion levels (maximum of 1.9% DME), dictated by thermodynamics, the DME concentration drops relatively rapidly. Clearly, the purge times used here, shorter than the adsorption times, do not regenerate the system completely and therefore result in a relatively fast steam breakthrough.

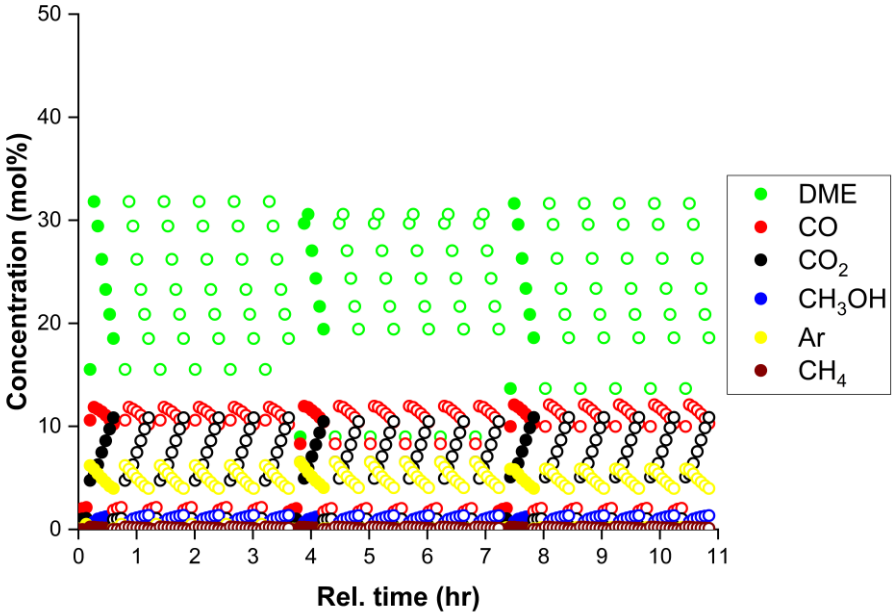

FIGURE 7-2: EXPERIMENTAL DATA AT 250 °C AND 25 BAR(A) FOR A CO_2 FEED WITH STOICHIOMETRIC HYDROGEN, WITH ARGON TRACER (24.5% CO_2, 73.6% H_2, 1.9% AR, GHSV 93 HR^{-1}), MEASURED FOR REACTOR COLUMN 6 (FILLED DOTS). FOR REACTOR COLUMNS 1-5 THE DATA FROM COLUMN 6 IS EXTRAPOLATED (COPIED, OPEN DOTS).

7.3.2. Lower temperature operation

Sorption enhanced DME synthesis was initially operated at 275°C [1, 17], which was lowered to 250 °C with improving performance, provided that both the catalyst activity and regeneration are sufficient [3, 4]. As discussed in Chapter 3, also the initial modelling study indicated temperatures around 250 °C to be optimal for SEDMES [2]. The direct synthesis of DME is thermodynamically favored at lower temperatures. However, the catalyst activity requires temperatures around 250 °C. In sorption enhanced synthesis, the temperature also affects the adsorption capacity. As indicated by the study of the adsorbent material (Chapter 4), the adsorption capacity benefits from operation at lower temperatures [16]. Although with a pressure swing regeneration, the operating temperature must be balanced for both good adsorption and desorption properties, maximizing the cyclic working capacity.

As shown in Figure 7-3, the multi-column testing demonstrates SEDMES at temperatures as low as 220 °C with very similar performance to the original higher temperature operation. This result seems very promising with respect to the heat management of the system. Both methanol synthesis and direct DME synthesis are exothermic reactions, limiting the conversion and deactivating the methanol catalyst by hydrothermal sintering, and therefore require a cooled reactor, such as a multi-tubular reactor concept [18, 19]. In sorption enhanced DME synthesis, the exothermic adsorption is added to the already exothermic system. As discussed in Chapter 3, SEDMES temperature control appears not to be an issue in a multi-tubular cooled reactor. Larger tube diameters can be adopted compared to conventional direct DME synthesis. However, operation at lower temperatures would allow a higher maximum temperature rise, and therefore makes higher conversions possible and it allows even larger tube diameters for a multi-tubular reactor as described in Chapter 3. Where the complex multi-tubular reactor concept is also a costly part of the SEDMES process, larger reactors would benefit the economic valorization of CO_2 conversion [11].

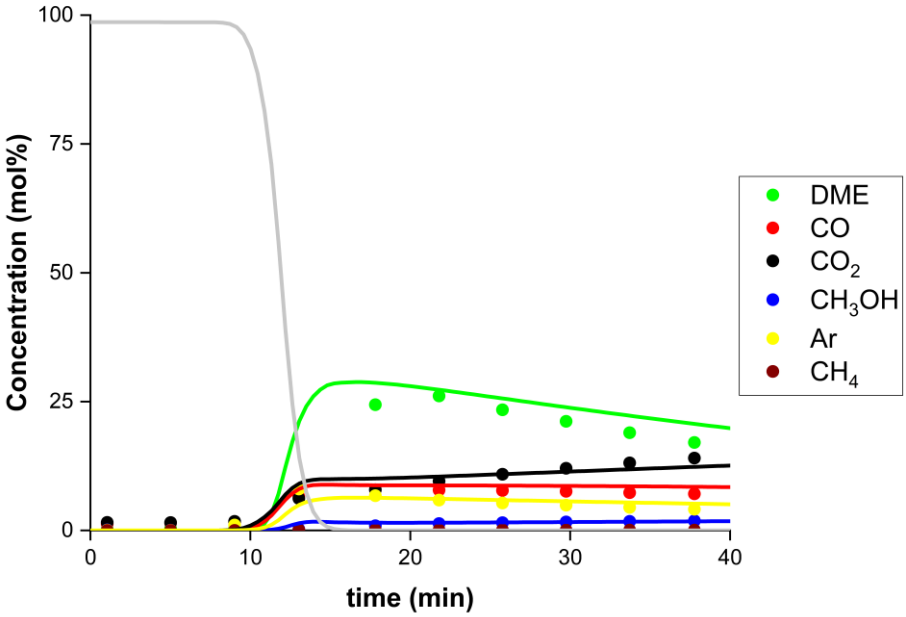

FIGURE 7-3: EXPERIMENTAL DATA AT 220 °C AND 25 BAR(A) FOR A CO_2 FEED WITH STOICHIOMETRIC HYDROGEN, WITH ARGON TRACER (24.5% CO_2, 73.6% H_2, 1.9% AR, GHSV 93 HR^{-1}), (DOTS; DME (GREEN), CO (RED), CO_2 (BLACK), METHANOL (BLUE), ARGON (YELLOW), METHANE (BROWN), NITROGEN (GREY)) AND MODEL PREDICTION (LINES).

7.3.3. Cyclic steady-state

Figure 7-3 also shows that the SEDMES reactor model adequately describes the transient concentration profiles at cyclic steady-state. However, not only the behavior at cyclic steady-state is described by the model. The SEDMES reactor model is a dynamic cycle model, simulating each step of a cycle towards cyclic steady-state. The model predicts the dynamic behavior of the system, both the various steps in a cycle and consequently the subsequent cycles, very well, as demonstrated in Figure 7-4 by the approach to CSS observed experimentally and predicted by the model. Initially, in the first cycle shown in Figure 7-4, the adsorbent material is relatively dry. For the chosen operating conditions and cycle design, more water is adsorbed during the reactive adsorption step than desorbed during the regeneration. This results in an accumulation of water loaded on the adsorbent material, hence a lower working capacity and a decreasing carbon selectivity to DME until a cyclic steady-state is achieved, where an equal amount of water is adsorbed and desorbed during a cycle.

The approach to a new cyclic steady-state goes relatively quick, especially if the CSS values are close to the old values. In Figure 7-5 it can be seen that the experimental carbon

selectivity at 250 °C reaches the predicted cyclic steady-state within approximately 5 cycles. Whereas, the working capacity is slightly higher (8.8%) at this elevated temperature, a small increase in the carbon selectivity to DME and a small decrease in the carbon selectivity to CO_2 can be observed during the first cycles.

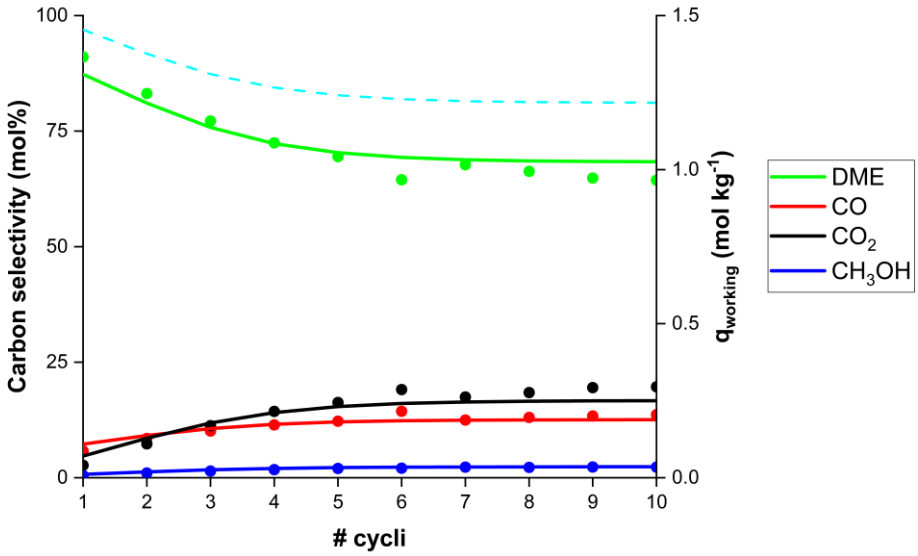

FIGURE 7-4: EXPERIMENTAL CARBON SELECTIVITY (DOTS) TO DME (GREEN), CO (RED), CO_2 (BLACK) AND METHANOL (BLUE) AND MODEL PREDICTION (LINES) AS FUNCTION OF THE NUMBER OF SUBSEQUENT CYCLES. THE MODEL WORKING CAPACITY (DASHED BLUE LINE) IS SHOWN ON THE RIGHT AXIS. CONDITIONS: 220 °C AND 25 BAR(A) FOR A CO_2 FEED WITH STOICHIOMETRIC HYDROGEN, WITH ARGON TRACER (24.5% CO_2, 73.6% H_2, 1.9% AR, GHSV 93 HR^{-1}).

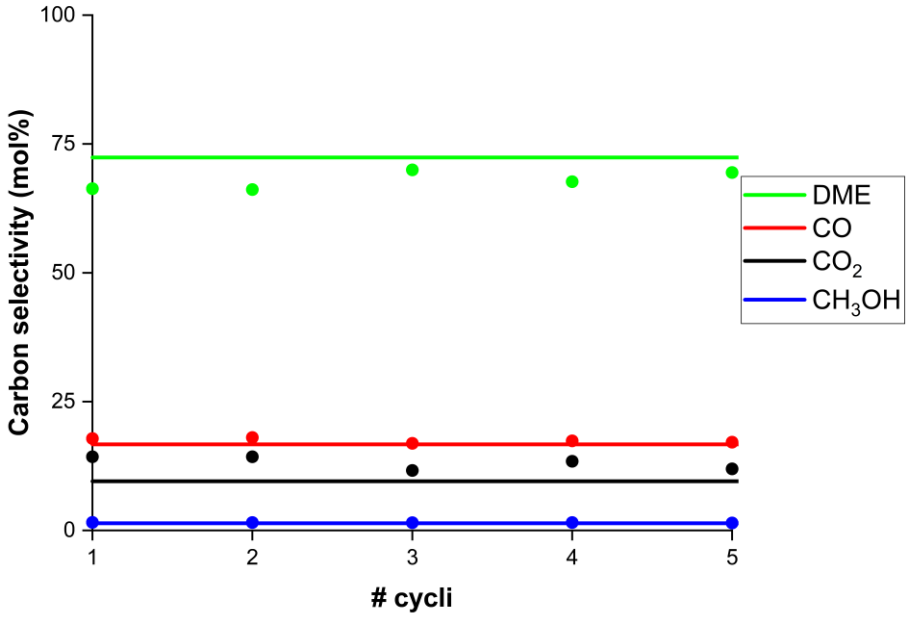

FIGURE 7-5: EXPERIMENTAL CARBON SELECTIVITY (DOTS) TO DME (GREEN), CO (RED), CO_2 (BLACK) AND METHANOL (BLUE) AS FUNCTION OF THE NUMBER OF SUBSEQUENT CYCLES. MODEL PREDICTION FOR CYCLIC STEADY-STATE (LINES). CONDITIONS: 250 °C AND 25 BAR(A) FOR A CO_2 FEED WITH STOICHIOMETRIC HYDROGEN, WITH ARGON TRACER (24.5% CO_2, 73.6% H_2, 1.9% AR, GHSV 93 HR^{-1}).

7.3.4. Cycle design

Cycle design is an important factor for sorption enhanced processes, which entails many degrees of freedom. During the experimental validation the cycle design was limited due to technical restrictions of the setup, e.g. resulting in a nitrogen, purge gas repressurization and an adsorption duration shorter than the purge duration. As elaborately discussed in Chapter 3, these are far from ideal considering the SEDMES cycle design. To maintain a high working capacity, the regenerative purge step is typically longer than the adsorption step [2, 4]. An inert purge gas, such as N_2, regenerates the system well, but needs to be collected separately to avoid mixing with the product gas. Alternatively, reactants (separately or mixed) could be used as purge gas. Although a slight loss in working capacity could be expected, it would prevent product dilution or an additional process step. For the repressurization step, both the feed (syngas) and product (DME) could be considered. Despite the high DME purity in the adsorption product for a product repressurization, the loss in effective productivity can be costly. Therefore, a feed repressurization would be the first option to consider.

Furthermore, the overall process will result in boundary conditions for the cycle design. For the following study the preliminary conditions are set as the most favorable from operational prospective, i.e. continuous feed (adsorption and purge) and product (DME) flow. For a cycle design with 1 pressure equalization step at least 6 columns are required to fulfill these boundary conditions, considering 6 steps of equal duration (Figure 7-6).

Column 1	ADS	PEQ DN	BD	PURGE	PEQ UP	REP
Column 2	REP	ADS	PEQ DN	BD	PURGE	PEQ UP
Column 3	PEQ UP	REP	ADS	PEQ DN	BD	PURGE
Column 4	PURGE	PEQ UP	REP	ADS	PEQ DN	BD
Column 5	BD	PURGE	PEQ UP	REP	ADS	PEQ DN
Column 6	PEQ DN	BD	PURGE	PEQ UP	REP	ADS

FIGURE 7-6: 6-COLUMN CYCLE DESIGN (ADS=ADSORPTION STEP, PEQ DN=PRESSURE EQUALIZATION STEP DOWN, BD=BLOWDOWN STEP, PURGE=PURGE STEP, PEQ UP=PRESSURE EQUALIZATION UP, REP=REPRESSURIZATION STEP).

Feed flowrate

As explained clearly in Chapter 3, the selection of the adsorption feed flow rate is a trade-off between the carbon selectivity, i.e. the high single-pass DME yield, and the productivity. Figure 7-7 shows this trade-off for the 6-column cycle design. Where a lower gas hourly space velocity (GHSV) results in high carbon selectivity to DME, the productivity drops significantly for lower space velocities. In its turn, the productivity increases for increasing GHSV, as can be expected for higher flow rates, until a maximum is reached. At this point the loss in conversion with increasing flow is greater than the benefit from the increase in flow rate itself, the system will start approaching conventional direct DME synthesis. The overall process design, including separation and recycle, therefore needs to balance selectivity and productivity to select the best conditions specific to the process.

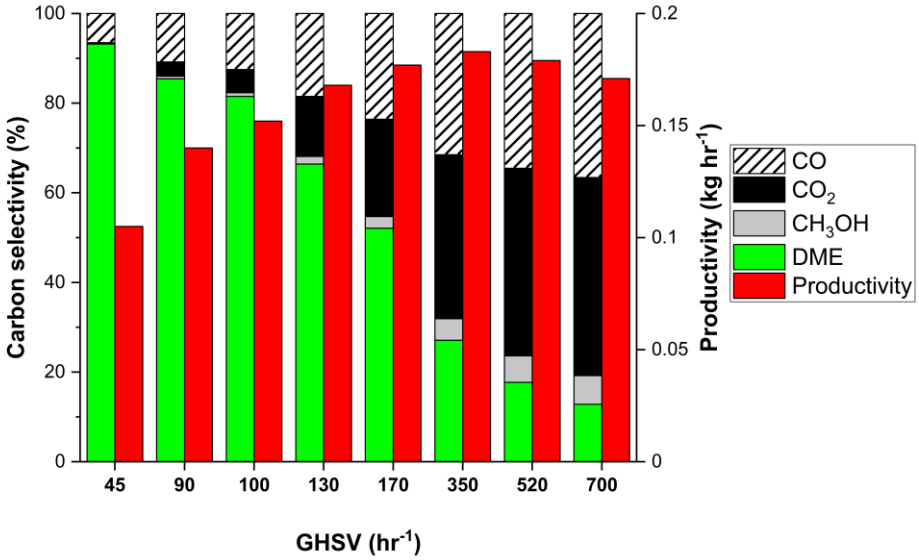

FIGURE 7-7: CARBON SELECTIVITY AND PRODUCTIVITY AS A FUNCTION OF THE GAS HOURLY SPACE VELOCITY OF THE FEED SYNGAS (HR^{-1}); TOTAL CYCLE TIME IS 90 MINUTES. CONDITIONS: 250 °C AND 25 BAR(A) WITH FEED COMPOSITION IN TABLE 7-3.

Cycle time

As also discussed in the previous chapter, the carbon selectivity can be chosen and optimized by determining the relative time of the reactive adsorption step due to the dynamic nature of sorption enhanced processes. In Figure 7-8 the total cycle time, all steps are of equal duration, is varied. A shorter cycle time improves the carbon selectivity to DME, because the adsorption step is cut off before more steam, and therefore CO_2, breakthrough. The productivity initially increases as well, going from 90 minutes to 60 minutes cycle time. However, it drops for an even shorter cycle time of 45 minutes. By stopping the adsorption step too soon in this case, the subsequent pressure equalization step is not able to maintain the remaining DME in the system by transferring it to a repressing column (Figure 7-9). As a result, the DME will end up in the blowdown product, lowering the adsorption productivity for this case.

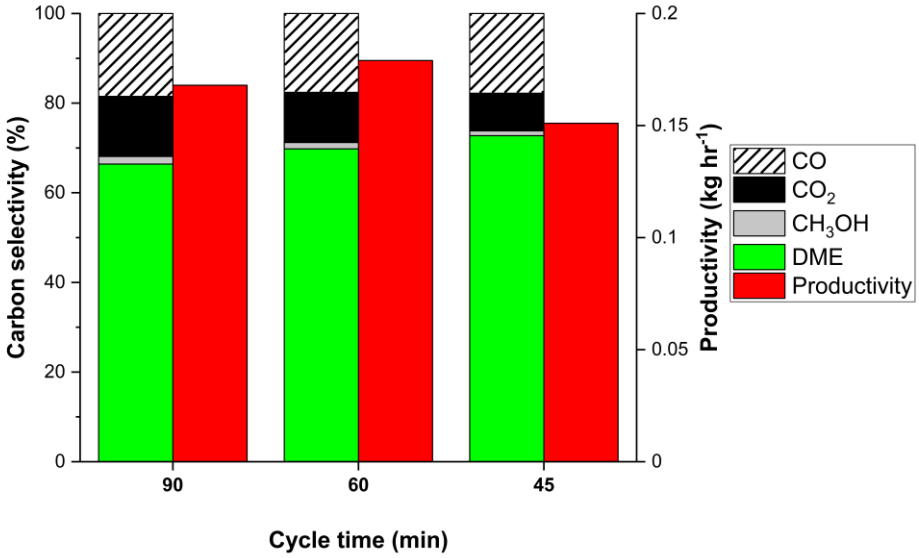

FIGURE 7-8: CARBON SELECTIVITY AND PRODUCTIVITY AS A FUNCTION OF THE TOTAL CYCLE TIME (MIN); GHSV IS 130 HR^{-1}. CONDITIONS: 250 °C AND 25 BAR(A) WITH FEED COMPOSITION IN TABLE 7-3.

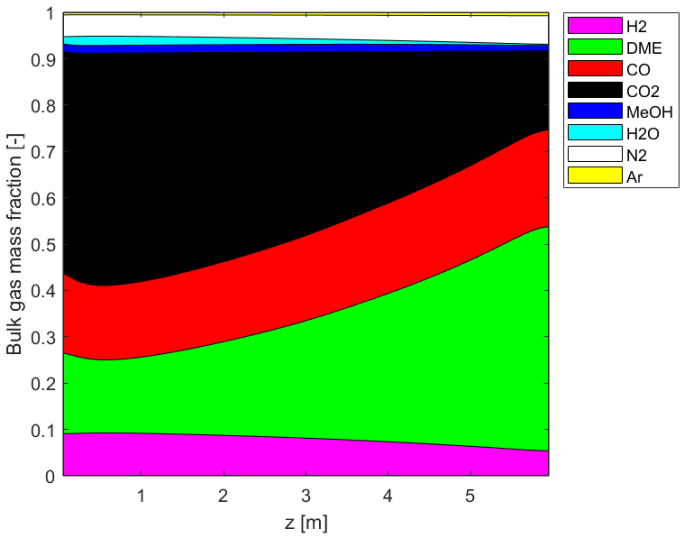

FIGURE 7-9: GAS PHASE CONCENTRATIONS VERSUS AXIAL COORDINATE AT THE END OF THE PEQ DOWN FOR THE 45 MINUTE CYCLE.

Purge gas recycle

As mentioned before, an inert purge gas, such as N_2, regenerates the system well, but needs to be collected separately to avoid mixing with the product gas. Alternatively, reactants (separately or mixed) could be used as purge gas. Although a slight loss in working capacity could be expected, it would prevent product dilution or an additional process step. Additionally, an increasing purge flow rate will increase the cyclic working capacity [2]. Whereas the purge is expected to be a (closed) recycle, a higher purge flow rate can be allowed from a system point-of-view, without a significant pressure drop increase. The higher flow rate compensates for the small loss in working capacity when using a reactant purge. Figure 7-10 shows indeed that a high carbon selectivity to DME, in combination with a higher productivity can be achieved by using an increased flow rate of a syngas purge.

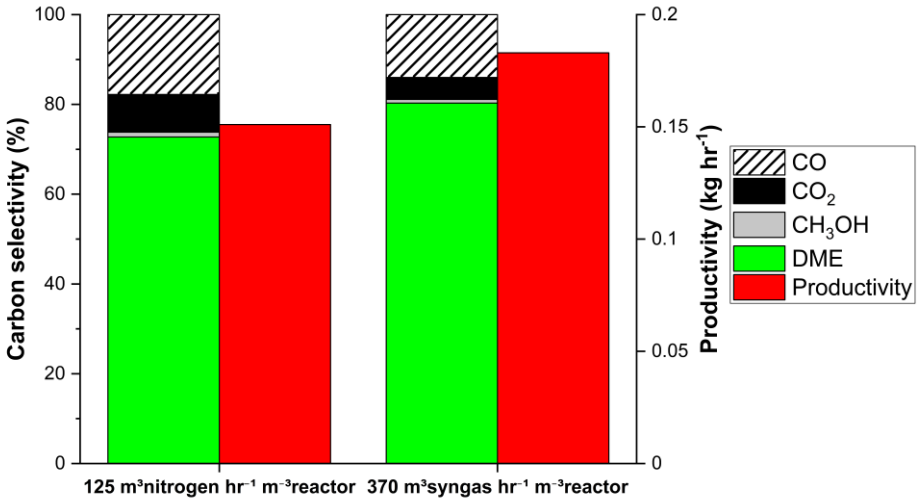

FIGURE 7-10: CARBON SELECTIVITY AND PRODUCTIVITY FOR 2 DIFFERENT PURGE GAS CASES. CONDITIONS: 250 °C AND 25 BAR(A) WITH FEED COMPOSITION IN TABLE 7-3.

Pareto plot

As has become clear in the preceding chapters and sections, SEDMES is a complex and highly nonlinear process with a large degree of freedom. This results in a high flexibility, but also in many dependent parameters to be optimized for a specific case. Carbon selectivity (to product DME and reactant CO_2) and DME productivity are considered as the key performance parameters. Given the results presented, it has become clear that the main optimization addresses the trade-off in carbon selectivity to DME and/or CO_2 versus the

DME productivity. The simulation results obtained for the 6-column cycle design, for which an overview is given in Table 7-2, indeed show a front similar to a Pareto frontier (Figure 7-11, Figure 7-12), common to sorption enhanced reaction processes. In good agreement with experimental results, a high carbon selectivity to DME can be obtained (over 95%). Similarly, the carbon selectivity to CO_2 can be reduced to less than 1%, simplifying the downstream separation. However, both extreme selectivities come at a loss in productivity. Still a very high productivity can be obtained for a carbon selectivity over 80%, where the breaking point in the front appears.

TABLE 7-2: OVERVIEW OF THE VARIOUS SIMULATIONS USED FOR THE PARETO PLOT.

	Min.	**Max.**
Cycle time variation [min]	6	360
(for different feed flow rates)		
Feed flow rate variation [kg/hr]	0.16	2.52
(for different cycle times)		
Repressurization flow rate variation [kg/hr]	10.8	86.4
Pressure variation [bara]	25	50
Matrix		
GHSV [hr^{-1}]	90	130
Cycle time variation [%]	75	125
Number of PEQ [-]	1	2

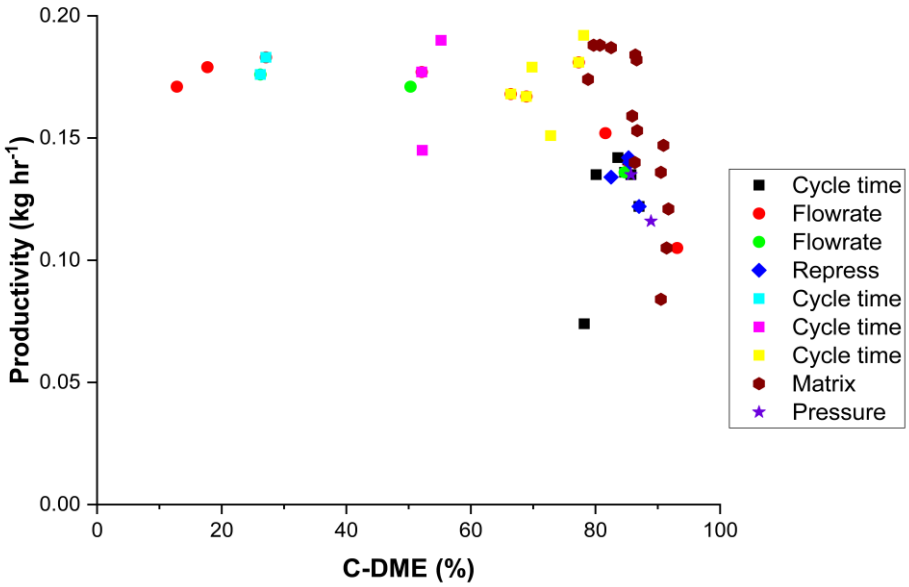

FIGURE 7-11: PARETO PLOT, SHOWING THE TRADE-OFF BETWEEN CARBON SELECTIVITY TO DME AND PRODUCTIVITY.

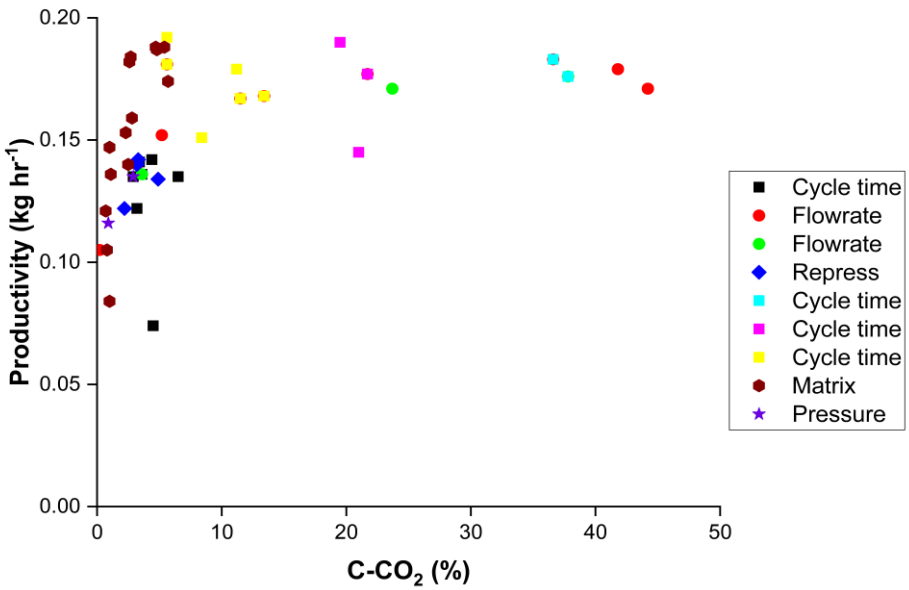

FIGURE 7-12: PARETO PLOT, SHOWING THE TRADE-OFF BETWEEN CARBON SELECTIVITY TO CO_2 AND PRODUCTIVITY.

7.3.5. Improved cycle design

Different process operating and boundary conditions, as well as the optimization goal result in different optimal cycle designs and therefore have a different trade-off in carbon selectivity and productivity. Close integration of SEDMES cycle design, overall process systems engineering and techno-economic evaluation are therefore essential.

The preliminary cycle design, including 1 pressure equalization step, requires 6 columns to provide continuous feed and products streams for facilitated technical design. However, due to the estimated CAPEX associated to a SEDMES unit [11], in the further development of the cycle design the number of columns would ideally be reduced. A 3-column cycle design (Figure 7-13) has already shown good cyclic performance [2]. However, preliminary process boundary conditions must be relieved. Especially when pressure equalization is disregarded to minimize the number of columns, the blowdown recycle becomes more important. Without pressure equalization the remaining product and reactants are not transferred to another reactor column and the blowdown product should be recycled after water knockout to avoid valuable losses. The trade-off between carbon selectivity and production has shown that the highest single-pass yield does not result in the highest productivity. From a techno-economic perspective, a small recycle of non-condensables (CO and H_2) after a simple flash separation would be of interest, considering high productivity at high, but not maximum, carbon selectivity. These considerations would result in a flow scheme as shown in Figure 7-14.

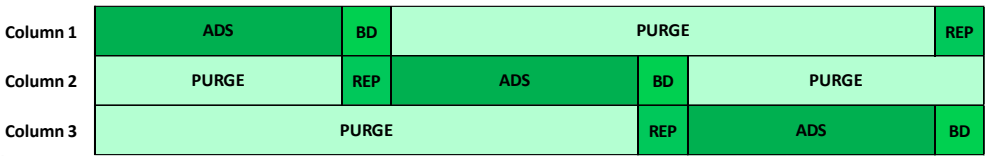

FIGURE 7-13: 3-COLUMN CYCLE DESIGN WITH CONTINUOUS SYNGAS FEED (ADS=ADSORPTION STEP, BD=BLOWDOWN STEP, PURGE=PURGE STEP, REP=REPRESSURIZATION STEP).

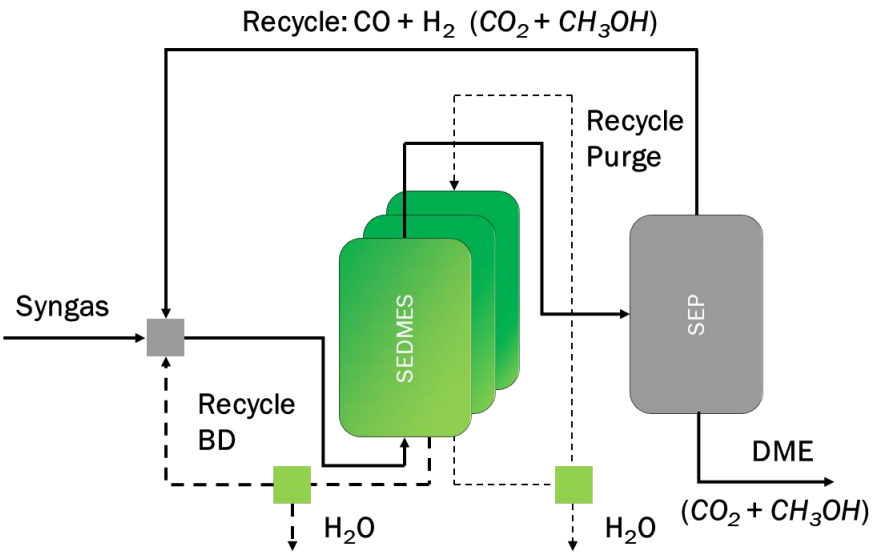

FIGURE 7-14: SCHEMATIC OF THE SEDMES FLOW SCHEME INCLUDING BLOWDOWN RECYCLE, PURGE RECYCLE AND PRODUCT RECYCLE. UNCONVERTED CO_2 AND METHANOL END UP IN THE DME PRODUCT OR ARE RECYCLED WITH CO AND H_2.

Figure 7-15 shows the results for the 3-column cycle design with a blowdown recycle, compared to the same design without recycle. The recycle assures that no valuable feedstock and product are lost and DME is collected as product in the adsorption step, showed by the increased productivity (21%). However, the recycle increases the space velocity of the feed which again poses the trade-off between carbon selectivity and productivity (Figure 7-7). Therefore two recycle cases are shown, corresponding to a multi-tubular reactor with either 4000 or 6000 tubes (GHSV 105 and 70 hr^{-1} with respect to the syngas feed shown in Table 7-3, corresponding to the FLEDGED 10MW thermal biomass input [20]). The larger reactor, with a lower feed flow rate, results in a higher single-pass DME yield (85% carbon selectivity to DME) and despite the lower production rate per tube, the total productivity is increased by 31%. Whereas the reactor size increases with 50%, a first cost estimate based on methanol synthesis reactors gives a 30% cost rise [21]. A full techno-economic optimization should determine the optimum productivity.

TABLE 7-3: SYNGAS FLOW AND COMPOSITION FOR 10MW THERMAL BIOMASS INPUT.

Total mass flow [kg/s]	0.424		
Composition [$\%_{vol}$]			
H_2	70.35	**CH_4**	0.01
CO_2	14.76	**Ar**	0.15
CO	12.88	**N_2**	1.85

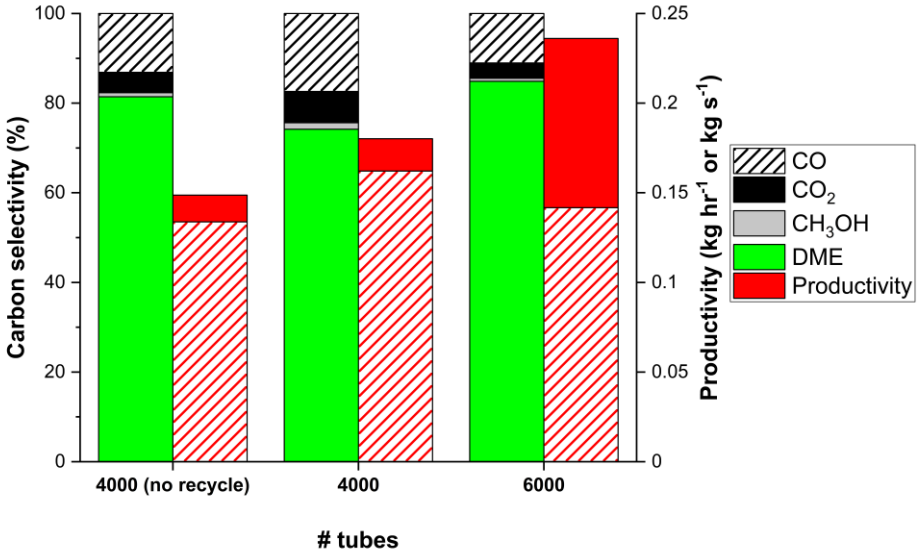

FIGURE 7-15: CARBON SELECTIVITY, SINGLE TUBE PRODUCTIVITY (STRIPED RED, KG HR^{-1}) AND TOTAL PRODUCTIVITY (RED, KG S^{-1}) WITH AND WITHOUT BD RECYCLE.

Moreover, a high single-pass conversion is not the only way to increase the total productivity. The alternative is a product recycle. But again, a product recycle of unconverted H_2 and CO, will increase the feed flow rate with a lower single-pass conversion as a result. Clearly, the cycle design should be closely integrated with the overall process flowsheet. Recently, the techno-economic benefit of sorption enhancement for the production of DME from CO_2 and H_2 directly is investigated [11]. Although the power-to-X case studied, is not the same as the biomass to DME process, lessons could be learned for the SEDMES case. The first design of a SEDMES separation section consists of three steps, a flash drum where the non-condensables (CO and H_2) are separated, a cryogenic distillation column where CO_2 is separated and finally a distillation column where remaining traces of water and methanol are separated to achieve the desired purity of DME. The remaining fraction of water and methanol is so little that separation seems not feasible, as would be required in conventional DME synthesis, and the stream is best recycled to the reactor inlet. To avoid valuable reactant loss, both the CO and H_2 stream and the CO_2 stream are recycled. Depending on the DME content in the blowdown stream, the choice can be made to recycle the stream directly to the reactor inlet, as suggested in this chapter, or add it to the product stream and separate the DME first.

Although the main cost contributing factors in power-to-DME are related to H_2 production and not to the DME production, the SEDMES reactors dominate the cost of the DME synthesis section. SEDMES improves the H_2 conversion to DME, reducing the loss of the

valuable green H_2. On an operational level, the separation of DME and CO_2 is recognized as the most energy intensive process. The resulting bottom product (DME) exceeds the limits of the ISO standard (methanol), and therefore, a second distillation column is required to separate only a very small fraction of methanol. In conclusion, the SEDMES cycle design and process flowsheet in general, but for the biomass to DME case in particular, should further focus on maximizing productivity (minimizing reactor CAPEX), avoid or improve the separation of DME and CO_2, and possibly avoid the final purification step by minimizing by-product methanol. Combined these aspects can be optimized further by techno-economic analysis, addressing the economic and carbon mitigating benefits of SEDMES over conventional DME synthesis technology.

7.4. Conclusions

In this chapter, for the first time, SEDMES technology is validated experimentally on a multi-column test-rig under industrially relevant conditions. Pressure swing regeneration is confirmed as the mode of regeneration. SEDMES is a transient and dynamic process, resulting in many degrees of freedom. The SEDMES reactor model not only describes the transient behavior during cyclic steady-state well, also the dynamic approach to the cyclic steady-state is modelled well.

The multi-column experiments have demonstrated that SEDMES can be operated at 220 °C, which is lower than expected based on previous data. Operation at lower temperatures would allow for a higher maximum temperature rise and would ease the heat management further. Where the complex multi-tubular reactor concept is also a costly part of the SEDMES process, larger reactors would benefit the economic valorization of the process.

Cycle design is an important point of attention for sorption enhanced processes, since many degrees of freedom have to be considered. The preliminary cycle design, including 1 pressure equalization step, requires 6 columns to provide continuous feed and products streams. However, due to the estimated CAPEX of the SEDMES reactors, further development of the cycle design should consider reducing the number of columns. A 3-column cycle design has shown a good cyclic performance as well. When pressure equalization is disregarded to minimize the number of columns, the blowdown recycle becomes important. Also, from a techno-economic perspective, a small recycle of non-condensables (CO and H_2) after a simple flash separation would be of interest to achieve high productivity at high, but not maximum, carbon selectivity. This example illustrates the importance of combining the SEDMES cycle design, the overall process systems engineering and techno-economic evaluation. Combined these aspects can be optimized and address the economic and carbon mitigating benefits of SEDMES over conventional DME synthesis technology. In contrast to conventional DME synthesis, SEDMES allows more efficient carbon and renewable hydrogen utilization to DME.

Nomenclature

a_p	Particle interfacial area (m^2 m^{-3})
c_i	Concentration of component I (mol m^{-3})
Cp	Gas thermal conductivity (J kg^{-1} K^{-1})
Cp_p	Particle thermal conductivity (J kg^{-1} K^{-1})
d_p	Particle diameter (m)
D_z	Axial dispersion coefficient (m^2 s^{-1})
G	Ergun constant (-)
ΔH_{ads}	Adsorption enthalpy (J mol^{-1})
$\Delta H_{r,i}$	Reaction enthalpy (J mol^{-1})
M_i	Molecular weight of component i (kg mol^{-1})
N_i	Mole flux of component i (mol m^{-2} s^{-1})
P	Reactor pressure (bara)
q_i	Adsorbent loading (mol kg^{-1})
r_i	Reaction rate of component i (mol m^{-3} s^{-1}) or (mol kg^{-1} s^{-1}) or (kmol kg^{-1} hr^{-1})
R	Ideal gas constant (J mol^{-1} K^{-1})
t	Time (s)
T	Temperature (K)
u	Superficial gas velocity (m s^{-1})
U	Overall heat transfer coefficient (W m^{-2} K^{-1})
v	Interstitial gas velocity (m s^{-1})
z	axial coordinate (m)

Greek letters

ε_b	Bed voidage (-)
λ	Axial thermal conductivity (W m^{-1} K^{-1})
ρ	Density (kg m^{-3})
ρ_p	Particle density (kg m^{-3})
ω_i	Weight fraction of component i (-)

Bibliography

[1] J. van Kampen, J. Boon, F. van Berkel, J. Vente, M. van Sint Annaland, Steam separation enhanced reactions: Review and outlook, Chemical Engineering Journal 374 (2019) 1286–1303.

[2] J. van Kampen, J. Boon, J. Vente, M. van Sint Annaland, Sorption enhanced dimethyl ether synthesis for high efficiency carbon conversion: Modelling and cycle design, Journal of CO_2 Utilization 37 (2020) 295-308.

[3] J. van Kampen, S. Booneveld, J. Boon, J. Vente, M. van Sint Annaland, Experimental validation of pressure swing regeneration for faster cycling in sorption enhanced dimethyl ether synthesis, Chemical Communications 56 (2020) 13540-13542.
[4] J. van Kampen, J. Boon, J. Vente, M. van Sint Annaland, Sorption enhanced dimethyl ether synthesis under industrially relevant conditions: Experimental validation of pressure swing regeneration, Reaction Chemistry & Engineering Advanced Article (2020).
[5] J.C. Abanades, J. Boon, P. Cobden, K. Coenen, D.S.M. Constantino, R.P.V. Faria, J.R. Fernández, F. Gallucci, M.C. Iliuta, A.E. Rodrigues, E. van Dijk, M. van Sint Annaland, Sorption Enhancement of Chemical Processes, 1 ed., Academic Press, 2017.
[6] A.E. Rodrigues, L.M. Madeira, Y.-J. Wu, R. Faria, Sorption Enhanced Reaction Processes, World Scientific, 2017.
[7] B.T. Carvill, J.R. Hufton, M. Anand, S. Sircar, Sorption-enhanced reaction process, AIChE Journal 42 (1996) 2765-2772.
[8] J. Boon, P.D. Cobden, H.A.J. van Dijk, M. van Sint Annaland, High-temperature pressure swing adsorption cycle design for sorption-enhanced water–gas shift, Chemical Engineering Science 122 (2015) 219-231.
[9] R.J. Detz, J.N.H. Reek, B.C.C. van der Zwaan, The future of solar fuels: when could they become competitive?, Energy & Environmental Science 11 (2018) 1653-1669.
[10] V. Dieterich, A. Buttler, A. Hanel, H. Spliethoff, S. Fendt, Power-to-liquid via synthesis of methanol, DME or Fischer–Tropsch-fuels: a review, Energy & Environmental Science 13 (2020) 3207-3252.
[11] G. Skorikova, M. Saric, S.N. Sluijter, J. van Kampen, C. Sánchez-Martínez, J. Boon, The Techno-Economic Benefitof Sorption Enhancement: Evaluation of Sorption-Enhanced Dimethyl Ether Synthesis for CO2 Utilization, Frontiers in Chemical Engineering (2020).
[12] H. Graaf, E.J. Stamhuis, A.A.C.M. Beenackers, Kinetics of low-pressure methanol synthesis, Chemical Engineering Science 43 (1988) 3185-3195.
[13] G. Berčič, J. Levec, Intrinsic and Global Reaction Rate of Methanol Dehydration Over γ-Al_2O_3 Pellets, Industrial & Engineering Chemistry Research 31 (1992) 1035-1040.
[14] K.L. Ng, D. Chadwick, B.A. Toseland, Kinetics and modelling of dimethyl ether synthesis from synthesis gas, Chemical Engineering Science 54 (1999) 3587-3592.
[15] J. Boon, J. van Kampen, R. Hoogendoorn, S. Tanase, F.P.F. van Berkel, M. van Sint Annaland, Reversible deactivation of γ-alumina by steam in the gas-phase dehydration of methanol to dimethyl ether, Catalysis Communications 119 (2019) 22-27.
[16] J. van Kampen, J. Boon, M. van Sint Annaland, Steam adsorption on molecular sieve 3A for sorption enhanced reaction processes, Adsorption (2020).
[17] D. Liuzzi, C. Peinado, M.A. Peña, J. van Kampen, J. Boon, S. Rojas, Increasing dimethyl ether production from biomass-derived syngas via sorption enhanced dimethyl ether synthesis, Sustainable Energy & Fuels 4 (2020) 5674-5681.

[18] D. Song, W. Cho, G. Lee, D.K. Park, E.S. Yoon, Numerical Analysis of a Pilot-Scale Fixed-Bed Reactor for Dimethyl Ether (DME) Synthesis, Ind. Eng. Chem. Res. 47 (2008) 4553–4559.
[19] S. Guffanti, C.G. Visconti, J. van Kampen, J. Boon, G. Groppi, Reactor modelling and design for sorption enhanced dimethyl ether synthesis, Chemical Engineering Journal 404 (2021) 126573-126585.
[20] M. Romano, G. Guandalini, A. Poluzzi, C. Elsido, E. Martelli, M. Astolfi, P. Chiesa, S. Guffanti, G. Groppi, I. Martínez, G. Grasa, R. Murillo, D. Liuzzi, C. Peinado, S. Rojas, S. Hafner, M. Schmid, J. van Kampen, G. Skorikova, J. Boon, A. Pitkäoja, J. Ritvanen, K. Myöhänen, T. Jayabalan, L. Joubert, G. Marlair, S. Schucht, E. Real, L. Létinois, F. Sessa, J. Laffely, J. Palonen, G. Rexwinkel, P. Huttenhuis, J.C. Aparicio, R. Garcia, Flexible Dimethyl ether production from biomass gasification with sorption enhanced processes: Final technical report, Milano, 2020.
[21] W.L. Luyben, Design and Control of a Methanol Reactor/Column Process, Principles and Case Studies of Simultaneous Design, Wiley, 2011.

Chapter 8. Conclusions and outlook

Efficient carbon utilization to dimethyl ether by steam adsorption enhancement

Dimethyl ether (DME) is one of the most promising alternative fuel solutions among the various ultra clean, renewable, and low-carbon fuels under consideration worldwide [1]. As it can be produced from syngas, defined here as a mixture of CO, CO_2 and H_2, originating from fossil and renewable feedstocks alike, it is projected to play an important role in the energy transition [1]. DME is also one of the valuable products considered for chemical recycling by carbon dioxide conversion [2], both direct (CCU) as well as indirect conversion via biomass-based syngas.

Conventionally, DME is produced from synthesis gas with methanol as an intermediate chemical. The following equilibrium reactions are involved:

Methanol synthesis	$CO_2 + 3\ H_2 \rightleftharpoons CH_3OH + H_2O$	(1)
	$CO + 2\ H_2 \rightleftharpoons CH_3OH$	(2)
Water-gas shift	$CO + H_2O \rightleftharpoons H_2 + CO_2$	(3)
Methanol dehydration	$2\ CH_3OH \rightleftharpoons CH_3OCH_3 + H_2O$	(4)
Direct DME synthesis	$3\ CO + 3\ H_2 \rightleftharpoons CH_3OCH_3 + CO_2$	(5)
Sorption enhanced DME	$2\ CO_2 + 6\ H_2 \rightleftharpoons CH_3OCH_3 + 3\ H_2O$	(6)

Indirect DME production comprises the production of intermediate methanol (1,2), and methanol dehydration (4). The incomplete methanol and DME yields require extensive separation sections and recycles. The single-step direct DME synthesis (5) proceeds via intermediate methanol as well, yet offers a reduction in process steps and increased overall conversion to DME [3-6]. Although the direct DME synthesis process outperforms the indirect process in terms of efficiency, separation and recycling remain a requirement. In the direct DME synthesis, the O-surplus of the feed ends up in CO_2, resulting in equal molar amounts of DME and CO_2 produced. Since the reaction is equilibrium limited, the downstream separation section produces recycle streams of synthesis gas ($CO+H_2$), CO_2, and methanol. Synthesis gas and methanol can be recycled back to the DME synthesis reactor, while the CO_2 is at best recycled in synthesis gas generation via dry or tri-reforming [7-14]. However, starting from a renewable, CO_2-rich feedstock and/or captured CO_2 to produce DME this is not an option. In fact, one of the major challenges in power-to-liquid (PtL) processes is the direct utilization of CO_2 [15], making most approaches for renewable fuel production unattractive [16]. For CO_2 utilization, the production and efficient handling of steam remains a major bottleneck [2, 17, 18]. In this thesis sorption enhanced DME synthesis is introduced as a promising process intensification for the production of DME from biomass-based, CO_2-rich syngas or CO_2 and hydrogen directly.

In **Chapter 2** the enhancement by steam separation is shown to be a promising process intensification for many types of reactions in which water is formed as a by-product, such as the utilization of CO_2 [7]. Reducing the steam partial pressure by in situ adsorption or membrane separation, results in conversion enhancement due to equilibrium displacement. With respect to DME synthesis, the in situ removal of H_2O ensures that the oxygen surplus of the feed no longer ends up in CO_2 as is the case for direct DME synthesis. As a result, CO_2 can be converted directly to DME with high carbon efficiency, rather than being the main byproduct of DME production (5,6). Both membrane and adsorption technology are of interest for in situ steam separation. However, sorption enhanced DME synthesis appears to be the most promising from a carbon efficiency point of view due to its high single-pass conversion of CO_2 to DME.

A model framework for sorption enhanced DME synthesis is developed and SEDMES is studied as a full cyclic process of adsorption and inherent regeneration in **Chapter 3** [19]. Cooled reactor operation of the reactive adsorption step is required to achieve high performance of the system. SEDMES temperature control in a multi-tubular fixed bed reactor, however, is not a critical issue [20]. The maximum bed temperature stays well below the limits reported in the literature (300 °C) to preserve the CZA catalyst stability. Accordingly, larger tube diameters (up to 46.6 mm) can be adopted compared to conventional direct DME synthesis, with less than 2.5% loss in DME yield compared to smaller diameters.

A key parameter for optimizing the SEDMES process is the working adsorption capacity of the system. In **Chapter 4**, it is shown that molecular sieve 3A has an adequate adsorption capacity at elevated temperatures, which increases rapidly at higher partial pressures of steam [21]. This makes the LTA adsorbent suitable for sorption enhanced reaction processes, such as SEDMES, enabling a high single-pass yield. Steam adsorption on the material is described with a multi-site GSTA isotherm, allowing further flexibility in the number of distinct adsorption sites, and additional capillary condensation. The multi-site isotherm can be best described as a dual-site GSTA isotherm (dual-Langmuir) corresponding to the respective α and β cages of the material. The adsorption mass transfer rate can be described with a linear driving force approximation, which is sufficiently accurate for all reactor and process modelling purposes. The mass transfer resistance during adsorption on zeolite 3A is shown to be dominantly determined by micropore resistance, due to the small cage aperture.

Experimental proof-of-concept for sorption enhanced DME, with commercial and novel materials, is discussed in **Chapter 5** [6]. The performance of several Copper-Zinc oxide-Alumina catalysts for the synthesis of methanol and the direct synthesis of DME, using additional γ-Al_2O_3 as acid catalyst, from a CO_2-rich (biobased) syngas is studied. CZA catalysts have been doped with Zr and Ga oxides, which increases the CO/CO_2 product ratio, but fails to improve methanol production. This is probably due to the higher activity of the

doped catalysts for the reverse WGS reaction and the concomitant production of H_2O, which results in activity loss for the catalysts. In addition, the presence of water prevents the production of methanol and its subsequent dehydration to DME. In contrast to direct DME synthesis, SEDMES offers two specific advantages for the catalyst: the system is operated at low steam pressures and is periodically regenerated due to its adsorptive nature. Proof-of-concept was demonstrated with DME concentrations of ca. 70%, well above the equilibrium for conventional synthesis. The undoped, commercial and novel, CZA catalysts show the highest production rate of methanol from CO_2-rich syngas and therefore also demonstrate the best SEDMES performance.

The activity and stability of the commercial dehydration catalyst, γ-Al_2O_3, was further investigated [22]. The γ-Al_2O_3 has a high activity and selectivity for the production of DME from methanol at 250 °C. However, adsorbed steam reduces the catalytic activity of γ-Al_2O_3. At 250 °C and steam partial pressures of 14 bar and higher, the conversion to crystalline boehmite has been confirmed through PXRD measurements. While crystalline boehmite remained present after testing methanol dehydration at 350 °C, it was shown that the activity for methanol dehydration restores in situ at 250 °C. This confirms that the deactivation by steam is reversible under DME synthesis conditions.

Reaction kinetics for the dehydration catalyst, as well as the methanol synthesis catalyst, have been determined by fitting the parameters in methanol synthesis and dehydration reaction kinetic models from literature [23]. The activation energies determined for both the methanol synthesis and methanol dehydration kinetics are lower than the values originally reported, attributed to the higher activity of present-day catalysts. Next to the study of the adsorbent material in **Chapter 4**, this investigation of the catalysts, and the combination of all materials involved results in a validated dynamic reactor model, which is used for upscaling of SEDMES technology and predictions of large scale DME synthesis.

A validated pressure swing regeneration cycle for sorption enhanced DME synthesis is demonstrated on a bench-scale reactor [23, 24]. In **Chapter 6** SEDMES is again demonstrated to be a highly flexible process for converting CO_2-rich (bio-based) syngas and CO_2 directly to DME with a high single-pass conversion. The relevant testing performed in this chapter indeed proves the efficiency of PSA regeneration, generally preferred for its facilitated design, shown in **Chapter 3**. Here, 80% single-pass carbon selectivity to DME is demonstrated with pressure swing regeneration, which already allows for a factor four increase in productivity, with further optimization still possible.

In **Chapter 7**, SEDMES technology is developed further by experimental validation on a multi-column test-rig under industrially relevant conditions. In this setup the continuous production of DME by sorption enhancement is demonstrated for the first time in open literature. The essential pressure swing regeneration, as discussed in **Chapter 6**, is confirmed as the preferred mode of regeneration. The SEDMES reactor model describes

both the transient nature of the process during cyclic-steady-state, as well as the approach to cyclic steady-state.

The multi-column experiments have demonstrated that SEDMES can be operated at 220 °C, which is lower than expected based on previous experimental and modelling results reported in this thesis. In **Chapter 3** SEDMES temperature control is discussed not to be a critical issue in a cooled reactor concept, such as a multi-tubular reactor. However, operation at lower temperatures allows for a higher maximum temperature rise and would ease the heat management further. Where the cooled, multi-tubular reactor concept is also expected to have a relatively large cost, larger reactors would benefit the economic valorization of the process.

Cycle design is an important aspect for sorption enhanced processes, since it involves the optimization of many degrees of freedom common to a reactive adsorption process. The preliminary cycle design, including 1 pressure equalization step, requires 6 columns to provide continuous feed and products streams. However, due to the estimated CAPEX of the SEDMES reactors, further development of the cycle design would ideally reduce the number of columns. A 3-column cycle design has shown good cyclic performance, however preliminary process boundary conditions have to be relieved. Especially when pressure equalization is disregarded, the blowdown recycle becomes important to avoid loss of valuable product. The trade-off between carbon selectivity and productivity has shown that the highest single-pass yield does not result in the highest productivity. From a techno-economic perspective, a small recycle of non-condensables (CO and H_2) after a simple flash separation would be interesting, considering the high productivity at high, but not maximum, carbon selectivity. This illustrates the necessity of integrating the SEDMES cycle design, overall process systems engineering and techno-economic evaluation. Combined, these aspects can be optimized while addressing the economic and carbon mitigating benefits of SEDMES over conventional DME synthesis technology. In contrast to the conventional technology, SEDMES allows more efficient utilization of carbon and renewable hydrogen. Downstream DME purification can be simplified and large reactant recycles, and the losses associated with it, can be reduced.

In conclusion, during the work presented in this thesis, sorption enhanced DME synthesis has matured from a technology concept [25-28] to a technology validated in a relevant environment [23]. Crucial to the understanding of steam separation enhanced processes, SEDMES is investigated by a combined experimental and modelling approach. Essential aspects for reactive steam adsorption, including high temperature working capacities and heat management, have been addressed. With the technology validated and the modelling framework available, techno-economic and life cycle analyses have to be performed to investigate the economic and carbon mitigating benefits of the high efficiency of the carbon and hydrogen utilization by the SEDMES technology.

A recent study looked into the techno-economic benefit of sorption enhancement for the production of DME from CO_2 and H_2 directly [29]. With a production cost of €1.3 per kg DME by the PtX SEDMES process at a small scale of only 23 kt/year, the costs are higher than the current market price. Although the production cost is higher than the current market price for fossil-based DME, the results are promising compared to other studies on DME production from CO_2 by conventional DME synthesis processes at even larger scales. The main cost contributing factors are related to H_2 production, required for CO_2 utilization. The electricity cost has the largest impact on the production price, followed by the CAPEX of the PEM electrolyser. In this thesis, SEDMES is demonstrated to be a powerful technology for efficient conversion of H_2 into DME, which is an essential benefit due to the determining role of hydrogen in the total production cost.

Biobased DME is potentially cheaper than DME produced from CO_2 and renewable hydrogen. Competitive production costs as low as €0.25 per kg are even reported [30, 31]. Due to the hydrogen deficiency of biomass for the production of DME [32], either renewable hydrogen needs to be added or carbon has to be captured. Moreover, capturing CO_2 using biomass is rather efficient and could contribute to negative emissions. Besides latest generation biomass sources, municipal solid waste as feedstock could play an important role in the circular economy [33]. Compared to alternative biomass sources, (municipal) waste could offer advantages in terms of cost saving since collection and disposal are a requirement. Considering a different feedstock than renewable hydrogen from electrolysis, the reactors will have a larger contribution to the overall cost of the SEDMES process. As discussed throughout this thesis, further optimization of SEDMES should be pursued. Firstly, operating conditions can be improved. Catalysts active at lower temperatures, such as heteropoly acids, would allow operation at lower temperatures which is favorable for the adsorption capacity of the system. Also elevated pressure would increase SEDMES productivity due to both enhanced reaction kinetics (conventional methanol synthesis is performed up to 100 bar) and adsorption capacity. Although SEDMES is also able to achieve high conversion at low pressures, in contrast to conventional synthesis, process specific flowsheet integration has to indicate the optimal pressure based on cost optimization. Modelling, supported by experimental results, indicate that fast or even rapid cycling seems promising for increasing the productivity. Under the current conditions it has been shown that the heat in SEDMES is very well manageable. Improved heat management would allow for larger reactor diameters and therefore fewer separate vessels, reducing the total capital cost. Reduced mass transfer resistance between catalyst functionality and adsorbent, by integrated catalyst-adsorbent particles, improves the trade-off between catalyst activity and adsorbent capacity and therefore also enhances the productivity.

Sorption enhanced dimethyl ether synthesis has shown to be an efficient technology for carbon utilization, which plays an important role in worldwide efforts to limit global warming. All pathways, reported by the IPCC, to achieve the challenging target of only 1.5 °C

temperature rise result in net zero CO_2 emissions in 2050 and require net negative emissions after 2050 [34]. It can even be argued that we should prepare for achieving net negative CO_2 emissions before 2050, considering the still increasing emissions and the emission of greenhouse gasses other than CO_2 [35]. This stresses the importance of carbon capture, utilization and sequestration (CCUS). Both for the direct utilization of CO_2 and via the conversion of (waste) biomass, carbon and hydrogen efficiency will become leading. The SEDMES process can achieve this high efficiency, which is essential for a circular carbon economy, and DME as alternative fuel can be implemented relatively quickly and easily compared to other solutions (for the longer-term future), mainly due to compatibility with the existing infrastructure. Sorption enhanced DME synthesis is already a promising process intensification for the production of DME with high single-pass conversion of CO_2 to DME. The high single-pass yield reduces or even eliminates the conventionally large recycles and the loss of valuable carbon and renewable hydrogen. Also downstream purification could be simplified. SEDMES is less affected by feed dilution with impurities and can be operated at milder conditions compared to the conventional synthesis process. Ultimately, SEDMES is further optimized for the desired use case by a combination of cycle design and the specific overall process flowsheet, where it can play an important role for the required energy transition in the near future.

Bibliography

[1] T.A. Semelsberger, R.L. Borup, H.L. Greene, Dimethyl ether (DME) as an alternative fuel, Journal of Power Sources 156 (2006) 497-511.
[2] G. Centi, S. Perathoner, Opportunities and prospects in the chemical recycling of carbon dioxide to fuels, Catalysis Today 148 (2009) 191-205.
[3] U. Mondal, G.D. Yadav, Perspective of dimethyl ether as fuel: Part I. Catalysis, Journal of CO2 Utilization 32 (2019) 299-320.
[4] K.L. Ng, D. Chadwick, B.A. Toseland, Kinetics and modelling of dimethyl ether synthesis from synthesis gas, Chemical Engineering Science 54 (1999) 3587-3592.
[5] F. Dadgar, R. Myrstad, P. Pfeifer, A. Holmen, H.J. Venvik, Direct dimethyl ether synthesis from synthesis gas: The influence of methanol dehydration on methanol synthesis reaction, Catalysis Today 270 (2016) 76-84.
[6] D. Liuzzi, C. Peinado, M.A. Peña, J. van Kampen, J. Boon, S. Rojas, Increasing dimethyl ether production from biomass-derived syngas via sorption enhanced dimethyl ether synthesis, Sustainable Energy & Fuels 4 (2020) 5674-5681.
[7] J. van Kampen, J. Boon, F. van Berkel, J. Vente, M. van Sint Annaland, Steam separation enhanced reactions: Review and outlook, Chemical Engineering Journal 374 (2019) 1286–1303.
[8] T.B.H. Nguyen, E. Zondervan, Methanol production from captured CO2 using hydrogenation and reforming technologies: environmental and economic evaluation, Journal of CO2 Utilization 34 (2019) 1-11.

[9] A. Rafiee, K. Rajab Khalilpour, D. Milani, M. Panahi, Trends in CO2 conversion and utilization: A review from process systems perspective, Journal of Environmental Chemical Engineering 6 (2018) 5771-5794.
[10] M.T. Luu, D. Milani, M. Wake, A. Abbas, Analysis of di-methyl ether production routes : Process performance evaluations at various syngas compositions, Chemical Engineering Science 149 (2016) 143-155.
[11] S.-H. Lee, W. Cho, W.-S. Ju, B.-H. Cho, Y.-C. Lee, Y.-S. Baek, Tri-reforming of CH4 using CO2 for production of synthesis gas to dimethyl ether, Catalysis Today 87 (2003) 133-137.
[12] W. Cho, T. Song, A. Mitsos, J.T. McKinnon, G.H. Ko, J.E. Tolsma, D. Denholm, T. Park, Optimal design and operation of a natural gas tri-reforming reactor for DME synthesis, Catalysis Today 139 (2009) 261-267.
[13] I.H. Kim, S. Kim, W. Cho, E.S. Yoon, Simulation of commercial dimethyl ether production plant, in: S. Pierucci, G.B. Ferraris (Eds.) 20th European Symposium on Computer Aided Process Engineering – ESCAPE20, 2010, pp. 799-804.
[14] S.-H. Lee, W. Cho, T. Song, Y.-J. Ra, Scale up study of DME direct synthesis technology, Proceedings of World gas conference, 2009.
[15] V. Dieterich, A. Buttler, A. Hanel, H. Spliethoff, S. Fendt, Power-to-liquid via synthesis of methanol, DME or Fischer–Tropsch-fuels: a review, Energy & Environmental Science 13 (2020) 3207-3252.
[16] R.J. Detz, J.N.H. Reek, B.C.C. van der Zwaan, The future of solar fuels: when could they become competitive?, Energy & Environmental Science 11 (2018) 1653-1669.
[17] Accelerating Breakthrough Innovation in Carbon Capture, Utilization, and Storage, Report of the Mission Innovation Carbon Capture, Utilization, and Storage Expert's Workshop, 2017.
[18] A. Katelhon, R. Meys, S. Deutz, S. Suh, A. Bardow, Climate change mitigation potential of carbon capture and utilization in the chemical industry, Proc Natl Acad Sci U S A 116 (2019) 11187-11194.
[19] J. van Kampen, J. Boon, J. Vente, M. van Sint Annaland, Sorption enhanced dimethyl ether synthesis for high efficiency carbon conversion: Modelling and cycle design, Journal of CO_2 Utilization 37 (2020) 295-308.
[20] S. Guffanti, C.G. Visconti, J. van Kampen, J. Boon, G. Groppi, Reactor modelling and design for sorption enhanced dimethyl ether synthesis, Chemical Engineering Journal 404 (2021) 126573-126585.
[21] J. van Kampen, J. Boon, M. van Sint Annaland, Steam adsorption on molecular sieve 3A for sorption enhanced reaction processes, Adsorption (2020).
[22] J. Boon, J. van Kampen, R. Hoogendoorn, S. Tanase, F.P.F. van Berkel, M. van Sint Annaland, Reversible deactivation of γ-alumina by steam in the gas-phase dehydration of methanol to dimethyl ether, Catalysis Communications 119 (2019) 22-27.
[23] J. van Kampen, J. Boon, J. Vente, M. van Sint Annaland, Sorption enhanced dimethyl ether synthesis under industrially relevant conditions: Experimental validation of pressure swing regeneration, Reaction Chemistry & Engineering 6 (2020) 244-257.
[24] J. van Kampen, S. Booneveld, J. Boon, J. Vente, M. van Sint Annaland, Experimental validation of pressure swing regeneration for faster cycling in sorption enhanced dimethyl ether synthesis, Chemical Communications 56 (2020) 13540-13542.

[25] J. Boon, F. van Berkel, H. van Dijk, J. Vente, Separation enhanced dimethyl ether synthesis, 5th TMFB International Conference, Aachen, 2017.
[26] I. Iliuta, M.C. Iliuta, F. Larachi, Sorption-enhanced dimethyl ether synthesis — Multiscale reactor modeling, Chemical Engineering Science 66 (2011) 2241-2251.
[27] S. Ressler, M. Elsner, C. Dittrich, D. Agar, S. Geisler, O. Hinrichsen, Reactive gas adsorption, Integrated Reaction and Separation Operations, Springer2006.
[28] H.-J. Kim, H. Jung, K.-Y. Lee, Effect of Water on Liquid Phase DME Synthesis from Syngas over Hybrid Catalysts Composed of Cu/ZnO/$Al_2$0$_3$ and γ-Al_2O_3, Korean Journal of Chemical Engineering 18 (2001) 838-841.
[29] G. Skorikova, M. Saric, S.N. Sluijter, J. van Kampen, C. Sánchez-Martínez, J. Boon, The Techno-Economic Benefitof Sorption Enhancement: Evaluation of Sorption-Enhanced Dimethyl Ether Synthesis for CO2 Utilization, Frontiers in Chemical Engineering 2 (2020).
[30] M. Martín, Optimal year-round production of DME from CO2 and water using renewable energy, Journal of CO2 Utilization 13 (2016) 105-113.
[31] E. Peral, M. Martín, Optimal Production of Dimethyl Ether from Switchgrass-Based Syngas via Direct Synthesis, Industrial & Engineering Chemistry Research 54 (2015) 7465-7475.
[32] I. Martínez, V. Kulakova, G. Grasa, R. Murillo, Experimental investigation on sorption enhanced gasification (SEG) of biomass in a fluidized bed reactor for producing a tailored syngas, Fuel 259 (2020) 116252-116259.
[33] I. Martínez, G. Grasa, M.S. Callén, J.M. López, R. Murillo, Optimised production of tailored syngas from municipal solid waste (MSW) by sorption-enhanced gasification, Chemical Engineering Journal 401 (2020) 126067-126078.
[34] IPCC, Special Report, Global Warming of 1.5°C, Summary for Policymakers, 2018.
[35] R.J. Detz, B. van der Zwaan, Transitioning towards negative CO2 emissions, Energy Policy 133 (2019).

Curriculum vitae Jasper van Kampen

Jasper was born in 1991 in Sint-Oedenrode. After finishing secondary education at Gymnasium Beekvliet in Sint-Michielsgestel, he studied Chemical Engineering and Chemistry at the Eindhoven University of Technology (TU/e). After a side track in Chemistry at the University of Cambridge, he obtained his master's degree (MSc) in Chemical Engineering at the Eindhoven University of Technology (TU/e) with a specialization in Chemical and Process Technology in 2016. His graduation research on the optimization of furfural production by reactive stripping was carried out under supervision of prof. John van der Schaaf in the research group of Chemical Reactor Engineering.

In 2017 Jasper joined ECN (Energy research Center of the Netherlands) in Petten, as research scientist and continued his work at TNO (the Netherlands Organisation for applied scientific research) Energy Transition. He started his PhD project in 2017 within the Horizon 2020 framework project *FLEDGED* with prof. Martin van Sint Annaland at the research group of Chemical Process Intensification (TU/e) and with dr. Jurriaan Boon at the research group Sustainable Technologies for Industrial Processes (TNO). The most important findings of his PhD are described in this thesis.

ORCID 0000-0002-7085-5210

List of publications

J. van Kampen, J. Boon, J. Vente, M. van Sint Annaland, Sorption enhanced dimethyl ether synthesis under industrially relevant conditions: experimental validation of pressure swing regeneration, Reaction Chemistry & Engineering 6 (2021) 244-257.
S. Guffanti, C. Visconti, J. van Kampen, J. Boon, G. Groppi, Reactor modelling and design for sorption enhanced dimethyl ether synthesis, Chemical Engineering Journal 404 (2021) 126573-126585.

G. Skorikova, M. Saric, S. Sluijter, J. van Kampen, C. Sánchez-Martínez, J. Boon, The techno-economic benefit of sorption enhancement: Evaluation of sorption-enhanced dimethyl ether (DME) synthesis for CO2 utilisation, Frontiers in Chemical Engineering 2:594884 (2020).
J. van Kampen, J. Boon, M. van Sint Annaland, Steam adsorption on molecular sieve 3A for sorption enhanced reaction processes, Adsorption (2020).
J. van Kampen, S. Booneveld, J. Boon, J. Vente, M. van Sint Annaland, Experimental validation of pressure swing regeneration for faster cycling in sorption enhanced dimethyl ether synthesis, Chemical Communications 56 (2020) 13540-13542.
D. Liuzzi, C. Peinado, M. A. Peña, J. van Kampen, J. Boon, S. Rojas, Increasing DME production from biomass via Sorption Enhanced Dimethyl Ether Synthesis, Sustainable Energy & Fuels 4 (2020) 5674-5681.
J. van Kampen, J. Boon, J. Vente, M. van Sint Annaland, Sorption enhanced dimethyl ether synthesis for high efficiency carbon conversion: Modelling and cycle design, Journal of CO_2 Utilization 37 (2020) 295-308.

J. van Kampen, J. Boon, F. van Berkel, J. Vente, M. van Sint Annaland, Steam separation enhanced reactions: Review and outlook, Chemical Engineering Journal 374 (2019) 1286–1303.
J. Boon, J. van Kampen, R. Hoogendoorn, S. Tanase, F.P.F. van Berkel, M. van Sint Annaland, Reversible deactivation of γ-alumina by steam in the gas-phase dehydration of methanol to dimethyl ether, Catalysis Communications 119 (2019) 22-27.

Not related to this thesis

V. Krzelj, J. van Kampen, J. van der Schaaf, M. F. Neira D'Angelo, Furfural Production by Reactive Stripping: Process Optimization by a Combined Modelling and Experimental Approach, Industrial & Engineering Chemistry Research 58 (2019) 16126-16137.

Dankwoord

Dit proefschrift was nooit tot stand gekomen zonder de bijdragen, steun en kritiek van een groot aantal mensen. Hierbij wil ik dan ook iedereen hartelijk bedanken die heeft bijgedragen aan het tot stand komen van dit proefschrift. Zonder mensen tekort te doen, bedank ik in het bijzonder:
Jurriaan, Dick, Eric, Francesco, Frans, Galina, Gerard, Hans, Henk, Henny, Jaap, Jean-Pierre, Jebin, Johan, Leonie, Marija, Martien, Martin, Özlem, Paul, Raghu, Saskia, Sjaak, Soraya en al mijn huidige en voormalige collega's in Petten.
Martin, Fausto, Ivo, John, Judith en al mijn collega's en docenten aan de TU/e.
Bouke, Inge, Jasper, Jo-Ann, Juan, Jules, Niels, Roelof en alle studenten bij TNO en de TU/e.
Alessandro, Dalia, Gianpiero, Giulio, Matteo, Sergio, Simone, Stefania en iedereen waarmee ik verder plezierig heb samen mogen werken.
De docenten op Gymnasium Beekvliet, en in het bijzonder mevrouw Scheffers.
En tot slot mijn vrienden en familie, in het bijzonder, Kim, Jan, Maria, Roel, Floor en Joost.

Wonder en is gheen wonder

Simon Stevin